METHOD FOR CHARACTERISING AND QUANTIFYING VOLUMETRIC EDGE-WEAR IN CERAMIC-ON-CERAMIC HIP ARTHROPLASTY DEVICES

DARSHIL SUNIL KAPADIA

A thesis submitted to the University of Huddersfield
in partial fulfilment of the requirements for
the degree of Doctor of Philosophy

Department of Computing and Engineering,
The University of Huddersfield

September 2018

Copyright statement

Abstract

The number of primary total hip arthroplasty (THA) surgeries has been increasing worldwide over the last decades reaching over 200 per 100,000 population with a high degree of variability between countries[1-3]. National Joint registry 2017 report mentions that in the UK during the last decade, 711,765 primary surgeries have been carried out in comparison to 80,042 revision surgeries to replace joints that have failed either prematurely or at the end of their useful life[1]. The life expectancy of a hip prosthesis is commonly expected to be 15-20 years.

Of all current commonly used bearing surface combinations, the use of fourth generation ceramic-on-ceramic bearings have proved to be very efficient [4] and has grown in popularity for primary hip surgery in the decade preceding 2017 [1]. This is due to the low reported wear volumes associated with all ceramic bearings [5] as well as the fact that ceramic debris being bio-inert overcomes the commonly reported issues of systemic cobalt chromium ion concentration as reported in metal-on-metal bearings [6, 7] and issues of osteolysis induced by polyethylene wear debris in metal-on-UHMWPE [8, 9]. The interest in ceramic-on-ceramic is elevated also due to significant improvements in material properties and manufacturing process [10]. However, the ceramic-on-ceramic hip prosthesis are reported to squeak in-vivo [11, 12] which appears to be linked to edge-loading [13]. Also, it has been reported that an unusual stripe pattern of wear can occur in some retrieved acetabular cup liners [14] and it has further been postulated that this is caused by cup liner edge loading [15]. The combined measurement challenge of wear occurring at the edge of the acetabular liner of a low-wearing ceramic-on-ceramic prosthesis is therefore considerable.

Various wear measurement methods have been developed to measure wear in hip prostheses [12, 16-18], yet current recognised industrial practice regarding in vitro measurement of wear for hip joint prostheses involves either gravimetric assessment or co-ordinate measurement [19]. Due to the

considerable challenge in geometrical characterization of edge wear, current literature regarding the assessment of edge-wear in acetabular cup liners has been confined to in-vitro simulator studies and gravimetric measurement to assess wear volumes. Geometric characterisation of wear is essential in determining the contact conditions during gait and subsequent calculation of point and magnitude of the maximum stress condition. It is, therefore, vital that a robust and reliable method for geometric measurement and analysis of edge wear is created.

Current methodologies for assessing wear on acetabular cups have focused on quantifying the amount of material loss on the bearing surface. The bearing surface is constituted by well-defined geometry and surface characteristics. As such methods are able to estimate the unworn surface and determine the amount of material loss. However, the main limitation of these methods was that wear could only be estimated on the well-defined spherical geometry of bearing surface. Hence, when edge wear is present at the boundary between the bearing surface and outer cup geometry it is normally thresholded during analysis process when using current methods. This can potentially underestimate the amount of wear present on acetabular cups.

This study provides details of the requirements and methodologies for the measurement and analysis of edge wear in ceramic-on-ceramic liners. Two methodologies have been developed based on measurements using a coordinate measuring machine and a roundness measuring machine. Both methods have been evaluated using ceramic liners tested in vitro under edge loading conditions, and the volume loss is compared to gravimetric measurements. The results show that both methods have the required resolution to measure volume loss of less that $1mm^3$ and are thus capable of providing a volume loss estimation for ceramic-on-ceramic acetabular liners.

Table of Contents

Abstract..... 3

Table of Contents..... 5

List of Tables..... 9

List of Figures 12

Dedications and Acknowledgements 19

Chapter 1. Introduction 20

1.1 Aim & Objectives 22

1.2 Novel Contribution ..... **Error! Bookmark not defined.**

1.3 List of Publications 24

Chapter 2. Literature Review 25

2.1 Natural Hip Joint.....25

2.1.1 Introduction 25

2.1.2 Bones & Cartilage.....26

2.1.3 Ligaments 27

2.1.4 Lubrication 28

2.2 Disorders in joint 31

2.2.1 Introduction 31

2.2.2 Osteoarthritis 31

2.2.3 Rheumatoid Arthritis.....33

2.3 Total Hip Replacement 35

2.3.1 Introduction 35

2.3.2 History.....36

2.3.3 Failure of Total Hip Replacement 41

2.3.4 Hip Prosthesis Design 42
2.3. Bio-Materials.....49
2.3.1 Introduction 49
2.3.3 Metals 50
2.3.4 Polymers.....53
2.3.5 Ceramics.....58
2.4 Bearing Combinations & Failure Mechanisms 63
2.4.1 Metal-on-Polyethylene (MoP) 63
2.4.2 Metal-on-Metal (MoM).....66
2.4.3 Ceramic-on-Ceramic (CoC).....71
2.5 Biomechanics & Testing 76
2.5.1 Human Gait 77
2.5.2 Hip Joint Forces 79
2.6 Methods of Volumetric Wear Measurement.....83
2.6.1 Gravimetric measurement 84
2.6.2 Co-ordinate Measuring Machine (CMM) 85
2.6.3 Roundness Measurement Machine (RMM) 98
2.6.4 Review of Existing Wear Measurement Methods 100
Chapter 3: CMM Method Development.....107
3.1 Summary 107
3.2 Background 107
3.3 Method Development 108
3.4 First Attempt to Re-Construct Unworn Surface Geometry.....111
3.5 RMM roundness test performed to examine form of the acetabular liners through roundness traces.....112
3.6 Unworn Liner Study 117

3.7 Coverage Angle Test 121
3.8 Updated Method for Re-construction of Unworn Surface Geometry .. 126
3.9 Volumetric analysis for the cohort of Simulated Liners 131
3.10 Results 135
3.11 Inter-operator Variability for CMM method 139
Chapter 4: RMM Method Development 143
4.1 Measurement Procedure 143
4.1.1 Vertical Trace Test 144
4.1.2 Roundness Trace Measurement 147
4.2 Volumetric Analysis 150
4.3 Results 155
4.4 Inter-operator Variability for RMM method 158
Chapter 5: Case Study – Interval Wear Measurement 162
5.1 Study Design 162
5.2 Results – CMM Method 163
5.3 Results – RMM Method 173
5.3.1 RMM Repeatability 180
Chapter 6: Discussion 182
6.1 CMM Results from Method Development 184
6.2 RMM Results from Method Development 186
6.3 CMM Results from Interval study 188
6.4 RMM results from Interval study 189
6.5 CMM vs RMM Advantages and Limitations 190
6.6 Comparison of CMM, RMM and Gravimetric 195
Chapter 7: Conclusion 205
Chapter 8: Future Work 208

References.....210

Word Count : 55,130

List of Tables

Table 1: Prevalence of radiographic osteoarthritis in the hip [61]. 33

Table 2: Information of mechanical properties of metallic materials employed to fabricate hip prosthesis. σ_Y is yield strength, σ_{UTS} is ultimate tensile strength and E is Young's modulus. 51

Table 3: Displaying chemical composition of 316L stainless steel taken from ASTM F138 [129] 52

Table 4: Composition of Ti-6Al-4V as stated in ASTM F136 [135]. 53

Table 5: Mechanical properties of two medical grade of UHMWPE [140]. 55

Table 6: Composition of PMMA bone cement [154]. 57

Table 7: The mechanical characteristic of different generation of ceramics [57]. .. 62

Table 8: Tabulated results of the minimum edge deviation in height for all six liners of the unworn cohort-B. 121

Table 9: Tabulated results from the coverage angle assessment of the acetabular liners of the unworn cohort-B. 125

Table 10: Table comparing calculated wear volumes of measured surface mesh and reconstructed surface geometry. 130

Table 11: Linear wear, Wear sector length and volumetric wear results obtained by analysing all the six acetabular liners through CMM method. 136

Table 12: Table displaying the comparison between the results obtained by Gravimetric method and CMM method. 137

Table 13: Tabulated results of the repeatability study for the analysis process of the CMM method. This table displays mean, median range and std. deviation between the results obtained by two individual users. 140

Table 14: Results of the inter-operator variability study for analysis of volumetric wear by the CMM method. This table displays difference in the mean, median, range and std. deviation between the results obtained by two individual users... 141

Table 15: Wear sector, linear wear and volumetric wear obtained from the roundness measurement method. 155

Table 16: Volumetric wear results obtained from RMM method are tabulated against Gravimetric results with difference calculated. 158

Table 17: Results of the inter-operator variability study for analysis of volumetric wear. This table displays difference in the mean, median, range and std. deviation between the results obtained by 2 individual users. 159

Table 18: Tabulated linear wear penetration for all six acetabular liners at each interval determined by through deviation analysis of CMM method. 166

Table 19: Tabulated volumetric wear results of all three intervals. 167

Table 20: Tabulated volumetric wear results obtained by the CMM and the gravimetric method. 168

Table 21: A table displaying the variations between the results obtained from CMM method and gravimetric method for interval 1. 169

Table 22: A table displaying the variations between the results obtained from CMM method and gravimetric method for interval 2. 171

Table 23: A table displaying the variations between the results obtained from CMM method and gravimetric method for interval 3. 172

Table 24: Tabulated volumetric wear results of all liners of cohort C at each interval as measured by the RMM method. 174

Table 25: Tabulated volumetric wear results obtained from the RMM and the gravimetric method. 175

Table 26: A table displaying the variations in the results obtained from the RMM method and the gravimetric method for liners of cohort C at interval 1. 176

Table 27: A table displaying the variations in the results obtained from the RMM method and the gravimetric method for liners of cohort C at interval 2. 178

Table 28: A table displaying the variations in the results obtained from the RMM method and the gravimetric method for liners of cohort C at interval 3. 179

Table 29: Results of the repeatability study conducted on the measurement of the third interval on liner C-6. This table displays the mean, median, range and std. deviation of the obtained results. 181

Table 30: Volumetric wear results of cohort C obtained by the CMM and the RMM method at each interval. 193

Table 31: The given table compares the volumetric wear results of cohort-A as measured by the CMM, the RMM and the Gravimetric methods. 195

List of Figures

Figure 1: Hip Joint. A. Transverse acetabular ligament B. Ligament of the head of the femur. [29]..... 26

Figure 2: Articulating surfaces of the hip joint – pelvic acetabulum and head of the femur [30]. 27

Figure 3: Fibrous membrane and ligaments of the hip joint. A. Fibrous membrane of joint capsule. B. Iliofemoral and Pubofemoral ligaments. C. Ischiofemoral ligament [20]..... 28

Figure 4: Schematic of hip joint locating the hyaline articular cartilage and synovial membrane [34]..... 29

Figure 5: Image displaying a healthy hip (left) and osteoarthritic hip (Right) [43].32

Figure 6: Image displaying comparison between a healthy joint and rheumatoid arthritis affected joint [48]. 34

Figure 7: Surgery details for total hip replacement [53]. 36

Figure 8: Types of hip prostheses. A - Judet, B - Moore, C - Thompson, D - Ring, E - Sivash, F - McKee-Farrar, G - Charnley, H Müller [60] 38

Figure 9: Basic design and assembly of the hip prosthesis and their components [78]..... 43

Figure 10: Image displaying cemented hip prosthesis fixation using PMMA [81]. . 44

Figure 11: CT scan of screw fixated acetabular cup [83]..... 45

Figure 12: Porous uncemented implant displaying bone growth onto the porous surface [81]. 46

Figure 13: Image displaying hip prosthesis with modular femoral head and neck [100]..... 47

Figure 14: An image of metal-on-metal hip resurfacing prosthesis [114]. 50

Figure 15: Acetabular and tibial components fabricated from UHMWPE [127]..... 55

Figure 16: Temporal changes in percentages of each fixation methods used in primary hip replacements in the UK as mentioned in the national joint registry 2017 [74].....58

Figure 17: An image displaying the McMinn prosthesis/Birmingham hip resurfacing system [201].....69

Figure 18: Cross-section image of a ceramic acetabular component displaying the sharp edge generated by grinding and polishing bearing surface [232]. 74

Figure 19: Stripe wear on femoral head (A) and edge wear on acetabular cup liner (B) [153]. 75

Figure 20: Image showing swing phase and stance phase of a single gait [244]...78

Figure 21: An image showing the graph of the ground reaction forces from a walking gait cycle [246].....78

Figure 22: Image displaying a 'Butterfuly diagram' as presented by Pedotti [268]. This diagram represents ground reaction force vector at 10ms intervals [244].....81

Figure 23: Contact force vector F of a patient during nine activities as measured by Bergmann et al. Upper diagrams: Force vector F and direction Ay of F in the frontal plane. Lower diagrams: Force vector F and direction Az of F in the transverse plane [249].....82

Figure 24: Carl Zeiss Prismo Navigator CMM (www.zeiss.com). A modern generation CMM.....85

Figure 25: The first CMM introduced by Ferranti [272]. 87

Figure 26: CMM configuration for a Fixed Bridge type [272].....89

Figure 27: A CMM with fixed bridge configuration [272]. 90

Figure 28: A CMM with cantilever configuration [272]. 91

Figure 29: A horizontal arm-type CMM with dual arm configuration [272].....92

Figure 30: A CMM with gantry-type configuration [272]. 93

Figure 31: The original three dimensional touch trigger probe invented by Sir David McMurtry in 1972 [272]. 96

Figure 32: The above image displays the total points measured on a produced mesh for visualisation of the measurement strategy..... 110

Figure 33: Result of deviation analysis performed between the surface reconstructed by the first experiment and the measured surface. 112

Figure 34: CAD model of a custom made three-sphere fixture. 113

Figure 35: Image displaying the roundness traces as measured on RMM in the bearing area of the acetabular liner 2. Image (A) on the left is the actual roundness trace without elimination of any data and the image (B) on the right is the roundness trace that displays the form of the bearing surface when the wear patch is ignored. 114

Figure 36: Image displaying the roundness traces as measured on RMM of beyond the edge area of the acetabular liner 2. The figure displays the form of the unworn area beyond the edge. 115

Figure 37: Image displaying the roundness traces as measured on RMM at the edge of the acetabular liner 2. Image (A) on the left is the actual roundness trace without elimination of any data and the image (B) on the right is the roundness trace that displays the form at the edge area when the wear patch is ignored. 116

Figure 38: Image displaying two roundness traces of the bearing surface of liner 2 from the unworn cohort measured at different height to study the form of the bearing surface. 118

Figure 39: Image displaying two roundness traces of the surface above the edge of liner 2 from the unworn cohort-B measured at different height to study the form of the surface above edge. 119

Figure 40: Image displaying two roundness traces that made the first and the last contact with the tilted edge at the corresponding height. 120

Figure 41: Schematic explaining the procedure employed to test the coverage angle of the liners from the unworn cohort-B. 122

Figure 42: An image displaying the required geometry to compute the coverage angle. 123

Figure 43: Image displaying the coverage angle assessment of liner 2 from the unworn cohort-B as an example. 124

Figure 44: A flow chart diagram of the updated procedure employed for the reconstruction of the unworn geometry. 127

Figure 45: Grid generated from horizontal and vertical planar sections superimposed on the segmented mesh. 128

Figure 46: A bar graph displaying the results from the deviation analysis performed to test the deviation between the reconstructed surface and measured surface for all six liners of the unworn cohort-B..... 129

Figure 47: Image showing possible measurement error or debris deposit caught on the deviation analysis. (A) Possible debris on the surface. (B) Scanning error. ... 130

Figure 48: Image showing the required grid to reconstruct the unworn geometry. 132

Figure 49: Reference geometry generated from the identified grid to replicate the as manufactured surface. 133

Figure 50: Example of deviation analysis to characterise edge wear and evaluate linear wear penetration. 134

Figure 51: Wear measurement narrowed down from full liner to wear sector in order to limit the errors induced..... 135

Figure 52: Image showing the observed wear distribution extending from the bearing surface to the surface beyond the edge. 136

Figure 53: Image displaying wear at the clamping area on the exterior part of the liner. 138

Figure 54: The image displays a bar graph with standard deviation error bars comparing the results of the CMM method and the Gravimetric method. 138

Figure 55: Bland-Altman Plot with line of equality showing inter-operator variability of the CMM method and regression line stating absence of proportional bias problem. 142

Figure 56: Image displaying a ceramic acetabular liner being measured on a Talyrond 365 (left) with a full picture of the Talyrond 365 (right). 144

Figure 57: Image displays a 3D surface map of liner 4 from the worn cohort-A.. 146

Figure 58: An example of 2D profiles generated from the measured 3D surface of liner 4 from the worn cohort-A in order to determine the linear wear penetration. 147

Figure 59: The displayed image shows four roundness traces at different height of the acetabular liner 4 from the worn cohort-A. The approximate location of these four roundness traces are displayed on the below given surface map in Figure 60. 149

Figure 60: Image displays a 3D surface map of liner 4 from the worn cohort-A and the dotted lines shows an approximate location of four roundness traces displayed in figure 59..... 150

Figure 61: A block diagram displaying the analysis procedure of the RMM method. 151

Figure 62: Image displaying the stitched 110 roundness traces using developed MATLAB script..... 152

Figure 63: Unwrapped and form removed surface of the cup liner in cylinder co-ordinate (MATLAB). 153

Figure 64: Image displaying the proximal surface and wear boundary (MATLAB). 154

Figure 65: Image displaying the edge wear distribution beyond the bearing surface. The dotted line denotes the edge on the worn area of the liner. 156

Figure 66: Image showing wear distribution and linear wear penetration in acetabular liner 4 and liner 6. This data is segmented to focus on the wear patch. 157

Figure 67: Bar graph comparing the volumetric wear results of cohort-A as measured by the RMM method and the Gravimetric method. 158

Figure 68: Bland-Altman Plot with line of equality showing inter-operator variability and regression line stating absence of proportional bias problem..... 161

Figure 69: Image displaying the deviation analysis results of liner 4 at interval - 1 with the colour map..... 165

Figure 70: Image displaying the deviation analysis results of liner 4 at interval - 2 with the colour map..... 165

Figure 71: Image displaying the deviation analysis results of liner 4 at interval - 3 with the colour map..... 166

Figure 72: A bar graph comparing CMM results against Gravimetric results for interval - 1. 169

Figure 73: A bar graph comparing CMM results against Gravimetric results for interval - 2. 170

Figure 74: A bar graph comparing CMM results against Gravimetric results for interval - 3. 172

Figure 75: Image displaying the 3D surface of liner 4 at interval - 1 with the colour map. 173

Figure 76: Image displaying the 3D surface of liner 4 at interval - 2 with the colour map. 174

Figure 77: Image displaying the 3D surface of liner 4 at interval - 3 with the colour map. 174

Figure 78: Bar graph displaying the volumetric wear of liners from cohort-C at interval-1. 176

Figure 79: Bar graph displaying the volumetric wear of liners from cohort-C at interval-2. 178

Figure 80: Bar graph displaying the maximum linear wear and volumetric wear of liners from cohort-C at interval-3. 179

Figure 81: Image displaying the extent of smear effect highlighted after thresholding process [303]. 187

Figure 82: Image displays 3D surface of liner 5 from Cohort C at third interval. . 191

Figure 83: Deviation analysis of liner 5 of cohort C at third interval. 192

Figure 84: Image displays a bar graph that compares volumetric wear results of cohort C obtained by the CMM and the RMM method at interval 1..... 193

Figure 85: Image displays a bar graph that compares volumetric wear results of cohort C obtained by the CMM and the RMM method at interval 2..... 194

Figure 86: Image displays a bar graph that compares volumetric wear results of cohort C obtained by the CMM and the RMM method at interval 3..... 194

Figure 87: A bar graph displaying the volumetric wear results of cohort-A obtained from the CMM, the RMM and the gravimetric method. The dashed blue and orange line denotes the error range of the CMM and the RMM method respectively. 196

Figure 88: Graph displaying volumetric wear result obtained by CMM, RMM and Gravimetric at each interval for liner C-1. 197

Figure 89: Graph displaying volumetric wear result obtained by CMM, RMM and Gravimetric at each interval for liner 2. 198

Figure 90: Graph displaying volumetric wear result obtained by CMM, RMM and Gravimetric at each interval for liner 3. The picture of the liner displays the chipped rim. 199

Figure 91: Graph displaying volumetric wear result obtained by the CMM, the RMM and the Gravimetric at each interval for liner 4. 200

Figure 92: Graph displaying volumetric wear result obtained by the CMM, the RMM and the Gravimetric at each interval for liner 5. 201

Figure 93: Graph displaying volumetric wear result obtained by the CMM, the RMM and the Gravimetric at each interval for liner 6. Picture of the liner displays the chipped rim. 202

Dedications and Acknowledgements

The research presented in this thesis has been carried out at the Centre for Precision Technologies, Department of Computing & Engineering at the University of Huddersfield.

This thesis spans several years of work with testing and measurement methods development at the University of Huddersfield and many people have been involved and contributed to the presented ideas and understanding gained. The author acknowledges his debt to those who have helped along the way and influenced the understanding of, and the approach to, development of a measurement methodology as presented in this thesis.

In particular, I wish to express my gratitude to my supervisors, Dr. Paul Bills and Dr. Radu Racasan for their continued encouragement, guidance and invaluable suggestions during this work. In this I would also like to include my gratitude to my colleagues Dr. Luca Pagani, Dr. Andrew Townsend, Dr. Katie Adinall and Chris Dawson who provided support for this research along the way. Furthermore I am deeply indebted to rest of my colleagues at the Future Metrology Hub. Gratitude goes to the Future Metrology Hub and the University of Huddersfield who have financially supported this work.

Finally I want to thank my family, specially my grand-father who has always been a source of great inspiration and motivation. The encouragement and support from my parents and my friend Ketki Mistry has been invaluable and to them I give my sincere and heartfelt thanks.

Chapter 1. Introduction

The modern total hip replacement (THR) prosthesis was introduced in the 1960s and is rightly known to be one of the major medical revolutions of the 20th century, especially in treating chronic arthritis in elderly patients [20, 21]. The most common cause for THR surgery is severe pain and immobility which is a direct consequence of osteoarthritis. Osteoarthritis was predominant in 93% of the cases and there were 708,311 primary total hip replacements recorded in the UK itself during the 11 years period lasting from 2003 to 2014 [22].

THR prosthesis have been around for many decades. Traditionally in total hip joint replacement, the joint bearing pair would consist of a metallic femoral head articulating against Ultra High Molecular Weight Polyethylene (UHMWPE) acetabular liner component. Such bearings were termed as metal-on-polyethylene (MoP) bearings. However, the prosthesis design and technique is continuously evolving with the aim of improving patient's performance and longevity. The orthopaedic industry devotes an enormous amount of time and money to improve the design and performance of THR prostheses. Bearing surface play an important role in the performance of replacement prostheses and hence some of the major changes to improve hip prostheses performance include alternate bearings such as Metal-on-Metal (MoM), Ceramic-on-Ceramic (CoC) or Ceramic-on-Polyethylene (CoP) to minimise wear [23], as well as increasing size of femoral head to provide greater motion range and enhanced joint stability [24]. Other than that, various patient and surgical factors have been recognised that can lead to implant failure which now are taken into consideration in preclinical evaluation and implant design [25].

During the first five decades of THR, the principal long-term complication of metal-on-polyethylene was implant loosening owing to particle-induced osteolysis engendered mainly by polyethylene wear debris [26]. Similarly, in Metal-on-Metal devices concerns were raised associated

with the long-term biological reactions caused by metallic wear debris. Hence, attempts have been made to avoid biological complications such as osteolysis associated with conventional polyethylene particles induced by wear debris and also release of metal ions induced by metallic wear debris. With various reports of osteolysis and metallosis associated with wear debris from conventional Metal-on-Polyethylene and Metal-on-Metal articulations [27-38], the interest in Ceramic-on-Ceramic hip prosthesis was elevated. This is because ceramics are chemically inert and they possess all other qualities that are required from a bio-compatible material. The 4th generation ceramic-on-ceramic THR prosthesis has comparatively smaller wear volumes and hence is driven by an increasing demand on the longevity of joint replacement devices for young and more active patients.

The 4th generation ceramic-on-ceramic bearings produce twenty to eighty times lower wear rates as compared to recent crosslinked UHMWPE-on-metal bearing surface [39]. A study conducted by Tipper et al. [40] displayed a striking difference in the size of wear particles of UHMWPE (range: 100-50,000 nm) against the size of ceramic wear particles (range: 9-66 nm). Hence even though ceramic bearings have low wear rate, they produce considerable amount of wear particles. In ceramic-on-ceramic bearings, most of the wear occurs at the edge through edge-wear and hence is it essential to measure edge-wear. The current literature to test the ceramic-on-ceramic wear rate is limited to in-vitro testing and determining the wear volume through the gravimetric method [19]. However, the gravimetric method lack spatial characterization of wear extent and its location [16]. Due to the considerable challenge in geometrical characterization of edge wear, current literature regarding the assessment of edge-wear in acetabular cup liners has been confined to in-vitro simulator studies and gravimetric measurement to assess wear volumes. Geometric characterisation of wear is essential in determining the contact conditions during gait and subsequent calculation of point and magnitude of the maximum stress condition. It is, therefore, vital

that a robust and reliable method for geometric measurement and analysis of edge wear is created.

Previous methods used to analyse wear at the interface between the femoral head and the acetabular liner have solely been focused on the measurement of the bearing surface [17, 18, 41-43]. The main limitation of these methods was that wear could only be estimated on the well-defined spherical geometry of bearing surface. In the case of acetabular liner these methods aimed to identify the edge of the bearing surface and exclude the outer bearing surface geometry by thresholding it from the analysis. In some cases this area was not even included in the measurement process or was removed during the analysis.

This study details two novel geometric methods which are aimed to measure and analyse the bearing surface as well as the surface above it in order to characterise edge-wear in ceramic-on-ceramic acetabular liners and assess the wear volume.

1.1 Aim & Objectives

The aim of this study is to develop a reliable wear measurement method to characterise and quantify volumetric edge wear in ceramic-on-ceramic acetabular liners of total hip arthroplasty devices through the use of metrological techniques. The developed method should be appropriate to assess volumes of material loss in retrieved ceramic-on-ceramic hip arthroplasty devices.

This thesis comprises of various objectives in order to fulfil the above aim, detailed as follow:

i. Ceramic material was studied as a bio-material for the use of hip arthroplasty devices and the material properties of ceramic were compared against the other existing bio-materials employed to manufacture hip prostheses. Formation of edge wear in ceramic-on-

ceramic acetabular liner was investigated by studying simulator tests with edge loading conditions.

ii. The existing gravimetric method, the CMM method and the profilometry measurement method were studied in order to understand the current state-of-the-art of the wear measurement techniques employed to assess edge wear in acetabular liners of hip arthroplasty devices.

iii. Measurement and analysis test were performed to develop a novel CMM method that can characterise and quantify volumetric wear rate in and beyond the bearing surface of ceramic-on-ceramic liners of the total hip replacement device. Various tests were performed to characterise edge wear, including coverage angle test and profilometer traces to explore the bearing surface and surface beyond the edge.

iv. An analysis method was developed to reconstruct a digital geometry of the unworn surface. A Surface reconstruction test was conducted on the acetabular liners from cohort-B (a cohort of six off the shelf unworn liners) to test the robustness of the surface reconstruction process employed to regenerate a digital unworn surface. Linear deviation and variation in volume between the measured surface and reconstructed geometry were studied.

v. Measurement and analysis test were performed to develop a novel RMM method that can characterise and quantify volumetric wear rate in and beyond the bearing surface of ceramic-on-ceramic liners of the total hip replacement device.

vi. In order to validate the performance of the developed CMM and RMM method, both the methods were applied on the liners of cohort-A (a cohort of six edge wear simulated liners) and the results were compared against the results of the gold standard gravimetric method to test the agreement. The volumetric assessment by the CMM method and the RMM method was conducted blindly without any pre-wear data for the method to be suitable for measuring retrieved implants.

vii. A case study was performed which again utilised cohort-C (six acetabular liners) on which edge wear was simulated at three intervals to trace the progressing wear using both of the developed methods. This study was also conducted blindly without using any pre-wear data.

Both case studies have given various insights regarding the possibility of employing the developed metrological methods for edge wear measurement.

1.2 List of Publications

- Kapadia, D., Racasan, R., Pagani, L., Al-Hajjar, M., & Bills, P. (2018). Methods for Characterization of Edge Wear in Ceramic-on-Ceramic Acetabular Cups. In Beyond the Implant: Retrieval Analysis Methods for Implant Surveillance. ASTM International.

- Kapadia, D., Racasan, R., Pagani, L., Al-Hajjar, M., & Bills, P. (2017). Method for volumetric assessment of edge-wear in ceramic-on-ceramic acetabular liners. Wear, 376, 236-242.

- Kapadia, D., Racasan, R., Al-Hajjar, M., & Bills, P. (2017, February). CHARACTERISING AND QUANTIFYING EDGE WEAR IN CERAMIC-ON-CERAMIC ACETABULAR CUPS. In Orthopaedic Proceedings (Vol. 99, No. SUPP_4, pp. 50-50). The British Editorial Society of Bone & Joint Surgery.

- Kapadia, Darshil, Racasan, Radu, Al-Hajjar, Mazen and Bills, Paul J. (2016) *Characterizing edge-wear in ceramic-on-ceramic acetabular cups.* In: International Society for Technology in Arthroplasty (ISTA) 29th Annual Congress, October 5-8 2016, Boston, MA, USA.

Chapter 2. Literature Review

2.1 Summary

This chapter details information required by the reader to understand the development and the importance of the methods. The chapter details the basic information regarding the natural hip joint and THR devices, history and surgeries. The chapter informs reader about the state-of-the-art bio-materials and wear measurement techniques.

2.2 Natural Hip Joint

2.2.1 Introduction

The hip joint is a synovial coupling of the femoral head and acetabulum of pelvic bone that connects the lower limb to the pelvic girdle. The hip joint (Figure 1) is a multi-axial ball and socket joint with the purpose to bear weight and provide stability rather than large range of movements [44]. The stability of the hip joint is determined by the strength of the joint capsule, the shape of the articular surface, ligaments and muscles. The hip joint is one of the most important joints in the human body as it provides humans with the ability to walk, run and jump while it endures the weight of the human body. It is one of the most flexible joints and provides a wider range of motion in comparison to all other synovial joints in the human body other than the shoulder joint.

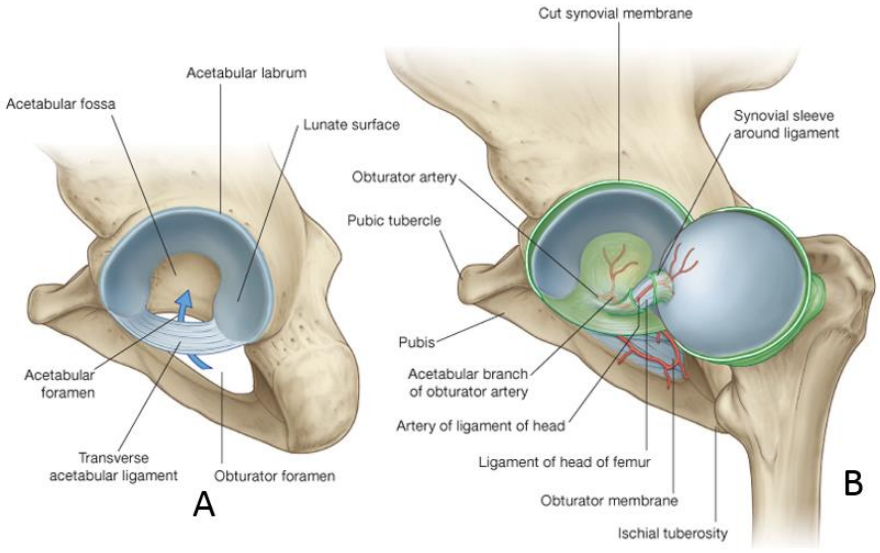

Figure 1: Hip Joint. A. Transverse acetabular ligament B. Ligament of the head of the femur. [44]

2.2.2 Bones & Cartilage

The articular surface of the hip joint consists of the acetabulum of the pelvis and the spherical head of the femur where the acetabulum allows the head of the femur to articulate in a ball and socket formation Fig 2. The acetabulum almost entirely surrounds the spherical head of the femur and provides joint stability. The articulating surface of both, acetabulum and head of the femur is covered by a layer of hyaline cartilage which acts to lubricate joint with synovial fluid. The head of the femur is completely covered by hyaline cartilage except for a tiny area known as fovea where the ligaments are attached to the acetabulum. The non-articular part of the acetabulum known as acetabular fossa gives attachment for the ligament of the head of the femur. A fibro-cartilaginous collar, known as the acetabular labrum, is raised slightly to grip the head of the femur and secure it in the joint [44].

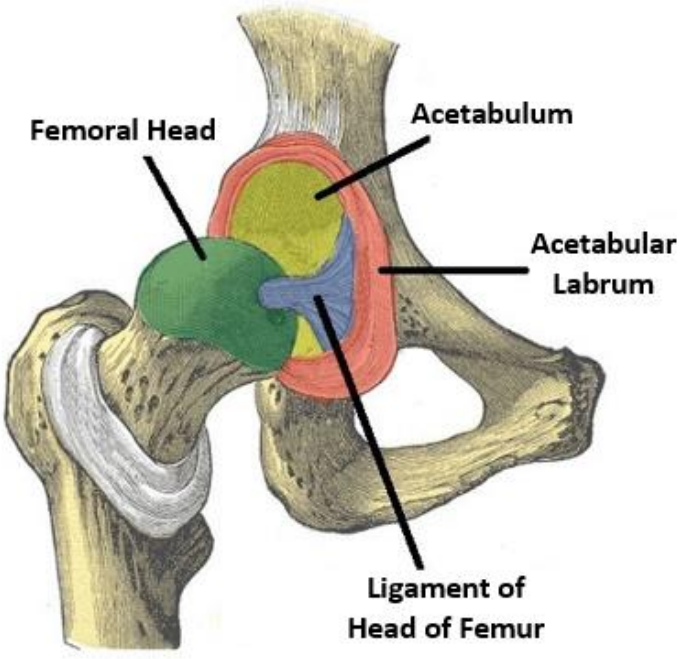

Figure 2: Articulating surfaces of the hip joint – pelvic acetabulum and head of the femur [45].

2.2.3 Ligaments

There are three ligaments that reinforce the outer surface of the fibrous membrane and provide stability to the hip joint. These three ligaments are known as iliofemoral, pubofemoral and ischiofemoral ligaments and can be seen in below given Figure 3. The iliofemoral ligament is on the anterior side of the hip joint and attaches the femur to the pelvis. The iliofemoral ligament is considered to the strongest ligament in the human body due to its capability to withstand the hyper-extention forces. The pubofemoral ligament is anteroinferior to the hip joint and fastens across the front of the joint from the pubis bone of the pelvis to the femur. Pubofemoral ligament is positioned such that it reinforces the hip joint capsule and can blend with the fibrous membrane and the deeper surface of the iliofemoral ligament. These two anterior ligaments can be seen in Figure 3-B. The posterior of the hip joint capsule is fortified by the ischio-femoral ligament that is attached from the ischium (acetabular rim) to the femur [44].

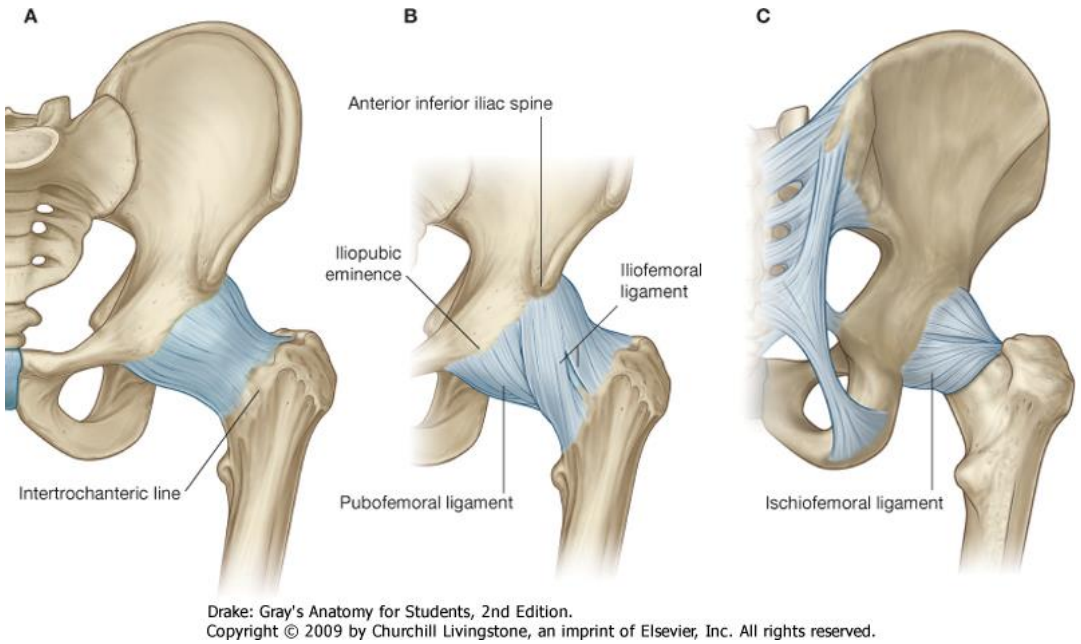

Figure 3: Fibrous membrane and ligaments of the hip joint. A. Fibrous membrane of joint capsule. B. Iliofemoral and Pubofemoral ligaments. C. Ischiofemoral ligament [20].

2.2.4 Lubrication

The articulating surface of both the acetabulum and the head of the femur, is covered with the load bearing hyaline cartilage as seen in Figure 4. For such a hyaline cartilage-covered articular joint, lubrication of the cartilaginous, bony, ligament like structures is provided by a synovial fluid generated from a specific layer of cells located at the surface of a delicate tissue called the synovial membrane or synovium [46]. The synovial membrane has been referred to as "controlling the environment of the joint" [47] as it participates in immune reactions to bacteria, detritus material (debris) removal, lubrication and cartilage nutrition [48].

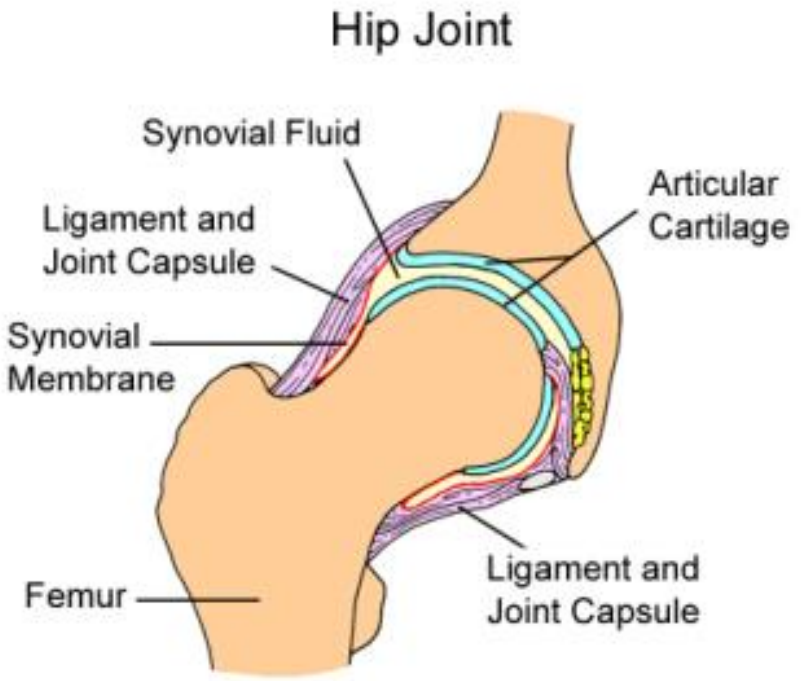

Figure 4: Schematic of hip joint locating the hyaline articular cartilage and synovial membrane [49].

The synovial fluid, also known as synovia, is an aqueous electrolyte solution containing, for example, lipids, proteins, hyaluronan (Hyaluronic acid) and phospholipids [50]. From a rheological perspective, synovial fluid is non-newtonian fluid that exhibits reduction in viscosity with an increase in shear rate. Due to the exceptional tribological properties of cartilage and synovial fluid the coefficient of friction ranges from 0.002 to 0.006 and wear is almost zero under normal biological conditions [51].

For many years, the mechanical performance of lubrication in natural hip-joint has been an issue of debate. While effortless articulation of the interfaces between numerous soft tissues indicates a universal lubrication system *in vivo*, it is the high load bearing of certain joints that really puts any theory to the test [52]. It is known that hip joints usually exhibit low friction and wear for an entire lifetime as they hold remarkable lubricating properties. Recently, the most common theory of natural hip-joint lubrication consists of a combination of lubrication mechanisms where the predominance of one over other depends on normal load and sliding velocity conditions. The swing phase

of the dynamic walking cycle, which is for example when the foot is not in contact with the ground and the exerted load is low and the sliding velocity is high, is thought to be dominated by the fluid-film lubrication mode. However, under heavy static loading, or once the foot comes in contact with the ground, mixed and boundary lubrication takes over [53, 54].

The friction forces in the hydrodynamic lubrication or fluid film lubrication systems are actually hydrodynamic drag forces generated at the solid-liquid interface instead of the just the outcome of mechanical or physical interactions against shearing surfaces. Wear is prevented or reduced in fluid film lubrication through disjoining hydrodynamic pressures created due to the flow of the restricted lubricant fluid film that endures the general loading pressure and separates the shearing surfaces or decrease the speed in order to limit the interaction between them. Hence, fluid film lubrication is commonly regarded as the most efficient lubrication system due to its ability to minimize friction forces and surface wear.

The fluid properties such as dynamic rheological behaviour, viscosity, and fluid film thickness when restricted between shearing surfaces plays a major role in the system by reducing the friction and wear to such an extent that the articulating surfaces and their properties have little to no influence on the performance of the system. However, the nature of biological surfaces that have low elastic modulus and complex morphologies can cause fairly large deformations through moderate stresses that can significantly affect the fluid film lubrication process. It is important to understand not only the dynamic and physical properties of the solid surface and lubricant fluid but also how these properties affect the solid-liquid interactions in order to understand the mechanism of fluid film lubrication functioning in the biological systems and how the process is naturally controlled and regulated.

There is still ongoing debate as to what the predominating lubrication regime is in synovial joints and it largely depends on the loading conditions and at which stage in a motion cycle the joint is at, but moreover it depends on the individual joint, its geometric properties and the general health of the

articulating surfaces and differing figures have been quoted for the coefficient of friction of human cartilage.

2.3 Disorders in joint

2.3.1 Introduction

There are a number of different causes of failure in a natural joint, which ultimately require joint replacement surgery to restore joint functionality and alleviate the pain. The most common diseases that affects and degenerate the natural joints to the point where joint replacement surgery becomes crucial are osteoarthritis and rheumatoid arthritis. Both the diseases are indicated by inflammation in the joint and failure in function with severe pain.

2.3.2 Osteoarthritis

Osteoarthritis is a degenerative joint disease recognised as the breakdown of articular hyaline cartilage particularly in weight bearing joints like hips, knees, spine, and ankles. The degradation of cartilage tissue is reliant upon loss of the amorphous portion of the matrix and the collagen structure that consequently cause either a local lesion or a form of erosion which subsequently result in deterioration of articular hyaline cartilage lining. Such occurrence can be a result of infection, joint disease or direct or indirect trauma to the articular hyaline cartilage [55]. The deterioration of such tissue will cause the bones to grind against each other in the joint that leads to pain and reduction in mobility [56, 57]. In severe cases the patient is unable to walk due to lack of movement in the joint.

Figure 5: Image displaying a healthy hip (left) and osteoarthritic hip (Right) [58].

Osteoarthritis is globally recognised as the most common form of arthritis disease that affects approximately 10% of men and 18% of women over 60 years of age [59]. The risks are greater among individuals who are categorized as obese [60]. The cause of arthritis is not only related to age and obesity, but it can also be caused due to high stresses in the joint attributable to wide range of sport activities [57]. Presently, osteoarthritis is one of the most commonly diagnosed diseases in general practice, with its occurrence expected to increase two times by the year 2020 mainly cause of an ageing population and an ever-increasing influence of obesity [58, 60]. Table 1 below displays the occurrence of radiographic osteoarthritis observed in the hip of males and females of different age range.

Age	Sex	Prevalence
<55	Men	1%
	Women	1%
55-65	Men	3%
	Women	2%
>65	Men	6%
	Women	4%

Table 1: Prevalence of radiographic osteoarthritis in the hip [61].

The early symptoms of osteoarthritis detectable from the articular surface are surrounding areas of fibrillation of the superficial layers of cartilage. With progress of the disease, more surface is involved and the tiny defects deepen further in the gaps. Eventually fissures reach the bone and tears the material from the fibrillated cartilage tips. Progressively the cartilage is lost leaving exposed bone.

2.3.3 Rheumatoid Arthritis

Rheumatoid arthritis is a chronic inflammatory joint disorder that often causes destruction to cartilage and damage bone leading to disability in patients [62]. It is characterised by systemic inflammation and persistent synovitis [63]. Rheumatoid arthritis was first recognised in the 19th century and became eminent in the 20th century. The name 'rhuematoid arthritis' was first introduced in 1850s, however classification criteria have only been defined 50 years ago. A comparison between a healthy and a Rheumatoid arthritis affected joint can be seen below in Figure 6.

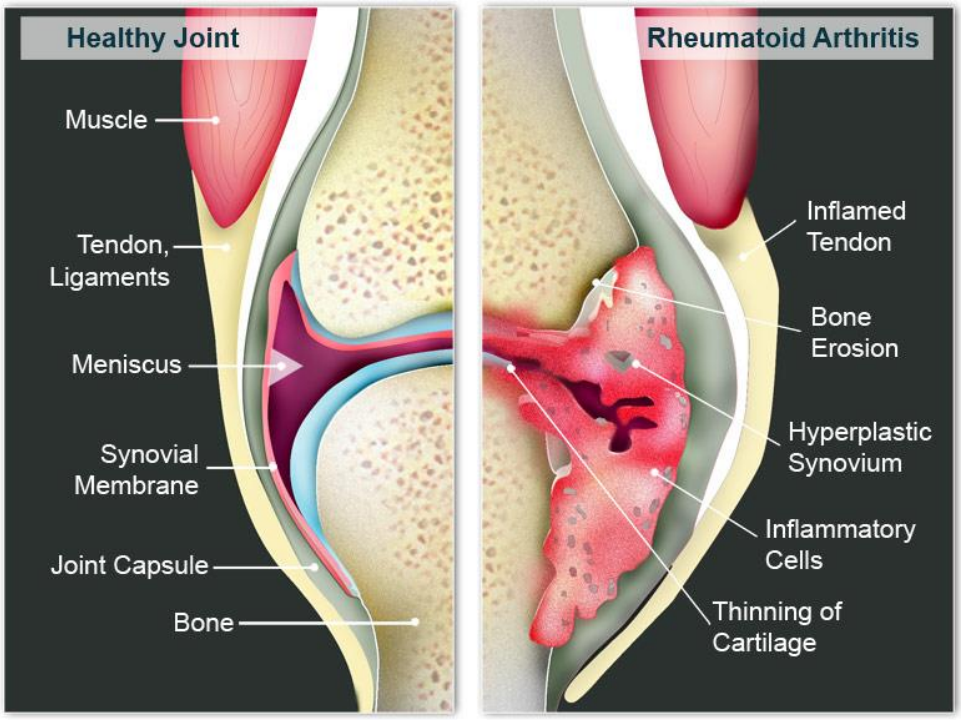

Figure 6: Image displaying comparison between a healthy joint and rheumatoid arthritis affected joint [63].

The initial cause of rheumatoid arthritis is not yet well-understood due to which the early diagnosis of rheumatoid arthritis is limited and challenging to identify. However it is commonly observed that immunity plays an important role in rheumatoid arthritis development and chronicity. Rheumatoid arthritis is usually triggered as inflammation in the synovial membrane, known as synovitis, which eventually progresses to erosion of bone and proliferation of the synovial fluid and the connective tissue [57]. Such active and uncontrolled rheumatoid arthritis often leads to damage to the joint, disability, decreased life quality, and cardiovascular and other comorbidities [63].

Through population-based studies it is observed that rheumatoid arthritis affects 0.5-1% of adults in developed countries and the disorder is most common in women and elderly people [63]. Symmons *et al.* estimated the prevalence of rheumatoid arthritis by mailing a screening questionnaire to 7050 individuals out of which 82% responded. The study estimated the occurrence of rheumatoid arthritis to be more than 1.16% in women and

0.44% in men among the population of the UK. The disorder is more frequent by three times in women compared to men. The frequency increases with age and is highest in women older than 65 years [64]. Incidence of rheumatoid arthritis varies geographically, and is observed to be more frequent in northern Europe and North America compared to other developing parts of the world such as rural west Africa [65, 66]. Genetic factors are attributable for 50% of the risk of developing rheumatoid arthritis [63]. Smoking is the primary environmental risk that increases the threat of developing rheumatoid arthritis by two times [67].

2.4 Total Hip Replacement

2.4.1 Introduction

A total hip replacement is a surgical procedure where the unhealthy or trauma affected cartilage and articulating femoral head of the hip joint is surgically removed and replaced with an artificial hip prosthesis fabricated from various man-made materials. Total hip replacement surgery allows a suffering patient with affected hips to regain the normal functions of the hip joint. Total hip replacement is one of the most appreciated developments in the history of orthopaedics. There are various types of modern total hip replacement, varying in shape, size of the femoral head, bearing materials and fixation method, although the basic design of the components essentially does not differ from the components implanted 40 years ago. The normal hip joint is a ball and socket articular joint, where the acetabulum acts as a socket and femoral head acts as a ball and articulates in the acetabulum.

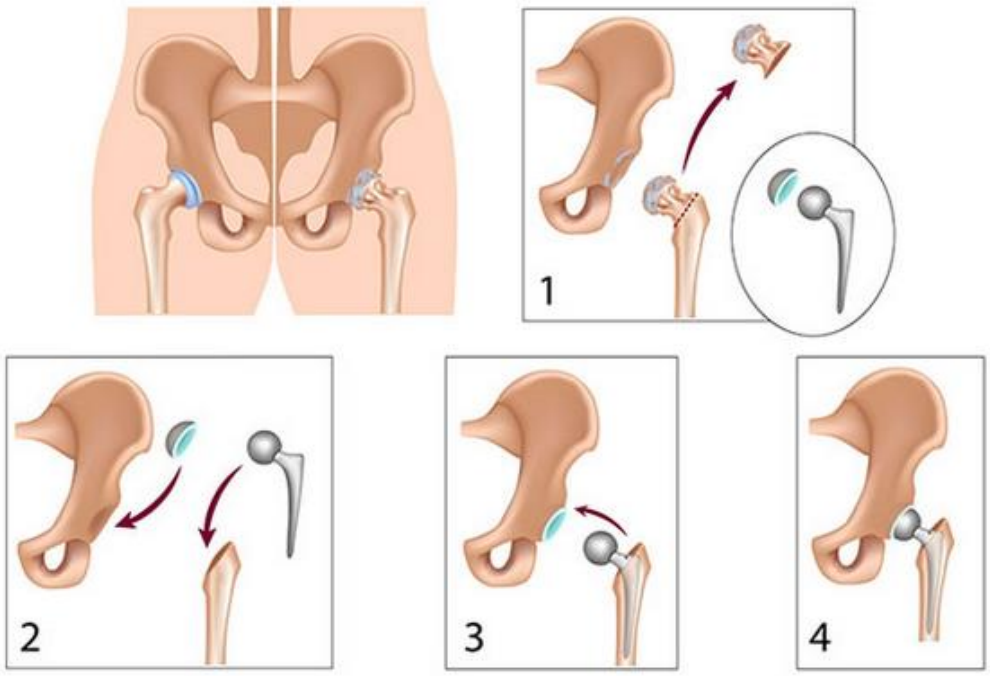

Figure 7: Surgery details for total hip replacement [68].

In total hip replacement surgery, the spherical head of the femur is removed and replaced by a femoral head. This femoral head sits on the femoral stem's neck and the stem is inserted into the medullary canal of the femur bone. The stem is secured in the canal using PMMA bone cement or porous coating on stem which allows bone growth. A hemispherical acetabular cup is fixed in to the acetabulum of the pelvis which allows the femoral head to articulate against it. There are other fixation methods which are discussed in detail in sub-section 2.3.4.2. The above Figure 7 represents a very basic surgical procedure and components position.

2.4.2 History

The total hip replacement procedure was first developed in 1938 by Philip Wiles who used femoral and acetabular components, fabricated from stainless steel. The cup was screwed in the acetabulum, the head was secured on to the neck of the femoral stem using a bolt and the stem was inserted in the femur [55]. Clinical results for this development remains unknown because of the interference of world war II [57]. In 1951, Haboush (US) and

McKee and Watson-Farrar (UK) introduced metal-on-metal implants [69, 70]. Other subsequent designs by Ring [71] in 1964, Müller in 1965 [72], endured failure rates as high as 50 percent caused mostly due to implant loosening and high wear of prosthesis components caused by high frictional torque [57, 73]. In early times, due to lack of machining technology the manufactured bearing surfaces could not meet the required tolerances. This resulted in equatorial bearing pair that made contact over a large portion of the bearing surface producing large torque due to friction. By decreasing the congruency of the bearing surfaces, a polar bearing is produced which decreases the frictional torques yet increases the contact stresses. Ring introduced a hip prosthesis design with a diametric clearance of approximately 0.5 mm between the femoral head and acetabular component [74]. These prostheses exhibited significantly reduced frictional torque [73, 74]. However, many of these hip prostheses proved to be a failure due to poor choice of materials and inappropriate bearing design. Stainless steel metal-on-metal hip prostheses exhibited very high wear of the bearing surface, high friction and corrosion [74]. Figure 8 displays some of the early prostheses.

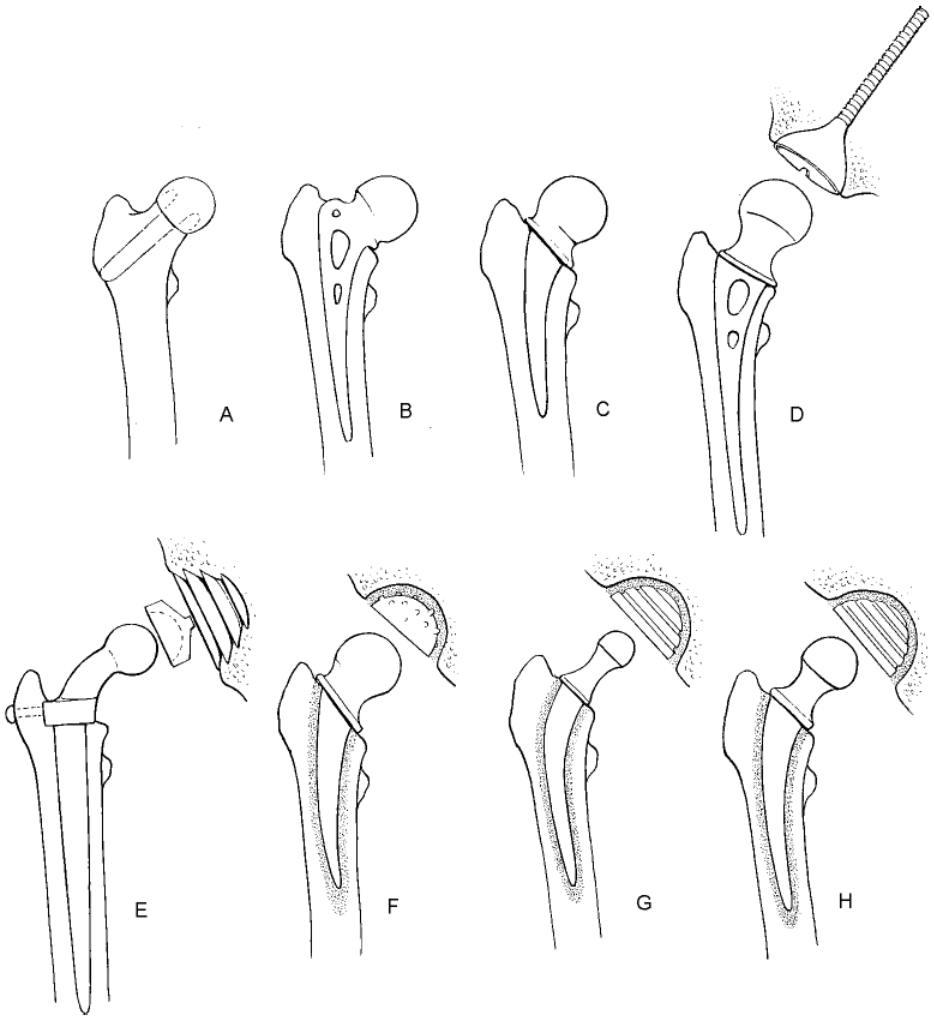

Figure 8: Types of hip prostheses. A - Judet, B - Moore, C - Thompson, D - Ring, E - Sivash, F - McKee-Farrar, G - Charnley, H Müller [75]

The modern total joint replacement was introduced in 1958 by Sir John Charnley by using the first ever metal-on-polymer hip prosthesis. The initial bearing materials chosen by Charnley were Polytetrafluoroethylene (PTFE) acetabular cup articulating against stainless steel femoral head, however it was observed that PTFE suffered from excessive wear and could only survive for two years [76, 77]. Later on in 1961, Charnley's research into the lubrication of animal joints led him to improvise the hip prosthesis by using Ultra-High Molecular Weight Polyethylene (UHMWPE) instead of PTFE as an acetabular component to reduce the interfacial friction against stainless steel femoral head. These metal-on-UHMWPE hip prostheses were termed as 'Low frictional Arthroplasty' (LFA). Charnley established surgical techniques,

instrumentation and procedures for total hip replacement surgery. Charnley's LFA hip prostheses have exhibited 20 years survival rates in 94% of the implanted hip prostheses. Such clinical results from these LFA hip prostheses encouraged Charnley's work worldwide and this bearing surface is still being widely used in cemented total hip replacement for less active elderly patients [78]. Eventually in 1980s and 1990s aseptic loosening and osteolysis were recognised as the major problems to limit the longevity of implanted hip prostheses. It was also found that the UHMWPE debris caused by the bearing surface were the major culprit leading to osteolysis. Hence the need arose for harder and more wear resistant materials.

In the early 1980s observations were made that several number of metal-on-metal hip prostheses from the post-1968 era were operating well and no radiological evidence of osteolysis was found in them. In 1985, six Huggler and eleven Müller metal-on-metal retrieved implants were analysed by Semlitsch *et al*. [79]. Except for one retrieved prosthesis, all had a clearance in diameter ranging from 0.12mm to 0.2mm. The average liner wear rate was 2.5–5 mm/year for a femoral head of 42 mm diameter except for one of the Huggler hip prostheses that exhibited excessive clearance. This linear wear rate was almost 40 times less compared to Muller's metal-on-polyethylene retrievals with 32mm head diameter. Such a low wear rate was also confirmed by other researchers [80, 81]. Hence, eventually in the late 1980s, parallel to the ongoing progress in traditional hard-on-UHMWPE bearings the possibility of using hard-on-hard bearing had gained attention [74]. The interest in Metal-on-metal bearings escalated after recognising the long-term survivorship and high wear resistance of such hard-on-hard prosthesis. Improvement in the outcome of metal-on-metal prostheses were expected through better manufacturing technologies by achieving enhanced tolerances and smoother surface finish.

In the early 1970s, the first ceramic-on-ceramic (CoC) total hip replacement prosthesis was developed by Boutin (France) [82]. Ceramic-on-ceramic hip prostheses were widely used in Europe as ceramics are highly

inert materials and possess highly smooth surface finish and exceptional resistance to wear [83]. Despite displaying such great properties, there still remained a threat of incidental fracture [84] with reported component fracture rates as high as 13% for ceramics manufactured before 1990 [85]. The fracture rates of femoral heads was reported to be 0.026% for first generation alumina ceramic, 0.014% for second-generation zirconia ceramic and 0.004% for ceramics manufactured after 1994 [86]. The third generation ceramic introduced as Biolox® Forte (CeramTec, AG, Plochigen, Germany) displayed continued improvement in manufacturing techniques and created a purer and denser ceramic, yet the third-generation was vulnerable particularly to the rim fractures [87]. The latest fourth-generation ceramics BIOLOX® Delta (CeramTec, AG, Plochigen, Germany) have displayed further advancement by limiting crack propagation with improved hardness, toughness and wear resistance [87].

In early 2000s, Firkins *et al.* introduced a low wearing differential hardness ceramic-on-metal (CoM) bearing combination. According to the basic law of wear, wear rate is inversely proportional to the hardness of the bearing surface material. Hence metal-on-metal and ceramic-on-ceramic, due to their hardness, have considerably lower wear rates compared to that of polyethylene. Recently, it has also been observed that the use of dissimilar material of the bearing couples gives lower wear rate compared to that of bearing couples manufactured from the same material. The reason for this reduced wear rate is the due to the reduction in adhesive wear and also due to harder surface remaining unworn and smooth [88]. CoM hip joint combination includes a ceramic head that articulates against cobalt chrome (CoCrMo) liner. An *in vitro* hip simulator study conducted by Firkins *et al.* in 2001 concluded that CoM bearing provides improvised wear performance [88]. The smooth surface of the ceramic benefits from the reduced abrasive wear on the metallic liner. It also reduces the hazard of liner fractures which are often observed in CoC bearings and reduces level of ion concentrations as compared to MoM bearings.

2.4.3 Failure of Total Hip Replacement

The life of a hip arthroplasty device is commonly expected to be 15-20 years. In the UK itself during the last 10 years 711,765 primary surgeries have been carried out compared to 80,042 revision procedures [22] to replace joints that have either faced premature failure or failed at the end of their useful life. However, even with such great success of total hip replacements several failure has been reported. Various complications like osteolysis and loosening, metallosis, impingement, dislocation, leg length discrepancy, adverse soft tissue reactions and pseudo-tumours have led to the revision of hip prostheses [1].

A common definition of failure in total hip replacement is the state when the implant requires revision or removal of one or both components. There are various other ways to define failure in total hip replacement. The performance of total hip replacement is also indicated by the use of an Oxford hip score. The Oxford hip score is determined by the feedback to a set questionnaire given by both, the patient and the clinician. A drop in this Oxford hip score below a set threshold suggests failure [89]. Another way to define failure is through radiographic assessment where hip prosthesis are scanned under X-ray and changes are measured.

Hip prosthesis failure can be divided into two category - septic and aseptic. Septic failure of the joint is attributable to infection in the tissue surrounding the joint which can occur during surgery or shortly after surgery. However infection rates have been greatly reduced after the introduction of clean air operation theatres and antibiotics [90, 91] and currently accounts for 3.5% of revision in the UK from 1st April 2013 to 31st December 2016 [1]. Aseptic loosening occurs due to mechanical failure of one or more components of hip prosthesis. Aseptic loosening is the most common source of failure in total hip replacement and is cited in 75.6% of all revision surgery in the UK from 1st April 2013 to 31st December 2016 [1]. Aseptic loosening is the result of wear in components of hip prosthesis and such wear releases wear debris in local enviornment. Wear can occur at any interface of the hip prosthesis,

however, most of the wear occurs at the bearing surface. Prosthesis wear releases wear debris in the environment surrounding the prosthesis. This wear debris is known to cause adverse cellular reaction which causes biological loosening of the prosthesis [28].

In addition to these common causes there are other various reasons for implant failure such as pain, deep infection, mal-position of implant or technical error during surgery, dislocation of the prosthesis, impingement between femoral head and acetabular cup of hip prosthesis, squeaking of prostheses [1].

2.4.4 Hip Prosthesis Design

2.4.4.1 Basic Design

There are various types of hips prosthesis available on the market, however the basic design remains unchanged. The femoral component of the hip prosthesis consists of an intramedullary stem, a neck and an articulating head. The stem provides stability and transfers load to the femur. The neck of the prosthesis is designed to be at particular angle with the stem and of a length to replicate the mechanics of a natural hip joint. The acetabular component is hemispherical cup and the femoral head is spherical ball and together they make a bearing surface and hence both the surface are highly polished for the smooth articulation. The below given Figure 9 displays the basic assembly and design of the hip prosthesis.

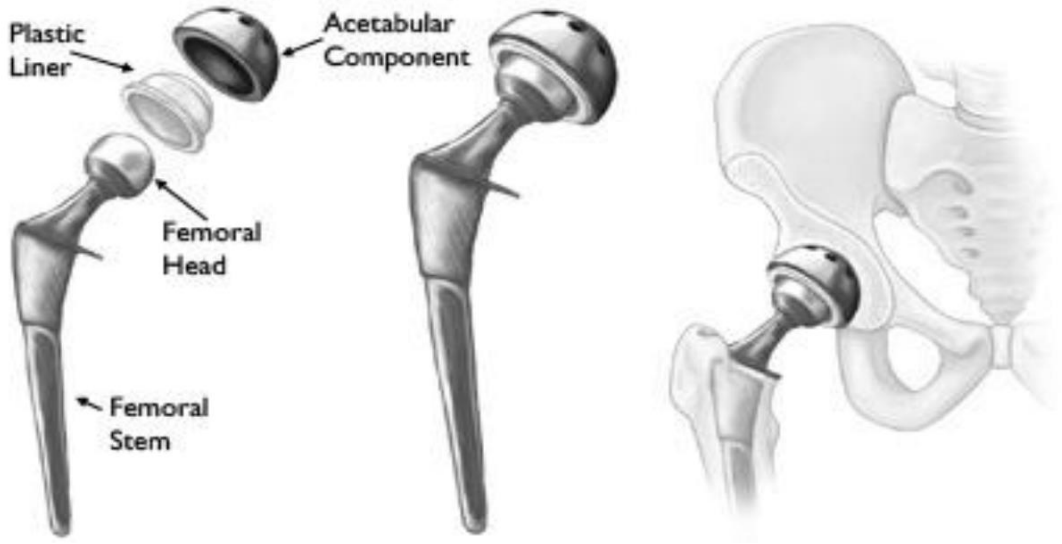

Figure 9: Basic design and assembly of the hip prosthesis and their components [92].

2.4.4.2 Modes of fixation

The mechanical stability of the hip prosthesis in the body relies upon the method by which the prosthesis are attached to bone. Loose prostheses are observed to induce pain to patients and revision surgery becomes essential, which is why the establishment and maintenance of fixation are important. The three known methods of fixation include the use of Polymethylmethacrylate (PMMA) bone cement, osseointegration and screw threads.

For cemented prosthesis, PMMA is utilised for fixation of both femoral stem and acetabular cup by pressurisation as seen in Figure 10. PMMA cement is not a glue but a grout and works on the principle of mechanical interlock rather than adhesion [20]. Hence pressurisation is required to drive the cement into the narrow spaces between the bone and prosthesis. It is comparatively easy to obtain pressurisation inside the femoral canal. Pressurisation techniques for acetabular have also been researched [93], however acetabular pressurisation is more challenging. PMMA is a low strength and brittle material hence to prevent fracture in bone cement it is essential to use sufficient thickness of bone cement [94].

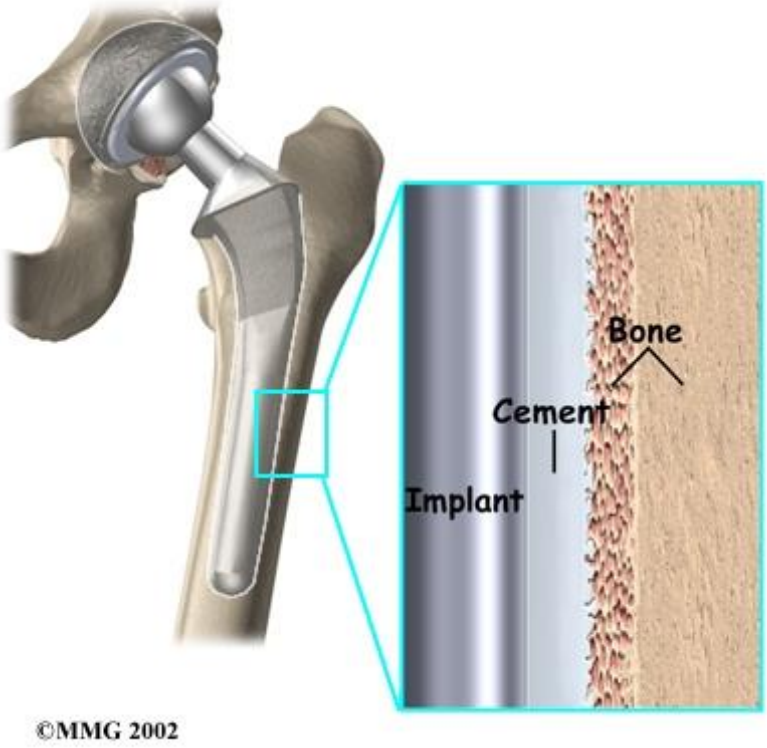

Figure 10: Image displaying cemented hip prosthesis fixation using PMMA [95].

Threaded screws have also been used for acetabular fixation as displayed in Figure 11. A few acetabular designs have used screw threads on their external surface. Such methods have displayed good short-term results in combination with bone ingrowth fixation, however for long-term results the failure rates are much higher [96]. Bone being a visco-elastic material will eventually loosen itself from the stress that a screw thread initially places on the bone, hence why it can be presumed that screw fixation provides only short term stability.

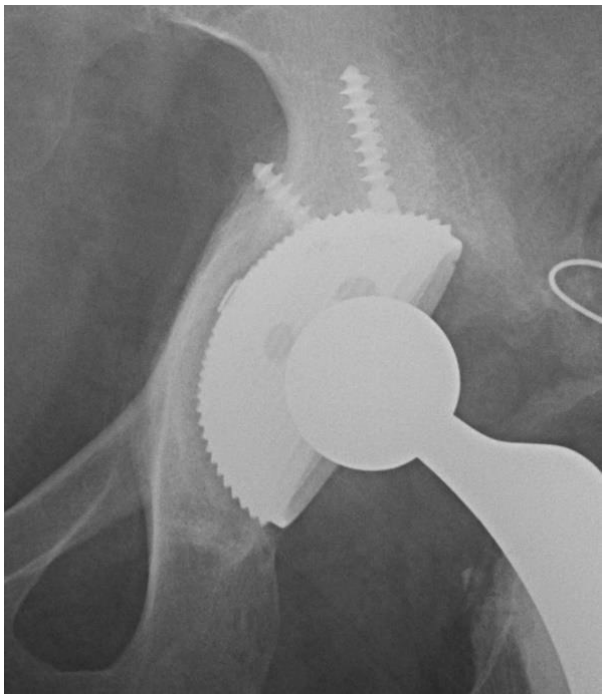

Figure 11: CT scan of screw fixated acetabular cup [97].

Bone ingrowth fixation is attained by allowing the bone to grow onto or into the components surface as seen below in Figure 12. Pilliar *et al.* studied the effect of movements on bone ingrowth and concluded that bone growth into the porous surface is achievable in presence of movement as small as 28 μm, however relative motions are required to be less than 150 μm [98]. Hence it is crucial for ingrowth fixation of a prosthesis to maintain the initial stability for the bone ingrowth to occur. In some cases such initial stability is achieved by interference fit or by screw fixation [75]. Pore size of the porous surface also plays an important role in the strength of prosthesis fixation. Pore sizes ranging from 50 μm to 800 μm have been investigated in past to determine the optimal range of pore size for strong bone ingrowth fixation [97, 99-102]. A research conducted in 1999 by Kienapfel *et al.* concluded that an optimal range of the pore size for a sturdy bone ingrowth ranges from 100 μm to 400 μm [103].

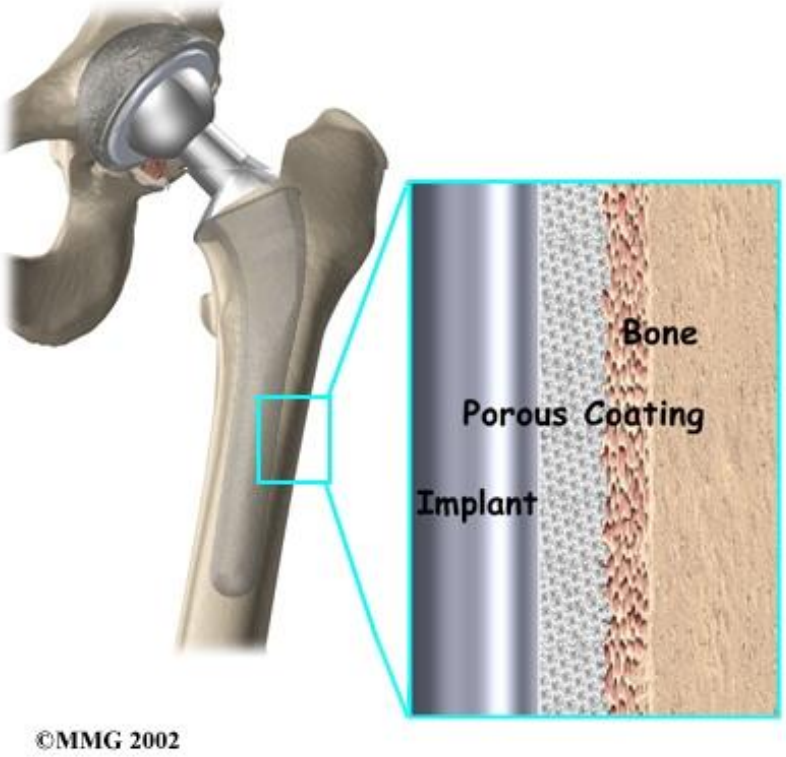

Figure 12: Porous uncemented implant displaying bone growth onto the porous surface [95].

2.4.4.3 Modularity

Initially femoral stem and femoral head were designed as a single component which made successful reconstruction of hip joint mechanics challenging [104]. However with the invention of modular components surgeons were benefitted as modularity provided them with versatility and the ability to adjust leg length and offset to establish optimal hip joint mechanics [105, 106]. Several authors reported manufacturers advertised the benefit of reduced inventory through modular components [107, 108]. A modular neck used at the primary surgery simplifies the revision surgery as it allows the modular neck to be removed, providing better visualisation and allowing surgeons to make changes in leg length and offset without revising femoral component [104]. It also allows the surgeons to mix-match femoral head and stem materials allowing introduction of more wear resistant materials for the bearing surface. Along with the impressive clinical benefits of modular neck

prosthesis, a number of concerns regarding modularity have been reported including component mismatch, source of ion and wear debris release, dislocation, as well as fretting and corrosion wear at the neck taper [106, 109-113].

Figure 13: Image displaying hip prosthesis with modular femoral head and neck [114].

2.4.4.4 Bearing Design and Tribology

It is essential for a hip joint prosthesis to replicate the motions of a natural hip joint which implies a requirement of the bearing surfaces which can glide on each other along with transmitting loads. The study of how such bearing surfaces behave is known as tribology. The etymology has to be referred to the Greek term *tribos* which means rubbing, hence the word tribology signifies "the science of rubbing" [115].

The bearing surfaces used for total hip replacement can be categorised in two groups, which are, hard-on-hard and hard-on-soft. For hard-on-hard bearing combination a femoral head made from hard material articulates against an acetabular cup/liner made from same or different hard material whereas in hard-on-soft bearing combination a fermoral head made of hard material articulates against an acetabular cup liner made from a soft material. Hard-on-hard category consists of bearing combinations like metal-on-metal,

ceramic-on-metal and ceramic-on-ceramic, whereas hard-on-soft category consist of metal-on-polyethylene and ceramic-on-polyethylene. Each category has its own advantages and disadvantages and are further discussed in detail in section 2.4. The risk that comes with introduction of alternate materials and novel designs of bearing surface into clinical use has been compensated by changes in patient demographics and their demand. Expectations from the total hip replacement have increased with younger patients who are more active and have desires to participate in sporting activities [116].

Metal-on-polyethylene articulating bearing surface was introduced by Sir John Charnley due to his interest in manufacturing a low friction bearing pair. Charnley used his famous pendulum friction test to demonstrate the enhanced performance of metal-on-polyethylene over metal-on-metal. In theory by the tribology analysis, mixed lubrication conditions are predicted for metal-on-polyethylene hips [117]. One of the most important factors is the surface finish of the bearing surfaces as even a tiny increment in surface roughness of hard material can cause increased wear of the UHMWPE counter-face [118]. Hall *et al*. studied 200 retrieved acetabular liners and observed lower volumetric wear rates in small femoral head due to smaller sliding distances [119]. The sliding velocity contact stresses also affects the wear rate in hip prosthesis. Higher sliding velocities can cause frictional heating and increased wear [120]. Bergmann *et al.* reported an *in vivo* temperature value as high as 43.1 °C in a patient after one hour of walking activity [121]. It is considered that biological injury occurs at 40 °C and this clarifies that frictional heating causes negative effects on the performance of hip prostheses [122]. As heating is frictional and friction is directly related to the surface finishing of the bearing surface, it makes the study of surface finish essential.

2.4.4.5 Surface Finish

For well-functioning articulation of femoral head and acetabular cup in a hip prosthesis, BS ISO 7206-2:2011 (2016) gives a guideline for appropriate

surface roughness required on articulating surfaces. It is reported in the standards that the maximum average roughness (Ra) for metallic and ceramic components should not be greater than 0.05 μm and 0.02 μm respectively. Such highly polished surfaces are necessary to maintain smooth articulation of the bearing surfaces by reducing frictions. Advancement in manufacturing technology and techniques allows to manufacture far more polished surfaces that reported for well-functioning hip prostheses. Some of the components studied by S L Smith in 2001 reported average surface roughness as low as 0.0016 μm (1.6 nm) on metal-on-metal femoral head and 0.0069 μm (6.9 nm) on metal-on-metal acetabular cup [123]. Recently, Cubillos *et al.* studied the average surface roughness of femoral heads made from stainless steel and Co-Cr-Mo and discovered the average Ra ranging from 0.014 to 0.018 μm [124]. Interestingly the Ra observed by S L Smith in 2001 falls in range of the findings of Cubillos *et al.* in 2018.

2.5 Bio-Materials

2.5.1 Introduction

Any material considered for designing a hip prosthesis has to be compatible with the host environment inside the human body. Such compatible materials are termed as biomaterials. Human body is well designed to guard itself against foreign objects and is very aggressive in that matter. Hence only highly inert materials are suitable to be used as implants. However it is well-known that no material is completely inert and is able to escape without provoking any host response from the body. A long term bio-compatibility can be divided into two categories, i.e. host response and material degradation. For example, metal implants degrade by corrosion whereas polyethylene causes host response and stimulates biological agents within the body. If the implant degradation products are soluble they may enter the blood stream and affect other tissues and organs in the body [75]. Concerns have been raised that metal ions accumulation in organs can cause

cancer, although reduction in incidence rates for joint arthroplasty has been documented [125-127].

Figure 14: An image of metal-on-metal hip resurfacing prosthesis [128].

2.5.3 Metals

Metals and metallic alloys possess high strength, fatigue resistance and toughness required for the load bearing function in hip prosthesis. Metals can achieve a polished surface with very low average roughness (Ra) for bearing surface and can be hardened to resist wear. However in an aggressive biological environment most metals degrade by corrosion and the metals that can withstand corrosion like gold and platinum are very low in strength and do not meet the design criteria (as well as being prohibitively expensive). To overcome this issue a process called passivation is applied on the metal which builds a layer of metal oxide on the surface to create a protective shell against the corrosion by not provoking any host response in the biological environment. Currently three metal alloys are used to manufacture hip prostheses, stainless steel, and cobalt chrome and titanium alloys. Below displayed in Table 2 are the mechanical properties of some metallic materials employed in fabricating hip prostheses.

Metal Alloy	σY (MPa)	σUTS (MPa)	E (GPa)	Reference
Stainless Steel				
316L cold worked	310	655	200	ASTM F138 [129]
316L Annealed	170	480	190	
Cobalt Chrome				
Wrought Co-Cr-W-Ni	310	860	242	ASTM F90 [130]
Cast Co-Cr-Mo	450	655	248	ASTM F75 [131]
Cold worked	1586	1793		ASTM F562 [132]
Titanium				
Ti-6Al-4V	800-900	900-1000	115	ASTM F136

Table 2: Information of mechanical properties of metallic materials employed to fabricate hip prosthesis. σ_Y is yield strength, σ_{UTS} is ultimate tensile strength and E is Young's modulus.

2.3.3.1 Stainless steel

Stainless steel is easy to fabricate and is a cost-effective material which made it an attractive implant material in the early days of THR. Chromium present in stainless steel helps to prevent corrosion by forming an oxide layer on the surface. A minimum level of 12% chromium is required to ensure passivation. Molybdenum provides resistance against pitting corrosion which is a localised form of corrosion responsible for producing cavities in the material. The reduced carbon content in stainless steel prevents intergranular corrosion (IGC) which is a corrosion that occurs at the grain boundaries. An example from ASTM F138 for chemical composition of stainless steel 316L, the most commonly used alloy of steel used in implant manufacture, is given in the Table 3 below.

	Element (wt. %)								
Alloy	**C**	**Mn**	**P**	**S**	**Si**	**Cr**	**Ni**	**Mo**	**Fe**
316L	0.03	2.00	0.03	0.01	0.75	17.00 - 19.00	13.00 - 15.5	2.00 - 3.00	Balance

Table 3: Displaying chemical composition of 316L stainless steel taken from ASTM F138 [129]

2.3.3.2 Cobalt Chrome Alloys

In the 1930s, Smith-Peterson adopted cobalt chromium for his interposition arthroplasty. Before that cobalt chromium was used in dental applications as Vitallium. Subsequently cobalt alloys have been extensively employed in various other engineering fields like aerospace, space vehicles and energy generation industry. Corrosion resistance in cobalt chrome alloys are attributable to chromium, molybdenum and aluminium.

Cast cobalt chrome materials have a large grained structure giving poor mechanical properties and which tends to lead to corrosion. Hence it is essential to thermally process cast cobalt chrome materials. Use of such heat treatment along with aging permits the controlled distribution of hard particles known as carbides.

On the other hand, wrought cobalt chrome alloys possess finer grain structure with a suitable carbide distribution meaning that they have better mechanical and corrosion resistance properties compared to cast alloys. Casting can lead to porosity and grain boundary carbides which can be problematic for prostheses. To overcome such issues hot isostatic pressing process can be employed minimising porosity and improving fatigue strength of the alloy.

2.3.3.3 Titanium

Titanium has been used in prosthesis stems since the 1970s [133]. Titanium is used generally as a Ti-6Al-4V alloy which contains 6% aluminium and 4% vanadium which is treated thermally or thermo-chemically. Elements

present in the titanium alloy like carbon, hydrogen, oxygen and nitrogen are highly soluble at room temperature and need to be controlled at every processing stage to prevent the alloy from becoming brittle. The alloy possesses high strength and ductility and has high resistance to corrosion. However, unlike cobalt chrome alloys, titanium alloys are reported to degrade by fretting corrosion [134]. Table 4 below displays composition of the most commonly used titanium alloy Ti-6Al-4V.

	Element (wt. %)							
Alloy	**N2**	**C**	**H2**	**Fe**	**O2**	**Al**	**V**	**Ti**
Ti-6Al-4V	0.05	0.08	0.012	0.25	0.13	5.50-6.50	3.50-4.50	Balance

Table 4: Composition of Ti-6Al-4V as stated in ASTM F136 [135].

2.5.4 Polymers

Polymers provide the required articulating surface required for the orthopaedic prosthesis applications. Polymers are commonly used in conjunction with metals or ceramics for load bearing purpose as they have much lower stiffness compared to human bones. The most commonly used polymers in total joint replacement applications are ultra-high molecular weight polyethylene (UHMWPE) and Polymethylmethacrylate (PMMA).

2.5.4.1 Ultra-high Molecular Weight Polyethylene (UHMWPE)

Ultra-high Molecular Weight Polyethylene (UHMWPE) is a unique polymer that possess exceptional mechanical properties. The most notable properties of UHMWPE are its impact resistance, chemical inertness, wettability and abrasion resistance. In the orthopaedics industry, UHMWPE has been widely used as a bearing material in total joint arthroplasty for the past 45 years. Between april 2003 and December 2016 approximate 2.28 million total joint arthroplasty procedures were performed in the UK and the majority of these procedures utilised UHMWPE as a bearing material [1].

During this period, 48% of total hip arthroplasty utilised UHMWPE [1]. UHMWPE is commonly used to fabricate acetabular cup liners of hip prostheses and tibial trays of knee prostheses. Despite the success, one of the factors limiting implant longevity is wear and damage of the UHMWPE components.

Wear of UHMWPE develops due to abrasion and adhesion mechanisms. A layer of polyethylene accumulates on the hard counter of the bearing surface which is an outcome of adhesive wear of UHMWPE. Abrasive wear is caused by damaged hard surfaces or by hard debris particles. The debris may be a fragment of bone or particle of bone cement which can abrade the bearing surfaces directly [136].

In 1960s, Sir John Charnley introduced UHMWPE by using it to fabricate acetabular cups [133, 137] and this is still commonly used as the primary counter-face articulation material with metallic and ceramic femoral heads. This is majorly attributed to the outstanding mechanical properties like friction coefficient as low as 0.03, high wear resistance and self-lubricating *in vivo.* Attempts have been made to improve UHMWPE for orthopaedic applications by introducing carbon-fibre reinforced material. In 1970s, Oonishi in japan implanted a highly cross-linked UHMWPE which was produced by dosing upto 1000kGy of gamma irradiation in air [136]. In late 1980s, DePuy orthopaedics and DuPont introduced UHMWPE known as Hylamer which was a highly crystalline form of UHMWPE [138]. The clinical results of Hylamer has been mixed and remain controversial with some performances worse than conventional UHMWPE and some satisfactory or improved performances [103]. In late 1990s, crosslinked UHMWPE with thermal treatment was introduced in order to improve the wear resistance of UHMWPE components [139]. Through a hip simulator study Wang *et al.* showed that increased cross-linking resulted in greatly reduced wear [140]. Table 5 below displays mechanical properties of two different grades of UHMWPE and cross-linked polyethylene (crossfire^{TM} by Stryker) used in orthopaedics.

Figure 15: Acetabular and tibial components fabricated from UHMWPE [141].

	UHMWPE		
Mechanical Property	**1020**	**1120**	**CrossfireTM**
Density	0.935	0.93	
Yield Stress	22.8	23	25.4
UTS	39.6	49.5	61.1
Impact toughness	195	197	200

Table 5: Mechanical properties of two medical grade of UHMWPE [140].

There are various grades of UHMWPE used to fabricate orthopaedic implants. Using a numbering system known as Hoechst each grade is assigned with a four digit GUR code for example 1120 from the Table 5. The first digit indicates whether that particular UHMWPE is of medical grade or not where 1 stands for medical grade. The second digit is 1 if the polymer contains calcium stearate and 0 if otherwise. The third digit specifies the molecular weight where the digit is 2 for weight lower (~ 4 million g/mol) and 5 for higher (~ 6 million g/mol). The fourth digit always remain 0.

Although crosslinked UHMWPE displayed high wear resistance wear compared to UHMWPE, the fatigue resistance is decreased with the decrease

in crystallinity that occurs post-irradiation melting. Concerns were raised regarding increased occurrence of rim fracture under impingement which was directly attributable to the decreased fatigue strength [142, 143]. A recent advancement in UHMWPE is the introduction of vitamin E stabilized UHMWPE, where Vitamin E is used as an antioxidant to prevent oxidation in crosslinked UHMWPE. Post-irradiation melting is replaced by vitamin E stabilization in order to prevent the loss of crystallinity without decreasing wear or oxidation resistance [144].

2.5.4.2 Polymethylmethacrylate (PMMA)

Polymethylmethacrylate (PMMA), also known as bone cement, is a standard material used to fixate prosthesis to host bone. It serves as a grout and adapts the surface inconsistency of the surrounding bone tissue to the surface of the implanted prosthesis [145]. Bone cements do not possess innate adhesive properties, but they depend on close mechanical interlock between the inserted prosthesis and irregular bone surface [146]. The bone cement is capable to transfer the body weight and service loads that is exerted on the prosthesis to the bone and hence increase the load bearing properties between the stem and the bone. Polymethylmethacrylate (PMMA) was initially created by Otto Rohm in 1901 [147]. In 1940s, Jean Judet and Robert Judet used PMMA for their acrylic femoral arthroplasties [148]. However, in late 1950s Sir John Charnley employed the use of PMMA to fixate acetabular and femoral components in total hip replacement and its use soon became popular [149].

PMMA is typically supplied as two components, a polymer powder and a monomer liquid, which are commonly required to be mixed in a ratio of 2:1. 83% - 99% of the fine powder (30 – 150 μm) consist of PMMA or copolymer. Other components included in the powder are chlorophyll dye, antibiotics, benzoyl peroxide as an initiator, and a radio-opacifier: either barium sulphate ($BaSO_4$) or zirconium oxide (ZrO_2) [145]. Radio opacifier agents are used in the cement for post-operative assessment of the prosthesis. The mechanical

strength of bone cement is compromised due to barium sulphate [150, 151]. Also it has been reported that barium sulphate affects the polymerization temperature and induce increased bone resorption [152, 153]. Zirconium dioxide has less effect on the mechanical properties of the cement as it is 100 times less soluble than barium sulphate.

The liquid comprised with 97% - 99% of methylmethacrylate monomer along with traces of hydroquinone which acts as a stabilizer to prevent the monomer from polymerisation through light or heat exposure[148]. A polymerisation activator, mostly N,N-dimethyl-p-toluidine (DmpT), is also present in the liquid which acts as an initiator and activates the polymerisation at room temperature (Cold curing cement) when mixed with the powder [145]. Table 6 below displays the composition of commercially available PMMA (Palacos® R; Heraeus Medical GmbH, Wehrheim, Germany).

Constituent	**Amount**
Powder	
Poly (methyl methacrylate)	33.55 g
Zirconium dioxide	6.13 g
benzoyl peroxide	0.32 g
Chlorophyll	1.0 mg
Liquid	
Methyl methacrylate	18.4 g
N,N dimethyl-p-toluidiene	0.38 g
Chlorophyll	0.4 mg
Hydroquinone	64ppm

Table 6: Composition of PMMA bone cement [154].

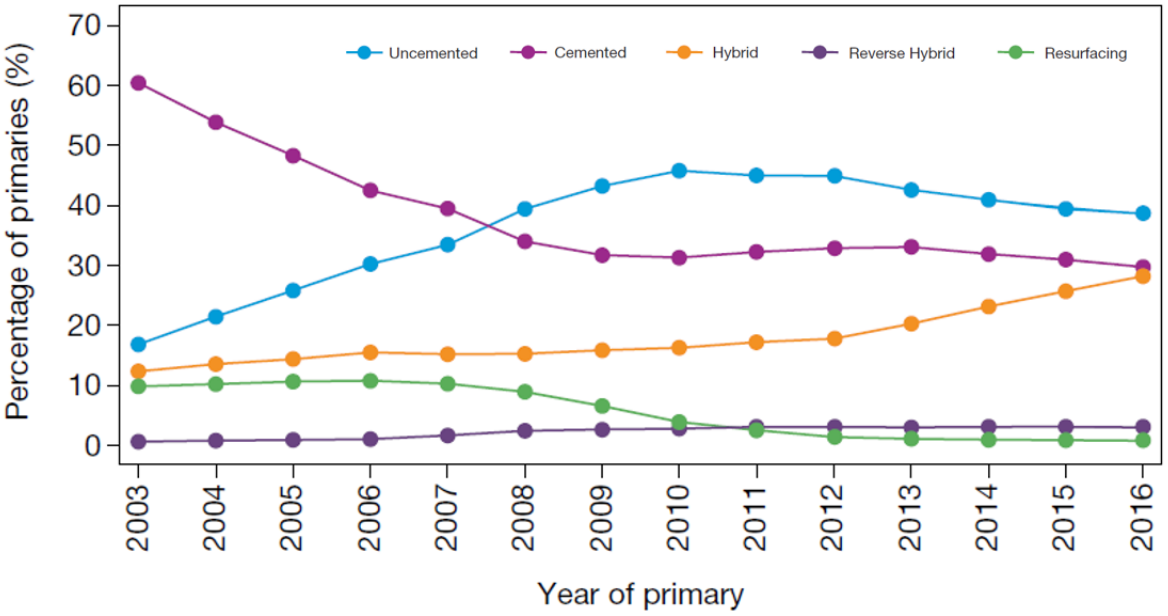

Figure 16: Temporal changes in percentages of each fixation methods used in primary hip replacements in the UK as mentioned in the national joint registry 2017 [1].

2.5.5 Ceramics

Ceramics are non-metallic and inorganic materials which are processed by mixing a material along with water and an organic binder. Later the mixture is pressed into a mould to obtain the required form and dried to evaporate the water. Sintering or firing is performed at a very high temperature to increase the density of the residual material. Factors like the distribution and size of the grains, porosity and the purity of the powder determines the biological and mechanical properties [155]. The wide use of bio-ceramics in medicine is attributable to their high strength, stability, excellent corrosion and wear resistance, non-toxicity and outstanding bio-compatibility as a result of their high level of oxidation [87, 156].

Ceramics employed in the orthopaedic industry are categorised as bioactive or inert according to the host environment response when implanted in a human body. The bioactivity of ceramics can be characterised as their ability to bond biologically (osteo-integrate) with the bone. Whereas ceramic that are inert simply elicits a minor fibrous reaction. Clinically, inert fully-

dense ceramics are employed to fabricate bearings in total joint arthroplasty due to their remarkable resistance to wear and tribological properties. Ceramics are also capable to achieve a high degree of surface finish through polishing which tribologically is an attractive property. Ceramics have improved wettability which displays lower friction properties compared to metals when in articulation against UHMWPE in bearing surface. Unlike inert ceramics, bioactive ceramics are used as coatings on the prosthesis to enhance their fixation by stimulating or accelerating bone growth due to their osteo-conductive properties [155].

2.5.5.1 Alumina

Alumina is a standardised material since 1984 (ISO 6474) [155]. Alumina belongs to oxide ceramic group that is made of pure metal oxides. A surgical grade dense alumina is attained by sintering alumina powder at temperatures that ranges from 1600°C to 1800°C. Through this process the material achieves maximum oxidation, permitting chemical inertness, thermodynamic stability and exceptional corrosion resistant properties. As a biomaterial, alumina was chosen for its extreme hardness (>2,000 HV) that was four times harder compared to its metal equivalents [157]. It also possesses outstanding compressive strength however it is brittle and has limited bending and tensile strength. The young's modulus of alumina is 300 times higher compared to that of a cancellous bone. Alumina ceramic material when used against itself in the bearing possesses excellent tribological properties with a reported linear wear rate 4000 times lower compared to that of metal-on-polyethylene [158]. The frictional coefficient of alumina-on alumina is as low as 0.09 compared to 0.21 for metal-on-polyethylene. Such excellent frictional characteristics are attributable to a high wettability due to the hydrophilic nature of the material surface and the ability to operate with fluid film lubrication which considerably decreases adhesive wear. It is because of these properties that alumina components produce a limited amount of volumetric wear and moderate biological reaction to ceramic wear

debris. Clarke *et al*. estimated wear volume to be 2000-5000 times less in alumina-on-alumina compared to metal-on-polyethylene [159]. The survival rate at ten years for cemented alumina cups was 88.6% when aseptic loosening was considered as the cause of failure [160]. Patients younger than 50 years of age had a survival of 94% at ten years [161, 162]. However, alumina has large grain size, high porosity, low density and limited plasticity which made the material vulnerable in terms of crack propogation which lead to fracture rapidly. Moreover the poor socket design of prostheses lead to reported fracture rates as high as 10% - 13% [86].

2.5.5.2 Zirconia

In 1985, Zirconia ceramic was introduced as second generation ceramic for manufacturing femoral heads of total hip replacements prosthesis as it possessed higher strength, toughness and reduce the risk of fracture compared to alumina [163]. Pure zirconia is an unstable material and cannot be used due to the extreme ability to transform from one phase to another accompanied by shape and volume changes which may cause material to degrade and induce cracks. Hence during fabrication zirconia is stabilised by adding stabilizing oxides such as MgO or CaO to control the phase transformation which improves its mechanical properties [136]. The zirconia femoral head development was majorly performed by Kyocera (Osaka, Japan) and St. Gobain Advanced Ceramics Desmarquest (Evreux, France). These two manufacturers were market leader in manufacturing zirconia femoral heads. In the period between 1985 and 2000, St. Gobain Advanced Ceramics Desmarquest company had sold more than 350,000 femoral heads globally. With only 28 fractures reported in that period, zirconia displayed fracture rate of only 0.01% [164]. By ensuring the systematic use of proof tests on all the components, the fracture rates had reduced to as low as 0.002% by mid-1990s [165]. Zirconia material was standardised in 1997 (International Standard Organisation, ISO 13356) [155]. In 1998, in order to meet the increasing demand of zirconia femoral head, St. Gobain Advanced Ceramics

Desmarquest company replaced the batch furnace (kiln) with a tunnel furnace. This change in sintering process led to the change in microstructure of the manufactured zirconia femoral heads. In 2000, two major orthopaedic companies, DePuy and Smith & Nephew, had reported unusual fractures and a fracture rate of 8%. This new fracture rate was extremely high compared to 0.002 which was reported in previous 15 years. As a consequent, St. Gobain Advanced Ceramics Desmarquest discontinued to manufacture zirconia femoral heads. Some studies reported that zirconia was vulnerable to high temperatures and wet environments which weakened zirconia and resulted in increased surface roughness [166] causing higher wear rates. As a result of such unfavourable fracture rates and reports against zirconia made it unfit as a biomaterial for orthopaedic prostheses.

2.5.5.3 Hot Isostatic Processed Alumina (BIOLOX® Forte)

BIOLOX® Forte (CeramTec AG, Plochingen, Germany) is a commercial name for the hot isostatic processed (HIPed) alumina, third generation ceramics, used in the orthopaedic industry. The third generation of ceramics was introduced in 1990s to overcome the fracture issues faced by first and second generation ceramics. The third generation alumina displayed better performance than the earlier generations of ceramic due to the additional process of hot isostatic pressing subsequent to the sintering process. Hot isotatic pressing process resulted in smaller grain size, lesser impurities and denser ceramic [15, 87]. Laser engraving is chosen over mechanical engraving in order to avoid initiation of weak stress area [167]. Lower temperatures used during the hot isostatic process aided to minimise grain growth which resulted in smaller grain size in the final product [57]. The mechanical characteristics of this third generation ceramics are displayed below in Table 7.

2.5.5.4 Alumina Matrix Composite (BIOLOX® Delta)

BIOLOX® Delta (CeramTec AG, Plochingen, Germany) is a commercial name for alumina matrix composite (AMC) ceramics, the fourth generation

ceramics, used in the orthopaedic industry. This modern ceramic is a compound of zirconia toughened alumina (ZTA), strontium (SrO), yttria (Y_2O_3) and chromia (Cr_2O_3) [168]. The nano-sized yttria stabilized tetragonal zirconia particles present in the material transforms and create a compressive stress field as soon as the crack comes in contact with it. This guards the material against the crack propagation within the microstructure [169]. Chromium oxide is also introduced in order to increase the hardness of the material [169]. Oxide additives generate platelet-like crystals which dissipate energy by deflecting cracks [170]. The end product is a mixture of approximately 82% alumina, 17% zirconia, and less than 1% of chromium oxide and strontium oxide [171]. Hence by combining the desired properties of zirconia and alumina, BIOLOX® Delta (CeramTec AG, Plochingen, Germany) has further addressed the limitations of all the previous generations of ceramic used in orthopaedic industry. The mechanical characteristics of fourth generation ceramics are displayed and compared to its previous generations below in Table 7.

Properties	First and Second Generation Ceramic	Third Generation HIPed Alumina (BIOLOX® Forte)	Fourth Generation Alumina Matrix Composite; (Biolox Delta®)
4-Point bending strength (Mpa)	500	580	1000
Density (g/cm^3)	3.96	3.98	4.37
Average grain size (μm)	< 3.2	< 1.8	< 1.5
Fracture toughness K_{Ic} ($Mpa.M^{1/2}$)	4 - 5	4 – 5	6.5 - 8.5

Table 7: The mechanical characteristic of different generation of ceramics [57].

2.6 Bearing Combinations & Failure Mechanisms

There are significant expectations from the materials employed for the bearing surfaces of total hip replacement prosthesis. The material is expected to articulate with a low friction coefficient in order to minimize the torque transferred to the adjacent host bone. It must also be durable and stable for approximately 20 years (i.e. over 30 million cycles). Moreover, wear of the materials must be low, and the wear particles generated must be inert enough to not instigate adverse tissue reactions. A number of different material combinations have been employed as bearing surfaces in total hip replacement prosthesis [117] and are discussed below.

2.6.1 Metal-on-Polyethylene (MoP)

In a Metal-on-Polyethylene bearing combination, a metallic femoral head articulates against a polyethylene acetabular cup liner to form a bearing surface of an artificial hip prosthesis. Polyethylene being soft material and metal being a hard material makes this a hard-on-soft bearing combination. The polyethylene used in such bearing sufaces includes polytetrafluoroethylene (PTFE), conventional non-cross-linked ultra-high molecular weight polyethylene (UHMWPE), cross-linked polyethylene (XLPE), highly cross-linked polyethylene and metals used for such bearing surface includes stainless steel (316S), cobalt chrome alloy (CoCrMo) and titanium alloy (Ti_6Al_4V). The metallic femoral head is manufactured with a highly polished smooth surface, in an attempt to reduce wear and friction of the softer counterpart polyethylene.

2.6.1.1 History

In late 1950s, Metal-on-polyethylene was first introduced as a low friction arthroplasty (LFA) bearing surface. In order to minimize frictional torque, the femoral head used had a smaller diameter than that of a natural hip joint.

However they suffered excessive wear and femoral head penetration into acetabular component [53]. Due to such catastrophic experience, in year 1962 Charnley employed the use of UHMWPE as acetabular component material and this material is still dominating the total hip arthroplasty market. In mid 1960s, Müller modified Charnley's metal-on-UHMWPE by employing the use of cast cobalt chromium molybdenum (CoCrMo) to manufacture femoral head and increasing the bearing diameter from 22.225 mm to 32 mm. The diameter size was increased in order to prevent dislocation in hip implants. However, it is recognised that the polymeric volumetric wear rate is proportional to total sliding distance, and hence is proportional to head diameter. Also, penetration is inversely proportional to femoral head diameter. Due to this, Müller hip arthroplasty device displayed higher wear rates with lower penetration compared to metal-on-UHMWPE device developed by Charnley. This was confirmed radiologically by Livermore *et al.* [172] and in laboratory by Clarke *et al.* [173] and Derbyshire *et al.* [174]. In 1970s, Ling and the University of Exeter collaborated to develop Exeter metal-on-polymer hip implant device. Exeter hip prosthesis has collarless femoral stem which allows the stem to be inserted down the cement mantle. Both, Charnley and Exeter metal-on-polymer hip prosthesis have exhibited high survivorship rates over 20 years [53].

2.6.1.2 Survivorship & Wear Rates

Metal-on-Polyethylene bearings manufactured from conventional non-cross-linked UHMWPE have exhibited higher magnitude of wear volumes in both *in vitro* and *in vivo*. Simulator test results have displayed wear volumes of 23.2 mm^3/million cycles and 32.8 mm^3/million cycles for 22.225 mm and 28 mm heads, respectively [173]. In attempts to decrease the wear volumes, acetabular components manufactured from cross-linked polyethylene (XLPE) were introduced. Endo *et al*. studied and compared volumetric wear rates of conventional UHMWPE against XLPE acetabular and concluded a 30% reduction of volumetric wear in moderately XLPE acetabular components

[175]. Development of highly cross-linked polyethylene (HXLPE) has exhibited even better results when compared to conventional UHMWPE and studies of wear volumes report reductions ranging between 73% to 87% [139, 176].

As mentioned previously, wear volume is directly proportional to sliding distance and hence is proportional to head diameter size. Thus a larger femoral head increases the volumetric wear rates of metal-on-polymer hip prosthesis [177]. An *in vivo* study compared wear volumes in 22mm, 28mm and 32mm head diameter size of metal-on-polyethylene acetabular components and concluded increase in wear rate by 74% by comparing 28mm and 32mm acetabular components [172]. Through *in vitro* simulator study, Clarke *et al*. observed that the volumetric wear rate increased linearly by 7.8% per millimetre increase in head diameter size of metal-on-polyethylene hip prostheses [173]. However, *in vitro* simulator studies of HXLPE have displayed no increase in wear volumes associated with increasing head diameter even in diameter size as large as 46mm [178, 179]. Retrieval study at mean 5.7 year (range 5-8 years) follow-up exhibited higher wear volumes of HXLPE with large femoral head diameter of 36mm and 40mm when compared to smaller head diameter of 26mm, 28mm and 32mm [180].

2.6.1.3 Complications

HXLPE and XLPE have been associated with high fracture rates of acetabular liners [181-183]. This is due to radiation-induced decrease in ductility of the material which takes place in dose-dependent manner [184-186]. Retrieval studies have exhibited higher occurrence of rim cracks which is presumed to be predecessor of complete fracture in XLPE or HXLPE [187].

There is strong evidence that UHMWPE wear particles majorly generated from the bearing interface is major factor in development of osteolysis [188]. Macrophages engulf the UHMWPE wear debris by phagocytosis when the wear particles enter the periprosthetic tissue. This leads to a release of cytokines that develops an inflamed granulomatous tissue local to the bone. This activates osteoclasts that resorb the bone which than leads to osteolysis and

hence loosen the prosthesis [188]. Several studies have observed the influence of wear particles on the phatogenesis of osteolysis and implant loosening [189-191]. UHMWPE wear debris have been observed to be related with macrophages, giant cells and areas of osteolysis in tissues retrieved from both acetabular and femoral components during revision due to aseptic loosening [192-196]. Several authors have reported correlation between wear of UHMWPE acetabular component and osteolysis [197, 198]. Studies suggests that the distribution of debris is not confined to periprosthetic tissue and have been identified in the draining lymph nodes and is presumed to access through tissue's lymphatic vessel [199-201].

2.6.2 Metal-on-Metal (MoM)

In a metal-on-metal is a hard-on-hard bearing surface with a metallic femoral head articulating against a metallic acetabular component. The metals commonly used for such metallic bearings are stainless steel, cobalt chromium alloys or titanium alloys. Metal-on-metal bearing surface is uniquely characterised as a self-polishing bearing surface as it is capable to wear off any scratches through joint movements. This characteristic is also one of the factors that allow metal-on-metal bearing to produce low wear [116].

2.6.2.1 History

In mid 1950s McKee developed the first metal-on-metal hip prosthesis. These prostheses consisted of a femoral head with a large diameter of 35-40 mm head articulating against acetabular cup of similar size and employed cobalt chromium alloy for both counter-parts of the bearing surface. Other such subsequent designs were developed in 1962 by Ring and in 1965 by Müller. Such metal-on-metal prosthesis designs were introduced without sufficient testing and suffered from high initial failure rates [116]. Metal-on-metal bearings were abandoned in 1970s dues to concerns associated with metal sensitivity and high frictional torques. However, the surviving

prostheses of this abandoned design displayed a high level of long term result with survivorship of over 20 years [72]. Metal-on-metal exhibited 40-100 times lower volumetric wear rates compared to that of metal-on-polyethylene bearings [202, 203]. Hence, metal-on-metal bearings gained interest and were re-introduced when studies showed that metal-on-polyethylene bearings suffered long term failure due to osteolysis induced by the polyethylene wear debris [204]. In early 1980s, Müller re-engineered the metal-on-metal design but had to abandon the design himself due to the concerns raised by the durability of the titanium nitride (TiN) coatings that he used [72]. Studies looking into the wear of metal-on-metal bearing surfaces have shown that the wear rate is very much dependent on the material properties, tribological design and surface finish technique [205, 206]. After acquiring such knowledge, in 1987 the first modern metal-on-metal hip prosthesis, known as Metasul™, was introduced into Europe by Sulzer Orthopaedics. Metasul employed a cobalt chrome alloy for both femoral head and acetabular cup. The material structure and modern manufacturing technique allows to create a smooth highly polished surface with average surface roughness for the head and the cup both being less than 10nm or even 5nm which caused reduction in frictional torques.

Modern Metal-on-Metal total hip replacements are divided into two categories, i.e. a conventional total hip replacement prosthesis and a hip resurfacing system. Hip resurfacing, also known as surface arthroplasty, procedure is a bone conserving alternative to the conventional total hip replacement procedure. In hip resurfacing procedure, instead of removing the femoral neck, the femoral head is trimmed and capped with a metallic femoral component and the acetabulum is replaced by an acetabular component. Hence hip resurfacing procedure provides ease of revision by minimising the bone removal by the use of smaller implants and leaving enough bone material for total hip replacement surgery to be performed if needed in future. The use of smaller device also helps the patient in regaining mobility quicker through

post-operative rehab programs and hence reduces the post-surgery recovery time.

It is considered that Wiles, in 1983, performed the first surface replacement surgery by implanting a femoral component over an existing femoral head supported by a smith-petersen nail [207]. In 1950s, Charnley failed in his hip resurfacing surgery attempt which used teflon/teflon (polytetrafluoroethylene) and metal/teflon prostheses. Through this failure he realised the osteolysis problems associated with wear of teflon material and excessive wear associated with large diameter hard-on-soft bearings and raised a warning against resurfacing arthroplasty [208]. In 1970s, after the introduction of UHMWPE acetabular liners, various hip resurfacing procedures with the use of metal-on-UHMWPE were performed around the globe [209-213].

In 1990's, Derek McMinn introduced the modern resurfacing prosthesis known as McMinn prosthesis. This McMinn prostheses, as shown below in Figure 17, were later termed as Birmingham Hip Resurfacing (BHR) system. Initially, Birmingham hip resurfacing system displayed promising success rate, and by observing these many manufacturers introduced competing prostheses. Some such prostheses include, Articular Surface Replacement (ASR, Depuy), the Cormet (Corin) and many others.

Figure 17: An image displaying the McMinn prosthesis/Birmingham hip resurfacing system [214].

2.6.2.2 Survivorship & Wear Rates

Radial clearance is defined as the gap between the two bearing surfaces which is determined by measuring the variance between the diameters of the bearing surfaces of the acetabular cup and the femoral head. Small clearances lead to equatorial contact, high frictional force and high torque, which causes loosening of prosthesis and failure. Large clearances results in smaller contact areas and therefore causes high contact stresses, and loss of fluid film lubrication, which lead to high wear rates [57]. Radial clearance of recent metal-on-metal hip implants ranges from 20-40 μm which in early prostheses used to be 75-100 μm [53].

The wear in metal-on-metal bearings can be categorised into two phases; the bedding-in phase and the steady phase. The bedding-in phase is the initial phase during which the quantity of volumetric wear rate that occurs

is higher and the subsequent steady state phase is the sustained period of lower volumetric wear rate. This phases have been reported *in vitro* [215-218] and *in vivo* [202, 219] studies. A study conducted by Chan *et al.* observed the mean bedding-in volumetric wear rate to be 0.4 mm^3/million cycles which later reduced to 0.08 mm^3/million cycles under standard gait condition on hip simulator [220]. Sieber *et al*. analysed a cohort of 118 retrieved metal-on-metal prostheses and reported a mean annual linear wear rate of 25 μm/year in explants retrieved after first year which eventually dropped to 5 μm/year for explants that were retrieved after the third year [202].

An *in vitro* pin-on-plate study conducted by Tipper *et al*. [221] exhibited volumetric wear rate as low as 0.1 mm^3/million cycles for modern metal-on-metal prostheses. Scholes *et al. conducted* metal-on-metal hip simulator study of 28 mm femoral head size diameter that exhibited volumetric wear rates ranging from 0.2 mm^3/million cycles to 2.5 mm^3/million cycles [222]. This rate of volumetric wear is significantly low compared to reported volumetric wear rates of 32.8 mm^3/million cycles and 9 mm^3/million cycles for 28 mm metal-on-UHMWPE and metal-on-HXLPE bearing respectively [173]. The early clinical tests of Metasul prosthesis displayed a mean annual wear rate of 0.3 mm^3 [202]. There were other short/medium term studies conducted [202, 223, 224] which reported similar results.

2.6.2.3 Complications

Regardless of encouraging wear performance of metal-on-metal bearings, the concerns related to the long-term effect of wear debris still persists. The size of the metallic wear particles are significantly smaller (10-60nm) compared to those from UHMWPE which commonly ranges from 0.1-10 μm [116]. As a consequence, although the wear volume is greatly reduced, the number of wear particles may have increased by a factor of 100 [215, 221]. The long term effect of increased ionic metallic debris generation is not yet well understood. Initially Blac highlighted the potential adverse effects of

the breakdown of metal debris into metal ions [225]. Release of such metal debris and metal corrosion can be followed by aseptic fibrosis, local necrosis or loosening of the prosthesis and this phenomena is termed as metallosis [226]. Cobalt and chromium have been linked with hypersensitivity [227] that can causes intoxication and inflammation to the surrounding host bone and tissue. Metallosis has been clinically observed in patients with metal-on-metal hip prosthesis. Blac studied a case in which metallosis was observed to be the cause of failure in 9 hip prosthesis [226].

Willert *et al.* [227] recently reported on a group of patients who had early post-operative pain. The histological findings indicated few metal particles but were consistent with a possible lymphocyte-dominated immunological response. Due to these concerns various research have been conducted in order to minimize the volume of wear generated in metal-on-metal bearings. In 2008, Langton *et al.* [228] analysed 76 ASR hips and investigated the effect of component size and their orientation on the concentration of metal ions. The study concluded that it was essential to accurately position the acetabular component in order to reduce the metal ion concentration in the blood. In the same year De Haan *et al.* found 27 revisions attributable to the malposition of the acetabular component and reported that malpositioning of the component was associated with high serum level and metallosis [229]. Hesketh *et al.* [230] conduct an *in vitro* experiment to explore the effects of wear and corrosion on the performance of metal-on-metal hip prostheses. The study found that damage related to corrosion of metal significantly contributed to the formation of metal ions and also advised that the corrosion damage could be higher in *in vivo* environment.

2.6.3 Ceramic-on-Ceramic (CoC)

Alumina ceramic is four times harder material (>2000 HV) than its metal equivalents [169], and hence was introduced to overcome the problems of wear and friction in metal-on-metal and metal-on-polyethylene bearing surfaces. In comparison to metal-on-UHMWPE bearings the wear rate

exhibited by ceramic-on-ceramic bearings was reported to be 500 folds lower. The evidence also states that alumina-on-alumina bearing performs well in younger patients and displayed lower rate of problems associated with aseptic loosening [160]. However the material exhibited high rate of fracture, squeaking and stem loosening [160, 231].

2.6.3.1 History

In the early 1970s, alumina-on-alumina ceramic bearings were first introduced by Pierre Boutin for total hip arthroplasty [87]. Since then ceramic bearings have improved to overcome some of the previous limitations, specially fracture, which was a direct consequence of the sintering process that resulted in large grain size and propagation of crack [232]. In 1985, Zirconia was introduced as a second generation ceramic and was treated with hot isostatic pressing which resulted in fewer impurities and smaller grain size [86]. Zirconia, displayed higher fracture toughness and bending strength yet inferior wear characteristics as compared to that of alumina ceramic [87]. In 1990s, third generation Biolox® Forte was introduced as a purer and denser ceramic. However, even with the increased density and purity, Biolox® Forte was still vulnerable to rim factures of the acetabular liner [87]. Later in 2000, CeramTec commercialised Biolox® Delta (Biolox® Delta, CeramTec, AG, Plochingen, Germany) as the fourth generation ceramic which is the latest generation of orthopaedic ceramics available in the market [233].

2.6.3.2 Survivorship & Wear Rates

Since the 1970s, ceramic-on-ceramic bearings for both *in vivo* and *in vitro* testing have exhibited low wear rates [234]. Modern Ceramic-on-ceramic has even lower wear rates for both linear and volumetric wear and it is also possess high resistance to third body wear which is why they exhibited excellent clinical outcomes [87]. Hamilton studied mid-term results of BIOLOX® Delta ceramic-on-ceramic bearings and reported a mean Harris hip score of 94.4 at 31.1 months follow up [171]. Outstanding patient satisfaction

has been reported for BIOLOX® Delta ceramic-on-ceramic bearings has been reported with no evidence of osteolysis or fracture [235]. For third generation hot isostatic processed ceramics studies report high little or no osteolysis for 10 year follow up [30]. Park *et al*. [236] and Murphy *et al*. [237] reported 98% and 97% survivorship respectively, Kress *et al*. [238] and Lee *et al*. [239] reported 99% survivorship.

Ceramic-on-ceramic exhibits superiority when compared to any other bearing combination. At 10 year follow up, metal-on-polyethylene reported osteolysis in 26% patients compared to none in ceramic-on-ceramic patients [30]. Nevelos *et al*. tested HIPed alumina-on-alumina bearings under various mechanical conditions and reported wear rate of 0.14 mm^3/million cycle for bedding in phase (first million cycle) and 0.05 mm^3/million cycle for steady state [240, 241]. The same author tested metal-on-UHMWPE under the same conditions and reported a wear rate of 35 mm^3/million cycle [242], which is considerably high compared to HIPed alumina-on-alumina. By comparing survivorship of ceramic-on-ceramic and metal-on-highly crossed-linked polyethylene (MoHXLPE) at 10 - 14 years follow-up, ceramic-on-ceramic exhibited significantly lower wear rates to that of MoHXLPE [243]. This is because of the scratch profile of metallic femoral heads that form raised sharp edges when scratched by debris entering the bearing surface, which greatly increase wear of polyethylene acetabular liners. A further study reported that smaller bearings of size 22.22 mm exhibited an even lower wear rate of 0.019 mm^3/million cycle [244].

2.6.3.3 Edge Wear

After the sintering process the finished bearing surface of ceramic acetabular liner is ground and polished to the required specification. A small preliminary surface is designed for the pre-machined component which intersects the ground and polished surface for the articulation [245]. When the surface is polished it leaves a hard edge at the intersection as seen in Figure 18.

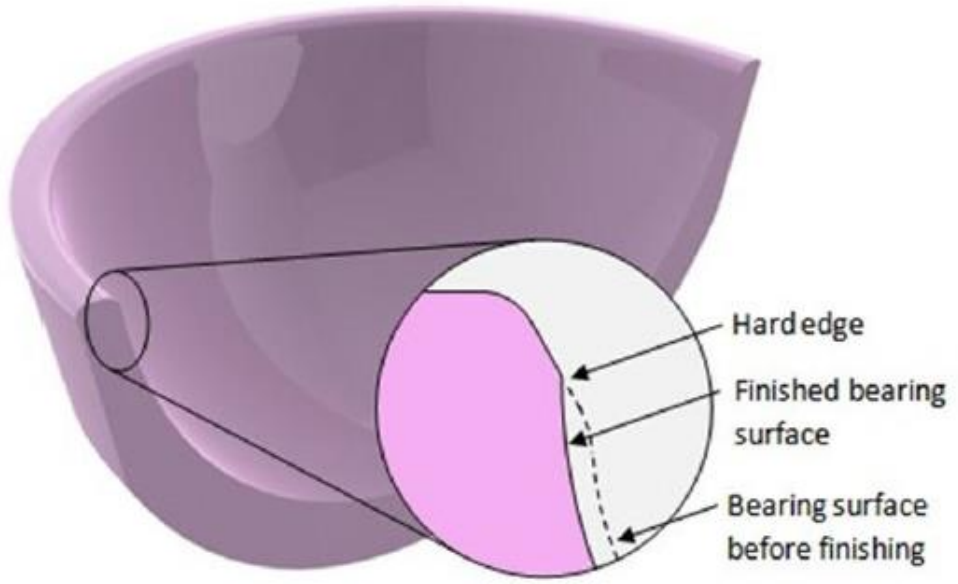

Figure 18: Cross-section image of a ceramic acetabular component displaying the sharp edge generated by grinding and polishing bearing surface [245].

When the force vector of the hip contact at the femoral head articulates against this hard edge of the acetabular liner, the stress is increased causing both surfaces to be damaged. The load on this edge is known as edge-loading, the wear caused on the edge of the acetabular liner by edge loading is termed as edge wear and the wear on the femoral head is known as stripe wear due to its appearance [245]. Edge wear is characterised as a slim area of disruption on the hard edge of acetabular liners and stripe wear is characterised as the long slender pattern of roughened damaged surface on the head as seen in Figure 19. This kind of wear is unique to ceramic-on-ceramic bearing surfaces. Stripe wear in initial alumina and zirconia (first and second generations) bearings were reported to be associated with steep cup angles, revision surgery and younger patients [246]. It was believed that edge wear complication would be eliminated with advancement in material technology and improved surgical technique. However, studies involving third generation HIPed alumina bearings reported edge wear as a persisting complication even though desired fixation and implant positioning techniques have been employed [241]. It was theorised that micro-separation occurs under the swing phase the centres of the bearing which leads to edge loading

at the heel strike. Later in 2000 Lombardi *et al.* confirmed this theory by 3D modelling and video fluoroscopy [247]. Walter *et al.* elaborated this further in his edge loading study [15]. Although the volumetric wear rate is comparatively very low in ceramic-on-ceramic bearings, the high incidence of stripe wear still remains a concern [15]. Even with such low wear rates and inert wear debris, study of long term data is still lacking.

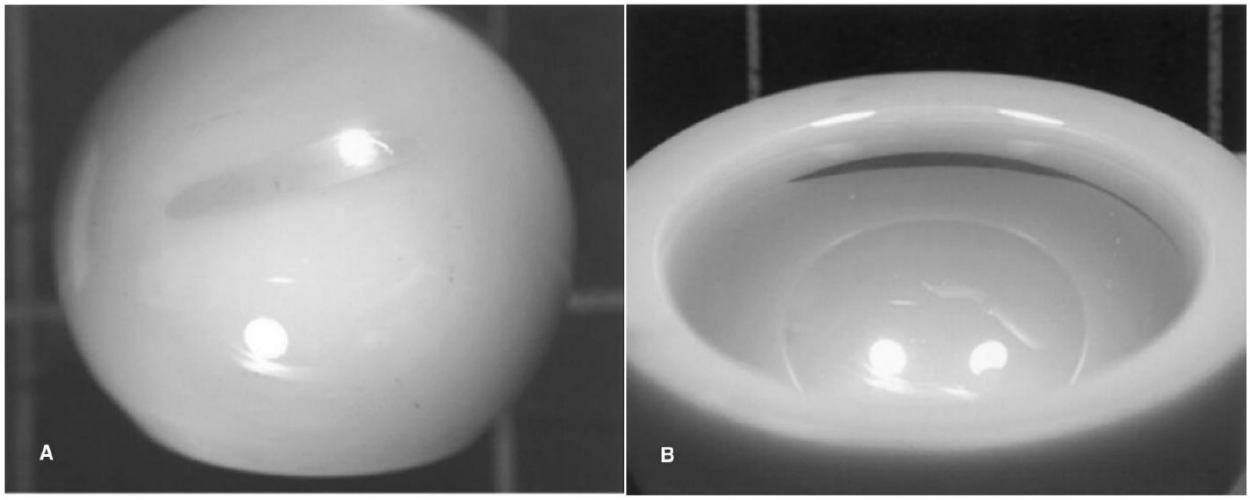

Figure 19: Stripe wear on femoral head (A) and edge wear on acetabular cup liner (B) [15].

2.6.3.4 Complications

Fracture is a major complication faced by ceramic-on-ceramic bearings. As mentioned previously, ceramic bearings have been extensively researched and advanced over the past four decades. Each generation has evolved in regards of composition and manufacturing process to address the limitations of the previous generation [87]. Fracture rates of first generation alumina ceramics were reported to be between 10% and 13% [86]. Zirconia ceramics exhibited better fracture resistance, but the inferior wear properties lead to the downfall. Fracture rate of approximately 0.02% was reported for BIOLOX® Forte for both femoral heads and acetabular liners [248]. Most recent fourth generation alumina matrix composite ceramics (BIOLOX® Delta) exhibited a fracture risk of 0.02% for the liner and 0.002% for the head [249].

Post-operative squeaking is also observed in ceramic-on-ceramic bearings and is recognised as a cause of early revision [250]. Charnley observed squeaking in hip while he was *in vitro* testing the ceramic-on-ceramic bearings designed by Boutin [251]. Reports also shows incidence of transient squeaking in 3.9% of metal-on-metal implants [252]. The cause of squeaking in ceramic-on-ceramic bearings is multifactorial depending on component orientation, surgeon factors and patient factors. However, squeaking is believed to be the result of vibrations from micro-separations. It has been postulated in a retrieval study that squeaking is induced by edge loading [253]. Incidents of squeaking in ceramic-on-ceramic bearings are reported to be 0.5% to 20% [11, 12, 254].

After exploring the advantages and disadvantages of ceramic-on-ceramic bearings, it is evident that the fourth generation ceramic-on-ceramic are superior to rest of the current alternatives. The outstanding biocompatibility of ceramics and extreme hardness assures the lowest values of aseptic loosening in the orthopaedic industry. This in conjunction with the high wettability of ceramics that aids in better lubrication of the bearing surface gives the lowest wear rates in hip joints. In comparison to alternatives like metal on UHMWPE the only factor that modern literature does not favour is the low rate of fracture in metal and UHMWPE compared to that in ceramic bearings.

2.7 Biomechanics & Testing

Biomechanics is a scientific discipline which studies human body through principles of mechanical engineering [255]. Pre-clinical endurance test on hip implants require defining realistic *in vivo* hip joint forces from patients. These hip joint forces requires simplification in order to be applicable for the simulator tests [256]. In this section, biomechanics of hip joint is explored to the study the movements of body and its effect on the hip joint.

2.7.1 Human Gait

The human gait is described as the locomotion achieved by the movement of human limbs. This subsection details the gait analysis of a hip joint. The time interval between two consecutive incidences of one of the repetitive actions of walking is one gait cycle. A gait cycle is divided into two phases – stance phase and swing phase (see Figure 20). In order to understand a single gait cycle, assume the cycle starts when the left feet is raised to swing further. This raising of left leg is the first step of the swing phase as described in Figure 20 and the left leg remains in the swing phase until it hits the floor again. Subsequent to touching the floor, the left feet enters the stance phase where it acts as a support to the right leg. During walking, there is an incidence when the body is supported by both the legs, and hence the stance phases overlap. Contrastingly in case of running, there is a period when there is no ground contact and the phases are separated. Heel strike initiates the stance phase and gives a temporary force spike that is followed by the ground reaction force which is a little more than the body weight (BW) due to the deceleration of the body. This along with the acceleration force caused by lifting the other toe generates a typical double peak curve as seen in Figure 21.

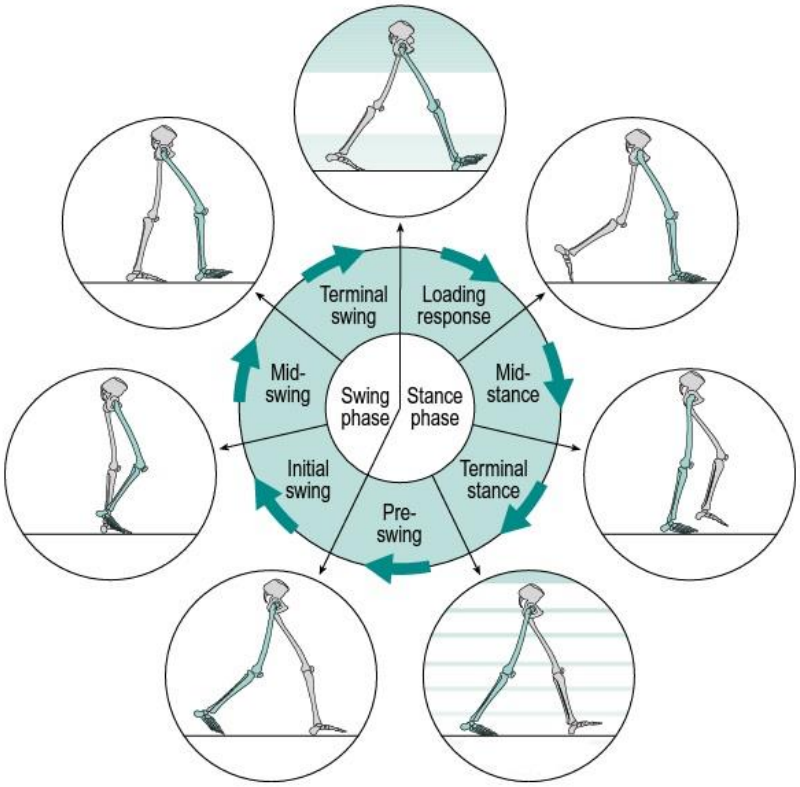

Figure 20: Image showing swing phase and stance phase of a single gait [255].

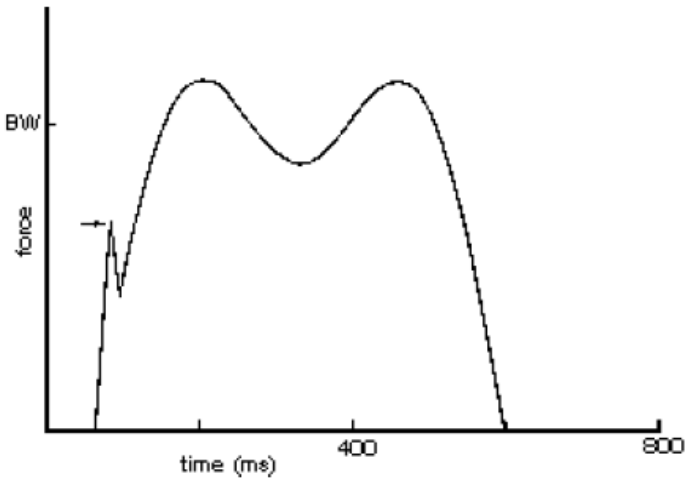

Figure 21: An image showing the graph of the ground reaction forces from a walking gait cycle [257].

2.7.2 Hip Joint Forces

The forces acting at the hip joint varies with the patient's body and the activities they perform. Hip joint forces differ with different gait patterns and every gait pattern exhibits a pattern of force at the hip joint. The magnitude of hip joint forces differs as per patient's body weight and hence are expressed in terms of body weight. High contact forces and implant twisting moments are thought to be associated with implant loosening [258]. Hip joint force information is essential to test and improve strength, wear and fixation stability of hip implants and to optimise the hip implant design and materials through computer simulation. They also provide essential guidelines to patients and physiotherapists to recognise the activities that should be avoided after a total hip replacement. Hip joint force information is also necessary for *in vitro* testing of the hip implants. Relationships between hip joint forces and gait patterns are not yet well understood, despite repeated findings that gait of a patient after a total hip arthroplasty does not completely return to normal [258].

There are two methods by which the forces at the hip joint junction can be determined. In the first method the reactions forces of the ground during the gait is determined along with the video analysis of the gait [259]. In this analysis the motions of the limb segments are traced and assumptions are made about the ligament and muscle connections and the timing of muscle action throughout gait to evaluate reaction forces at the joints. In the study, it is assumed that the forces within the muscles acting at any given period are at a very low level. However in this assumption, actions of the muscles that produce motion in opposite direction are not taken into account. Actions of such muscles can potentially be taken into account by including forces in bony elements during the optimisation routine. Such muscles are known to guard the bone against high stress levels. Most of the studies that employed this method were limited to walking, running and stair climbing [260-264].

For the second method the patient is implanted with an instrumented prosthesis to measure the direct loads at the hip joint [264-267]. The

instrumented implant records the actual forces at the hip joint. Implanting such prostheses is not a common practice due to regulatory concerns and challenges like insufficient mechanical strength and a long term power supply. However, there is an extensive amount of on-going research to develop such instrumented hip. Some of these research includes development of power supply to power instrumented hip prostheses, telemetry systems, a miniaturised customisable System-on-Chip [268-270]. Further to instrumented implants, recently a new concept of wearable sensing and feedback device is being researched. Wearable sensors have been designed with arrays of magnetometers, gyroscope and accelerometers that can be worn across by the patient to measure joint and segment kinematics [271, 272]. Systems like accelerometer have been employed to measure step count, cadence and walking speed [273, 274].

However, in 1995, Bergmann *et al*. [275] studied hip forces for the stair climbing activity by using a hip prosthesis that was instrumented with strain gauge and telemetry inside the hollow neck. To power the electronics of this instrumented hip, the patients were made to wear an induction coil induction coil during the measurement. The study found that the magnitudes of the largest force are commonly three times the body weight for normal walking and have little variation in their directions. For faster walks and jogging, the magnitude of the force can increase up to 5 times the body weight. Hip joint forces are lower in case of ascending the stair than that in descending the stairs and is 10% and 20% higher than normal walking [275]. Hip joint forces and their direction acting at the femur which are measured from the gait lab data can be converted to the pelvic coordinate system to evaluate the forces effect on the acetabulum.

In 2001, Bergmann *et al*. studied nine different routine activities in details by using instrumented implant method and studied the forces at the hip joint for each activity. The direction vectors of the force at the hip joint can be seen in Figure 23 below. It has been suggested that the muscle strength and walking speed of the patient are significant determinants of the

resultant force acting on the hip [276]. However there is a debate about the direction, magnitude and timing of the forces developed by the muscles. Bergmann *et al*. found that average peak forces of the patient during level walking at speed of 4km/h were within the range of 211% to 285% BW [260]. This was similar to the force as measured by other authors using instrumented implants [267, 277, 278]. When climbing stairs the average torque was reported to be 23% higher compared to normal level walking and for brisk walking the torque levels are of the same order [275]. However there are variations in torque during climbing the stairs depending on the patient, and the implant torque as high as 83% more than normal walking is observed for climbing stairs [260]. Bergmann had reported an incident of stumbling where the hip joint force that acted was as high as 870% BW [264].

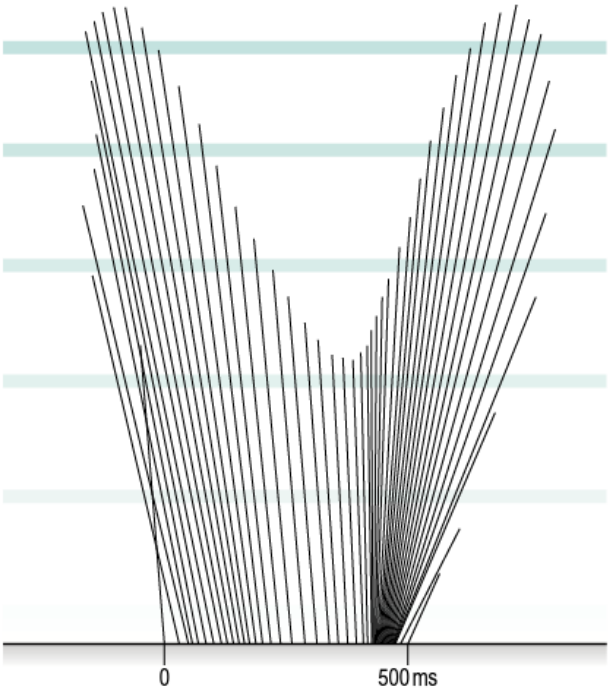

Figure 22: Image displaying a 'Butterfuly diagram' as presented by Pedotti [279]. This diagram represents ground reaction force vector at 10ms intervals [255].

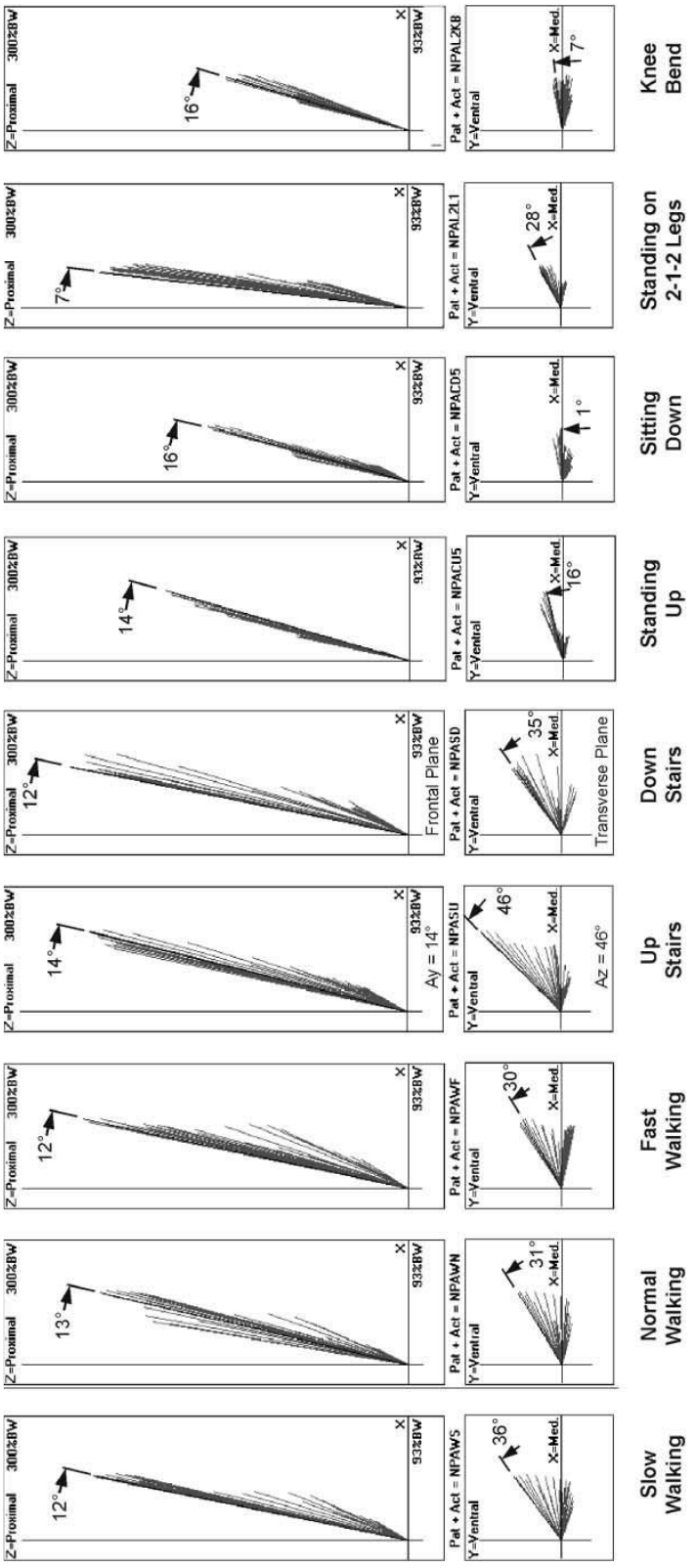

Figure 23: Contact force vector F of a patient during nine activities as measured by Bergmann et al. *Upper diagrams:* Force vector F and direction Ay of F in the frontal plane. *Lower diagrams:* Force vector F and direction Az of F in the transverse plane [260].

2.8 Methods of Volumetric Wear Measurement

Wear in orthopaedic prostheses have been the major factor in limiting the longevity of total hip arthroplasty prostheses. Wear assessment of hip prostheses is important to determine failure mechanism, functionality and to predict wear and longevity of the prostheses. It is the prime indicator of bearing's performance it allows the improvement of design, manufacturing and material quality in order to lengthen service live of the prostheses. The generation of particulate debris through wear at the interface is the major concern in relation to the operation of the bearing surfaces. Advancement in material selection has significantly reduced this wear. However, what was once easy to be measured is now outside the scope of measurement through feasibly affordable instrumentation.

Various methods like gravimetric, co-ordinate measuring machine, radiographic are currently employed for measuring wear in wear simulated and retrieved prostheses. In hard-on-hard bearings, linear wear and volumetric wear is observed to be very small as compared to hard-on-soft bearings. Bearings made from fourth generation alumina matrix composite ceramics (BIOLOX® Delta) the wear volume is observed to be as low as 0.13 mm^3/million cycle for 28-mm bearing size compared to wear rate of 1 mm^3/million in 28mm metal-on-metal and 5-10 mm^3/million in metal-on-crosslinked polyethylene [5]. It remains a challenge for currently used methods to measure the volumetric wear of such retrieved hip prosthesis bearing combinations and it is this challenge that forms the focus of the work outlined in this thesis. Gravimetric measurement is the main standardized method for quantifying volumetric wear of total joint prostheses.

Geometric measurements are now commonly employed to determine the wear volume of retrieved hip prostheses, having been developed over the last 10-15 years. Most of these geometric methods were developed, and hence can be used, to measure wear exclusively in metal-on-metal prostheses [17, 18, 43]. With the improvements in the accuracy and resolution of current coordinate measuring machines, it has become of interest to investigate the

potential of measuring very low wear rates as observed in fourth generation ceramic-on-ceramic bearings using geometric techniques. In the sub-sections below some such wear assessment methods that are currently commonly used are elaborated.

2.8.1 Gravimetric measurement

Gravimetric measurement is a laboratory method that is standardised (ISO 14242-2:2000) and most commonly employed method to assess volumetric wear hip prostheses. Gravimetric measurement is a useful method that uses a weight loss technique to evaluate the experimental volumetric wear of bearing surfaces of total hip replacement prosthesis. The hip prostheses are tested in a hip simulator machine which simulates the tribological conditions encountered in the human hip joint to artificially recreate the wear mechanism as it takes place *in vivo*. In this method the prosthesis is weighed prior to and after simulation on a high precision weighing scale and the difference in weight is used to calculate the volumetric wear of hip prosthesis based on pre-knowledge of the density of the worn material.

Like every measurement method, the use of gravimetric method has its limitations. It is only applicable for *in vitro* testing of total joint replacement performance as it requires pre-wear information of the prosthesis to be assessed. There have been documented problems in relation to measuring simulated wear volumes due to material transfer from a metallic counter-face which occurs exclusively in ceramic-on-metal or due to protein deposition, both of which can give rise to an increase in recorded weight measurement value after simulations [16, 57, 280]. Sometimes wear of *in vitro* tested components is observed at the fixation interface which cannot be separately accounted for. Such wear damage is negligible when higher wearing bearing surfaces are concerned, such as MoP, however for recent and advanced low wearing fourth generation ceramic hip prostheses the low level of wear that is experienced means that it is essential to ensure precision in wear

measurement and as such this damage can cause a significant error in the calculated value for wear.

Being a standard method, the ISO 14242-2:2016 requires the accuracy of the weighing balance to be 0.1 mg. However, the commercially available balances can measure weight as high as 560 g with an accuracy of upto 0.005 mg. Such high accuracy balance are essential in order to measure low wear ceramic-on-ceramic bearing surfaces.

2.8.2 Co-ordinate Measuring Machine (CMM)

A CMM is considered to be a powerful and important tool that can measure the overall geometry of complex components. It is commonly used to evaluate the required metrological information of a component such as size, location, form and orientation. CMM is considered as a standard tool in the orthopaedic industry for metrological assessment of manufactured components.

Figure 24: Carl Zeiss Prismo Navigator CMM (www.zeiss.com). A modern generation CMM.

A CMM physically measures a given work-piece by probing various points on the surface as defined by the user. These probed points are recorded as co-ordinates and are used to align the co-ordinate system as desired. Using this constructed alignment more points are recorded in a strategic manner to construct the feature and calculate the required size and form data on the provided software. Advanced features allow patterns and to set up more than one alignment in the work-space to perform batch work and can measure more than one component per routine.

The CMM has three axes that form a Cartesian reference co-ordinate system. The probes used by the CMM can be mechanical, optical or laser-based and are fixed to the end of the quill of the CMM. The location of a probe is detected by displacement transducers and the location of any point contacted by the probe on the surface is relayed dependent on the type of probe in operation. Regardless of the probe employed for measurement, the first step in operating a CMM is always to calibrate the stylus using a traceable calibrated artefact (usually a calibrated sphere). It is essential to calibrate the probe on a regular basis to prevent machine drift and to check for stylus damage. A calibrated probe allows the user to operate with confidence.

2.8.2.1 History

The invention of co-ordinate measuring machines came from early comparator machines which were industrialised in the former half of the twentieth century. They allowed user to perform several simple measurement tasks in a more precise and repeatable manner compared to what was previously achievable.

The first CMM (Figure 25) was developed and introduced by Ferranti Ltd of Dalkeith, Scotland [281] in the early 1950s and arrived in the British market in 1959. Initially it was designed as a companion product to numerical controlled machine tools in response to the requirement for more rapid and more flexible measurements. This was only possible with the development of a precise, long range and electronically compatible digital measuring system.

The use of an optical grating in combination with a moiré fringe sensing system made it possible. Rather than a conventional machine tool design the Ferranti CMM was a classic kinematic design which was supported by involving minimum constraints with provision of alignment of the moving elements. The Ferranti CMM opened a huge market in the industrial world and led to the advancement of similar machines with higher capacities and better accuracies and resolutions [282].

Figure 25: The first CMM introduced by Ferranti [282].

The basic principle of CMM technology has not been altered much since its first introduction by Ferranti, however recent advancement in the systems and analysis software have permitted CMMs to be more productive with much improved accuracy

2.8.2.2 CMM Configurations

Five types of CMM are commonly exist in industry; moving bridge, fixed bridge, cantilever, horizontal arm and gantry types. CMMs are versatile and are all applicable in numerous situations however some CMMs such as the gantry type have more definite applications.

The most common type of CMM in general use have a moving bridge configuration. This configuration of CMM allows the user to assess various small to medium sized components and such CMM are available in various sizes. This configuration can accommodate most manufactured components and allow measurement with small measurement uncertainty. A moving bridge configuration has a stationary table to support the work-piece and the moving bridge is supported by two columns and all three axes are able to move independently at the same time (see Figure 26). In this design there is a chance of phenomenon called 'yawing' to occur because of the two columns of bridge moving at different speeds and resulting the bridge to twist. Yawing can affect the accuracy of measurement at various location on the CMM table. However, a CMM design that implements dual drive (a drive for each column) and position feedback control system for both columns, and design that drives the moving bridge from its centreline can greatly reduce this effect on accuracy. The main disadvantage of this configuration is reduced accessibility due to the second moving or supporting column [282].

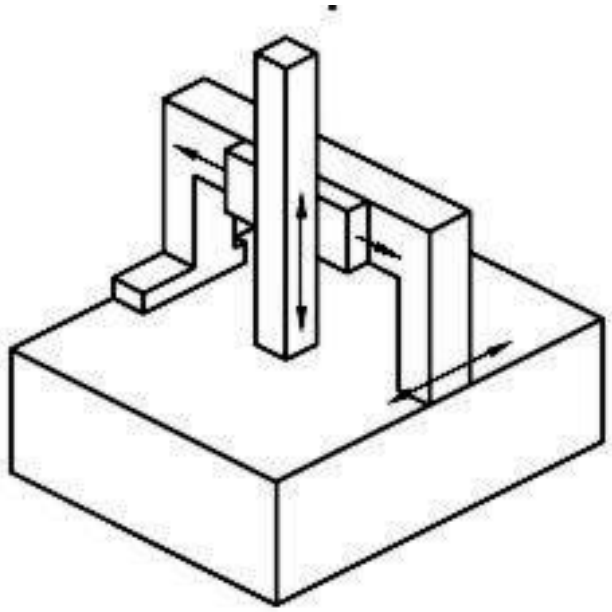

Figure 26: CMM configuration for a Fixed Bridge type [282].

In the fixed bridge configuration, unlike moving bridge configuration, the bridge is rigidly attached to the machine bed. However, the table upon which the work piece is mounted provides one of the three axes of the motion (see Figure 27). Such fixed bridge design eliminates the yawing problem faced by moving bridge design and provides high rigidity and better accuracy. Out of all the CMMs offered in the market, the most accurate CMM has fixed bridge configuration. This accuracy comes at the cost of low operating speed as it requires to move the heavy table with the part fixated on it which results in lower throughput of the machine. The maximum allowable weight is also a limitation for CMMs with such configuration. The requirement of extended guide ways to allow long table movements is a disadvantage as it requires larger space [282].

Figure 27: A CMM with fixed bridge configuration [282].

The CMMs with cantilever design are equipped with a cantilever arm that supports a carrier to move back and forth. The carrier supports the probe arm for vertical movements to move in Z axis (see Figure 28). The artefact to be measured is placed on a fixed table in cantilever design similar to that of the moving bridge. The table does not include the bearing guideways and hence can uphold heavy components without affecting the measurement accuracy. A cantilever configuration CMM with fixed table favours good accessibility to the work-piece and flexibility to mount it with three sides open, however overhead loading is generally not possible. The cantilever type CMMs usually have low mass of moving structures which makes it agile and grants the machine with higher output. All such advantages make this configuration makes it favourite general metrological applications. The bending is however a major disadvantage for cantilever type CMMs. There are chances for bending occurs when the carriage travels toward the extreme outer position. The cantilever CMMs have long table with comparatively smaller range for other

two axes and hence is more suitable for measuring long and thin components [282].

Figure 28: A CMM with cantilever configuration [282].

There are various configurations for horizontal arm-type CMMs (see Figure 29) which includes moving ram, moving table and dual ram designs. This exhibits the flexibility of horizontal arm-type CMM and they are majorly used by the automotive industry. For moving arm design of horizontal type CMMs the cantilever design gives relatively low dynamic stiffness as an inherent disadvantage of having cantilever. Moving table design is equipped with the table for one of the horizontal axes of motion and the moving column for the other. The measurement speed and accuracy for moving table design is dependent on the weight and size of the component being measured similar to that of all other CMMs equipped with a moving table. The dual-arm type design of CMM (see Figure 29) employs two identical mirror-image set of

horizontal measuring arms and moving axes which allows for measurement of two sides of a component at the same time. This makes the CMM twice as efficient and hence increasing the measurement productivity. The advantage with all types of horizontal arm CMMs is the exceptional accessibility to all sides of the part and efficient productivity. High speed of measurement is a typical characteristic of horizontal arm-type CMM. However the limited accuracy is the primary disadvantage.

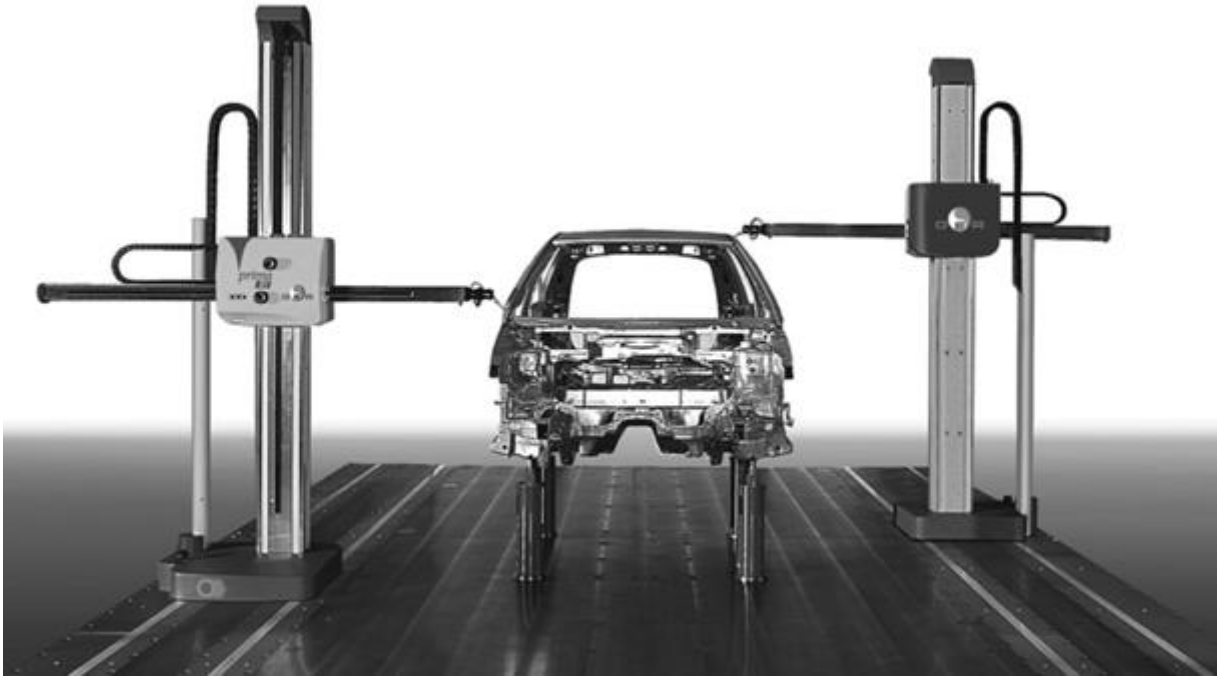

Figure 29: A horizontal arm-type CMM with dual arm configuration [282].

Gantry-type CMMs (see Figure 30) are designed and most suitable for scenarios where measurement of very large volumes ($10m^3$ or more) is required. The foundation of the machine is designed in a manner that deflection of the measurement frame is very much limited. This is essential in order to avoid the weight of the component from distorting the foundation and induce errors in measurement. Dual drive systems are often employed to prevent yawing in the travelling beam. The software correction algorithms have been developed to compensate the geometric distortion caused by loading and temperature effects which permits the gantry type CMMs achieve higher degree of measurement accuracy than previously achievable. Besides

the huge volume, the gantry-type CMMs has an advantage of high level of accessibility for operators. As only the horizontal beam is permitted movement the moving parts of machine weigh less which is why the accuracy achieved even for large volumes is in the medium range. The normal class in gantry type CMM is relatively low, however if better uncertainty is essential, the costs can increase due to the requirement of special structure and foundation [282].

Figure 30: A CMM with gantry-type configuration [282].

2.8.2.3 Hardware Components

Although the CMM configuration has a certain effect on its performance, there are various other factors that contribute to the overall efficiency of a CMM. One of such factors are the hardware components of the CMM. The hardware components include structural element, drive system, measurement

and displacement systems, bearing support, probe head, and control system [282].

The structural elements comprise of the machine base, table for the work-piece support, slideways, machine columns and ram. The characteristics of these structural elements directly affect the measurement performance and accuracy as they guide the measuring probe or the work-piece for the position feedback systems. Dimension stability is one of the most essential characteristics required for the structural elements. Granite is naturally seasoned and has low thermal conductivity and hence is recognised to be the most suitable material for structural elements and often used as a basic element in CMMs. However, granite is affected by liquids if not guarded and can alter its shape [282].

Bearing systems directly affect the measurement accuracy of a CMM and can influence the drive system characteristics and because of this they are very important. Generally, there are two types of bearings used in a CMM machine, i.e. air bearing (non-contact) and mechanical bearing (contact). Air bearings use a thin film of pressurised air to support the load. Air having low viscosity requires a tight gap of 1-10 μm. Mechanical bearings like ball bearings or sliding guideways are mostly employed for CMMs that are designed for high precision machine tools. Mechanical bearings are capable to endure heavier loads compared to air bearings and are mainly equipped in CMMs developed for harsh factory environments [282].

Displacement transducers, combined with a probe, determine the position of the work-piece in all the three linear axes of the CMM. A Variety of displacement transducers like laser interferometers, optical linear scales, magnetic scales and rotary encoders are employed for CMMs. However, the most commonly used displacement transducers are laser interferometer and optical linear scales. Optical scales utilise grating scales that has a pitch of approximately 100 lines per mm which are then read by electro-optical read head that senses interference fringes from the light reflection cause by the scale and reference grating. Laser interferometer scales are used in high

accuracy machines and their cost is relatively high compared to interferential scales. They work by the well-established light interference principles that are used for surface texture measurement. Basically, it has a laser light source two mirrors and an interferometer, where a beam splitter splits the laser into two separate beams, one part of laser is used as a reference and the other is used to create interference with that reference beam. Reference beam is directed to the fixed mirror and the other beam is directed to the moving mirror. A phase change takes place among the beams by displacing the movable mirror and when the beams combine again the beams interfere and produce countable fringes which can determine displacement. As the optical linear scale employs optical gratings on material standards as reference and laser interferometers uses laser wavelength in the medium, the factors that influence accuracy differ for both the systems. The major factor influencing the accuracy of optical linear scales are grating accuracy, temperature, and thermal expansion coefficient of the scale material. Whereas, major factor influencing is the refractive index of air, which is mainly affected due to humidity and temperature. Typically, optical scales have a resolution of 0.1 – 1 μm, whereas laser interferometers provides resolution of 1nm or smaller than that [282].

2.8.2.4 CMM Probe

Probe is an important hardware component that is used in all CMM as an interface between the machine and the work piece to be measured. All geometric measurements in coordinate metrology are established by positions and distances of a set of points detected on the physical surface of a work piece. Probing systems are employed to detect the position of these points with respect to the coordinate system of a CMM. In early days, CMMs used hard probes to contact the work piece surface manually until Sir David McMurtry of Rolls Royce Group invented touch trigger probe system (see Figure 31) in 1972. This invention carved the way for developing more

advanced probing systems and sophisticated CMMs with higher accuracy [282].

Touch trigger probe system is the most commonly used and most widely available type of modern probing system. In the touch trigger probing system an electrical signal triggers the reading of Cartesian position of the probed point on the measuring component when the probing force on the component exceeds an electronically or mechanically controlled value. The measurement uncertainties of electromechanical method used in the touch trigger probing systems are dependent on measurement direction and preload due to forces induced by acceleration and deceleration. Uncertainties caused by such forces form a triangular pattern and are termed as lobing errors [282]. With the use of piezo sensors in the probes that are sensitive to tension and compression these uncertainties can be reduced [55].

Figure 31: The original three dimensional touch trigger probe invented by Sir David McMurtry in 1972 [282].

Whereas a touch trigger probing system only detects a few distinct probing points, there are measuring systems that allow for maintaining

contact with the surface of the measuring component and collect thousands of points on their travel path along the surface. This process is known as scanning. Continuous measuring probing systems function by the inductive principle for displacement measurement. The movement of a magnetically soft core inside a coil results in a change of inductance according to the position of the core inside the coil and generates signal that are proportionate to the distance. The probes are able to measure in all the three axes at the same time as the probe head is fitted with three separate signal systems. Hence they can determine force and direction vectors directly from the displacement and simplifies probe bending correction [55, 282].

2.8.2.5 CAD Directed Inspection

Introduction of CAD/CAM systems has greatly evolved the dimensional measurement of three-dimensional artefacts that have freeform surfaces or complex contours. The CAD model of any artefact is geometric information of that artefact which is stored electronically in the CAD file. As CMMs operate by point-to-point sampling, they can be programmed to measure the artefact by using the artefact's geometric information stored in the CAD model. A CAD directed inspection generates various points on a CAD defined object according to surface definition and then commands the CMM automatically to execute the inspection [283]. It is similar to programming a CNC machine for a desired machining process. A major advancement in geometric inspection based on three-dimensional CAD model was the invention of direct computer controlled (DCC) inspection paths and routines by the use of a CAD model. DCC inspection routines uses the datum and surface geometrical information from the CAD model to guide the probe. The CAD directed inspection allows for the scanning process of an artefact mentioned in the previous subsection. CAD directed inspection is a powerful tool to evaluate the magnitude and position of part deviations from the designed model.

2.8.2.6 Reverse Engineering

Reverse engineering is a process of replicating an existing component without the help of engineering drawings or CAD models. In engineering, usually the product designer produces an engineering drawing or CAD model showing how the component is required to be manufactured, and then the object is manufactured as per the details in engineering drawing. Whereas in reverse engineering, the steps are inverted. Engineers first identify the components and study its structure, physical dimensions and geometrical features. Then a CAD model or an engineering drawing of the component is generated by utilising the identified dimensions and geometrical features. Then finally the original component is precisely manufactured from the generated CAD model or engineering drawing. Reverse engineering is desirable in various scenarios such as analysing competitor's component, updating obsolete component with modern technology, performing finite element analysis or other computational analysis on artefacts that has no design information.

High precision is of utmost importance while recording the dimensions and geometric features of the component that is required to be reverse engineered for the component to be accurately reproduced or analysed. CMMs can be employed to precisely define the dimensions and geometric features of a complex and free form components and to reverse engineer that component. CMM also allows to record coordinate points quickly compared to conventional tools either as a single point probing, contact scanning or laser non-contact scanning. These probed or scanned points are stored electronically as a point cloud that represents the coordinates of the component's surface. This measured point cloud is than exported to specialised CAD software to produce a CAD model or to analyse the surface.

2.8.3 Roundness Measurement Machine (RMM)

The roundness measurement machine (RMM) is effectively a contact surface profilometer that allows for circular measurement. They are used to

measure surface geometries such as cylinder, cone and sphere. Primarily contact profilometers are employed for surface metrology but can also be used for dimensional measurement. In roundness measurement machine a diamond tip stylus is moved in contact with the surface of the measuring component. The on which the component is placed rotates around the axis which is aligned with axis of the component prior to the measurement. Roundness measurement machine measures small surface deviation horizontally by reading the stylus displacement on the surface. Typically a RMM can measure horizontal features as small as 10nm. The end tip radius of the diamond styli ranges from 500nm to 25μm.

The major advantage of surface profilometer is the fully developed and well established methodology. Most of the surface finish standards are specifically made for contact profilometers. RMM is also a contact measurement system and hence is not sensitive to colour or surface reflectance from mirror polished surfaces. However a major disadvantage of RMM is the a diamond tip stylus, which is a very hard material, can possibly scratch the surface of the component being measured, particularly if the component is manufactured from soft material like plastic [284]. Hence roundness measurement machines are not used to measure orthopaedic prosthesis made out of materials like UHMWPE or highly polished metallic surface as they can be easily scratched by the diamond stylus tip. However, the fourth generation ceramics being a very hard material remain unaffected by the profilometer measurement.

Surface profilometry is now seen as a bridge between specialised surface characterization measuring machines such as white light interferometers and geometric measurement devices such as co-ordinate measurement machines as profilometers can carry out some functions of both. Profilometry is still a widely used technology and has great use in many different sectors of industry including automotive, biomedical and aerospace and consequently there is still a great degree of hardware and software development in this area.

2.8.4 Review of Existing Wear Measurement Methods

The characterisation and quantification of the wear of prosthesis materials, both, for *in vivo* clinical applications and *in vitro* laboratory simulations is still one of the most important topics for researchers [4–7]. Recently methods like gravimetric, CMM, radiographic and optical methods are employed to measure and evaluate the wear in total hip arthroplasty components.

Gravimetric method is the most common and standardized method to quantify volumetric wear of hip prosthesis. This method is effective for evaluating experimental *in vitro* volumetric wear, however the use of gravimetric is not feasible for evaluating the wear volumes of retrieved prostheses as it requires pre-wear measurement [17-19]. For this method, the bearing components are weighed before and after wear simulation and the difference between the two obtained values is calculated. The calculated value is the required loss of mass, which divided by density gives the volumetric wear. As per ISO 14242-2:2000, the method requires the balance to have an accuracy of ±0.1 mg [19]. Information obtained by gravimetric method is limited to volumetric wear, it is unable to characterise the surface wear and or plastic deformation of the prosthesis material. Also, in case of *in vitro* measurements, significant errors are noted due to metal transfer through metallic materials or bone cement attached to UHMWPE components [285, 286].

Co-ordinate measurement method has been an alternative method to gravimetric method for *in vitro* measurements [16, 18]. CMM method is a geometry based method that allows the user to quantify the wear volumes. The CMM method's ability to characterise the wear distribution along with quantifying the wear volumes is an advantage over the gravimetric method. Various studies states the advantage of the CMM method over the gravimetric method [285, 287-291].

For *in vitro* testing, the geometry of the component is measured before and after the wear simulation and then measurement data are compared to

assess the wear volumes. The use of CMM to define volumetric wear rates *in vitro* prostheses is standardised by ISO 14242-2:2000 [16, 19]. ISO 14242-2:2000 specifies the principle and detailed procedure to be followed by the user who intends to measure acetabular components by using the gravimetric method and the CMM method. The standard warns the users regarding the organic deposits that affects the measurements, usually in hard-on-hard bearing combinations and suggests cleaning techniques to the users. According to the standard the permissible axial-position error, D, of the CMM should not exceed $D = 4 + 4l \times 10^{-6}$ µm. The standard required the mesh spacing to be less than 1 mm in horizontal plane or along any arc for optimal measurement. The standard does not mention the details required to determine the wear distribution and its location which leaves the measurement analysis unclear. Hence, it can be said that information outlined in the standard is incomplete and the given details are not up to date with the current standard.

Another advantage of the CMM method over gravimetric method is that it does not require pre-wear measurement data and hence can be employed to assess explanted prostheses. In order to assess clinically retrieved prostheses, due to lack of pre-wear data the unworn regions of the component are used to reconstruct an estimation of an unworn geometry. Many authors have employed this method to assess simulated or clinically retrieved prostheses [43, 289, 292, 293].

In 2001, Anissian *et al.* employed the CMM method for an *in vitro* experiment to study the wear pattern of the metal-on-metal bearings (Metasul™, Suzler) [292]. The authors employed computerised CMM (CMM 5, SIP, Geneva, Swizerland) to measure linear wear in the femoral head and the acetabular liner. The accuracy of the selected CMM was not mentioned. The spatial resolution in the measurement area was kept less than 1µm. The chosen measurement strategy included a co-ordinate measurement at an interval of 7.5 degree on 12 concentric circles and a measurement at the pole which gave a total of 577 points per measured component. Interestingly, the

author defined the wear by using the maximum deviation from an ideal sphere. This method provided the maximum linear wear penetration and not the mean wear of the component. The details of the ideal sphere constructions were not given, however the author claimed an accuracy of the wear measurement to be ±2 μm.

In 2005, Morlock *et al.* analysed failed and clinically retrieved hip resurfacing prostheses from random institutes by the CMM method. The prostheses were measured using a Mitutoyo BHN 805. CMM measurement strategy employed 1mm ruby stylus to measure sixteen equidistant planar scans through the pole at an interval on 11.25° starting and ending at the equator with point spacing of 0.5 mm. Such measurement strategy led to maximum point space of 8 mm at the equator between each planar scan which will result in huge measurement triangulation errors. Authors recognised that the use of worn area for generating the reference best fit sphere can induce error and hence eliminated the worn surface from the best fit sphere data selection. They also made an interesting note of fitting an ellipsoidal reference surface instead of a best fit reference sphere for the deformed components in order to eliminate error especially at the equator region of the bearing components. However they discounted the triangulation error at equatorial region induced through the measurement strategy. The accuracy of the CMM used for this study was not mentioned in this publication, however Morlock published another study in 2008 [293] in which he analysed 267 retrieved hip resurfacing prostheses by the same method and mentioned the accuracy of CMM to be ±3 μm.

In 2007, Bills *et al.* [289] developed a metrological solution with an aim to gain better understanding of the tribology and the true *in vivo* performance of the hip prostheses. They employed a Zeiss Prismo CMM (Carl Zeiss Ltd., Rugby, UK) to measure UHMWPE acetabular components of various designs and sizes. The probing accuracy and the scanning accuracy of the employed Zeiss Prismo CMM was stated to be 0.7 μm and 1 μm respectively which was lower than previously suggested minimum accuracy of 2 μm for analysing

wear of hard-on-hard bearing [288]. The authors created an apporimate CAD model in order to define the measurement location of the measurement points. A methodology was developed to generate the reference unworn geometry due to the lack of pre-wear data. Procedure to generate the reference geometry involved measuring points in the unworn region of the bearing component. Subsequently, Non-Uniform Rational B-Splines (NURBS) were fitted through these measured points in the unworn region to develop reference geometry that imitates the unworn surface. The measurement grid of 0.5 mm × 0.5 mm was developed to measure the component. The bearing surface was isolated and the deviation between the measured bearing surface and the generated unworn reference geometry was computed in order to characterise the wear distribution and wear volumes were calculated.

In 2008, Witzbel *et al.* conducted a study with the purpose of investigating the clinical wear performance of the explanted Birmingham Hip Resurfacing (BHR) prostheses. The CMM employed for the study was CMM5 (SIP, Geneva, Switzerland) that had a spatial resolution of less than 1 μm. The measurement strategy employed by the authors measured a point at an interval of 5° on 18 concentric circles and at the pole which, as stated by author, gave a total of 1297 points for femoral head and 865 measurement for the acetabular components. However the measurement strategy as stated is confusing and suspected to be missing information as according to the measurement strategy, the number of points measured for femoral head and acetabular component must be equal, unless only 12 concentric circles were measured at 5° interval or 18 concentric circles were measured at 7.5° interval for the acetabular component. Regardless, the author developed a mathematical model in order to assess the linear and volumetric wear. The mathematical model was a representation of an ideal hemisphere which was divided into two regions, worn and unworn, for the assessment. The author defined linear wear as the maximum deviation of the worn region from the unworn region of the mathematically developed hemisphere and volumetric

wear was calculated as the weighted sum of the volumetric deviation in the worn region.

In 2011, Carmignato *et al.* conducted a study to evaluate the uncertainty of the CMM volumetric wear measurement method. The study used nine new femoral heads which were measured before and after the wear simulation by the gravimetric method and the CMM method. The gravimetric used a micro-balance (SARTORIUS AG, Germany) with an expanded measurement uncertainty of ±0.1 mg. The CMM (Zeiss PRISMO VAST 7, Germany) was employed to measure surface of worn and unworn femoral heads. The CMM was in a temperature controlled room at 20±1° and the components to be measured were stabilised by soaking them in the same temperate for 'sufficient time' as described by the author. A CAD model of a basic sphere with the same diameter to that of the femoral head was generated as a reference for measurement. The measured CMM data was then evaluated on a three-dimensional data modelling and evaluation software known as Polyworks (InnovMetric Software Inc., Canada). The author validated the CMM method by comparing the results with the gravimetric results and displaying a good agreement between the two methods. The author outlined five major sources of the uncertainty i.e. CMM probing, measured points distribution, alignment to reference datum, surface roughness and software used to determine volume.

In the same year, Bills *et al.* developed a method to measure and analyse retrieved bearings and also assessed and quantified the magnitude and effect of the measurement uncertainty on the measurement process. The study describes the importance of the expanded measurement uncertainty in measuring retrieved components and recommends the user to be cautious with the factors like point spacing and scan line distribution while performing wear measurement on retrieved components as they can have a considerable effect on the measurement result. The authors employed a Zeiss PRISMO CMM (Carl Zeiss, Germany) that had a maximum permissible error of $D = 1.9 + {}^{L}/_{300}$ (µm), probing error of 0.7 µm and scanning error of 1.3 µm. They analysed

six metal-on-metal hip prostheses of different size and consisted both modular and resurfacing design. The CMM measurement process included defining a polar grid and with point spacing of 0.3 mm in scanning mode where scanning speed was chosen to 2 mm/s. Further the measured point clouds were exported to CATIA (Dassault systèmes, France) for analysis. A best fit sphere was generated from the point cloud data by the use of least squares method as an estimate of the unworn surface. The correct fit and size of the generated sphere was recognised by the use of a fitting histogram. After analysing the components, the factors contributing to the expanded uncertainty were identified. The author mentioned three standard uncertainties, i.e. uncertainty of the calibration, measurement uncertainty, and uncertainty attributable to the material and manufacturing variations. From this study, a significant influence of uncertainty was observed and hence the author suggests to adapt the grid spacing with respect to the component size in order to minimize the uncertainty contributors.

There have been many publications [294-296] where authors utilised CMM measurements to examine creep, deformation and volumetric wear in orthopaedic implants.

Radiographic method allows for the estimation of the femoral head migration into the cup. This method can be employed prior to surgery of explanting a prosthesis. As radiographic method provides 2D imaging which at times makes it challenging to characterise wear. Limitation of radiographic method are factors like coarse image resolution, availability of initial radiographs, and wear pattern assumption [297, 298].

Each of the wear measurement method has advantages and limitations. Researches has been going on for developing effective methods. The literature works and new trends in metrological assessment of wear are reviewed. However, it has been observed that none of the method can measure wear above the bearing surface. This can significantly underestimate the volumetric edge wear measurement. Thus, a method that can quantify and characterise

wear beyond the bearing surface is essential to gain more precise estimate of volumetric wear.

Chapter 3: CMM Method Development

3.1 Summary

This chapter describes the development of the edge wear measurement method by the use of a CMM. It gives the details of the acetabular liners used for the testing and the details of the wear simulation process used to simulate wear on the acetabular liners. Further the chapter provides details of the measurement machines and the measurement strategy employed to measure the wear simulated acetabular liners. The method mentions details of the failed attempts, liners examination and various test performed to study the form of the acetabular liners. The chapter provide details of the procedure to reconstruct the unworn surface geometry in order to analyse the characterise and quantify volumetric wear. The wear results obtained through the use of the CMM method are documented and inter-operator variability is tested.

3.2 Background

For the development of a suitable CMM-based method, two cohorts of ceramic-on-ceramic acetabular liners were assessed and these cohorts are coded as cohort A and cohort B for the ease of understanding. Both, cohort-A and cohort-B, consist of six acetabular liners of 36mm diameter of ceramic-on-ceramic (BIOLOX® delta, Pinnacle®, DePuy Synthes, Leeds, UK). Firstly, wear was simulated on all the liners from cohort-A for which the Leeds II hip joint simulator (Institute of Medical and Biological Engineering, University of Leeds) was employed. The simulation process was configured to run for three million cycles specifically under edge loading conditions in order to simulate edge wear on the acetabular liner. The dynamic separation occurred through translational mismatch between the centres of rotation caused edge loading between the femoral head and acetabular liner during the simulated gait cycle [299]. The simulation procedure has been proven for generating wear that is clinically relevant on the femoral head and the acetabular liner and to produce bimodal wear debris distribution as observed clinically with ceramic-on-ceramic bearings [241, 300-302].

Under the test condition mentioned above the wear was simulated on the edge and the area surrounding the edge of the acetabular liner. At the end of the simulation process (three million cycles), the components were cleaned and decontaminated by the use of local standard operating procedures before they are measured in a temperature and humidity controlled environment using a microbalance (Mettler-Toledo XP205, UK) under which they were also measured for pre-simulation data before the test commenced. The wear volume was determined gravimetrically by dividing the mass loss by using the density of BIOLOX® delta which was 0.00437 g/mm^3.

3.3 Method Development

Upon completion of the simulator test, in order to develop a method to assess edge wear without any pre-wear geometric data, each acetabular liner from cohort-A was measured in a blind study at EPSRC CIMAM, University of Huddersfield. After examining the current geometric CMM method to assess volumetric wear in hip prosthesis [17], a CMM was employed to acquire the geometric data of the simulated acetabular liners. Hence, cohort-A was measured on a Zeiss Prismo (Carl Zeiss, Rugby, UK) CMM. A ruby stylus with a 2mm diameter was employed for the measurement of both the bearing surface and the rim of the acetabular liner up to the flat plane of the acetabular liner. The measurement strategy can be seen in Figure 32. The acetabular liners were securely fastened using three jaw chucks. The room temperature was controlled and maintained at 20°C±1 in accordance with current best practice [19].

To measure the required geometric features of bearing surface and rim of the acetabular liner, a 3D CAD surface model of the liners was constructed. In order to develop the 3D CAD model, reverse engineering primitives were utilised and the geometric features of the acetabular liner were defined by probing the surface. Firstly, the flat plane on the top of the rim and the spherical part of the bearing surface were probed to define the central axis of the sphere perpendicular to the flat plane. Subsequently, a single trace was

scanned from the pole of the bearing surface to the extended flat plane in order to generate a curve that is required to create the CAD surface. The measured curve was then revolved around the defined central axis of the sphere which than produced the required CAD surface of the acetabular liner. This CAD surface was used to define measurement strategy on the CMM software (Calypso) in order to scan the acetabular liner as per requirement.

Defining an appropriate measurement strategy is essential for accurate measurement. For measurement strategy, factors such as grid pattern, angle spacing between each scan line, point mesh spacing and scanning speed have to be considered. BS ISO 14242-2 recognises that mesh point spacing majorly influences the accuracy and efficacy of the result of a measurement analysis. Mesh point spacing is dependent on three factors which are scanning strategy, distance between scan lines and point pitch along a single scan line. These three factors together produce the mesh spacing described by the standard BS ISO 14243-2:2000 [19]. ASTM F2979-14 provides further guidance regarding the measurement strategy to be employed for measuring an acetabular component on the CMM. The below described measurement strategy is in agreement with the ASTM F2979-14 [303]. The measurements carried out in this study utilised the produced CAD surface and a scanned series of 720 vertical traces (0.5° interval from the central axis) were defined to cover both the bearing and rim surface as shown in Figure 32. The scanning of the traces began from the pole of the liner and extended to the flat plane located on the rim. It is essential to maintain a continuous contact between the surface of the component and the stylus and hence, a slow measurement scanning speed was defined at 3 mm/sec and the point pitch/spacing along each trace was set to 0.05 mm. Such density of mesh is thought to be necessary in case of ceramic-on-ceramic as the wear volumes are expected to be very low and it is a recognised fact by ISO 14242-2 that mesh spacing significantly influences the results of any analysis. The calibrated maximum permissible error MPE and MPE/THP of the employed CMM was 1.99µm+L/300 and 1µm@30sec respectively. For each acetabular liner, the wear

measurement consisted of over 400,000 points, allowing for a dense high-resolution mesh of the surface to be constructed. Such a dense point cloud is required in the case of ceramic-on-ceramic components as the linear wear penetration and wear volumes are expected to be comparatively very low compared to bearing surfaces manufactured from other biomaterials such as MoM components or UHMWPE acetabular liners.

The same measurement strategy was applied for each liner from cohort-A. Upon completion of the measurement, the measured point cloud data (see Figure 32) was exported to CATIA for analysis in order to characterise wear by deviation analysis and to quantify volumetric wear.

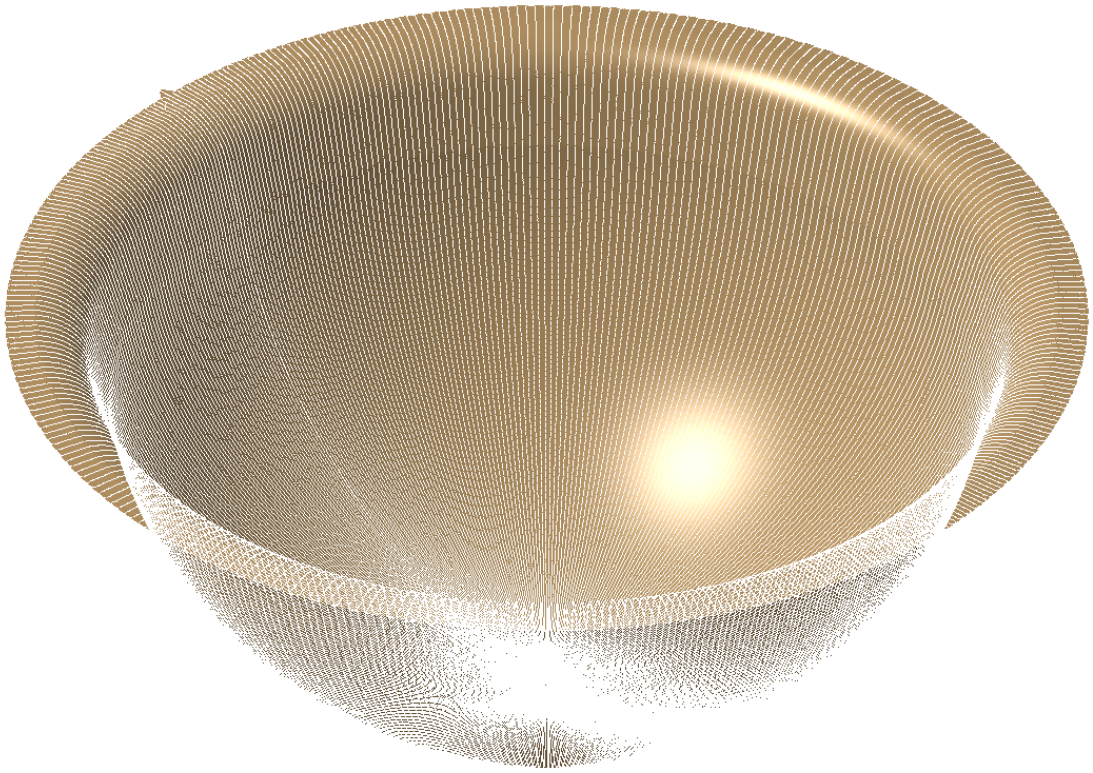

Figure 32: The above image displays the total points measured on a produced mesh for visualisation of the measurement strategy.

3.4 First Attempt to Re-Construct Unworn Surface Geometry

Analysis of the point cloud data obtained from CMM measurement was performed to characterise wear and to determine linear and volumetric wear. An attempt was made to develop a set of routines based on functions implemented in the CATIA V5 (Dassault Systèmes, France) software package.

In the first step of the analysis the point cloud data obtained from CMM measurement is meshed and prepared for analysis. The triangulation process converted individual points into a digital map of the surface that can be evaluated. Due to an increased number of points all relevant features such as the wear area and edge geometry appear visible to the operator when rendered.

In order to reconstruct a geometry that imitates the unworn surface, the first attempt made was similar to that of generating a 3D CAD surface on CMM for defining the scanning strategy. A vertical planar section was created on an unworn area of the acetabular liner and was converted into a curve that can be utilised for CAD modelling. This curve was then revolved around the Z-axis, which was the central axis of the bearing surface sphere perpendicular to the flat plane of the rim. The revolved surface was then assumed to be the unworn surface geometry. A deviation analysis between the reconstructed surface and measured surface mesh was computed and is displayed below in Figure 33.

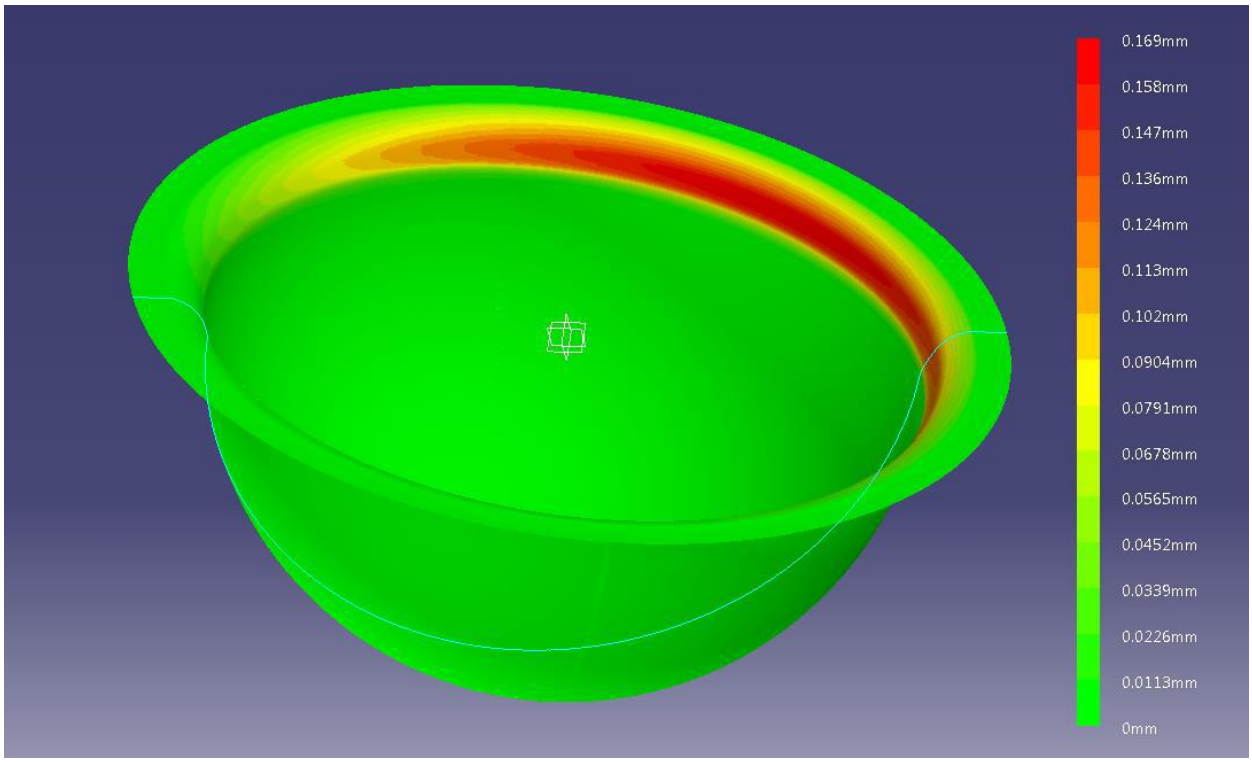

Figure 33: Result of deviation analysis performed between the surface reconstructed by the first experiment and the measured surface.

Through deviation analysis it was observed that the surface reconstruction was not successfully performed and wear could not be characterised. A maximum deviation of 0.169mm was observed in the area above the bearing surface which gave an insight of the acetabular liner's geometry and it was observed that the liners were ellipsoidal instead of spherical. Hence it was essential to examine the geometry of the acetabular liners in further detail before further analysing the liners.

3.5 RMM roundness test performed to examine form of the acetabular liners through roundness traces.

In order to examine their sphericity, the liners of cohort-A were measured on the RMM. The RMM employed was a Talyrond 365 (Taylor Hobson, UK) which has a stated gauge resolution of 30nm with a spindle runout value of 20nm. The stylus employed for the measurement was a diamond tip pointed stylus with an end radius of 5 μm in order to eliminate

mechanical filtering errors caused by using larger standard sized ruby styli. Due to the nano-meter precision of RMM, the room temperature was controlled at 20°C ±1 to prevent errors induced through thermal expansion.

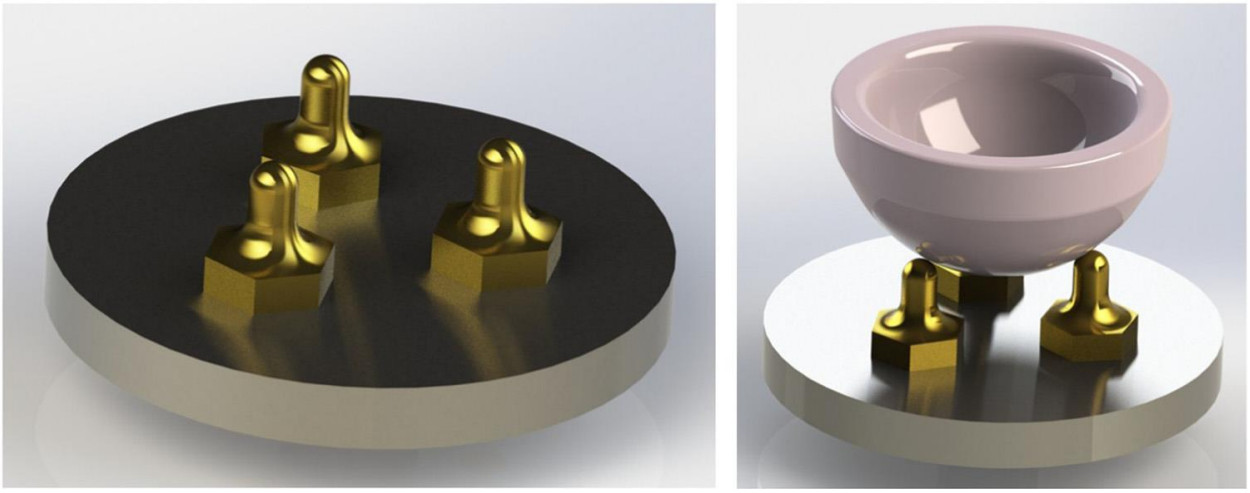

Figure 34: CAD model of a custom made three-sphere fixture.

The liner was mounted on a custom designed three-sphere fixture (see Figure 34). The three-sphere fixture was attached to a two-stage goniometer and an x-y translation stage. Prior to the measurement, an initial alignment was done manually by the operator to centre and level the component and then an automated centring and levelling routine was performed in order to attain an eccentricity of under 1µm between the centre axis of the spindle and the centre axis of the component. After achieving the required eccentricity, several roundness traces were measured on different areas of the liner including the bearing surface, the edge and the surface beyond the edge.

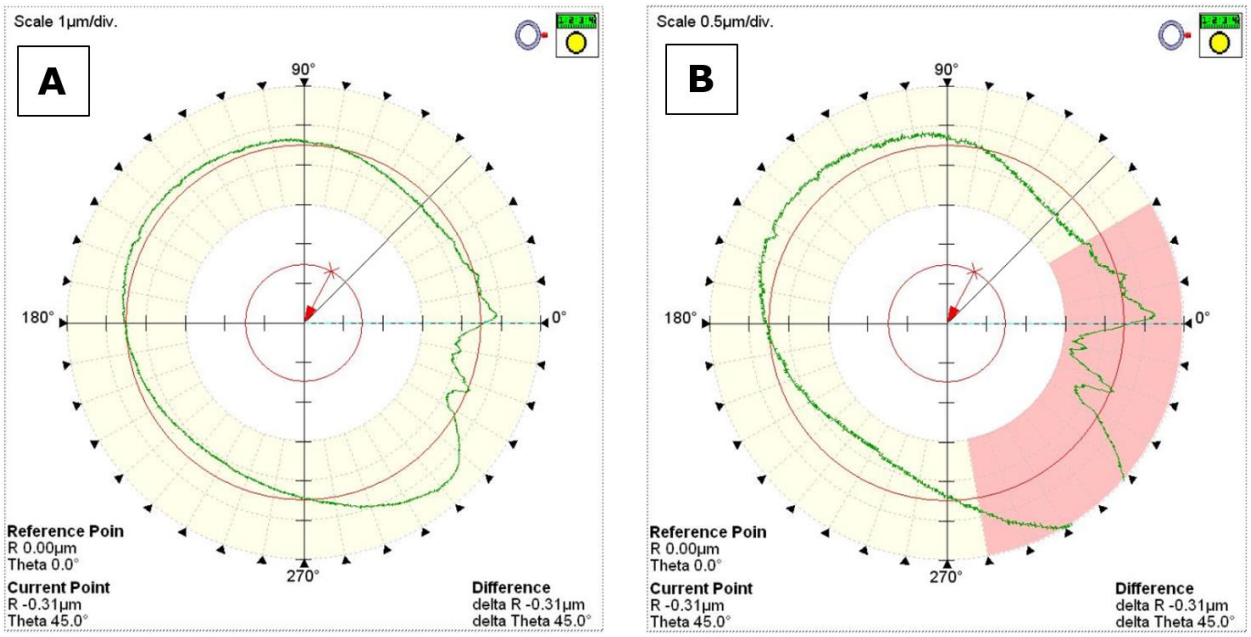

Figure 35: Image displaying the roundness traces as measured on RMM in the bearing area of the acetabular liner 2. Image (A) on the left is the actual roundness trace without elimination of any data and the image (B) on the right is the roundness trace that displays the form of the bearing surface when the wear patch is ignored.

Above Figure 35 displays the result of a roundness trace measured in the bearing surface of liner 2 from cohort-A. Figure 35-A displays the true measurement and the form of the bearing surface including the wear patch. The wear patch can be recognised as the disruption in the ellipsoidal form of the liner in Figure 35-A. In Figure 35-B displays the same measured trace however the wear patch is eliminated from the measurement to examine the true form of the bearing surface. Both, Figure 35-A and Figure 35-B, has a defined scale in the top left corner which defines the radial distance between each dotted circle. The scale in Figure 35-A is 1 µm/division whereas for Figure 35-B is 0.5 µm/division. Hence it can be noted that the resolution has increased with the reduction in scale as seen in Figure 35-B after eliminating the wear patch from the measurement. The straight dotted represents angular intervals at 10° angle. After studying the bearing surface, the edge area was explored.

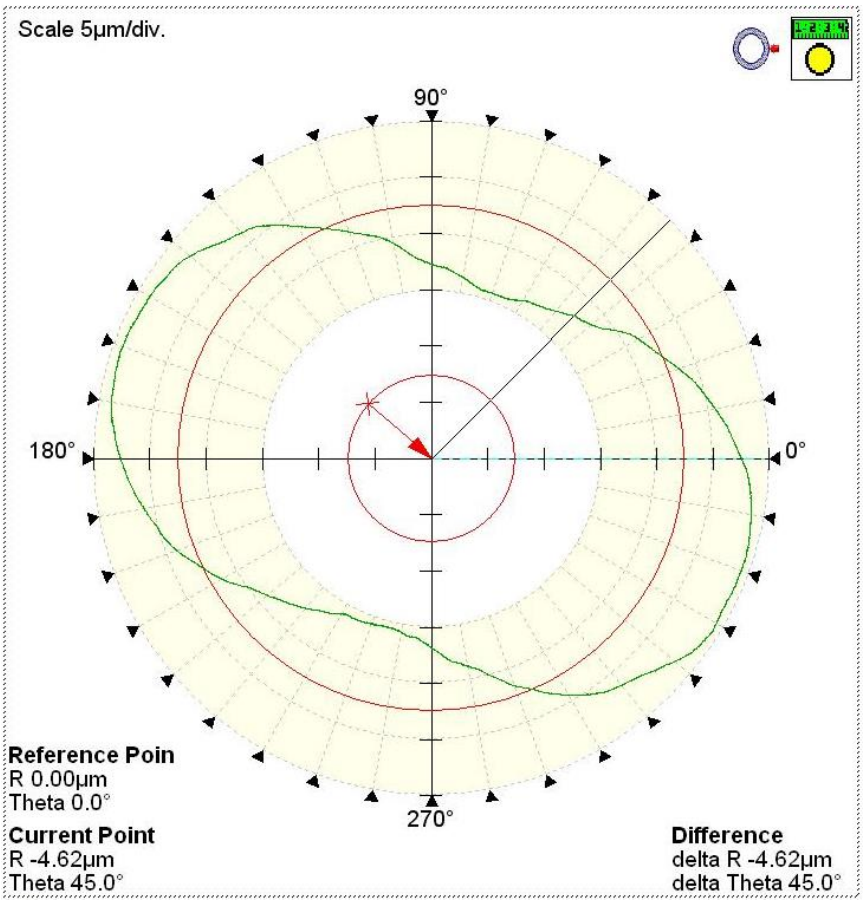

Figure 36: Image displaying the roundness traces as measured on RMM of beyond the edge area of the acetabular liner 2. The figure displays the form of the unworn area beyond the edge.

Above Figure 36 displays the result of a roundness trace measured in the unworn area above the edge of liner 2 from the given cohort-A. From Figure 36, the true form of the surface above the edge can be examined. The above Figure 36 also explains the results obtained through the initial attempt at using deviation analysis and the errors induced by using a revolved curve geometry as an unworn surface geometry in the initial analysis.

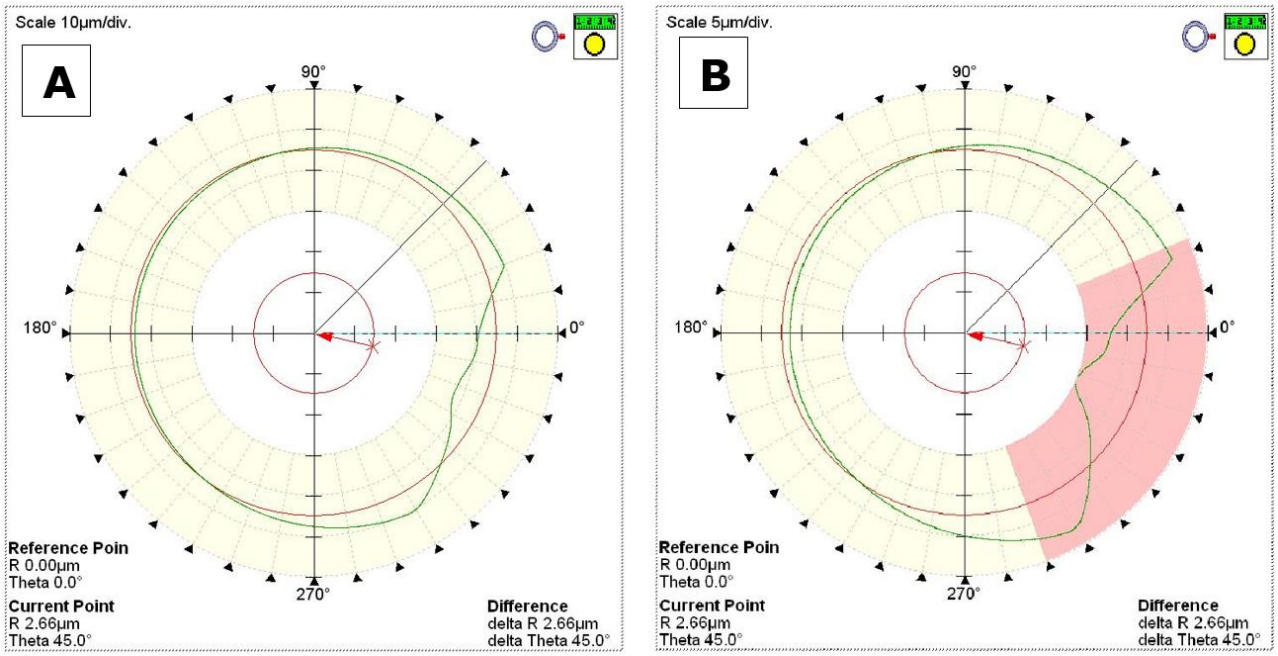

Figure 37: Image displaying the roundness traces as measured on RMM at the edge of the acetabular liner 2. Image (A) on the left is the actual roundness trace without elimination of any data and the image (B) on the right is the roundness trace that displays the form at the edge area when the wear patch is ignored.

Above Figure 37 displays the result of a roundness trace measured in the bearing surface of liner 2 from the given cohort-A. Figure 37-A displays the true measurement and the form of the bearing surface including the wear patch and Figure 37-B displays the same measured trace however the wear patch is eliminated from the measurement to examine the true form of the bearing surface. It can be noted that the given scale is 10µm and 5µm for Figure 37-A and Figure 37-B respectively, which is 10 times higher than that from the roundness trace of the bearing surface in Figure 35-A and Figure 35-B. The reason behind this is the form variation in the surfaces above the edge and the bearing surface. By comparing the roundness traces of the surface above the edge and the bearing surface it was observed that the surface above the edge is almost 10 times more uncontrolled compared to the bearing surface. Subsequent to observing these results, it became essential to examine unworn ceramic liners in order to gain better understanding of the form of the ceramic acetabular liners.

A one hundred and ten roundness traces were measured at a height interval of 0.5mm starting from the bearing surface till above the edge covering 5.5mm height around the wear patch in order to explore the overall form of the acetabular liner's surface. After studying all the roundness traces, it was observed that the ceramic acetabular liners had controlled bearing surface with minute form error, uncontrolled edge-geometry and ellipsoidal surface beyond the edge. Hence, it was evident that revolving basic geometrical shapes as employed in the first attempt, cannot be employed for reconstruction of the geometry of such uncontrolled elliptical edge and ellipsoidal surface beyond the edge of ceramic acetabular liners. A schematic view of the 5 microns ellipticity of the edge geometry can be observerd in Figure 37. Due to such non-consistent form of bearing surface, edge and the surface beyond the edge, the surface had to be treated as a true freeform in order to reconstruct the unworn geometry.

3.6 Unworn Liner Study

After studying the cohort-A of simulated acetabular liners, the cohort-B that consist of six unworn ceramic acetabular liners was examined to study the form of the as manufactured surface of ceramic liners. All the liners from cohort-B were measured on Talyrond 365 RMM. Similar to the previous procedure, the temperature was controlled at 20°C ±1 and the stylus employed was a diamond tip 5 micron stylus. The liners were placed on the custom designed three-sphere fixture and each liner went under centring and levelling process to establish an eccentricity of under 1µm between the centre axis of the spindle and the centre axis of the component. The RMM was configured to measure 100 roundness traces at the height interval 0.05mm measuring 5mm of the surface around the edge, starting from the bearing surface till the surface beyond the edge, in order to study the as manufactured surface on bearing, edge and above edge.

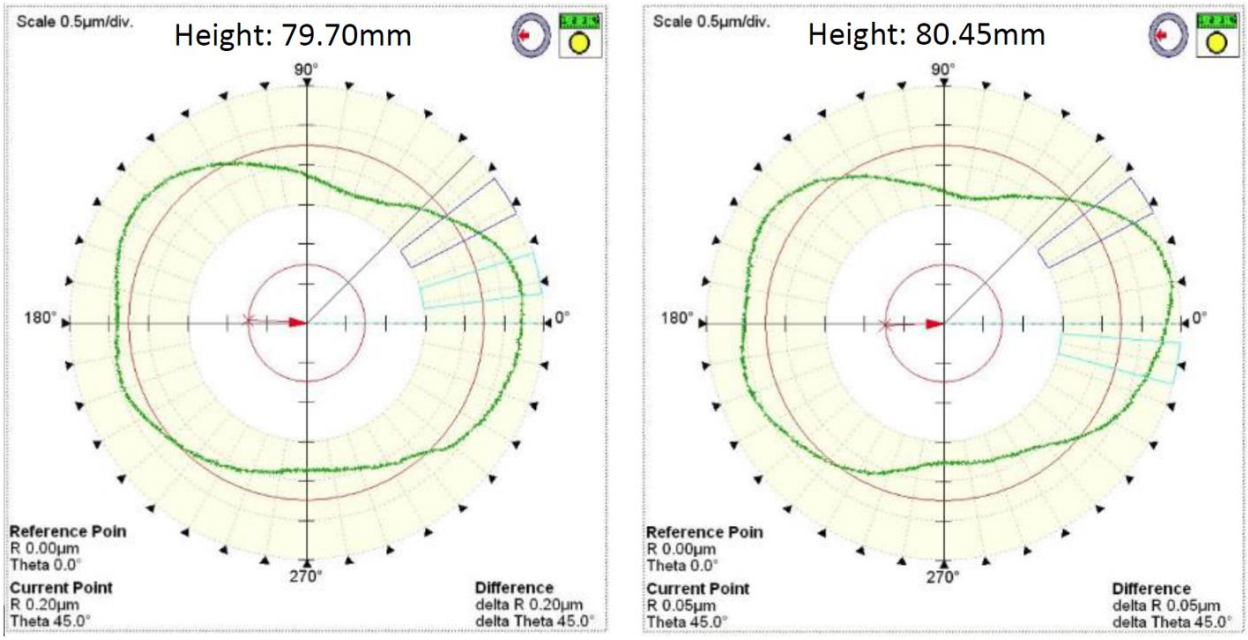

Figure 38: Image displaying two roundness traces of the bearing surface of liner 2 from the unworn cohort measured at different height to study the form of the bearing surface.

The above Figure 38 displays the result of roundness traces measured at the bearing surface of liner 2 from the unworn cohort-B. As displayed in Figure 38, both of the roundness traces are measured at different height and denotes the form of the bearing surface at that corresponding height. A minute form error was observed in the bearing surface of an unworn acetabular liner through examining these roundness traces. Such small form error of the bearing surface was observed in all six liners from the unworn cohort-B. After examining the bearing surface, the surface above the edge was examined.

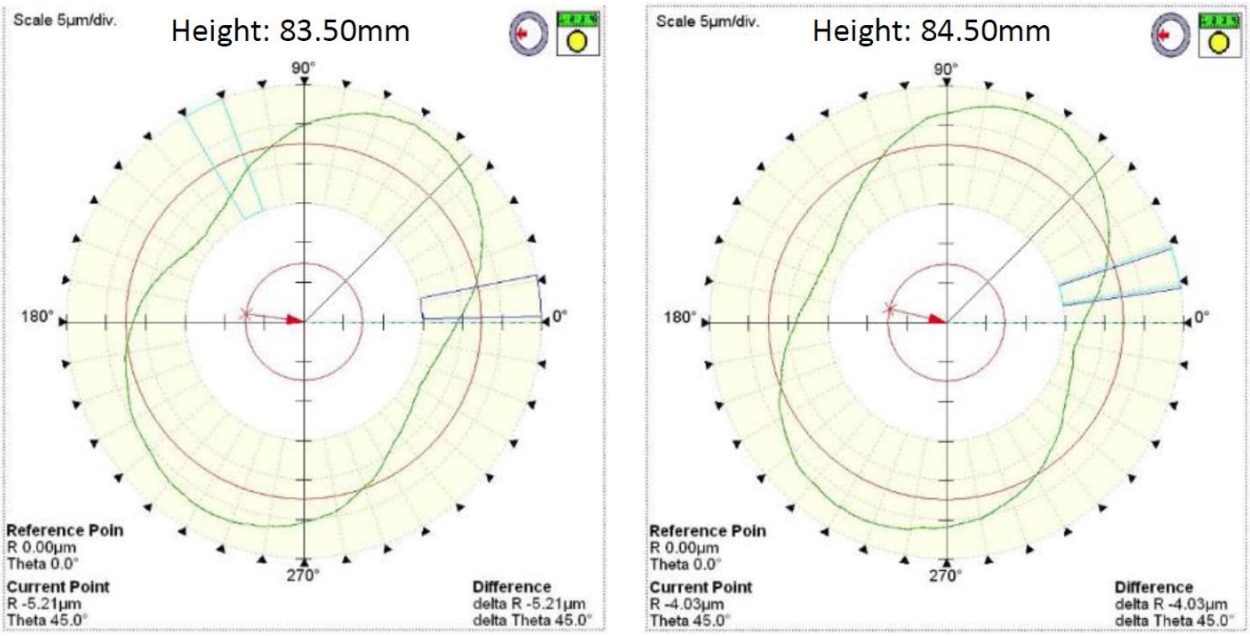

Figure 39: Image displaying two roundness traces of the surface above the edge of liner 2 from the unworn cohort-B measured at different height to study the form of the surface above edge.

The above Figure 39 displays the result of roundness traces measured at the surface above the edge of liner 2 from the unworn cohort-B. Both the roundness traces are measured at different height as mentioned in the Figure 39 and denotes the form of the surface at that corresponding height. The surface above the edge is observed to be free form again, however from the stated scale of 5µm/division it is evident that the surface above the edge is more affected by the form compared to the bearing surface. Such uncontrolled free form surface above the edge was observed for all six liners. After examining the surface above the edge, the edge variation was examined.

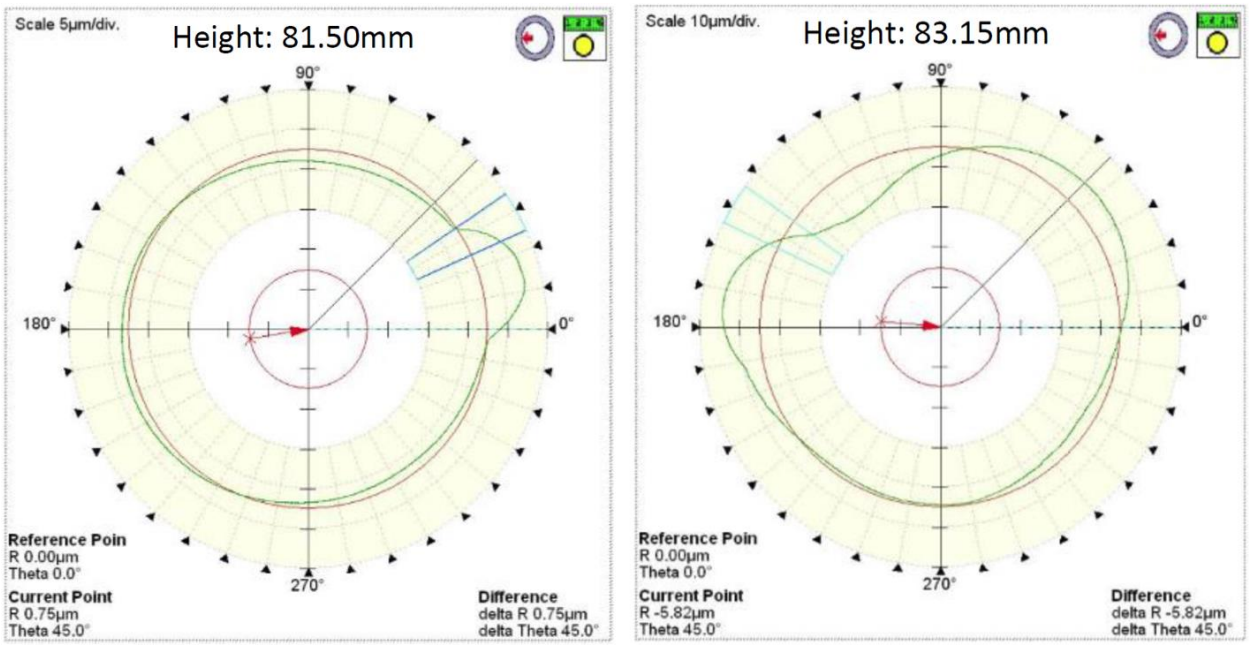

Figure 40: Image displaying two roundness traces that made the first and the last contact with the tilted edge at the corresponding height.

The above Figure 40 displays the result of two roundness traces measured at the edge of liner 2 from the unworn cohort-B. Both the roundness traces are measured at different height which is mentioned in the Figure 40and denotes the first and last contact with the edge. As the roundness traces start measuring from the bearing surface towards the surface above the edge, the first contact made with the edge was at the height of 81.50mm and the last contact made was at 83.15mm. Hence it is evident that the minimum edge deviation in height was 1.65mm (difference in height between the first and last edge contact). From this edge height deviation it is evident that the edge had a tilt which shows a defect regarding the coverage angle tolerance of the manufactured liners. All six unworn liners were studied in a similar manner to test the height variation of the uncontrolled edge. The result is tabulated below in Table 8. From the results, it can be observed that there was a significant edge deviation in height for liner 2 and liner 6 at 1.65mm and 1.20mm respectively. Through observing such significant deviation in edge height, it was suspected that a tilt exists between the central axis of the edge and the central axis of the acetabular liner which can affect the coverage angle

geometry. Hence coverage angle of each liner from the unworn cohort-B were tested and its details are mentioned in further section.

Liner No.	1	2	3	4	5	6
Edge (mm)	0.35	1.65	0.10	0.25	0.15	1.20

Table 8: Tabulated results of the minimum edge deviation in height for all six liners of the unworn cohort-B.

Overall, examining the unworn liners gave a broader understanding of the bearing surface and uncontrolled edge and the free form surface above the edge. However after observing the huge deviation in edge height it was essential to test the coverage angle of all six liners of the unworn cohort-B.

3.7 Coverage Angle Test

Coverage angle is defined as the angle between the two lines connecting the centre of the sphere and the end-points of the longest hemispherical arc of the bearing surface of the acetabular liner. The coverage angle is used to define the bearing area of the acetabular liners where the femoral head is allowed to articulate against the acetabular liner. In case of edge wear, it is important to assess the coverage angle in order to ensure that the femoral head is not articulating above the bearing surface. Any tilt/shift in the coverage angle can allow the femoral head to articulate outside the defined bearing area. Hence it is essential to assess the liners for the coverage angle.

After assessing the unworn liners of cohort-B on the RMM, they were measured on a CMM to measure the full coverage angle in each case. The liners were measured with same measurement procedure as mentioned above in section 3.2. The stylus employed for the measurement was Ø2mm ruby stylus. A scanning strategy was configured to measure 720 traces at an angular distance of 0.5° and the point pitch spacing was defined to be 0.05mm. After performing the measurement, the point cloud was exported to CATIA to analyse the coverage angle of each component.

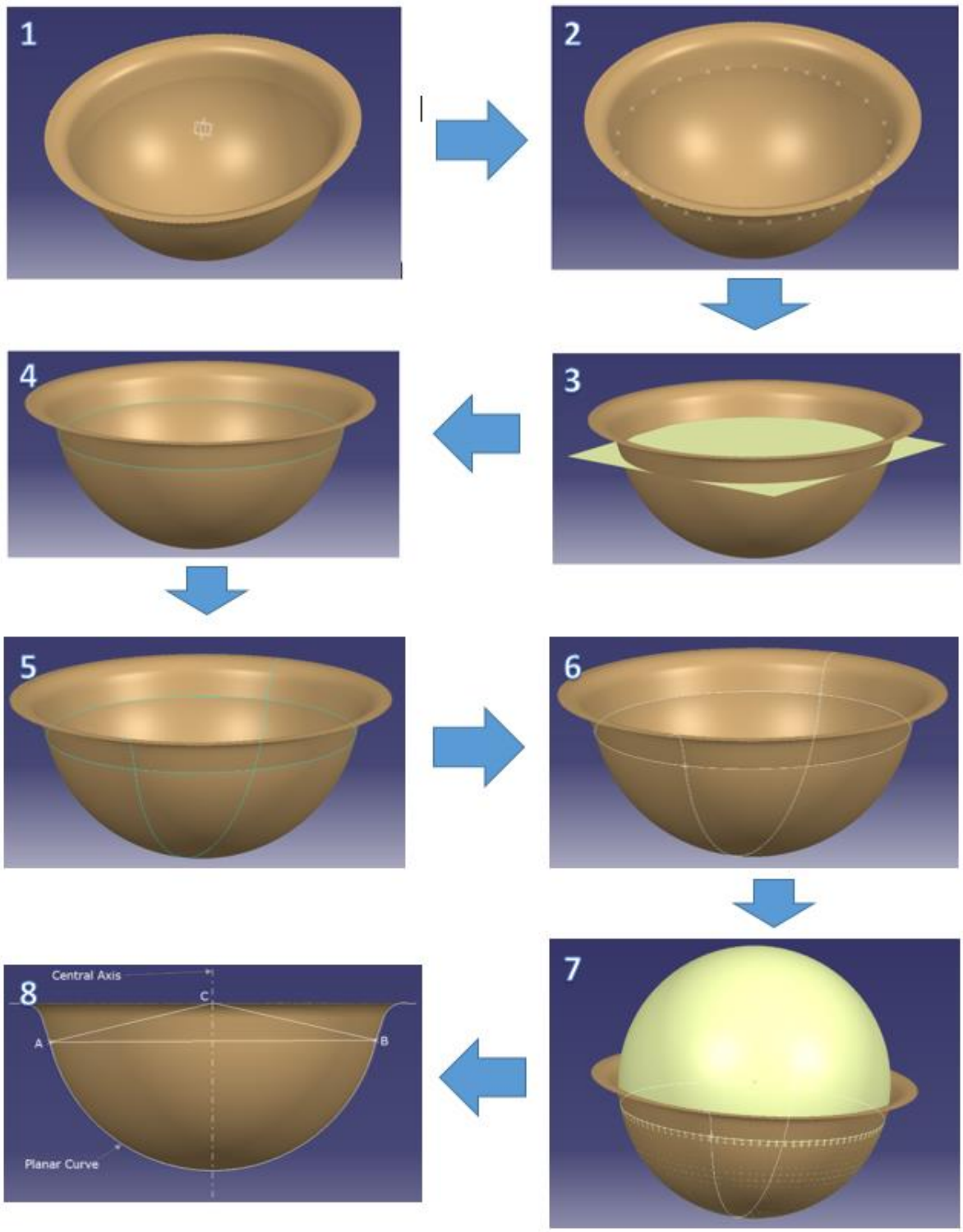

Figure 41: Schematic explaining the procedure employed to test the coverage angle of the liners from the unworn cohort-B.

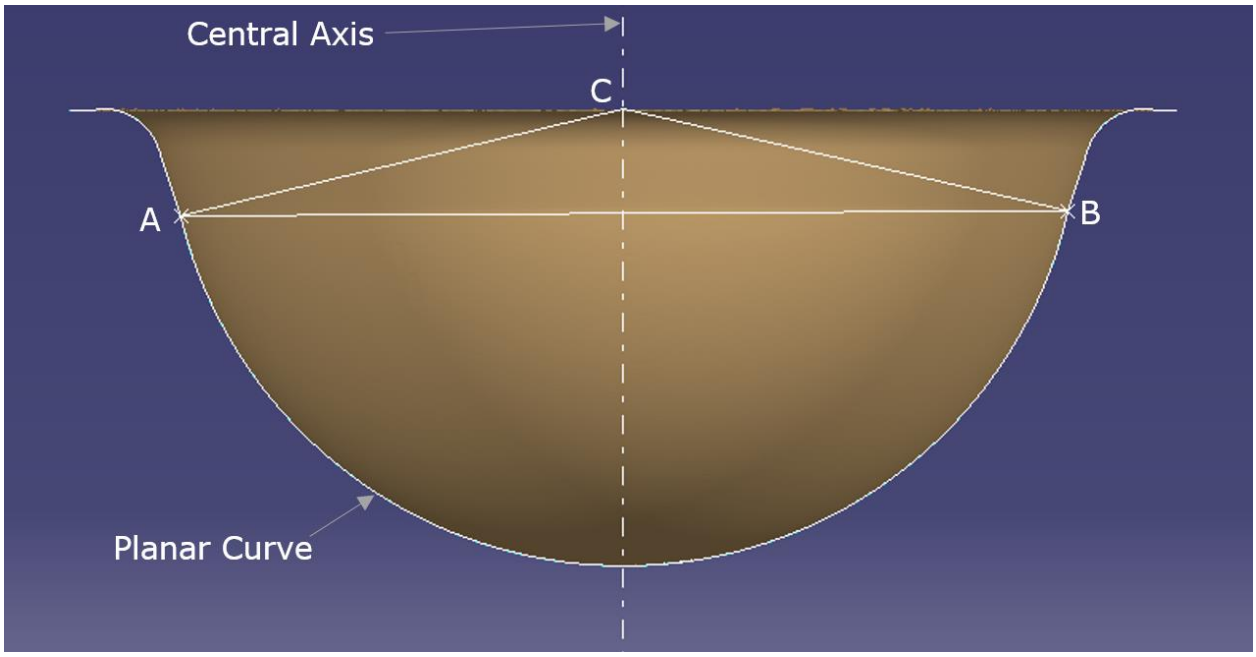

Figure 42: An image displaying the required geometry to compute the coverage angle.

In Figure 41 a schematic of the procedure to test the coverage angle is described and Figure 42 displays the geometry required in order to compute the coverage angle. In order to assess the coverage angle in CATIA, the first step was to import the measured point cloud data to CATIA and mesh the imported data. Then, in second step, various points were manually created on the edge in order to create a mean plane passing through the edge. In third step, using the generated points a mean plane is generated. In fourth step, by the use of the created mean plane, a planar section was generated on the mesh. This planar section traced the contour of the edge on the mesh. Then, in fifth step, a vertical plane that included two points with the maximum height deviation was visually located by rotating the mesh about the XZ-axis of the measured data and a planar section of this plane was generated. Then, in step six, both the planar sections were converted to planar curves and the intersection of these two planar curves generated the required two points that had visually recognised maximum edge height deviation. These two points are named as point A and point B as seen in above Figure 42. Further, in step

seven, a sphere is generated by using only the mesh of the bearing surface to locate the centre of the sphere which is required to assess the coverage angle. This centre of the sphere is termed C as seen in in above Figure 42. After creating all the required points, line AC and BC were created. Now, the geometry required for the measurement of the coverage angle was constructed. The angle between line AC and BC was computed in order to determine the required coverage angle. Further the angles between the central axis of the sphere and the two lines AC and BC were computed in order to compute deviation from the central axis and to detect the tilt in the edge geometry. An example of coverage angle assessment of liner 2 from the unworn cohort-B is displayed below in Figure 42.

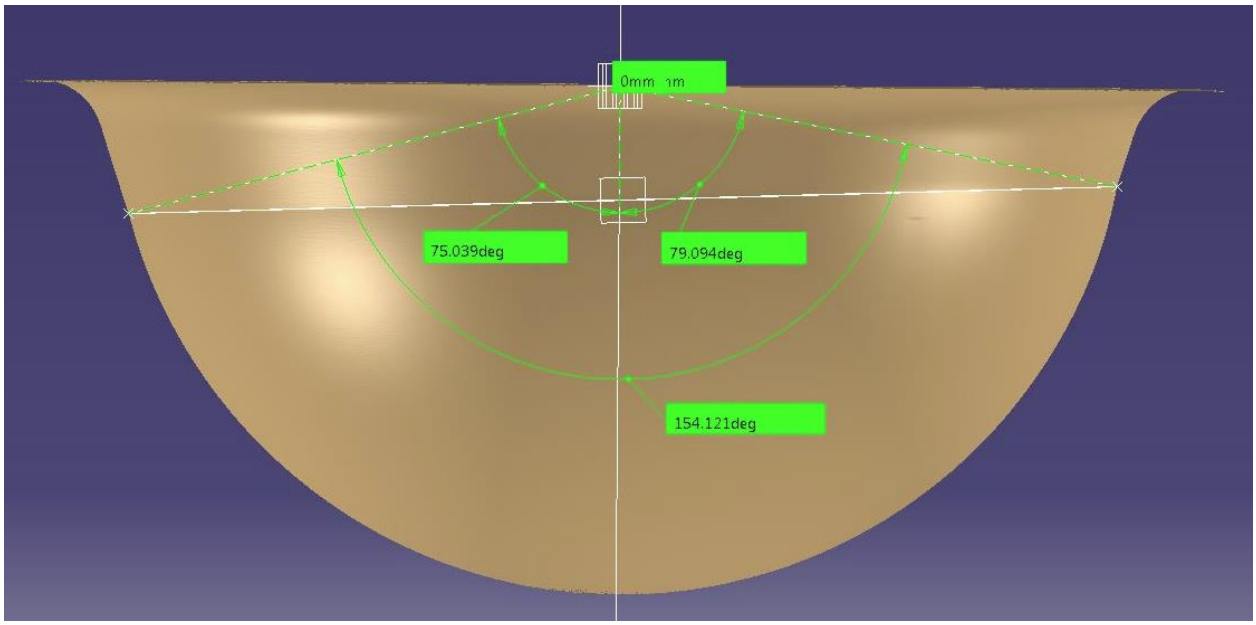

Figure 43: Image displaying the coverage angle assessment of liner 2 from the unworn cohort-B as an example.

From the example of liner 2, it can be observed that the coverage angle is 154.121°. However, there is a tilt of 2° from the central axis of the sphere which causes disparity in quartiles by 4° and increases possible contact or edge loading. The tilt of the edge is calculated by averaging the difference in the two angles formed between the central axis and the two lines AC and BC. Using this procedure, the coverage angle and the tilt were measured in all the

acetabular liners of the unworn cohort-B. The results of the assessed liners are tabulated below in Table 9.

Liner No.	1	2	3	4	5	6
Coverage Angle (°)	153.07	154.12	154.04	153.80	154.36	154.40
Tilt (°)	1.06	2.03	0.31	0.47	0.56	1.91

Table 9: Tabulated results from the coverage angle assessment of the acetabular liners of the unworn cohort-B.

From studying the above Table 9 it can be noted that, for the liners of unworn cohort-B, the coverage angle varies between 153.07° to 154.40° and the tilt in the edge varies from 0.31° to 2.03°. It is observed that liner 2 and liner 6 had the edge tilted by 2.03° and 1.91° respectively. Such a tilted edge is a manufacturing effect that could induce edge wear as the disparity in possible contact angle from one side of the component to the other and has been shown to be over 4° in two out of the given six liners [304]. The implication of the measurements from this small cohort is that for a given implantation angle there could be a significant variation in the position of the effective contact patch boundary. This increases the possibility of leading the edge loading as it positions the edge into the bearing surface [229, 305].

The assessment of the fresh unworn acetabular liners through performing the roundness test and coverage angle test by the use of RMM and CMM machines explored the form of the liners and gave a better understanding of the form variation in the as manufactured acetabular liners. It was observed that the acetabular liners had controlled bearing surface and a free form ellipsoidal surface above the edge. The edge of the acetabular liner was found to have a less controlled geometry than that of the bearing surface and a significant tilt in the position of the edge of the bearing surface and therefore coverage angle was observed in two of six liners from cohort-B.

Consequently the analysis process was required to reconstruct a geometry that incorporated a controlled bearing surface, a elliptical edge and an uncontrolled ellipsoidal surface in order to characterise and quantify wear in ceramic acetabular liner. This was the biggest challenge of the method development process.

3.8 Updated Method for Re-construction of Unworn Surface Geometry

After assessing the form of liners from the unworn cohort-B, a new concept was developed to reconstruct the unworn surface geometry which was suitable for liners that had controlled bearing surface, elliptical edge and an uncontrolled ellipsoidal surface beyond the edge. Before testing the method on the cohort-A of worn acetabular liners, the method was tested on the liners of unworn cohort-B which were measured to test coverage angle and an attempt was made to reconstruct a surface geometry that imitates the measured unworn surface. The measurement data from the CMM was imported to CATIA where the point cloud data was meshed and prepared for the analysis. The triangulated mesh is then segmented to delineate the wear area by creating two horizontal planar sections parallel to the flat surface of the rim (XY-plane as defined on CMM). The distance between the two horizontal planes is determined based on the wear distribution and its extent, extra unworn area adjacent to the wear area is purposely not segmented as it is essential for the reconstruction of the unworn geometry. The distance between two horizontal planes in the case of the below given example (see Figure 45) was 7.5mm.

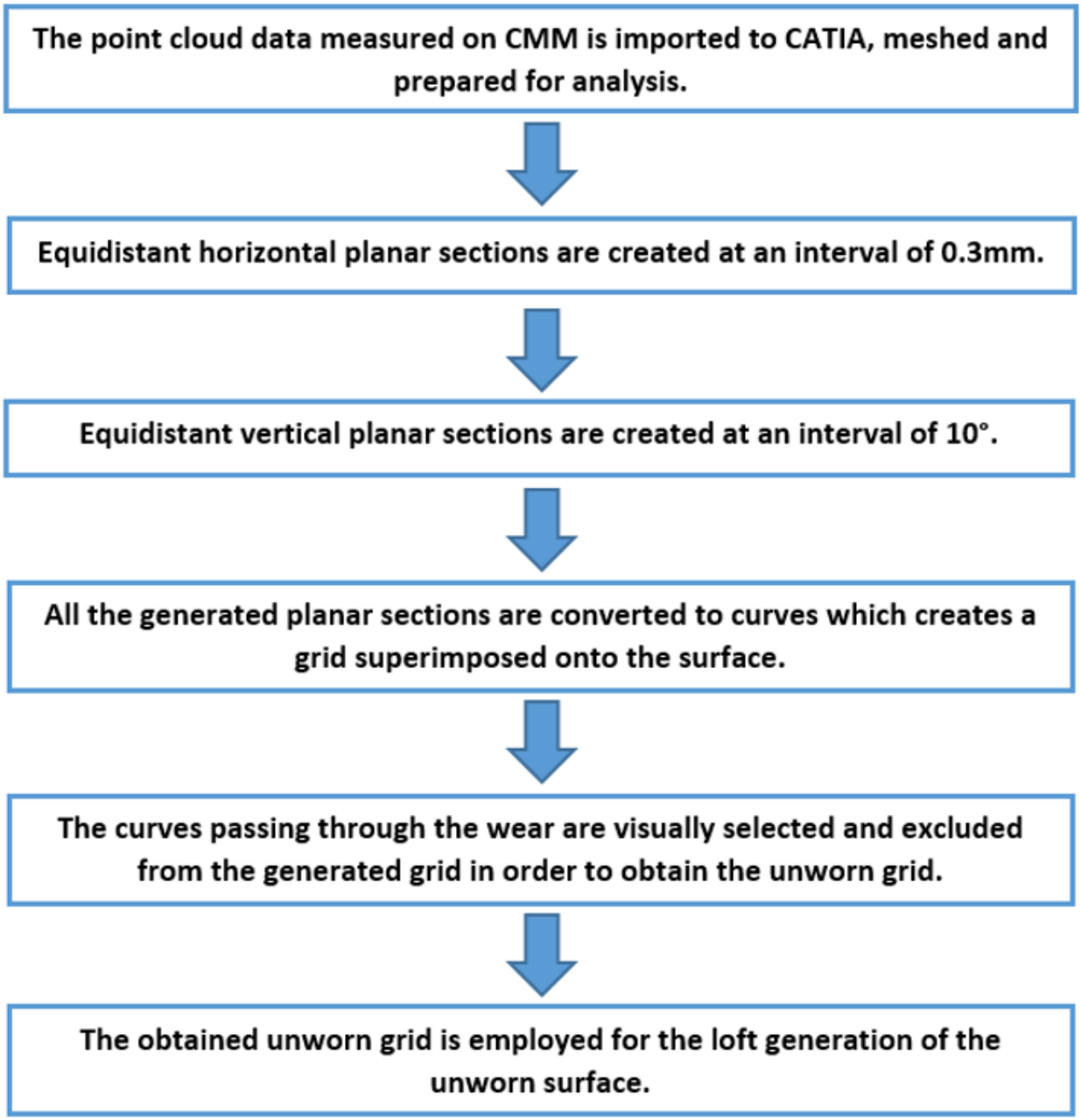

Figure 44: A flow chart diagram of the updated procedure employed for the reconstruction of the unworn geometry.

Subsequent to the segmentation process, horizontal planar sections are created parallel to the XY-plane at an interval of 0.3mm covering the height of the segmented mesh. Similarly, vertical planar sections at an interval of 10° from the XZ-plane or the YZ-plane are produced. These horizontal and vertical sections are further used to create a grid (see Figure 45) that is superimposed over the mesh and served as the basis for generating the

unworn reference geometry. The grid generation process is restricted to a tolerance of 0.1µm ensuring a high accuracy. A tool in CATIA known as 'Multi-Surface' allows to create a feature by making transition between the produced horizontal curves by using the produced vertical curves as guides. This allows for the re-construction and imitation of the unworn surface geometry as required in case of such free form surface observed in ceramic acetabular liners.

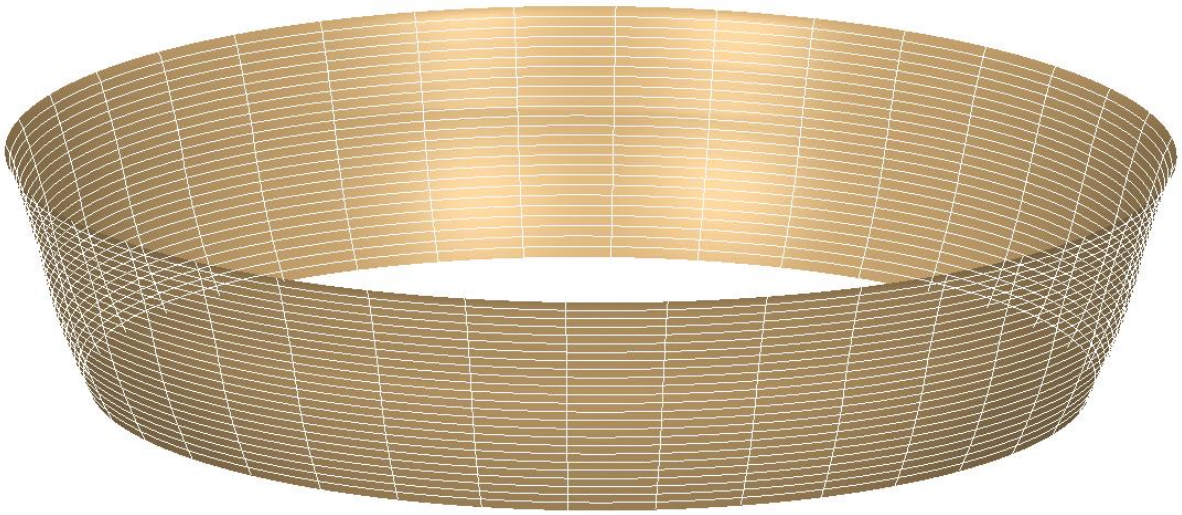

Figure 45: Grid generated from horizontal and vertical planar sections superimposed on the segmented mesh.

After reconstructing the surface geometry of the unworn liners, the accuracy of the re-constructed surface was tested by performing the deviation analysis between the mesh of the measured surface and the re-constructed surface geometry. These results are displayed through the bar graph below in Figure 46. The results of the test showed that the method was able to re-construct and replicate the free form as manufactured surface with over 84% of the points having a deviation of less than 1 µm and 96% of the points with deviation of less than 1.5 µm. Only approximately 1% of the surface is above 2 µm and ranges from 2 µm to 8 µm. For example, liner 5 displayed 0.06% deviation of less than 8 µm which is a scanning error caused by sliding of stylus against bearing surface due to the probing pressure at the curvature of

the bearing surface and also displayed a single blip of 17 µm which is suspected to occur due to a debris on the surface. Below in Figure 47, deviation analysis of liner 5 from the unworn cohort-B is displayed to examine the above mentioned scanning error and the blip caused potentially by a debris deposit. The highlighted circle 'A' is potentially a debris on the surface whereas the straight vertical yellow line highlighted by circle 'B' exhibits a measurement scanning error or possible debris deposit. The results were consistent for all the six liners showing that the method is able to account for part variability.

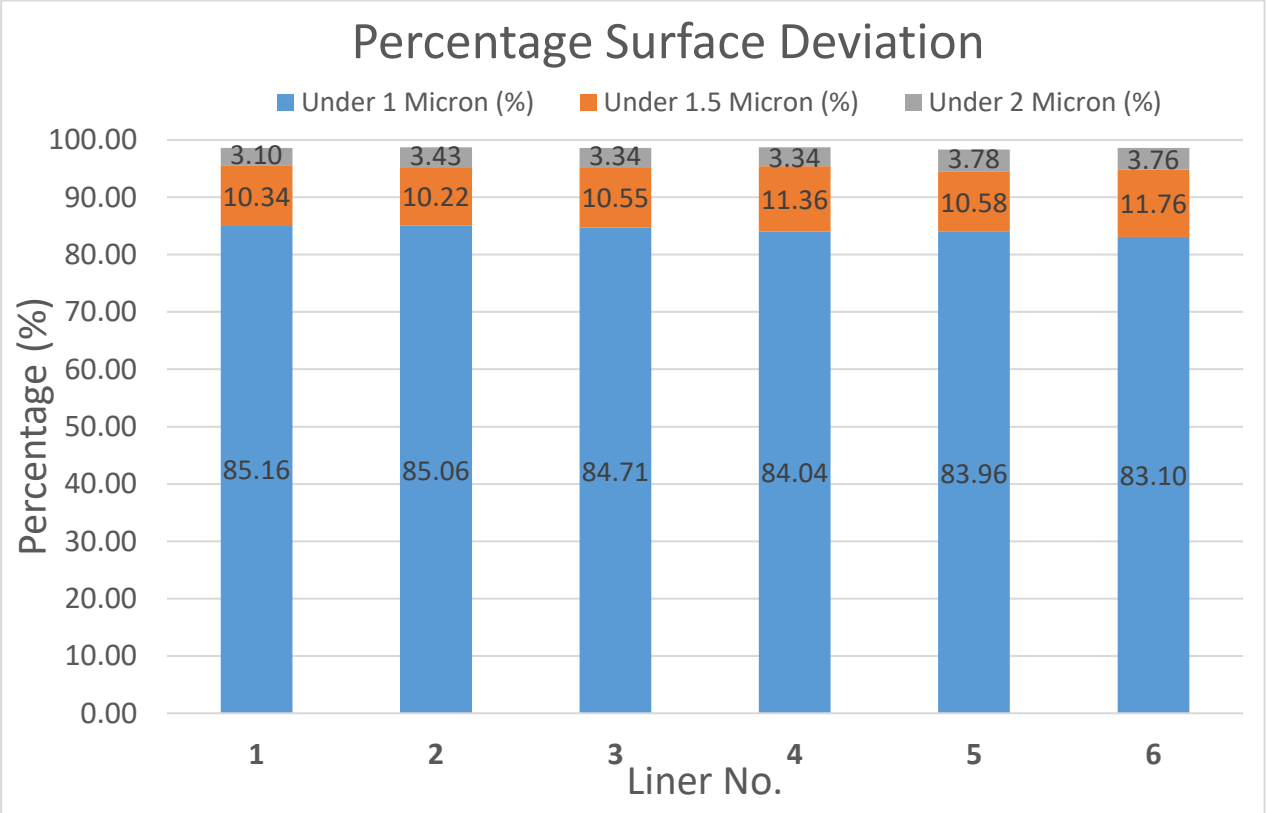

Figure 46: A bar graph displaying the results from the deviation analysis performed to test the deviation between the reconstructed surface and measured surface for all six liners of the unworn cohort-B.

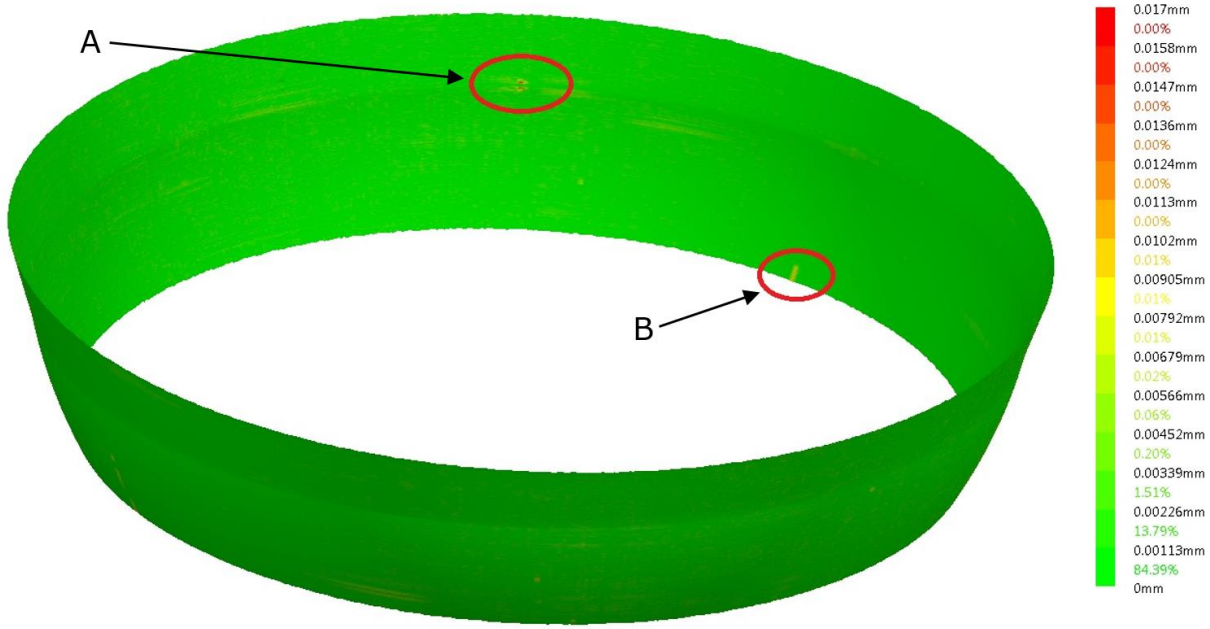

Figure 47: Image showing possible measurement error or debris deposit caught on the deviation analysis. (A) Possible debris on the surface. (B) Scanning error.

Once the surface was reconstructed successfully, the volume of the reconstructed surface geometry was compared to the volume of the measured segmented mesh to test the variation in the volumes. For this test both, the reconstructed surface and the measured surface were enclosed by the use of same planes in order to measure the correct volumes. The volumes of both the enclosed surfaces are computed in CATIA for all six unworn acetabular liners and compared with each other. The results are tabulated below in Table 10.

Total Volumetric Variation (mm^3)						
Liner No.	**1**	**2**	**3**	**4**	**5**	**6**
Mesh	6603.461	6746.062	6313.206	6736.562	6736.584	6748.807
Reconstruct	6603.430	6746.085	6313.264	6736.52	6736.725	6748.839
Variation	0.031	0.023	0.058	0.042	0.141	0.032

Table 10: Table comparing calculated wear volumes of measured surface mesh and reconstructed surface geometry.

From the above given Table 10 it can be noted that difference between the measured surface mesh and reconstructed surface ranges from 0.023 mm^3 to 0.141 mm^3. As expected, it was observed that liner 5 displayed the largest variation of 0.141 mm^3 which was suspected to be caused due to previously mentioned scanning error and possibly debris deposits on the liner at the time of measurement. In order to eliminate such errors, the error affected surface is segmented and volume measurement is limited to the wear distribution area. The process of eliminating such error and limiting the volume computation of the wear is detailed below in section 3.8. After eliminating these two observed errors through further segmentation and re-computing the volumes, the variation was reduced from 0.141 mm^3 to 0.033 mm^3. Thereafter, the updated variation in volume of the measured surface mesh and reconstructed surface ranges from 0.023 mm^3 to 0.058 mm^3.

3.9 Volumetric analysis for the cohort-A

After successfully testing the surface reconstruction method on unworn cohort-B, the method was employed to analyse the previously measured cohort-A of six simulated acetabular liners. The point cloud data from CMM measurement was imported to CATIA and triangulated to generate a surface mesh. This mesh was segmented in the same manner as done in the initial experiment. Horizontal planar sections were created parallel to the XY-plane at an interval of 0.3mm covering the height of the segmented mesh. Similarly, vertical planar sections at an interval of 10° from the XZ-plane or YZ-plane were produced. These horizontal and vertical planar sections were then converted into curves that created a grid which was superimposed onto the surface and served as the basis for generating the unworn reference geometry. The planar section to curve generation process is restricted to a tolerance of 0.1µm ensuring a high accuracy. The operator is able to visualise and exclude horizontal and vertical curves passing through the wear area ensuring an adequate delineation as shown in Figure 48.

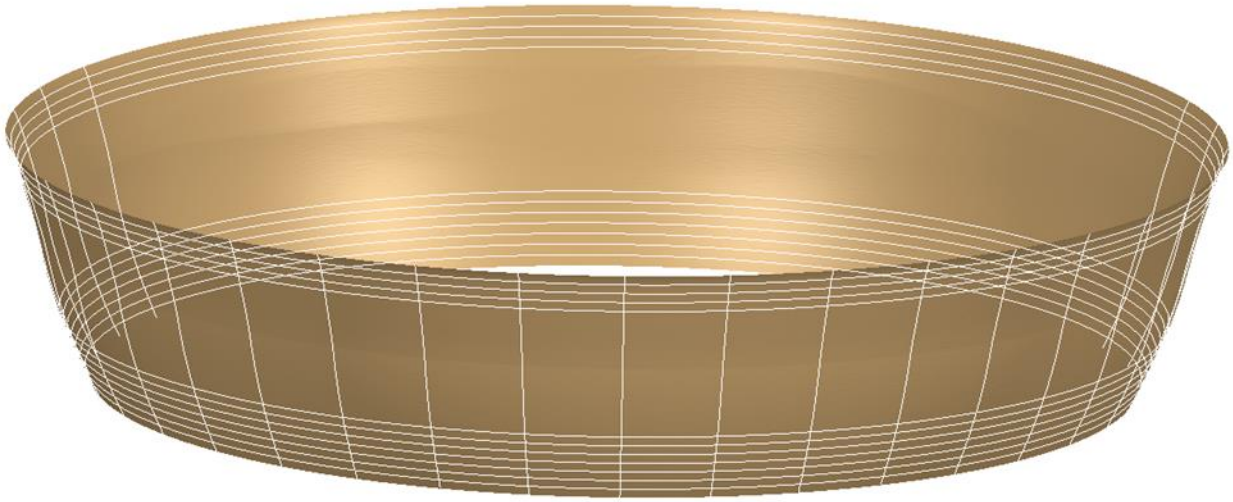

Figure 48: Image showing the required grid to reconstruct the unworn geometry.

The unworn surface geometry of the worn components of cohort-A are reconstructed through the use of such grid which has selected guides and curves as it only consists the unworn surface of the liner. The loft algorithm generates surface in the missing grid area according to the specified unworn data and replicates the corresponding as manufactured surface as seen in Figure 49 below. This procedure was iterated for each liner to generate its corresponding reference geometry that was compatible with the liner's unique form.

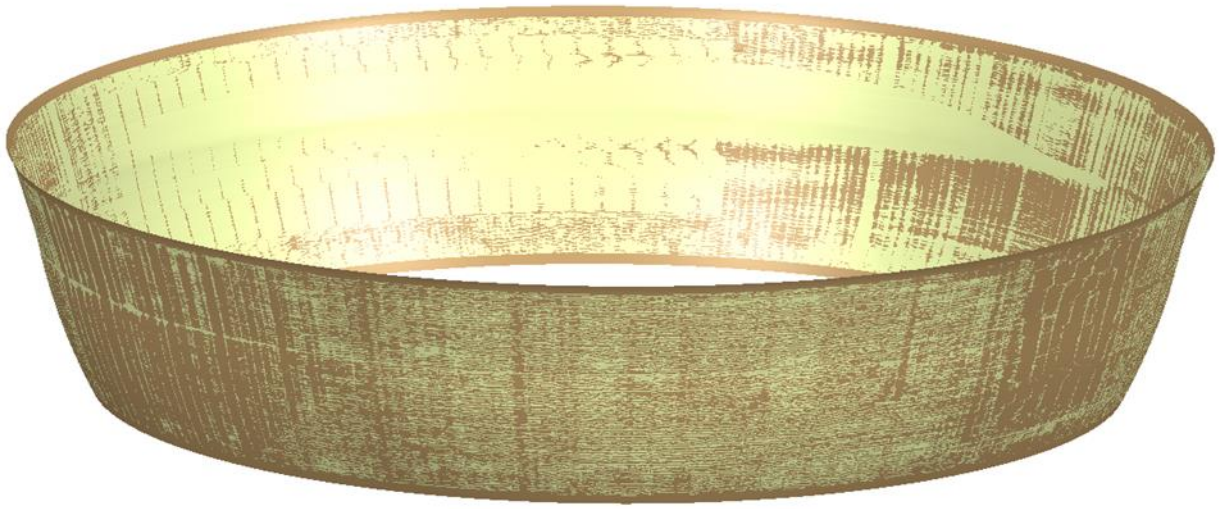

Figure 49: Reference geometry generated from the identified grid to replicate the as manufactured surface.

In the next step a deviation analysis was performed between the measured surface and the reconstructed reference surface. The deviation analysis generates a visual representation of the deviation between the two surfaces that is used to characterise edge wear distribution as shown below in Figure 50. The colour map and the intervals effectively display the wear penetration and percentage of the surface area covered under each colour range. Along with displaying the edge wear distribution and linear wear penetration, the deviation analysis is an efficient tool to identify debris and deposits on the acetabular liner.

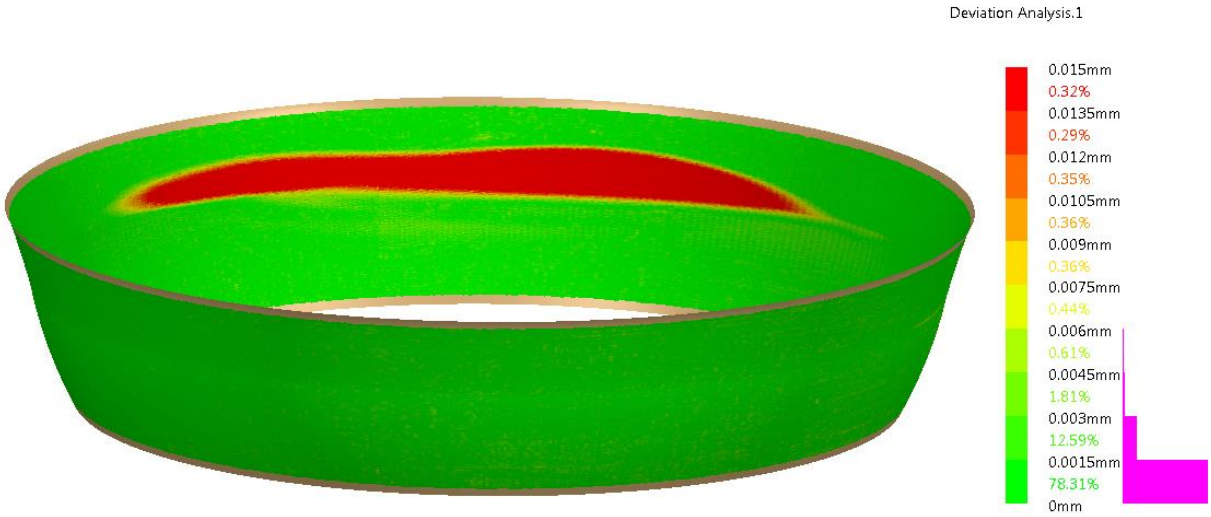

Figure 50: Example of deviation analysis to characterise edge wear and evaluate linear wear penetration.

Subsequent to characterising the edge wear on the liners, the final step of the analysis process involves determining the volume of wear. This is calculated as the difference in volume between the measured surface and the reconstructed as manufactured surface geometry. For CATIA to determine the volume of measured surface and generated surface both the surfaces are required to be enclosed. The difference in volume between the enclosed measured surface and enclosed generated reference geometry is the required volumetric wear.

On rare occasions scanning error or debris deposit were observed on the measured surface through the deviation analysis. In order to limit such errors from hindering the volumetric wear computation, the surface affected by the error is discounted from volume computation process. For discounting the surface affected by such error, both the enclosed surfaces are segmented down to just the area around to the wear patch using the same planes as seen below in Figure 51. This segmentation allows to focus the volume computation of just the wear distribution and small amount proximal area and discounts the volume of the error affected surface.

Figure 51: Wear measurement narrowed down from full liner to wear sector in order to limit the errors induced.

3.10 Results

The volumetric wear characterisation and quantification was carried out by the above developed method for the cohort-A of six simulated acetabular liners. Deviation analysis performed between the generated reference surface and measured surface effectively characterised wear distribution for each liner. After characterising the wear distribution it was observed that each liner had a singular area of localised wear. An example of such localised wear can be seen below in Figure 52. Deviation analysis was also capable to quantify linear wear penetration and the in-vitro linear wear penetration assessed through deviation analysis for the given cohort-A of six simulated acetabular liners ranged from 8.9 μm to 29.1 μm and the wear sector length as approximately measured from deviation analysis ranged from 50° to 110° as shown below in Table 11. It was observed from the wear distribution that the edge wear was spread out above the edge and into the bearing surface for all the six acetabular liners. An example of this observation can be seen below in Figure 52. This is an important observation as the existing co-ordinate measurement methods only measure wear in the bearing surface and do not measure wear beyond the bearing surface [17, 41-43, 289, 292, 306, 307].

After deviation analysis, volumetric analysis was performed to assess the edge wear volumes of all six acetabular liners and the volumetric wear as determined ranged from 0.081 mm^3 to 0.311 mm^3.

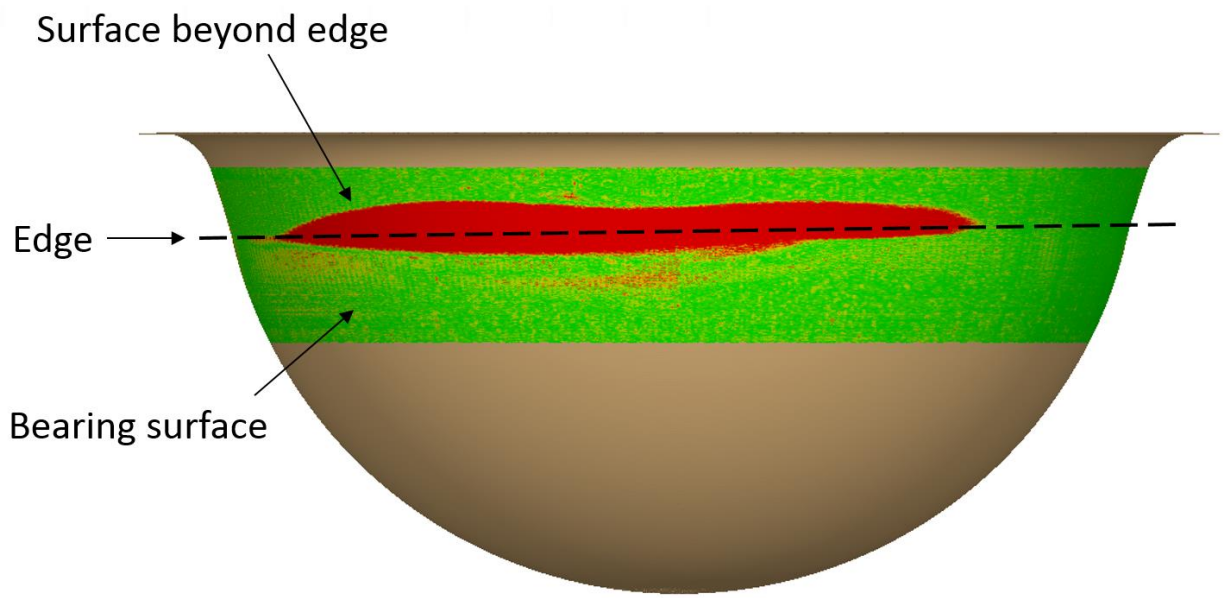

Figure 52: Image showing the observed wear distribution extending from the bearing surface to the surface beyond the edge.

Liner	1	2	3	4	5	6
Linear Wear (µm)	8.9	29.1	15.8	27.3	17.3	19.9
Wear Sector Length (°)	50	80	85	110	75	70
Volumetric Wear (mm^3)	0.081	0.250	0.084	0.311	0.105	0.129

Table 11: Linear wear, Wear sector length and volumetric wear results obtained by analysing all the six acetabular liners through CMM method.

By examining the results displayed in Table 11, there appears a correlation between the wear volumes, wear sector length and linear wear penetration yet there is not enough data to understand the significance. With longer sector length or deeper linear wear penetration, an increase in volumetric wear is observed. For example, by comparing liner 2 and liner 4 it can be noted that liner 2 has higher linear wear penetration yet the volumetric wear of liner 4 is higher. This is because the sector length of wear distribution of liner 4 is much longer than that of liner 2. Hence it can be noted that wear sector length and linear wear penetration both play an important role in determining volumetric wear.

After determining the wear volumes of cohort-A through use of the CMM method, these results were compared against the results obtained from the gold standard gravimetric method to test the agreement between both the methods. The volumetric wear as measured by gravimetric method and CMM method are tabulated in Table 12 given below along with the quantified difference between the results.

Cup No.	1	2	3	4	5	6
Gravimetric (mm^3)	0.112	0.414	0.179	0.432	0.164	0.247
CMM (mm^3)	0.081	0.25	0.084	0.311	0.105	0.187
Difference (mm^3)	0.031	0.164	0.095	0.121	0.059	0.060

Table 12: Table displaying the comparison between the results obtained by Gravimetric method and CMM method.

The below given Figure 54 exhibits a bar graph that graphically compares the wear volumes of each liner as measured by gravimetric method and CMM method. For errors bar in the bar graph, the standard deviation from the repeatability test of the analysis process of the CMM method is used. This repeatability of the CMM method is detailed below in section 3.10. However, for the gravimetric method, the repeatability of the employed weighing microbalance (Mettler-Toledo XP205, UK) is 7 µg which equates to as negligible as 0.0016 mm^3 as per the density of BIOLOX Delta. From Figure 54 it can be observed that the wear volumes measured by CMM method is lower than the wear volumes measured by gravimetric method for all the six acetabular liners. The reason behind this could be the fact that CMM method is focused on the edge wear and ignores wear on any exterior part of the acetabular liners, whereas gravimetric method cannot ignore any wear on the acetabular liner which can have occurred through mishandling or by clamping on the simulators. Figure 53 illustrates a good example of metal transfer onto the ceramic liners. Such metal transfer or wear in the exterior region of the acetabular liner is not a part of the wear study and gravimetric method cannot ignore it from the volumetric measurement and hence introduces errors in the wear study. Other possible reason can be the protein deposits on the ceramic

material which can minutely increase the weight of acetabular liners and induce errors in gravimetric measurements.

Figure 53: Image displaying wear at the clamping area on the exterior part of the liner.

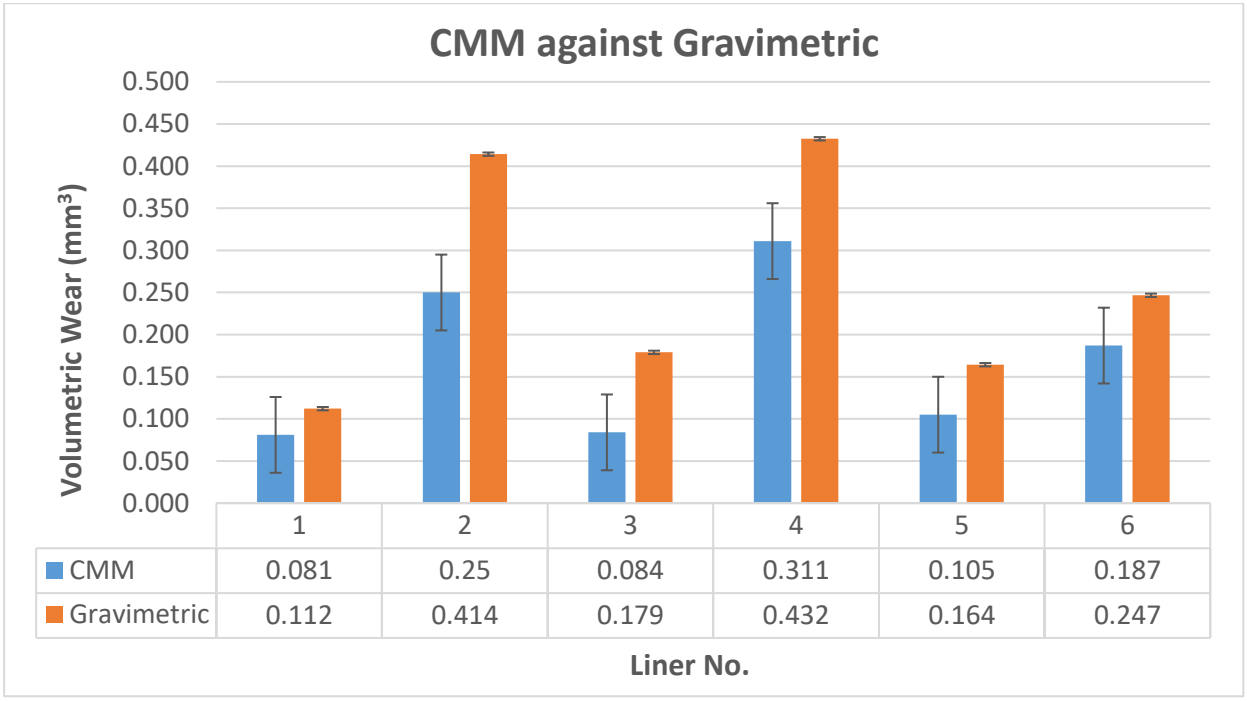

Figure 54: The image displays a bar graph with standard deviation error bars comparing the results of the CMM method and the Gravimetric method.

After accomplishing graphical comparison, the correlation between CMM method and gravimetric method was tested by Pearson's correlation test. The Pearson correlation value was found to be 0.969 at a significance value of 0.001 which displays a strong correlation between two methods.

After examining the results obtained from the developed CMM method, the limitation and accuracy of CMM measurement and the nm precision of RMM measurement, a development of new method was experimented that employs an RMM measurement and an analysis process that can characterise and quantify volumetric wear from the RMM measurement data. The intention behind developing the RMM method was to improve the accuracy of the measurement and possibly gain more precise volumetric wear results compared to CMM.

3.11 Inter-operator Variability for CMM method

A study was conducted to test the repeatability, reproducibility and the inter-operator variability of the analysis process of the CMM method. Acetabular liner A-6 was chosen from the set of wear simulated cohort-A to perform the study as liner A-6 exhibited high linear wear penetration yet the obtained volumetric wear was low. Hence, this was a good opportunity to test the CMM method's resolution.

A single CMM measurement of acetabular liner 6 from Cohort-A was analysed twenty times on CATIA for the repeatability study and was analysed 10 times by each operator for the inter-operator variability study. Each measurement followed the reconstruction and the analysis procedure of the CMM method as mentioned in section 3.7 and section 3.8. As the analysis process is sensitive to the selection of the thirty-six vertical planar section generated at an interval of 10°, each analysis for repeatability study included a shift of 0.5° in generation of the planar section. This gave 20 measurements that had a reconstructed surface geometry with an angular shift of 0.5° within 10° of the vertical planar section interval. This allowed for the study of the

uncertainty induced by the plane selection process. Similarly, for the inter-operator variability two operators analysed ten measurements per operator. Each measurement included an angular shift of 1° to the planar section interval of 10°. Both operators used the same angle shift for the comparison of the results. It must be noted that as the analysis process is user dependent and was hence performed in a blind manner where both the operators had no pre-wear data in order to test the inter-operator variability of the analysis process. Out of the two operators, operator-1 was an experience user whereas the operator-2 was only aware of the method and had no hands-on experience of the CMM analysis method.

	Max. Linear Wear Penetration (mm)	**Volumetric Edge Wear (mm^3)**
Mean	0.022	0.186
Median	0.022	0.188
Range	0.016 - 0.025	0.094 - 0.272
Std. Deviation	0.002	0.046

Table 13: Tabulated results of the repeatability study for the analysis process of the CMM method. This table displays mean, median range and std. deviation between the results obtained by two individual users.

The Table 13 displays the mean, median, range and standard deviation of the results obtained by measuring the maximum linear wear penetration and volumetric wear twenty times for the repeatability study. From Table 13 it can be observed that the standard deviation of the obtained maximum linear wear penetration is as low as 0.002 mm and the results ranged from 0.016 mm to 0.025 mm with the mean of 0.022 mm. The standard deviation of the volumetric wear was found to be as low as 0.046 mm^3 and the results ranged from 0.094 mm^3 to 0.272 mm^3 with the mean of 0.186 mm^3. Hence the method displays high repeatability in measuring the maximum linear wear penetration and the volumetric edge wear.

	Operator – 1 Volumetric Wear (mm^3)	Operator – 2 Volumetric Wear (mm^3)	Inter-operator Variability (mm^3)
Mean	0.187	0.196	0.061
Median	0.179	0.174	0.037
Range	0.128 – 0.272	0.067 – 0.351	0.007 – 0.178
Std. Deviation	0.045	0.085	0.051

Table 14: Results of the inter-operator variability study for analysis of volumetric wear by the CMM method. This table displays difference in the mean, median, range and std. deviation between the results obtained by two individual users.

The above given Table 14 displays the mean, median, range and standard deviation of the ten results obtained by each operator and that of the variability between their results. For the inter-operator variability study, it can be observed from the Table 14 that the standard deviation of the volumetric wear obtained by operator-1 and operator-2 was found to be 0.045 mm^3 and 0.085 mm^3 and the range of the obtained results was 0.128 mm^3 to 0.272 mm^3 and 0.067 mm^3 to 0.351 mm^3 with the variation range of 0.007 mm^3 to 0.178 mm^3. The means of the results obtained by operator-1 and operator-2 were calculated to be 0.179 mm^3 and 0.174 mm^3 respectively. The standard deviation of the results obtained by the operator-1 and operator-2 are found to be 0.045 mm^3 and 0.085 mm^3 respectively. The mean and the standard deviation of the inter-operator variability study of cohort C are calculated to be 0.045 mm^3 and 0.085 mm^3 respectively showing good inter-operator variability. As the study was conducted in a blind manner, the operators had no pre-wear data regarding the acetabular liners.

Further this study shows good agreement between the operators when considering individual datasets with an overall standard deviation of inter-operator variability of 0.051 mm^3. In below given Figure 55 a Bland-Altman plot is displayed to graphically examine the obtained results in detail. As operator-2 was more experienced with the analysis process, the analysis results of operator-2 are taken as reference instead of taking the mean of two

operators. The dashed line represents the 95% limit of agreement (1.96 Standard Deviation) range to examine the agreement of the analysis as analysed by two operators. This 95% confidence interval of agreement limits are -0.173 mm^3 to 0.155 mm^3. The mean of the paired differences in measurements from two operators is -0.01 mm^3 and is denoted by the solid line. Hence it can be observed that he variation between two users is noticeably low. The bias between two measurements can be estimated by the distance of mean line (dashed line) from the zero (dotted line). The t-score significance value is found to be 0.339 which is insignificant and agrees with the null hypothesis. This means the bias is non-proportional.

It is noted that the major contributing factor causing the variance in the volumetric wear measurement is the user dependent planar section identification process that affects the repeatability and reproducibility of the analysis process.

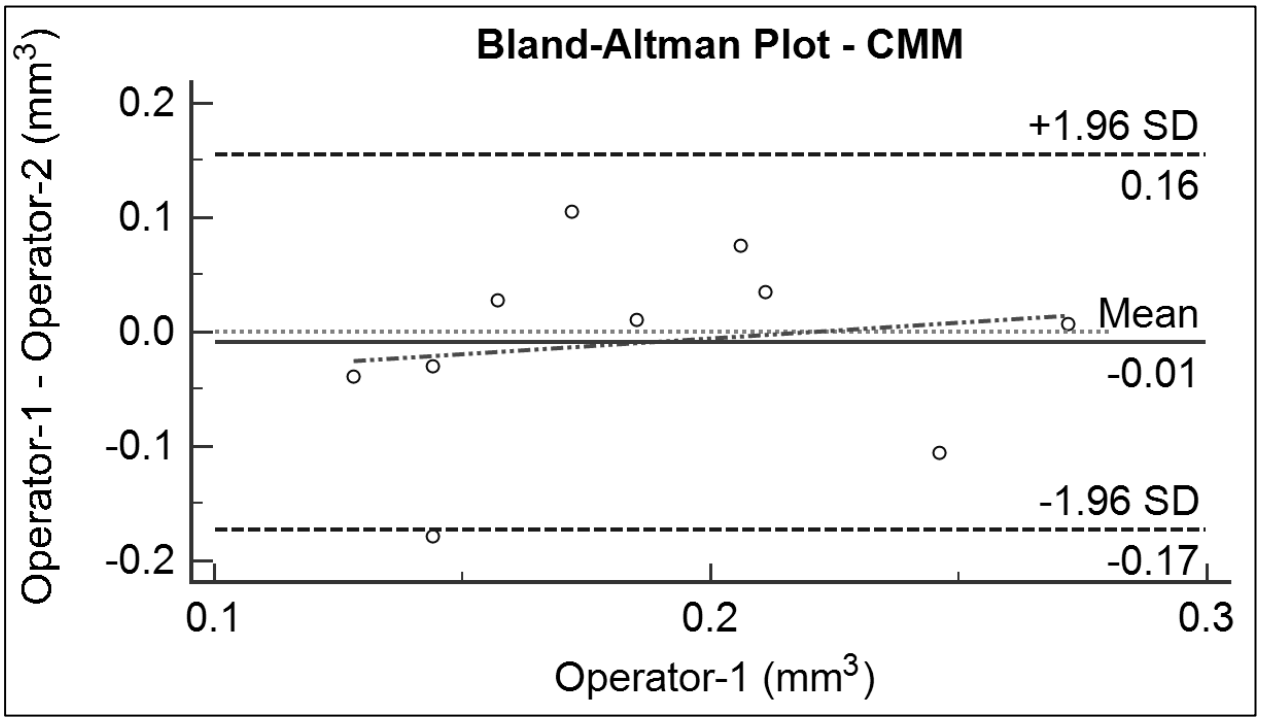

Figure 55: Bland-Altman Plot with line of equality showing inter-operator variability of the CMM method and regression line stating absence of proportional bias problem.

Chapter 4: RMM Method Development

4.1 Summary

This chapter describes the development of the edge wear measurement method by the use of a RMM. It gives the details of the acetabular liners used for the testing and the details of the wear simulation process used to simulate wear on the acetabular liners. Further the chapter provides details of the measurement machines and the measurement strategy employed to measure the wear simulated acetabular liners. The method mentions details of the vertical trace and roundness trace test performed to study the form of the acetabular liners. The chapter provide details of the procedure to reconstruct the unworn surface geometry using MATLAB programs in order to analyse the characterise and quantify volumetric wear. The wear results obtained through the use of the RMM method are documented and inter-operator variability is tested.

4.2 Measurement Procedure

After developing the CMM method, an experiment was made on the same cohort-A of six simulated acetabular liners to develop a method that utilised RMM data measured on a Talyrond 365 RMM. A pointed diamond stylus with the end radius of 5μm was employed in order to eliminate any possible errors induced through mechanical filtering. As mentioned previously, the Talyrond 365 RMM has the gauge resolution of 30nm with a spindle runout value of 20nm and is able to measure roundness and cylindricity of a given component (223).

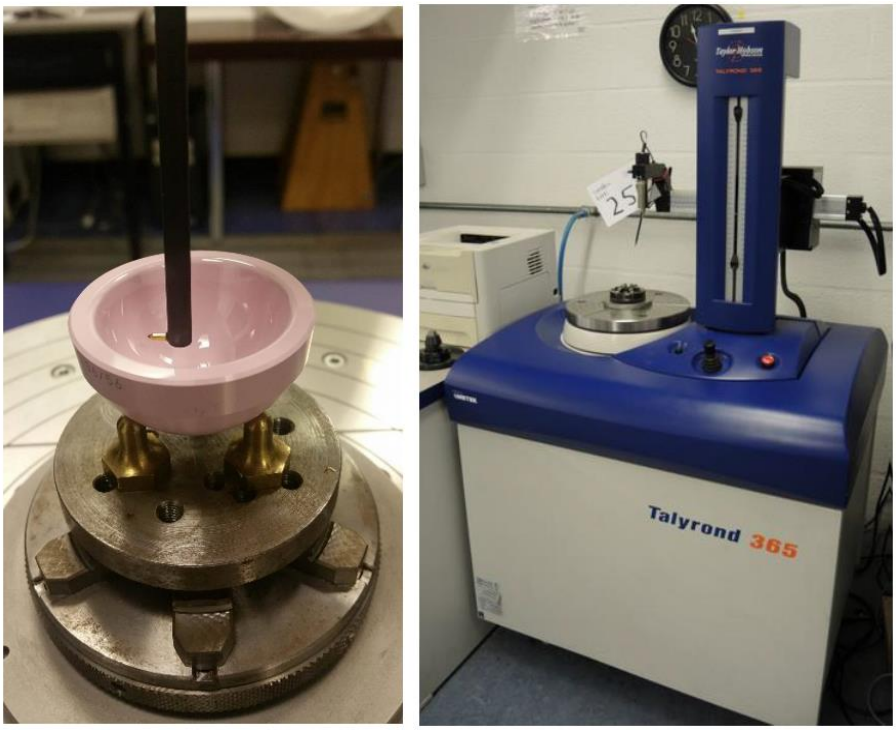

Figure 56: Image displaying a ceramic acetabular liner being measured on a Talyrond 365 (left) with a full picture of the Talyrond 365 (right).

4.2.1 Vertical Trace Test

For the development of the RMM method to characterise and quantify edge wear volumes without the use of pre-wear geometric data, the area surrounding the edge wear patch was measured on Talyrond 365 RMM. Due to the nano-meter precision of the employed RMM, although the thermal expansion coefficient of alumina oxide being as small as 8.1×10^{-6}/°C, the measurements were performed in a temperature controlled room where the temperature was maintained at 20°C ±1 in order to minimise any thermal expansion. Similar to the previously performed measurement, each liner was mounted on the custom designed three sphere fixture which was attached to a two-stage goniometer and an x-y translation stage. Operator performed an initial alignment to centre and level the liner manually prior to an automated centring and levelling process which established an eccentricity of under 1µm between the centre axis of the liner and the centre axis of the spindle.

In order to improve the measurement technique, unlike previously measured horizontal roundness traces to examine the form of the liners, this

time vertical traces were employed as they can measure more points and provide a denser point cloud for higher resolution of wear measurement. Prior to measurement, it was essential to identify the location and height of the wear distribution. In order to identify the wear distribution, a single vertical trace of the acetabular liner passing through the wear was measured. By the use of this vertical trace, the start and end position of the horizontal roundness traces in the vertical Z-axis that covered the required area of wear distribution at the edge and bearing surface were determined. It should be noted that, other than the height of the wear distribution, the permissible gauge travel length plays an important role in determining the first and last roundness trace. The RMM employed for this study, which is Talyrond 365, has a gauge travel length of 2mm that permits to perform measurement of approximately 5.5mm of the vertical height for a 36 diameter acetabular liner. However, there are other gauges available in the market that allows a travel length of 4mm which permits to measure larger area in terms of height.

Once the alignment is established and the measurement location is determined, measurement of 720 vertical traces were performed at an angular interval of 0.5° capturing the complete 360° of the required surface area of the given acetabular liner including the edge wear distribution. Each vertical trace recorded 3600 points and hence each liner measurement typically acquired 2,592,000 points (as per 720 vertical traces). The indexing spindle allows for continuous measurement which ensures that all vertical traces are measured with respect to the same axis. The talyrond 365 RMM stitches all the 720 vertical traces to generate a 3-dimensional surface, which effectively is a height map. This 3D surface representation of the measured surface area is a useful tool in order to characterise the wear distribution and is able to quantify linear wear penetration. An example of such height map is displayed below in Figure 57.

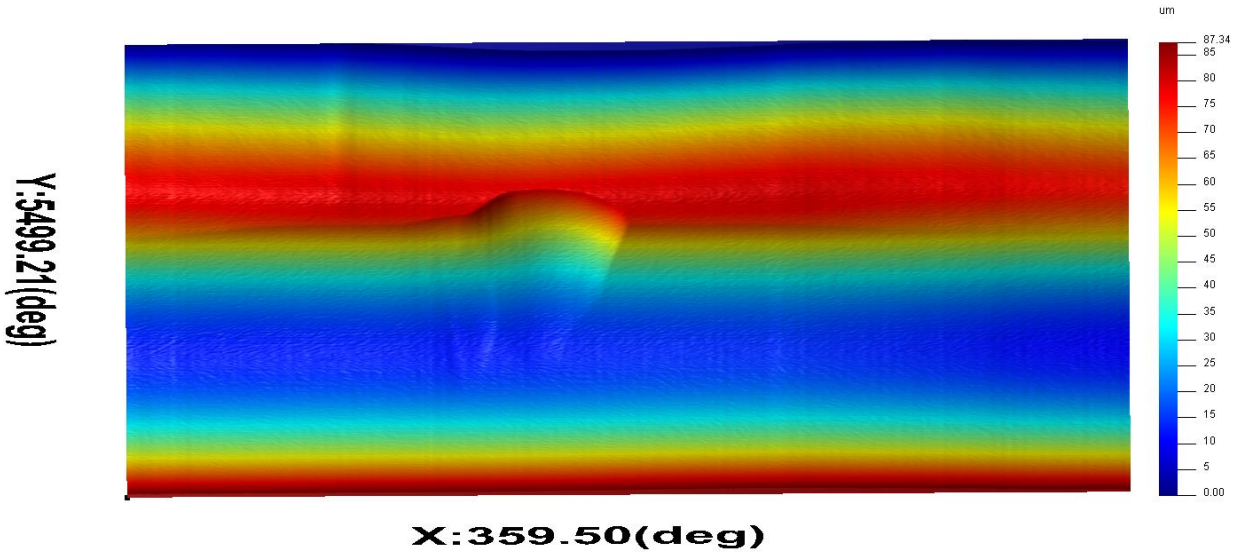

Figure 57: Image displays a 3D surface map of liner 4 from the worn cohort-A.

An example of the 3D surface map displayed above in Figure 57 provides information of wear distribution and allows user to estimate the linear wear penetration by the use of given colour map. Two 2D profiles are generated from the 3D surface in order to precisely determine the linear wear penetration. The generated 2D profiles are more effective at examining the surface as it allows the user to pin point the wear location and determine the wear depth in X-profile and Y-profile. An example of such 2D profiles is displayed below in Figure 58.

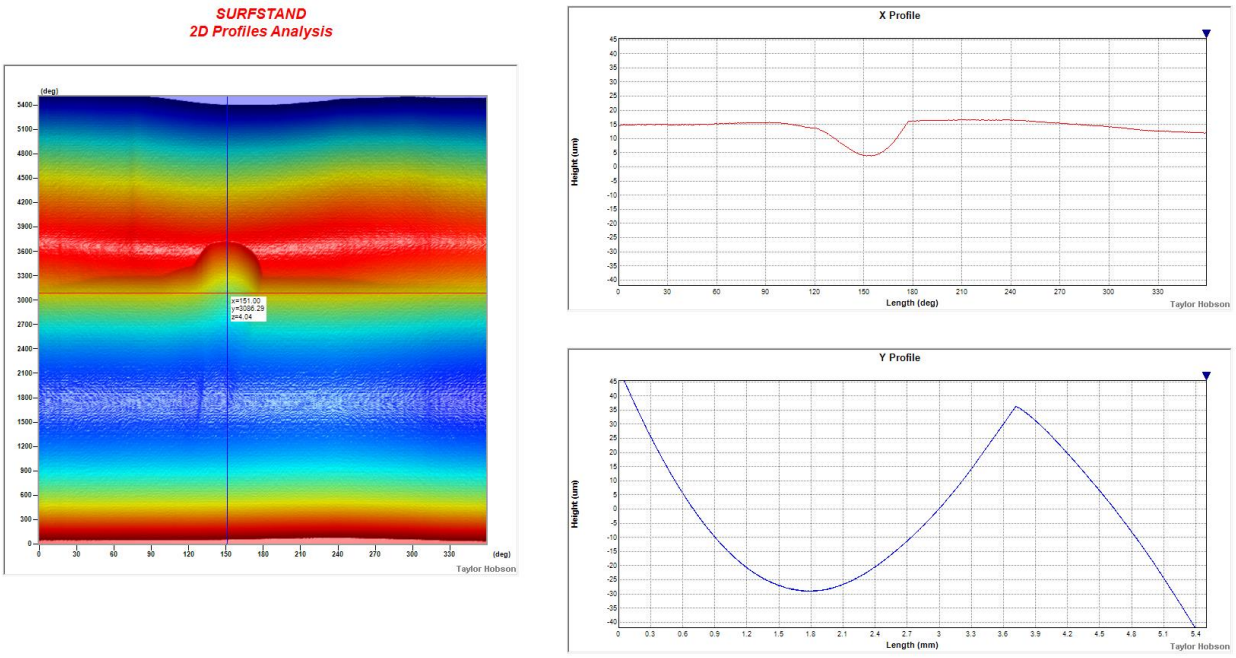

Figure 58: An example of 2D profiles generated from the measured 3D surface of liner 4 from the worn cohort-A in order to determine the linear wear penetration.

It was noted through examining the measured vertical traces that it is not possible to define a steady radius at a common height for all the measured individual vertical trace in such a manner that would align all the measured trace to form a cylinder. It must be noted that vertical traces measured on Talyrond 365 RMM does not measure the radial distance from the central axis of the spindle, but measures only the deviation from the contacted surface and hence the radius information is missing from the measurement. Due to this missing information the vertical traces could not be utilised to determine volumetric wear. This led the RMM method development back to the roundness traces, as the radius of the roundness traces could be obtained by the use of the Cartesian co-ordinates of a cylinder. This is explained in details in further section.

4.2.2 Roundness Trace Measurement

Prior to the measurement, the component was centred and levelled on the RMM and then the location and the height of the wear distribution was

identified using the same procedure as employed for the vertical trace test (Section 4.1.1). Again, similar to the vertical trace measurement, due to the permissible gauge travel length of 2mm, measurement of approximately 5.5mm of the vertical height for a 36 diameter acetabular liner was performed. Once the alignment was established between the component and the machine, measurement of approximately 110 horizontal roundness traces were performed at height interval of 0.05mm which measured 5.5mm of height in Z-axis including the wear distribution at the edge of the acetabular liner. The height interval of 0.05mm was selected as the height interval based on the minimum consistent height increment allowed by the Z axis for a roundness measurement. Each horizontal trace recorded 3600 points and hence each liner measurement typically acquired 396,000 points (as per 110 roundness traces). The indexing spindle allows for continuous measurement which ensures that all roundness traces are measured with respect to the same axis. Similar to the roundness test in section 3.4, each individual trace out of the 110 traces measured is effective to study the form and determine the linear wear penetration of the acetabular liner at that height. Four roundness traces of acetabular liner 4 measured at different height displayed below in Figure 59.

Subsequent to measuring the roundness traces, the Talyrond 365 RMM converts all the 110 roundness traces to linear form and stitch them to generate a 3-dimensional surface, which is effectively a height map. This 3D surface representation of the measured area is a useful tool in order to characterise the wear distribution and is able to quantify linear wear penetration. An example of such 3D surface is displayed below in Figure 60 along with the location of the roundness traces that are displayed in Figure 59.

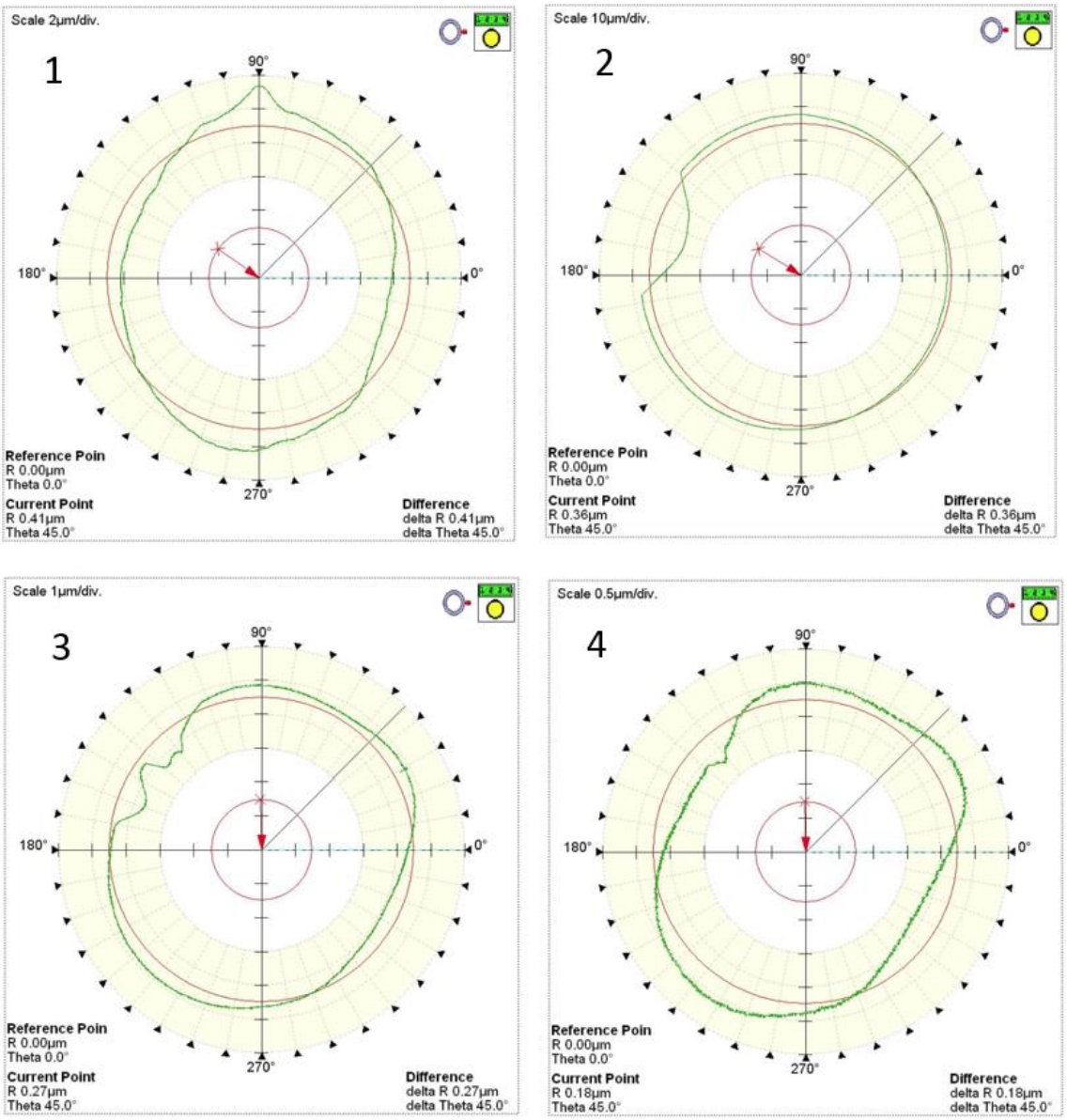

Figure 59: The displayed image shows four roundness traces at different height of the acetabular liner 4 from the worn cohort-A. The approximate location of these four roundness traces are displayed on the below given surface map in Figure 60.

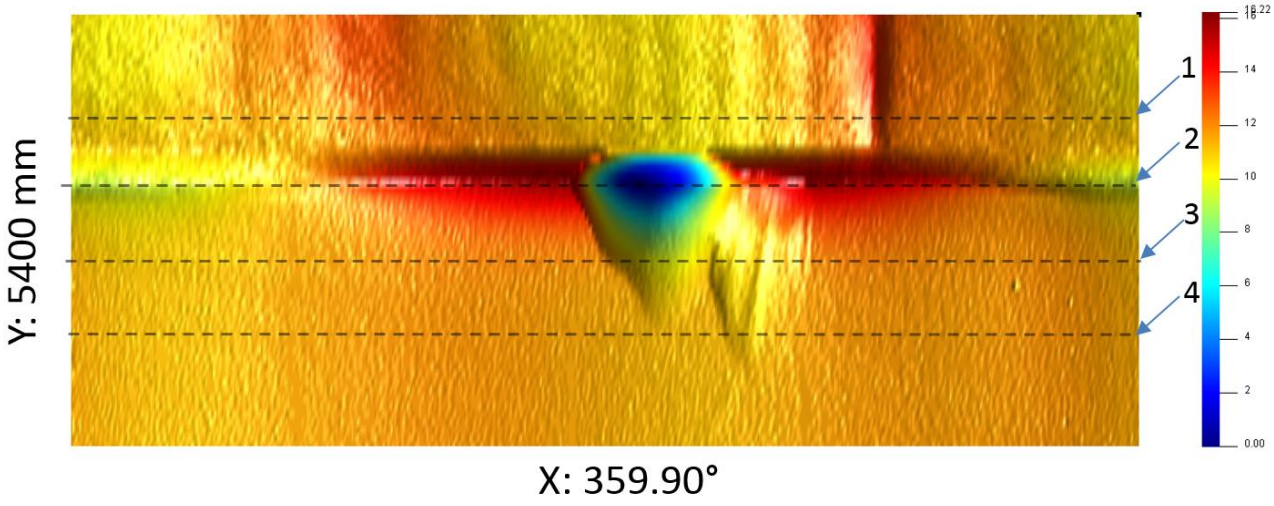

Figure 60: Image displays a 3D surface map of liner 4 from the worn cohort-A and the dotted lines shows an approximate location of four roundness traces displayed in Figure 59.

From the above displayed Figure 59 and Figure 60, the form of the liner 4 from the cohort-A can be examined. Figure 59 displays the four individual roundness traces measured at different height and Figure 60 displays an unwrapped surface of the cylinder generated by stitching the measured 110 roundness traces of liner 4 from the worn cohort-A. An approximate location of the four traces displayed in Figure 59 is marked and numbered in Figure 60 using a dotted lines. In order to compare the individual traces with the unwrapped 3D surface, it must be noted that the datum is located in the top right corner of the 3D surface and that the 0° angle on the X-axis of the 3D surface starts from the right side of the surface and increases towards the left.

4.3 Volumetric Analysis

In order to determine the volumetric wear, the measured raw data of 110 roundness traces were exported as individual point clouds in .csv file which provides the user with 110 individual .csv files.

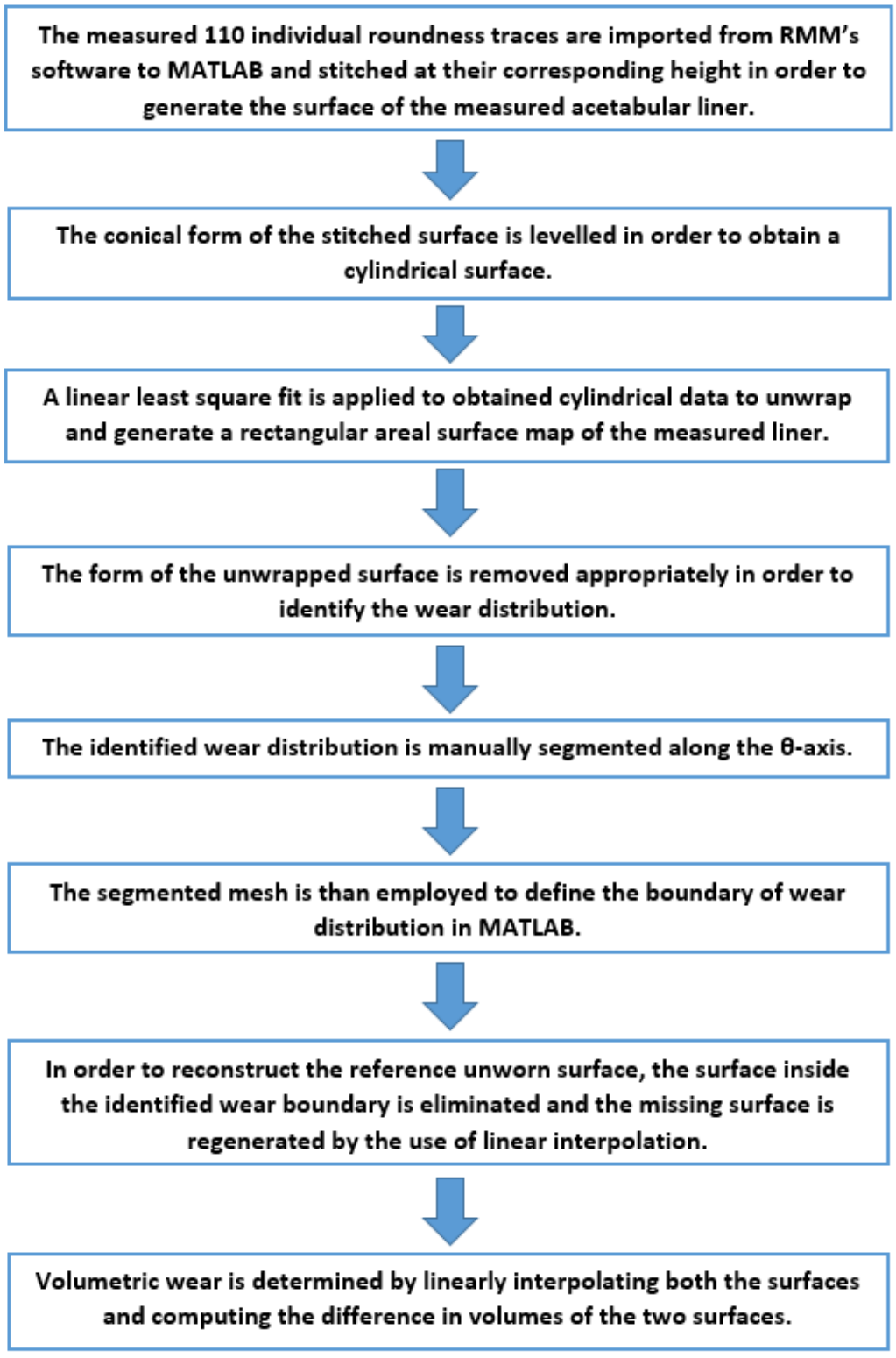

Figure 61: A block diagram displaying the analysis procedure of the RMM method.

The analysis of the obtained raw data is executed by the use of various procedures organized through the utilisation of a set of software programs

generated in MATLAB (The Mathworks Inc., Natick, USA). The volumetric analysis process begins by stitching all the 110 individual roundness traces at the corresponding height and generate the measured actual surface of acetabular liner. An example of this stitched surface is displayed in Figure 62. Than the conical form of the stitched data is levelled and a linear least square fit for all of the data, including the worn area, is applied to unwrap and generate a rectangular areal map of the acetabular liner. An example of this unwrapped surface can be seen in Figure 63 given below. The suggested method is not dependant on the estimated radius as it utilises a Cartesian co-ordinate system to unwrap the stitched roundness traces, and hence it is robust with respect to the estimated cylindrical form. The cylindrical coordinates (radius (r), angle (θ) and height (h)) are computed using the following formulas given below:

$$\begin{cases} r = \sqrt{x^2 + y^2} \\ \theta = \operatorname{atan}\left(\frac{y}{x}\right) \\ h = z \end{cases}$$

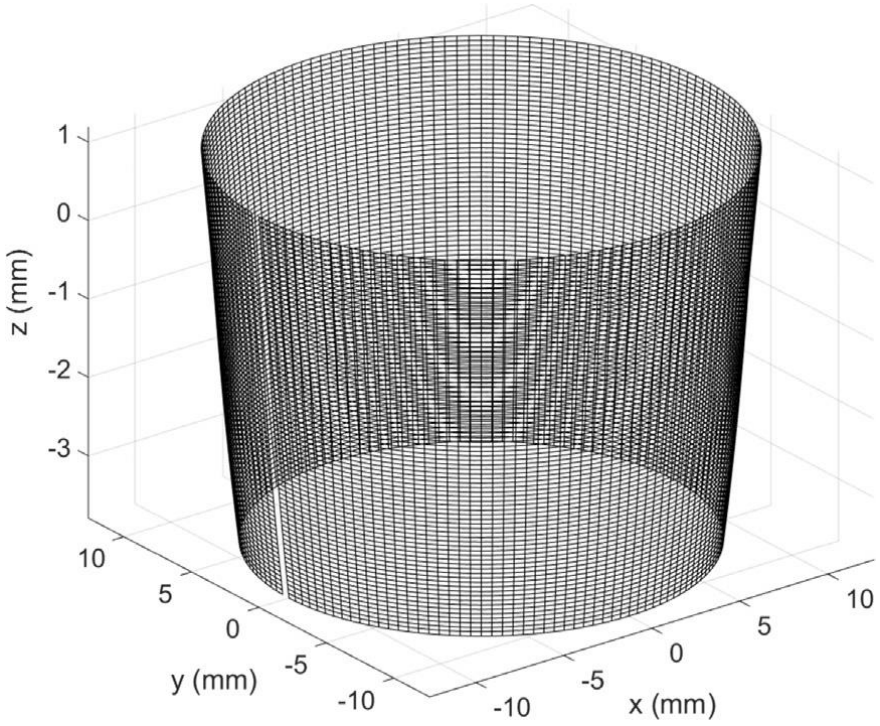

Figure 62: Image displaying the stitched 110 roundness traces using developed MATLAB script.

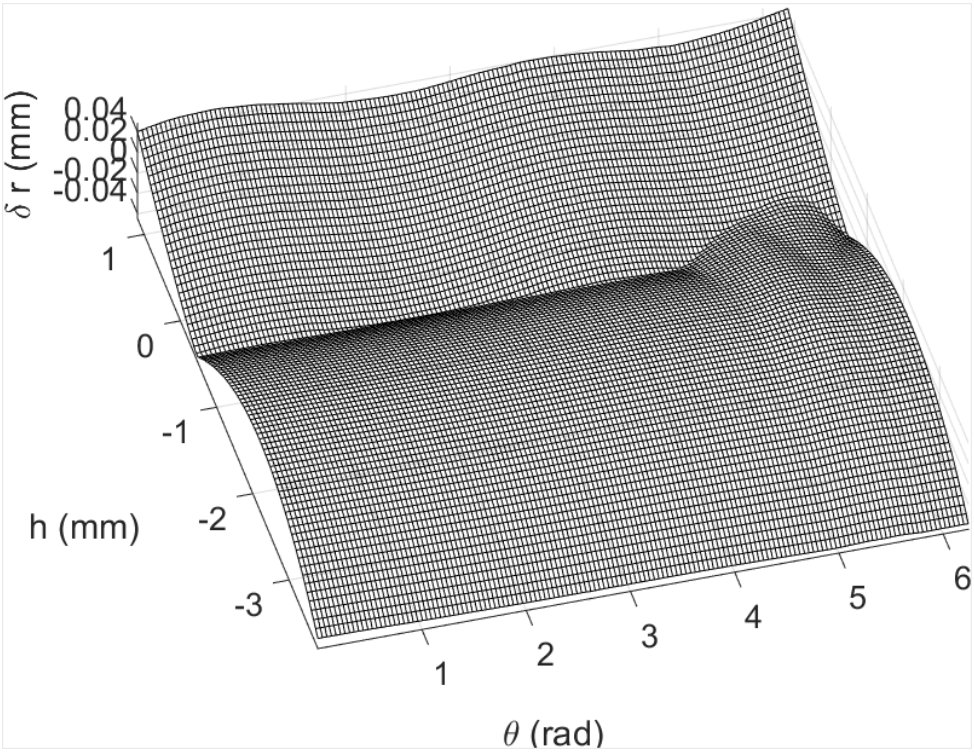

Figure 63: Unwrapped and form removed surface of the cup liner in cylinder co-ordinate (MATLAB).

After unwrapping the stitched data, the boundary of the wear distribution is identified in order to produce a surface that imitates the unworn as manufactured surface of the measured liner. A manual segmentation process is executed in order to perform this task. Firstly the form is removed by the use of a first degree polynomial in h direction and a second degree in θ direction, then the surface is segmented manually along the θ axis. The wear was clearly visible in all the measured liners after the form removal process. An example of this is displayed in Figure 64. The polygon file format is then saved and imported in an open source triangular mesh (3D point cloud) editing and processing software known as CloudCompare (http://www.cloudcompare.org/) where the point cloud is meshed and the wear region is zoomed in to perform accurate segmentation of the wear patch. This segmented mesh allows to define the boundary of wear distribution in MATLAB. Figure 64 below displays the MATLAB plot of the surface where the manually segmented wear boundary is marked by a red line.

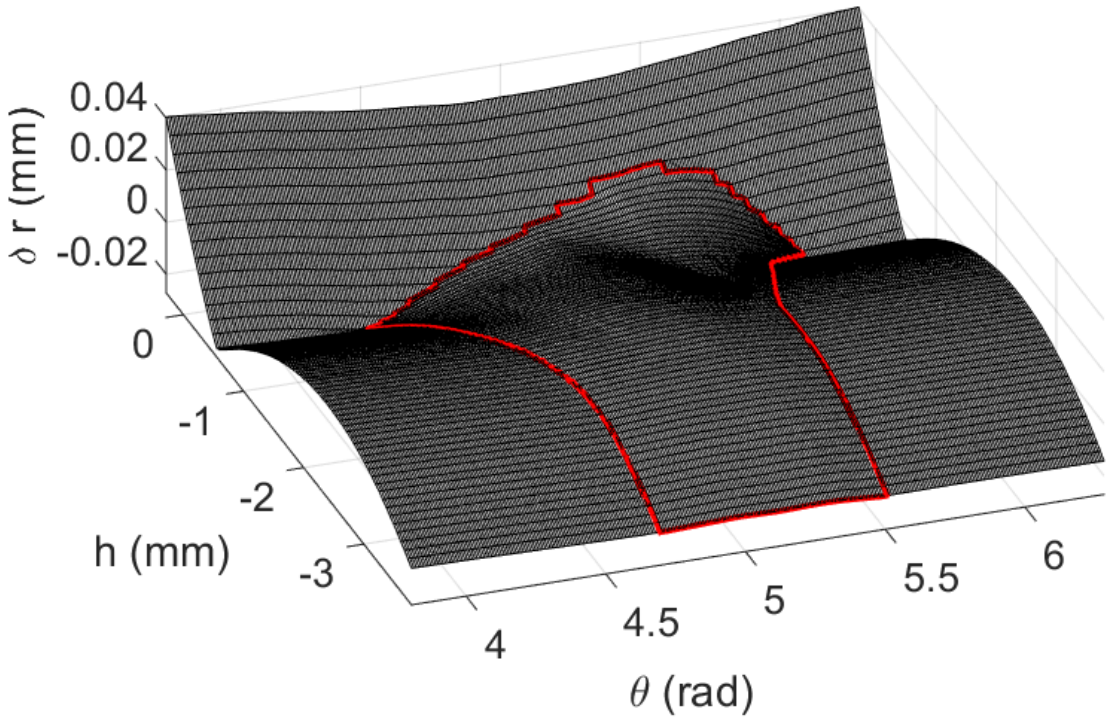

Figure 64: Image displaying the proximal surface and wear boundary (MATLAB).

As the segmentation process is performed manually, it is operator dependent and is subjective to the operator's perception of wear. Like CMM method, the RMM method also depends on the presence of unworn data adjacent to the worn area of the liner's edge in order to obtain a reliable datum to reconstruct the imitation of the original as manufactured surface.

Subsequent to importing the defined wear boundary to MATLAB, the next step is to reconstruct a surface which is an effective imitation of the unworn surface. For the reconstruction of the required unworn surface, the surface inside the identified wear boundary is eliminated and the missing surface is regenerated by the use of linear interpolation. It is important to note that the linear interpolation of cylindrical co-ordinates resembles to an arc of a circle in Cartesian co-ordinates. For this step the original form is used, without removing any polynomial form, in order to perform the correct volume computation. Finally, to determine the volumetric wear, both the surfaces are linearly interpolated and the difference in volumes of both the surfaces is computed. This difference in volume is the required volumetric wear.

After developing the RMM method, the method was tested by measuring the same cohort-A of six simulated acetabular liners that was employed for CMM method. The results obtained through the RMM method were then compared against the results obtained from the gravimetric method.

4.4 Results

All six acetabular liners of the simulated cohort-A were measured according to the developed measurement procedure. Measurement data of each liner surface was exported and rendered to generate a 3D surface. Through examination of these 3D surfaces it was observed that each liner had a singular area of localised wear and the wear distribution ranged from above the edge to the bearing surface as seen in Figure 65 below. The in-vitro linear wear penetration determined from the 3D surfaces of all six acetabular liners ranged from 10.59μm to 29.48μm and is tabulated below in Table 15. In each liner the 3D surface was segmented in order to establish the required mean plane value and eliminate areas of form error that is not proximal to the wear area. This allows for local normalisation of the data and limits the error from hindering the precision of the linear wear computation.

The greater level of resolution resulting from the segmentation process led to a greater level of definition of the edge wear distribution and highlighted an area immediately adjacent in which wear appears to 'smear' onto the bearing surface and above the edge. After examining the 3D surface, the measured circular traces were analysed using the developed MATLAB programs to assess the volumetric wear for each acetabular liner.

Liner	**1**	**2**	**3**	**4**	**5**	**6**
Linear Wear (μm)	10.59	23.92	14.71	29.48	16.44	29.66
Wear Sector Length (°)	65.5	94	90.5	111	93	84
Volumetric Wear (mm^3)	0.061	0.285	0.109	0.362	0.114	0.177

Table 15: Wear sector, linear wear and volumetric wear obtained from the roundness measurement method.

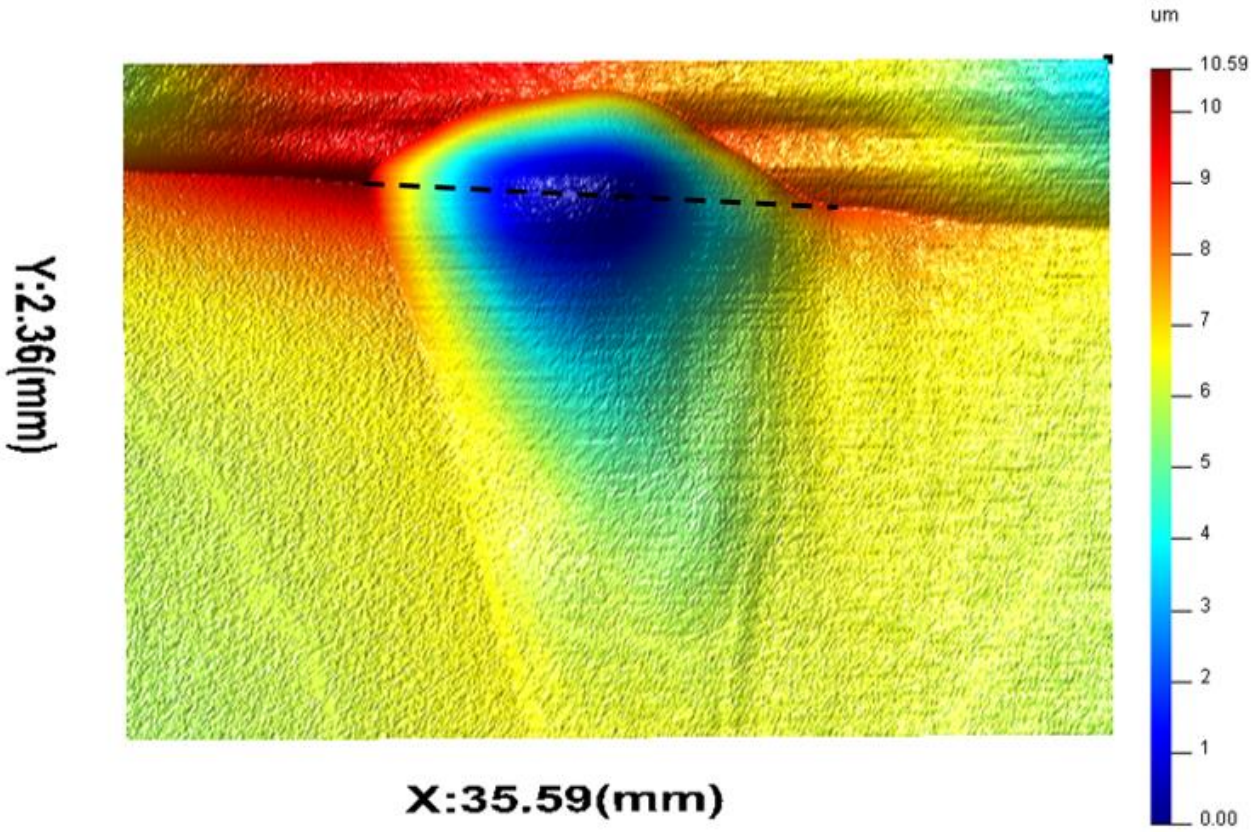

Figure 65: Image displaying the edge wear distribution beyond the bearing surface. The dotted line denotes the edge on the worn area of the liner.

The results of linear wear and volumetric wear obtained from roundness measurement method are shown in Table 15. The obtained linear wear and volumetric wear measured by RMM method for all six liners ranged from 10.59μm to 29.66 μm and 0.061 mm^3 to 0.362 mm^3 respectively. A correlation between linear wear and volumetric wear was observed. However, it was apparent from this cohort-A of simulated acetabular liners that there is some variance in the sector length over which edge wear has occurred. For example, it can be observed from Figure 66 below that liner 6 and liner 4 have a similar degree of linear wear penetration, yet the volumetric wear of liner 4 is significantly higher compared to that of liner 6 as the linear wear penetration of liner 4 is spread out for a longer sector length than that of liner 6. This difference is potentially due to a combination of several factors including positioning, test conditions, fixturing and local head-liner geometry. An estimation of the wear affected area can be made combination of the linear

wear depth and segmented sector length which is defined in the segmented surface as X and Y axes.

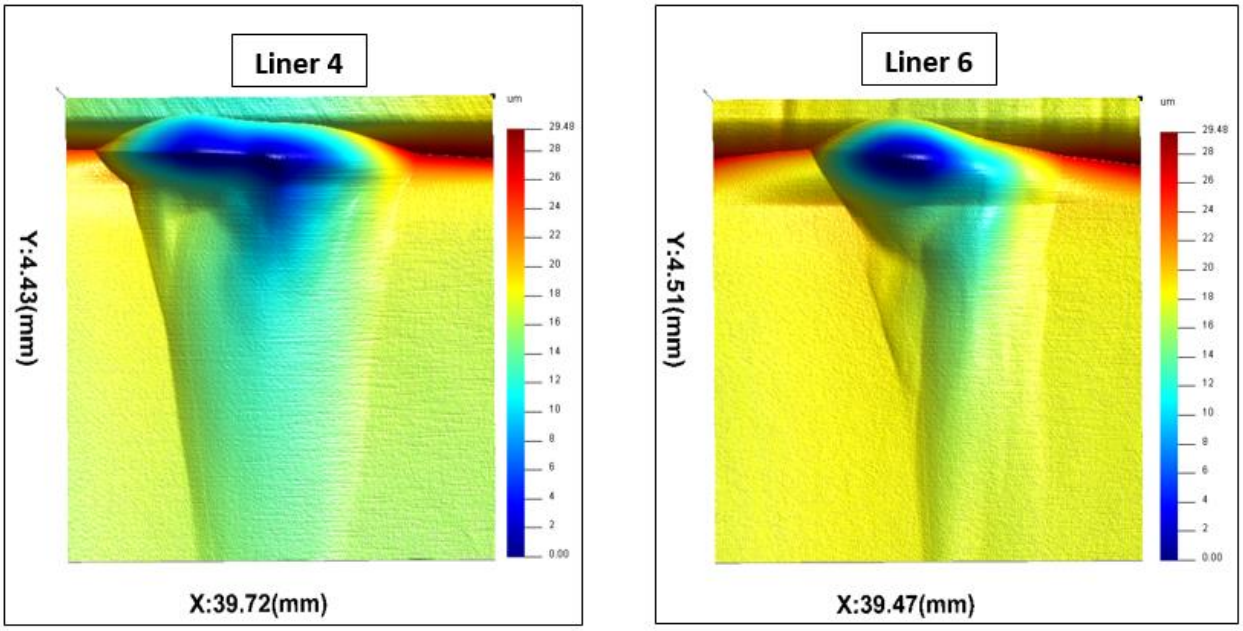

Figure 66: Image showing wear distribution and linear wear penetration in acetabular liner 4 and liner 6. This data is segmented to focus on the wear patch.

This cohort-A of ceramic acetabular liners were gravimetrically assessed to quantify volumetric wear subsequent to the wear simulation process. The results obtained by RMM method are tabulated against the results obtained from gravimetric method in Table 16 below and graphically represented in a bar graph below in Figure 67. The error bars of the RMM method added to the bar graph represents the standard deviation obtained from the repeatability study which is detailed in the next section. Again, as mentioned in the CMM method results (Section 3.9), the errors bars for the gravimetric method are as small as 0.0016 mm^3.

Total Volumetric Wear (mm3)						
Liner	**1**	**2**	**3**	**4**	**5**	**6**
Gravimetric	0.112	0.414	0.179	0.432	0.164	0.247
RMM	0.061	0.285	0.109	0.362	0.114	0.177
Difference	0.051	0.129	0.070	0.070	0.050	0.070

Table 16: Volumetric wear results obtained from RMM method are tabulated against Gravimetric results with difference calculated.

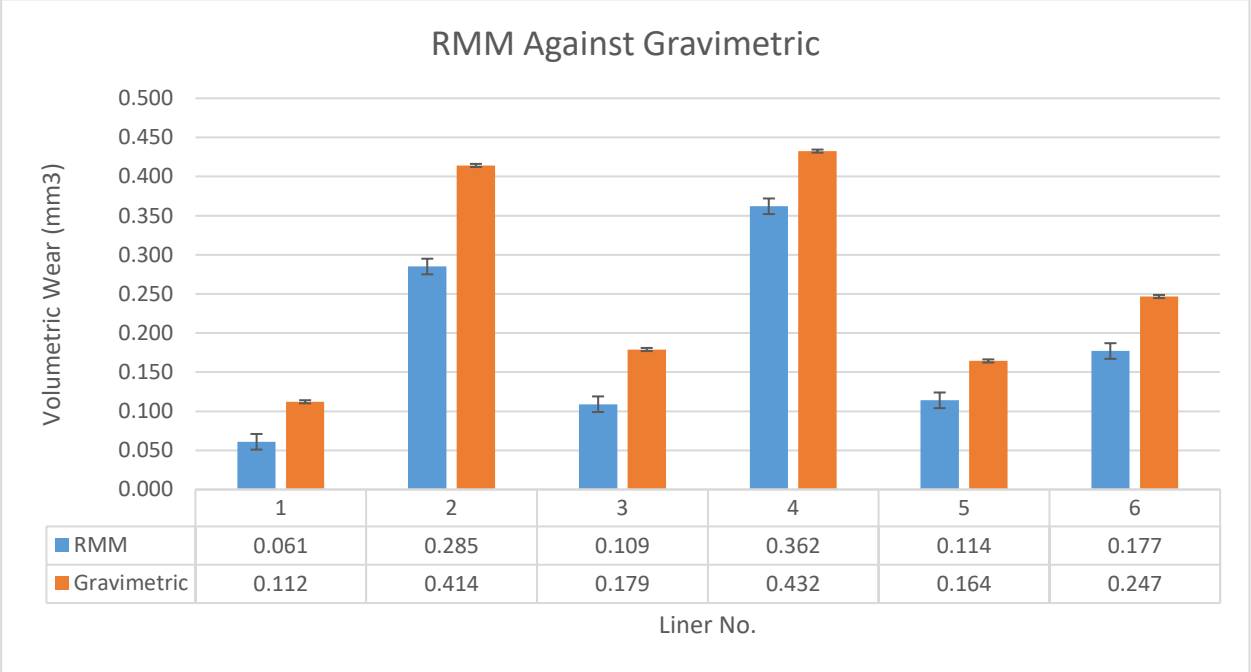

Figure 67: Bar graph comparing the volumetric wear results of cohort-A as measured by the RMM method and the Gravimetric method.

After examining graphical comparison, the correlation between RMM method and gravimetric method was tested by Pearson's correlation test. The Pearson correlation value was found to be 0.985 at a significance value of 0.001 which displays a strong correlation between two methods.

4.5 Inter-operator Variability for RMM method

A study was performed to test the repeatability and reproducibility of the measurement procedure and inter-operator variability of the analysis process

of the RMM method. The inter-operator variability was tested only on analysis process due to lack of a volunteer. Acetabular liner A-6 was chosen from the set of wear simulated cohort-A to perform the study as liner A-6 exhibited high linear wear penetration yet the obtained volumetric wear was low. Hence, this was a good opportunity to test the RMM method's resolution.

Acetabular liner A-6 was measured twenty times on the Talyrond 365 roundness measuring machine for this study. Each measurement followed the previously outlined RMM method procedure as mentioned in section 4.1.2 and the component was levelled and positioned on Talyrond 365 for each and every measurement. This ensured that the influences of the centring and levelling process on the measurement are considered while studying repeatability. It is important to note that the measurements were performed by a single operator. However the analysis process, being user dependent, was performed in a blind manner by two operators in order to assess inter-operator variability of the analysis process.

Blinded analysis process was performed by two operators to assess inter-operator variability of the analysis process. Both operators followed the analysis process specifications outlined in section 4.2, this included form removal process as well as any segmentation required in order to estimate the material loss volume.

	User – 1 Volumetric Wear (mm^3)	**User – 2 Volumetric Wear (mm^3)**	**Inter-operator Variability (mm^3)**
Mean	0.1780	0.1810	0.0071
Median	0.1790	0.01816	0.0071
Range	0.1603 – 0.1899	0.1749 – 0.1846	0.0000 – 0.0151
Std. Deviation	0.0090	0.0031	0.0043

Table 17: Results of the inter-operator variability study for analysis of volumetric wear. This table displays difference in the mean, median, range and std. deviation between the results obtained by 2 individual users.

The results obtained from the inter-operator variability and the repeatability study are tabulated in Table 17 and shows a good agreement in results obtained by two operators in terms of determined value of mean, median and range. As the study was performed in a blind manner on a simulated acetabular liner, the operators had no pre-wear information related to liner geometry. It can be observed that the standard deviation of the entire measurement and analysis process is found to be 0.009 mm^3 for first user and 0.003 mm^3 for second user. Hence, it can be said that the RMM method displays high repeatability of the measurement and analysis process and good reproducibility between operators.

Further this study shows good agreement between the operators when considering individual datasets with an overall standard deviation of inter-operator variability of 0.004mm^3. In below given Figure 68, a Bland-Altman plot is displayed to graphically examine the obtained results in detail. Normal distribution of variations in the obtained results was confirmed by Sharipo-Wilk test, and the normality was accepted with significant P-value of 0.164 (Alpha value = 0.05) (SPSS). As operator-2 was more experienced with the analysis process, the analysis results of operator-2 are taken as reference instead of taking the mean of two operators. The dashed line represents the 95% limit of agreement (1.96 Standard Deviation) range to examine the agreement of the analysis as analysed by two operators. This 95% confidence interval of agreement limits are -0.019 to 0.013 mm^3. The mean of the paired differences in measurements from two operators is -0.003mm^3 and is denoted by the solid line. The bias between two measurements can be estimated by the distance of mean line (dashed line) from the zero (dotted line). The t-score significance value is found to be 0.312 which is insignificant which agrees with the null hypothesis that the bias is non-proportional.

It is noted that the major contributing factor causing the variance in the volumetric wear measurement is the user dependent wear boundary identification process that affects the repeatability and reproducibility of the analysis process. Other factor is the centring and levelling procedure from the

measurement process that contributes to variance in the volumetric wear measurement.

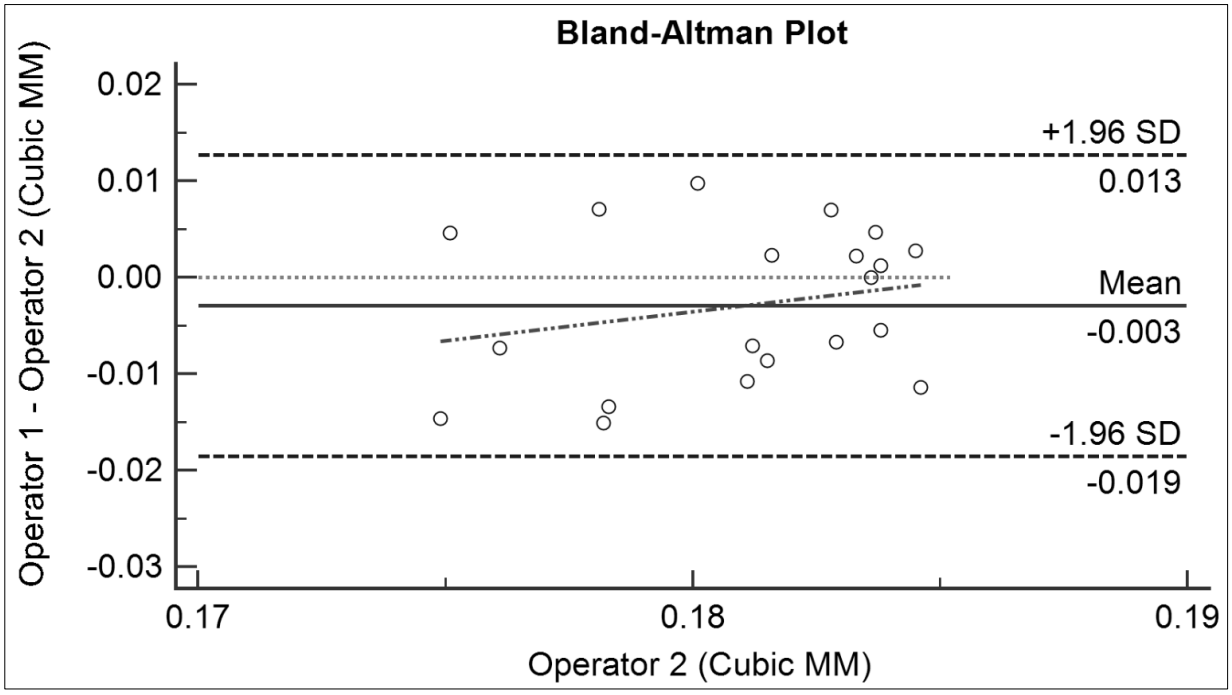

Figure 68: Bland-Altman Plot with line of equality showing inter-operator variability and regression line stating absence of proportional bias problem.

Chapter 5: Case Study – Interval Wear Measurement

5.1 Summary

This chapter provide the details of the case study performed to test the developed CMM and RMM methods. The chapter describes the type of liner employed for the study, the details of simulation performed on the liners and the study design of the case study. The results obtained by each method are compared against the gold standard gravimetric method to test the performance of each developed method.

5.2 Study Design

Subsequent to method development, a case study was performed to test both the developed methods. For this case study, a new cohort coded as cohort-C was measured. Cohort-C consist of six 36mm diameter ceramic-on-ceramic acetabular liners of hip arthroplasty device (BIOLOX® delta, Pinnacle®, DePuy Synthes, Leeds, UK). The liners of cohort-C were simulated on the Leeds II hip joint simulator (Institute of Medical and Biological Engineering, University of Leeds) under edge loading conditions similar to that of cohort-A which was employed for the method development. For this study the acetabular liners were simulated for three million walking cycles, with measurement intervals at every million cycles. The purpose of this study was to test both, CMM and RMM, method's capability to trace the formation and progression of volumetric wear in order to confirm that the method is robust for quantifying volumetric wear. Similar to the method development study, edge loading between the femoral head and acetabular cup liner for this case study occurred during gait due to dynamic separation driven by translational mismatch between the centres of rotation of the femoral head and acetabular cup liner [28].

Under the given test condition the wear was simulated at the edge region of the acetabular liner. After completion of each interval (one million cycle), the components were cleaned from contaminants using local standard

operating procedures prior to performing measurements in a temperature and humidity controlled environment using a microbalance (Mettler-Toledo XP205, UK). The liners were measured in a temperature and humidity controlled environment before commencing the simulation in order to obtain pre-simulation data. The wear volume was determined by gravimetric method at each interval by dividing the mass loss by the density of the BIOLOX® delta material which was given as 0.00437 g/mm^3.

Once gravimetric measurement was completed, measurement of the acetabular liners was performed in a blind manner at EPSRC CIMAM, University of Huddersfield. The components were measured on both co-ordinate measuring machine and a roundness measuring machine for assessment through both the methods. A Zeiss Prismo CMM (Carl Zeiss, Rugby, UK) was used to measure both the bearing surface and the rim of the liner up to the flat plane. An individual reference geometry that imitates the unworn as manufactured surface was generated for all six acetabular liners of the cohort-C and then the wear characterisation analysis was performed as detailed in section 3.7 and section 3.8.

For RMM method, a Talyrond 365 (Taylor Hobson) was used to measure the maximum permissible height around the edge wear distribution and the measured traces were than analysed on MATLAB generated software as detailed in section 4.2 to assess volumetric wear. The results obtained from both, CMM method and RMM method, were compared against the gold standard gravimetric method.

5.3 Results – CMM Method

The given cohort-C of six 36mm ceramic acetabular cup liners were measured on a CMM and analysed as a blind study to characterise and quantify volumetric wear at each interval. The measurement procedure and the volumetric analysis employed for this measurement was same as mentioned in section 3.2, section 3.7 and section 3.8 respectively. To quantify the

volumetric wear, a reference geometry imitating the unworn surface was generated individually at each interval for each acetabular liner of the given cohort-C. The analysis process consisted of two parts which were deviation analysis and volumetric assessment. Deviation analysis was performed to observe the deviation between the generated reference surface and the measured surface which effectively characterised wear distribution at each interval. Again it was observed that each acetabular liner at every interval had a singular area of localised wear. Deviation analysis was also capable to quantify linear wear penetration at each interval and an example of this is provided below in the three figures (Figure 69, Figure 70 and Figure 71) display the deviation analysis at interval 1 interval 2 and interval 3 respectively for liner 4. The colour map and percentage displayed in all the examples given below denotes the linear wear penetration and the percentage of the surface linear wear penetration in the corresponding range. It must be noted that the percentage are calculated with respect to the reconstructed surface and not the mesh of the measured surface. The colour map and percentage is displayed in all three examples of deviation analysis in order to visualise linear wear penetration and the vertical scale is purposely made constant for the reader to be able to compare the progression of linear wear penetration with each interval. The histogram provided with the colour map also gives information regarding the fitting of the reconstructed unworn surface by allowing the user to examine the percentage of reconstructed surface under the required threshold. For example, from the below reconstructed surface of liner 4 of cohort C, it can be noted that the 93.34%, 92.02% and 89.74% of the surface remains under a deviation of 4 μm from the measured surface. The colour map also allows the user to identify any outliers, for example it allows the user to differentiate between wear distribution and a debris deposit or scanning error.

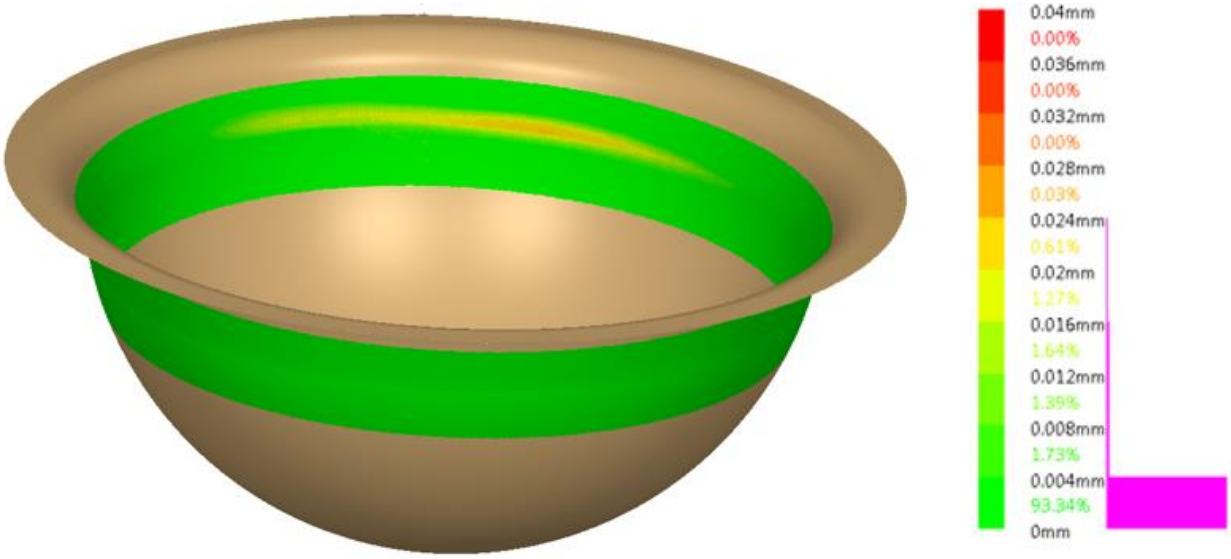

Figure 69: Image displaying the deviation analysis results of liner 4 at interval - 1 with the colour map.

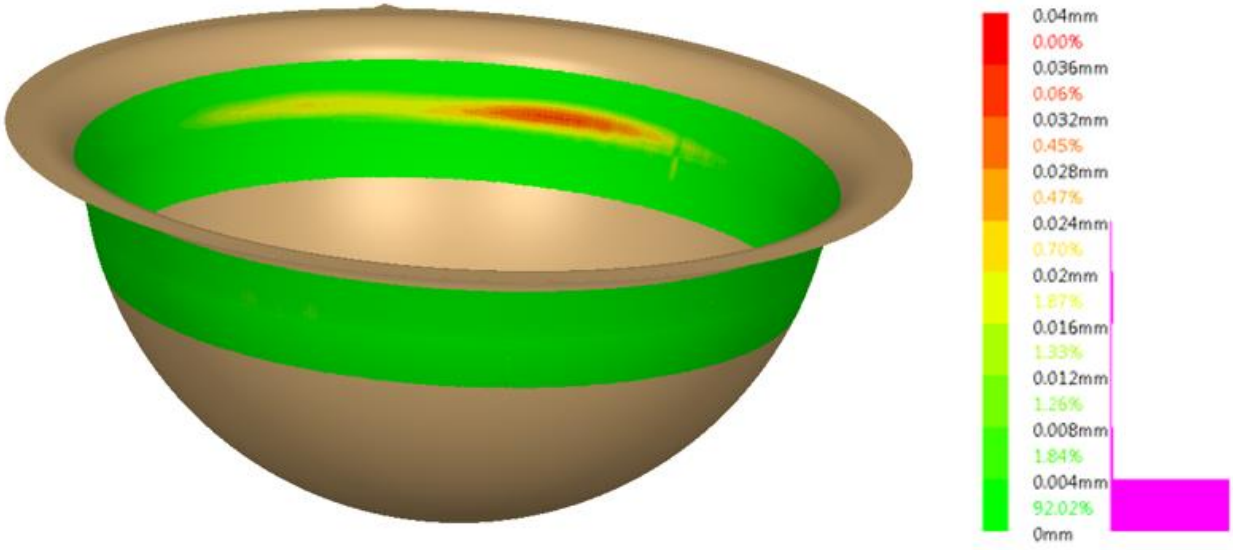

Figure 70: Image displaying the deviation analysis results of liner 4 at interval - 2 with the colour map.

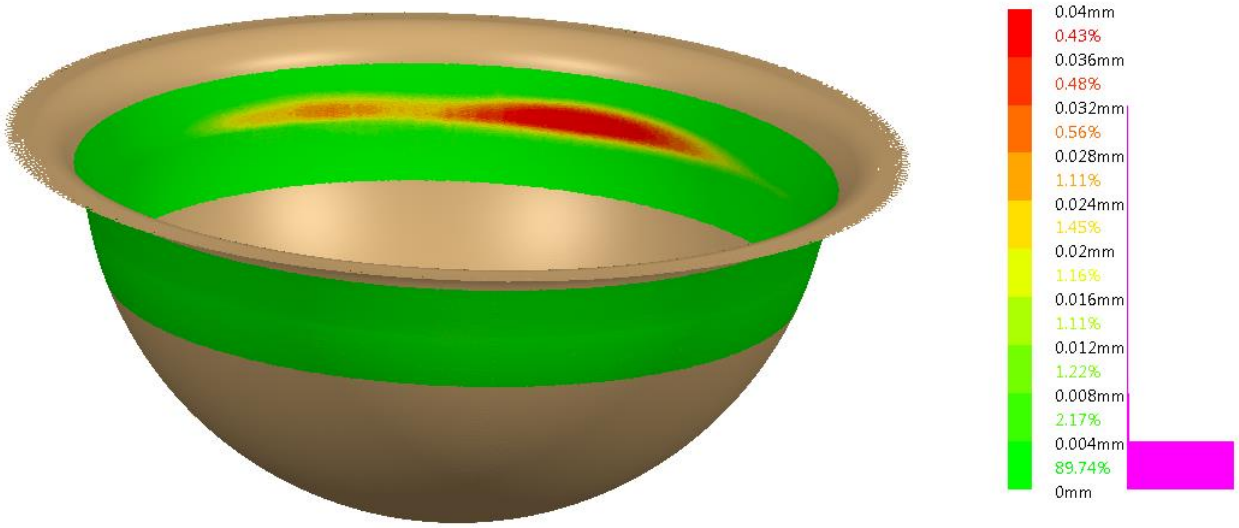

Figure 71: Image displaying the deviation analysis results of liner 4 at interval - 3 with the colour map.

By comparing the above three figures, the ability of the CMM method to trace the progression of wear is evident. It can be observed that the highest linear wear penetration range in liner 4 for interval 1 is 0.024 mm to 0.028 mm at 0.03%, for interval 2 is 0.0032 mm to 0.0036 mm at 0.06% and for interval 3 is 0.0373 mm to 0.04 mm at 0.24%. The deviation analysis highlighted that the edge wear distribution was spread out above the edge and into the bearing surface for all the six acetabular liners from the first interval itself. The determined linear wear penetration through deviation analysis for all six acetabular liners at each interval is tabulated below in Table 18.

Linear wear Penetration (mm)						
Liner	**1**	**2**	**3**	**4**	**5**	**6**
Interval - 1	0.0405	0.0284	0.0385	0.0259	0.0294	0.0310
Interval - 2	0.0440	0.0429	0.0440	0.0338	0.0318	0.0364
Interval - 3	0.0551	0.0454	0.0473	0.0481	0.0323	0.0382

Table 18: Tabulated linear wear penetration for all six acetabular liners at each interval determined by through deviation analysis of CMM method.

After deviation analysis, volumetric analysis was performed to assess the edge wear volumes of all six acetabular liners at each interval. The measured surface and the generated reference surface were enclosed and the difference in volumes was computed. Again, in each case the volume measurement was narrowed down to the area of wear distribution to limit form errors, measurements errors or errors induced through debris in order to compute wear volumes as precisely as possible. The volumetric wear results of CMM method at each interval are tabulated below in Table 19.

Total Volumetric Wear (mm^3)			
Liner	**Interval 1**	**Interval 2**	**Interval 3**
1	0.6980	0.9530	1.3380
2	0.4260	0.6800	0.7290
3	0.5060	0.9660	1.2430
4	0.4010	0.7310	0.8620
5	0.3890	0.6090	0.9130
6	0.4680	0.8030	0.6960

Table 19: Tabulated volumetric wear results of all three intervals.

From the above results in Table 19, volumetric wear progression can be noted for all the liners except for liner 6. Some error is observed with liner 6 at the interval 3 as, instead of increase in wear volume at the third interval, a decrease can be noted. This is suspected to be a measurement error and re-measurement was not possible as the cup liners had already been returned, hence the error induced through measurement couldn't be confirmed. However, the analysis process was performed three times on the same measurement of liner 6 in order to trace the errors induced through analysis process and the maximum variance in results obtained was 0.007 mm^3. It was observed that the first interval had endured maximum wear compared to interval 2 and interval 3. This is due to the bedding-in period

which was in interval 1 and steady wear period was for second and third interval.

After determining the wear volumes of cohort-C through CMM method, the results of CMM method were compared against the results obtained from the gold standard gravimetric method to test the authenticity of the results obtained from CMM method. The quantified volumetric wear by both, CMM and gravimetric method is tabulated below in **Error! Reference source not found.**.

Total Volumetric Wear (mm^3)						
Liner	**Interval 1**		**Interval 2**		**Interval 3**	
	CMM	**Gravimetric**	**CMM**	**Gravimetric**	**CMM**	**Gravimetric**
1	0.6980	0.6100	0.9530	0.8517	1.3380	1.4000
2	0.4260	0.5200	0.6800	0.6892	0.7290	0.9200
3	0.5060	0.7700	0.9660	1.0311	1.2430	1.4200
4	0.4010	0.5400	0.7310	0.7574	0.8620	1.0800
5	0.3890	0.4600	0.6090	0.5680	0.9130	0.8800
6	0.4680	0.6400	0.8030	0.8352	0.6960	1.1300

Table 20: Tabulated volumetric wear results obtained by the CMM and the gravimetric method.

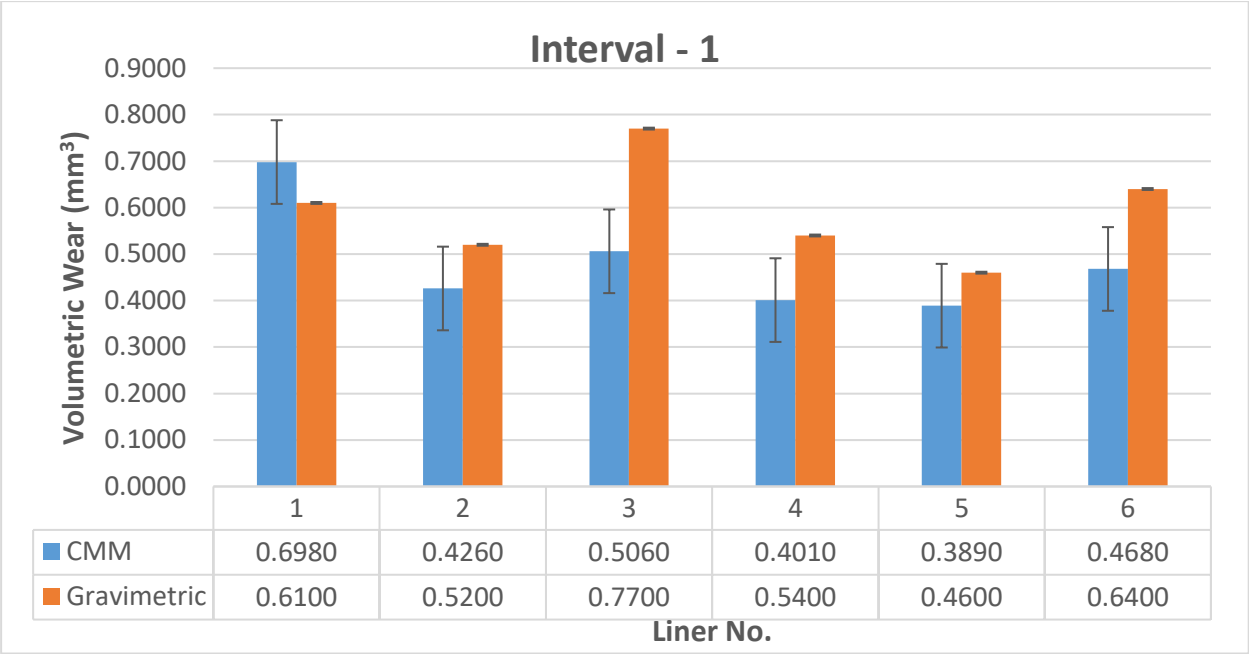

Figure 72: A bar graph comparing CMM results against Gravimetric results for interval - 1.

Interval – 1						
Liner No.	**1**	**2**	**3**	**4**	**5**	**6**
CMM (mm^3)	0.6980	0.4260	0.5060	0.4010	0.3890	0.4680
Gravimetric (mm^3)	0.6100	0.5200	0.7700	0.5400	0.4600	0.6400
Difference (mm^3)	0.0880	0.0940	0.2640	0.1390	0.0710	0.1720

Table 21: A table displaying the variations between the results obtained from CMM method and gravimetric method for interval 1.

The above bar graph displayed in Figure 72, exhibits the volumetric wear results of interval 1 obtained through the CMM method and the gravimetric method. It was speculated that the wear volume of liner 1 as measured by CMM method was the only result that is higher than the result obtained by gravimetric method. Due to the result obtained through CMM method being higher than the results obtained through gravimetric method it is suspected to be involved with errors within either of the results as gravimetric method is always suspected to measure higher wear than the CMM method. This is because CMM method only accounts for the edge wear

whereas gravimetric method accounts for the wear on the full the liner surface including the rear surface employed for clamping. The above Table 21 shows the absolute variation between the results obtained through CMM method and gravimetric method for all the six liners. The variation between results obtained by CMM method and gravimetric method ranged from 0.071 mm^3 to 0.264 mm^3. The liner 3 and liner 6 at this interval were found to be chipped and is suspected to be the reason of high variance in wear volumes as measured by the CMM method and the gravimetric method. Another reason to increase this suspicion is that the volumetric wear results of liner 3 and liner 6 as measured by the CMM method and the RMM method were found to be similar, i.e. 0.506 mm^3 and 0.468 mm^3 for the CMM method and 0.537 mm^3 and 0.473 mm^3 for the RMM method respectively. After excluding liner 3 and liner 6 measurements from the cohort, the range of variation is reduced down to 0.071 mm^3 to 0.139 mm^3.

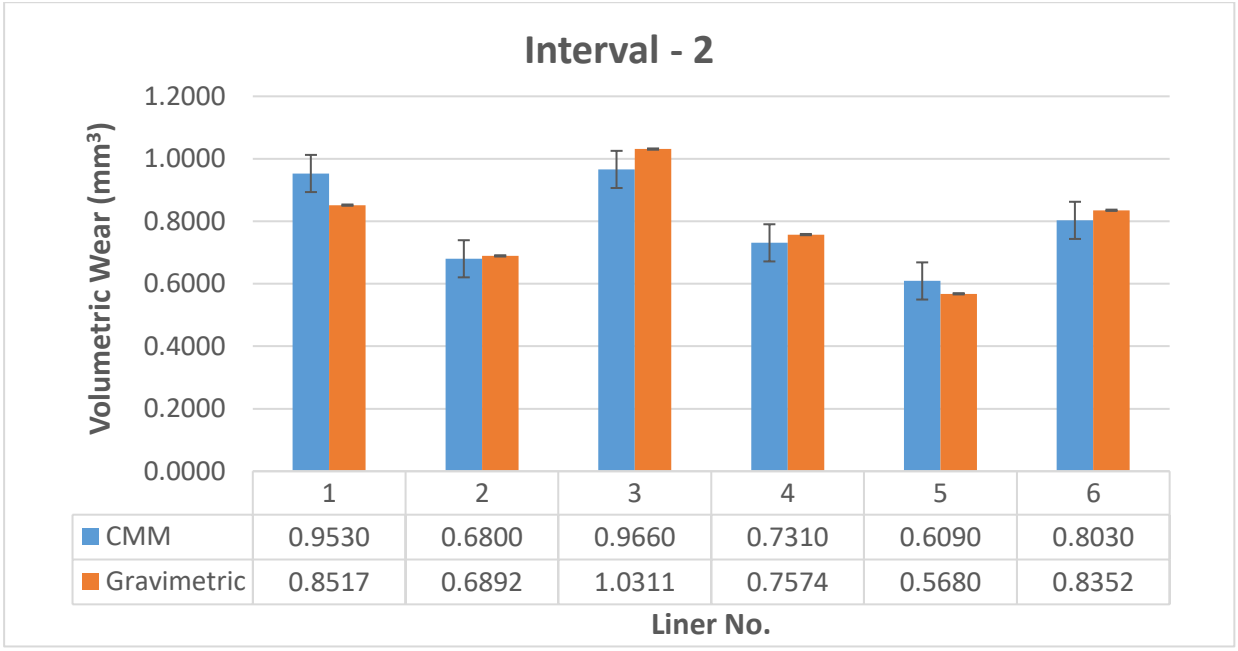

Figure 73: A bar graph comparing CMM results against Gravimetric results for interval - 2.

Interval - 2						
Liner No.	**1**	**2**	**3**	**4**	**5**	**6**
CMM (mm^3)	0.9530	0.6800	0.9660	0.7310	0.6090	0.8030
Gravimetric (mm^3)	0.8517	0.6892	1.0311	0.7574	0.5680	0.8352
Difference (mm^3)	0.1013	0.0092	0.0651	0.0264	0.0410	0.0322

Table 22: A table displaying the variations between the results obtained from CMM method and gravimetric method for interval 2.

The above bar graph displayed in Figure 73, exhibits the volumetric wear results for interval 2 obtained through the CMM method and the gravimetric method. From the graph displayed in Figure 73, it was speculated that the wear volume of liner 1 as measured by CMM method was again higher than the result obtained by gravimetric method. The variations in the results as seen from the bar graph were less compared to the variations of interval 1. The above Table 22 shows the variation between the results obtained through CMM method and gravimetric method at second interval for all the six liners. The variation between results obtained by CMM method and gravimetric method ranged from as low as 0.009 mm^3 to 0.101 mm^3 for second interval.

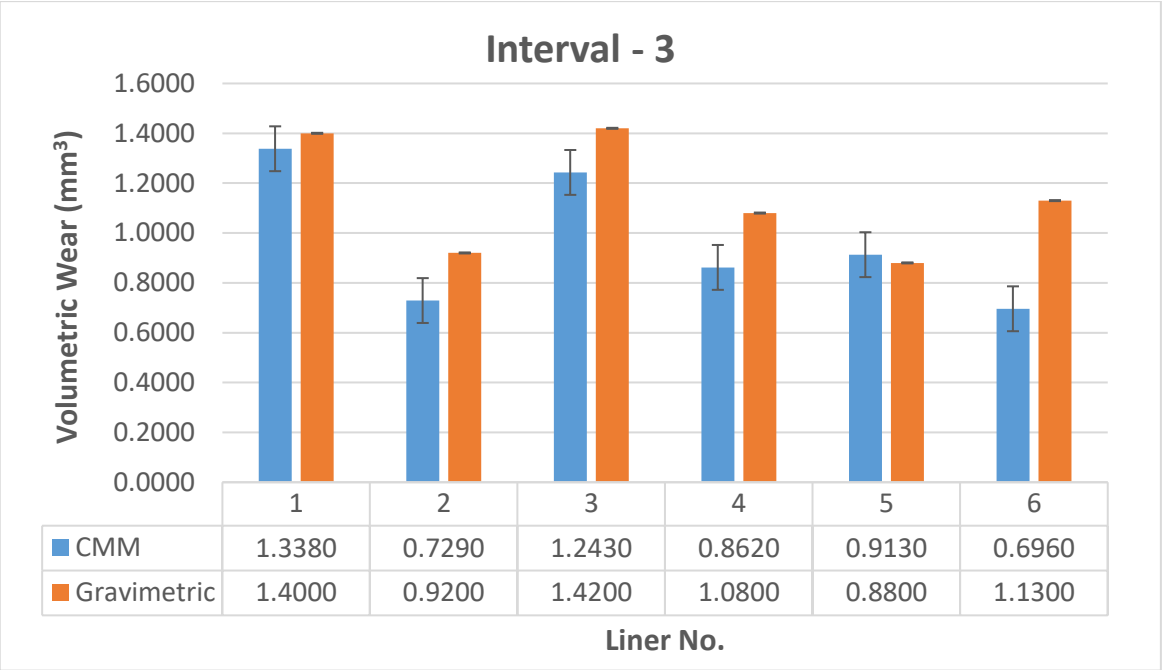

Figure 74: A bar graph comparing CMM results against Gravimetric results for interval - 3.

Interval – 3						
Liner No.	**1**	**2**	**3**	**4**	**5**	**6**
CMM (mm3)	1.3380	0.7290	1.2430	0.8620	0.9130	0.6960
Gravimetric	1.4000	0.9200	1.4200	1.0800	0.8800	1.1300
Difference	0.0620	0.1910	0.1770	0.2180	0.0330	0.4340

Table 23: A table displaying the variations between the results obtained from CMM method and gravimetric method for interval 3.

The above bar graph displayed in Figure 74, exhibits the volumetric wear results for interval 3 obtained through the CMM method and the gravimetric method. Again in third interval it is observed that the linear wear penetration is in good correlation with the quantified wear volumes by CMM method and gravimetric method. However a high variation in the quantified wear volumes can be speculated for liner 4 and liner 6. The above Table 23 shows the variation between the results obtained through CMM method and gravimetric method at third interval for all the six liners. By studying the tabulated variations results in Table 23 it can be noted that the variation in liner 4 and liner 6 are as high as 0.218 mm^3 and 0.434 mm^3 respectively. The

variation between results obtained by CMM method and gravimetric method ranged from as low as 0.033 mm^3 to 0.434 mm^3 for third interval.

5.4 Results – RMM Method

The liners of cohort-C were measured and analysed in a blind manner through the RMM method. All six acetabular liners were measured according to the measurement procedure as mentioned previously in section 4.1.2. Through examination of the 3D surfaces it was speculated that each liner had a singular area of localised wear for all three intervals similar to that found in cohort-A. The in-vitro linear wear penetration results that were determined from the 3D surfaces of all six acetabular liners at each interval are tabulated in Table 24. Below given Figure 75, Figure 76 and Figure 77 displays an example of progression in wear of liner 4 at interval 1, interval 2 and interval 3 respectively.

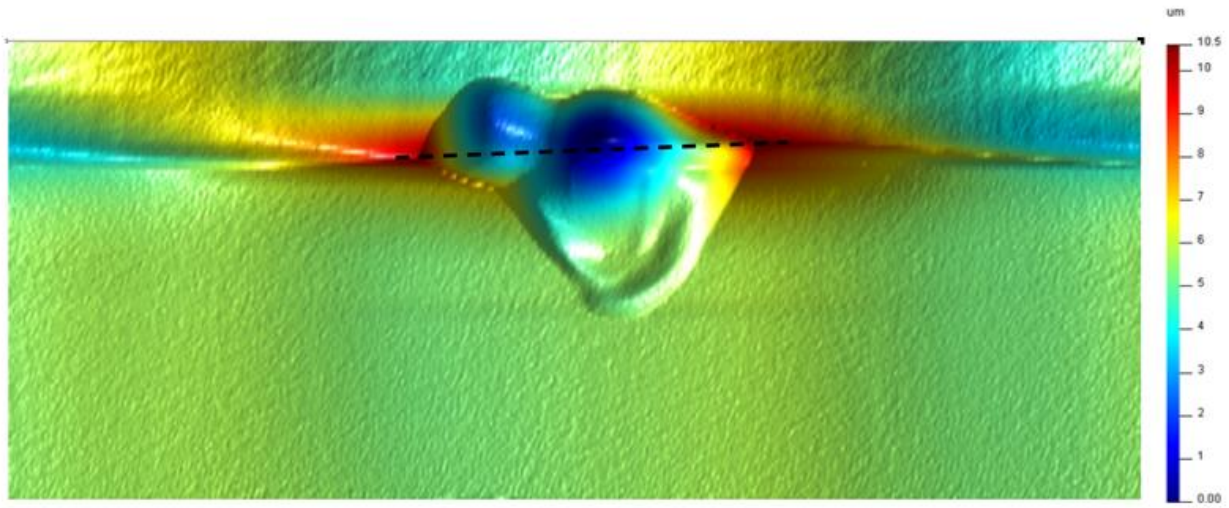

Figure 75: Image displaying the 3D surface of liner 4 at interval - 1 with the colour map.

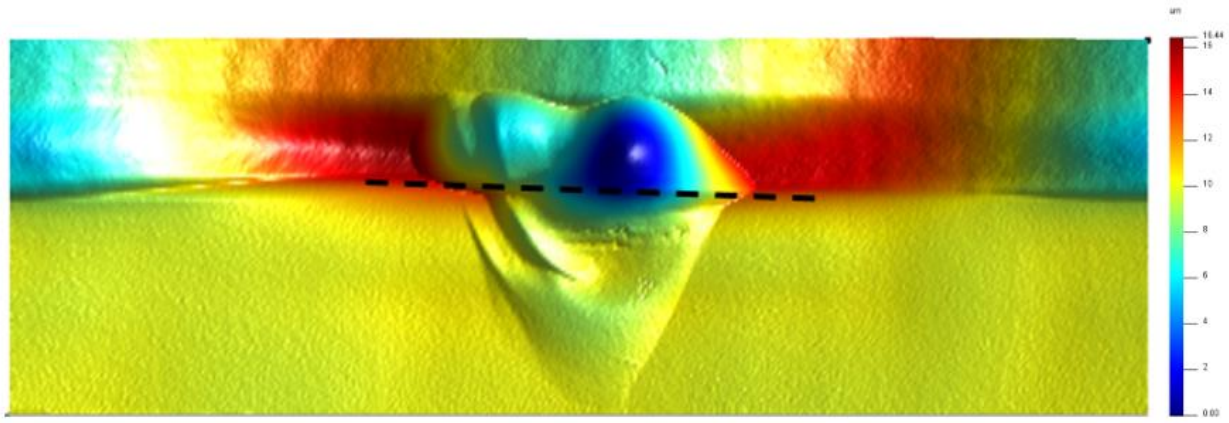

Figure 76: Image displaying the 3D surface of liner 4 at interval - 2 with the colour map.

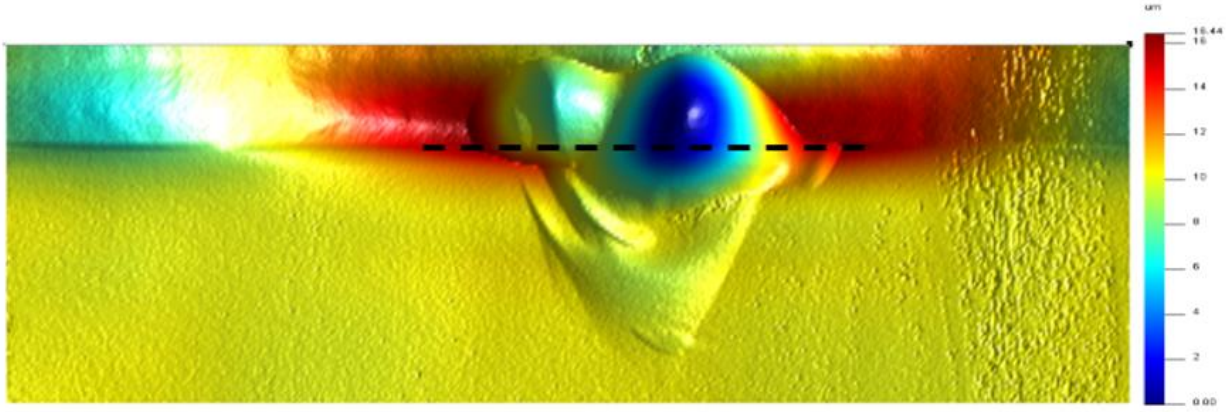

Figure 77: Image displaying the 3D surface of liner 4 at interval - 3 with the colour map.

By comparing the above three figures, the ability of the RMM method to trace the progression of wear is evident. The 3D surface efficiently highlighted that the edge wear was distributed above the edge and into the bearing surface for all the six acetabular liners from the first interval itself. The determined linear wear penetration through 3D surface for all six liners from cohort-C at each interval is shown below in Table 24.

Linear wear Penetration (mm)						
Liner	**1**	**2**	**3**	**4**	**5**	**6**
Interval – 1	0.042	0.036	0.040	0.026	0.031	0.032
Interval – 2	0.043	0.041	0.042	0.038	0.032	0.035
Interval – 3	0.053	0.045	0.046	0.047	0.032	0.038

Table 24: Tabulated volumetric wear results of all liners of cohort C at each interval as measured by the RMM method.

After examining the 3D surface, the developed analysis process of RMM method was performed on all the measured roundness traces in MATLAB to assess the volumetric wear of all acetabular liners from cohort-C at each interval. The obtained combined total volumetric wear results of all six liners at each interval are shown below in Table 25. As observed through CMM results, the RMM results also observed the effect of bedding-in period in first interval and steady wear period from the second interval.

After determining the wear volumes of cohort-C through the RMM method, the results of the RMM method were compared against the results obtained from the gold standard gravimetric method to test the authenticity of the results obtained though the RMM method. The quantified volumetric wear by both, the RMM and the gravimetric method, is shown below in Table 25.

Total Volumetric Wear (mm^3)						
Liner	**Interval 1**		**Interval 2**		**Interval 3**	
	RMM	**Gravimetric**	**RMM**	**Gravimetric**	**RMM**	**Gravimetric**
1	0.5152	0.6100	0.7861	0.8517	1.2230	1.4000
2	0.4140	0.5200	0.6590	0.6892	0.8650	0.9200
3	0.5370	0.7700	1.1180	1.0311	1.2643	1.4200
4	0.4290	0.5400	0.7002	0.7574	1.1280	1.0800
5	0.3871	0.4600	0.6645	0.5680	0.9100	0.8800
6	0.4732	0.6400	0.7825	0.8352	1.0160	1.1300

Table 25: Tabulated volumetric wear results obtained from the RMM and the gravimetric method.

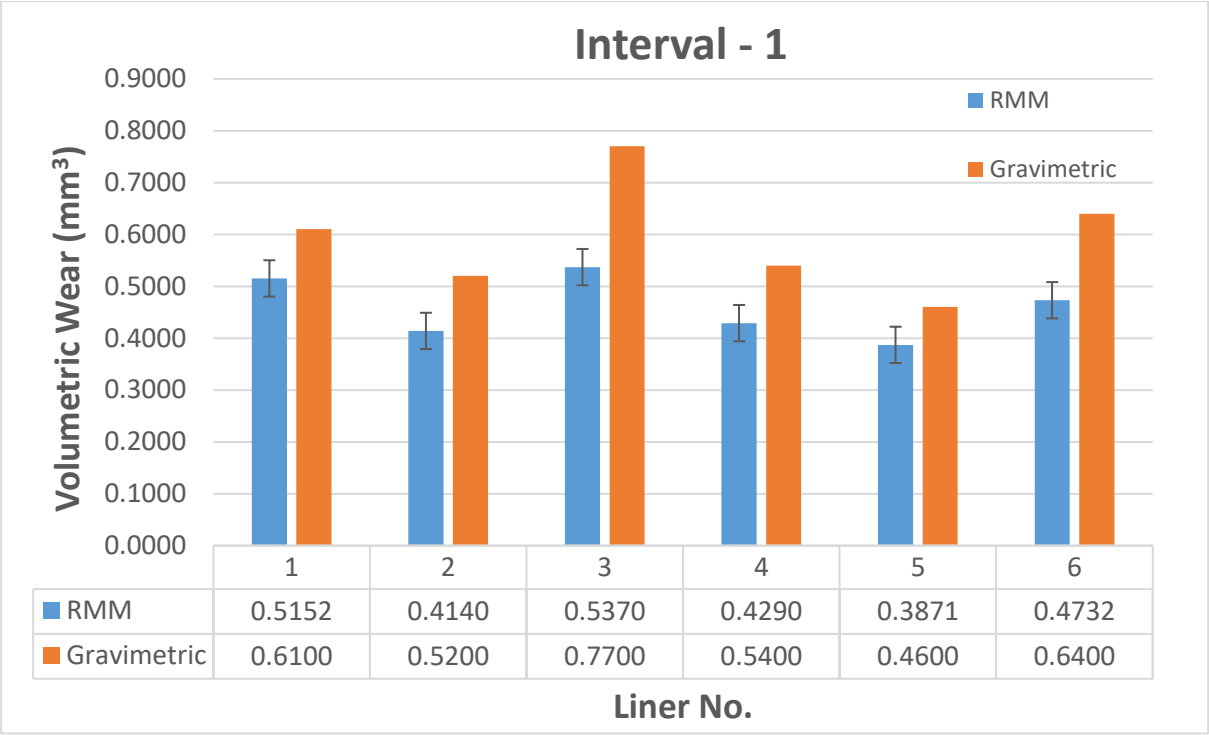

Figure 78: Bar graph displaying the volumetric wear of liners from cohort-C at interval-1.

Interval – 1						
Liner No.	**1**	**2**	**3**	**4**	**5**	**6**
RMM (mm^3)	0.5152	0.4140	0.5370	0.4290	0.3871	0.4732
Gravimetric (mm^3)	0.6100	0.5200	0.7700	0.5400	0.4600	0.6400
Difference (mm^3)	0.0948	0.1060	0.2330	0.1110	0.0729	0.1668

Table 26: A table displaying the variations in the results obtained from the RMM method and the gravimetric method for liners of cohort C at interval 1.

The above bar graph displayed in Figure 78, exhibits the volumetric wear results of interval 1 obtained through the RMM method and the gravimetric method. It can be observed that the volumetric wear quantified by the RMM method is consistently lower compared to the volumetric wear quantified by the gravimetric method. The reason for the RMM method being consistently lower compared to the gravimetric method is because of the travel length limitation of the employed gauge. The travel length of gauge on the RMM only allowed for a measurement of 5.5mm height on the RMM which didn't allow to measure the wear scar completely. Another reason is, like the

CMM method, the RMM method only accounts for the edge wear whereas the gravimetric method accounts for the wear on the full the liner surface including the rear surface employed for clamping. The above Table 26 shows the absolute variation between the results obtained through the RMM method and the gravimetric method for all six liners. The variation between results obtained by the RMM method and the gravimetric method ranged from 0.072 mm^3 to 0.233 mm^3. As mentioned earlier, the liner 3 and liner 6 at this interval were found to be chipped and is suspected to be the reason of high variance in wear volume results of the RMM method and the gravimetric method. However, the volumetric wear results of liner 3 and liner 6 as measured by the CMM method and the RMM method were found to be similar, i.e. 0.506 mm^3 and 0.468 mm^3 for the CMM method and 0.537 mm^3 and 0.473 mm^3 for the RMM method respectively. After excluding liner 3 and liner 6 measurements from the cohort, the range of variation is reduced down to 0.072 mm^3 to 0.111 mm^3. In terms of percentage, after discounting the liner 3 and liner 6, the variation is found to be in the range of 15.54% to 20.56%. It should be noted that the measured wear volumes are minimal and hence the variation percentage are noticeably high.

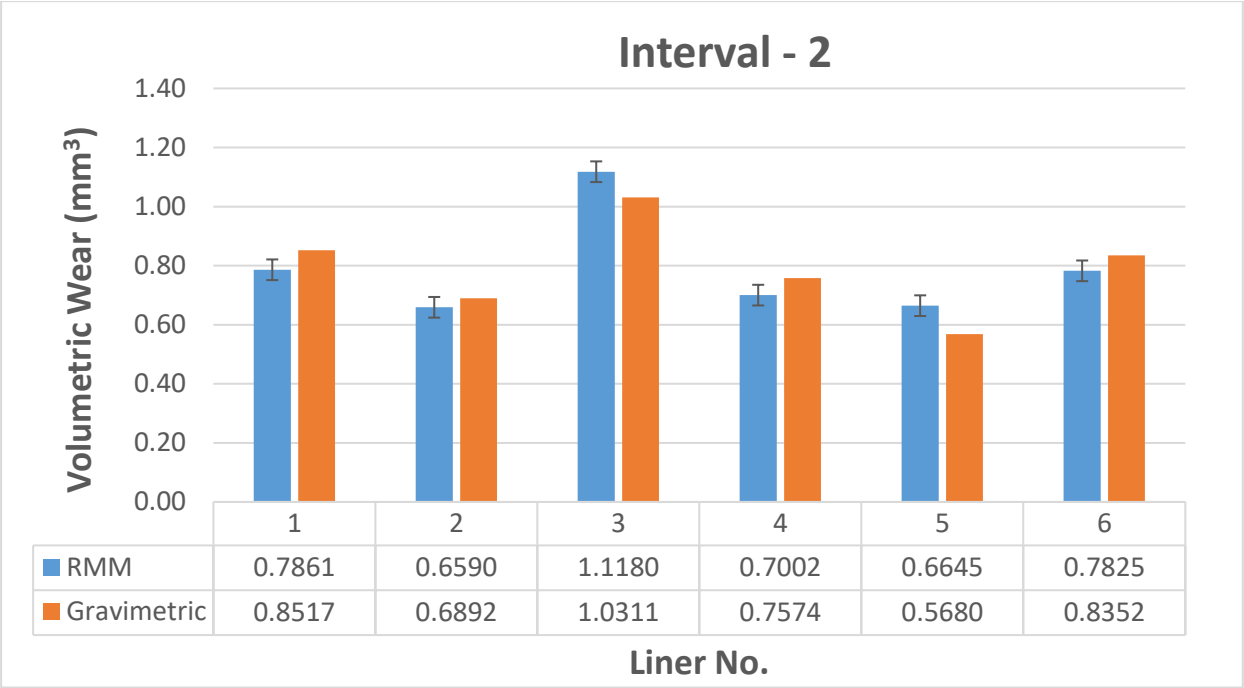

Figure 79: Bar graph displaying the volumetric wear of liners from cohort-C at interval-2.

Interval - 2						
Liner No.	**1**	**2**	**3**	**4**	**5**	**6**
RMM (mm^3)	0.7861	0.6590	1.1180	0.7002	0.6645	0.7825
Gravimetric (mm^3)	0.8517	0.6892	1.0311	0.7574	0.5680	0.8352
Difference (mm^3)	0.0656	0.0302	0.0869	0.0572	0.0965	0.0527

Table 27: A table displaying the variations in the results obtained from the RMM method and the gravimetric method for liners of cohort C at interval 2.

The above bar graph displayed in Figure 79, exhibits the volumetric wear results of interval 2 obtained through the RMM method and the gravimetric method. From the graph displayed in Figure 79, it was speculated that the wear volume of liner 3 as measured by the RMM method was higher than the result obtained by the gravimetric method, however, the variation was minimal. The variations in the results as seen from the bar graph were less compared to the variations of interval 1. The above Table 27 shows the variation between the results obtained through the RMM method and the gravimetric method at second interval for all the six liners. The variation between results obtained by the RMM method and the gravimetric method

ranged from as low as 0.030 mm^3 to 0.0965 mm^3 for second interval. The variation in percentage is found to be in the range of 4.39% to 17%. Compared to the interval 1, the percentage variation in interval 2 had decreased. This is because the measured wear volume is higher than that of interval 1.

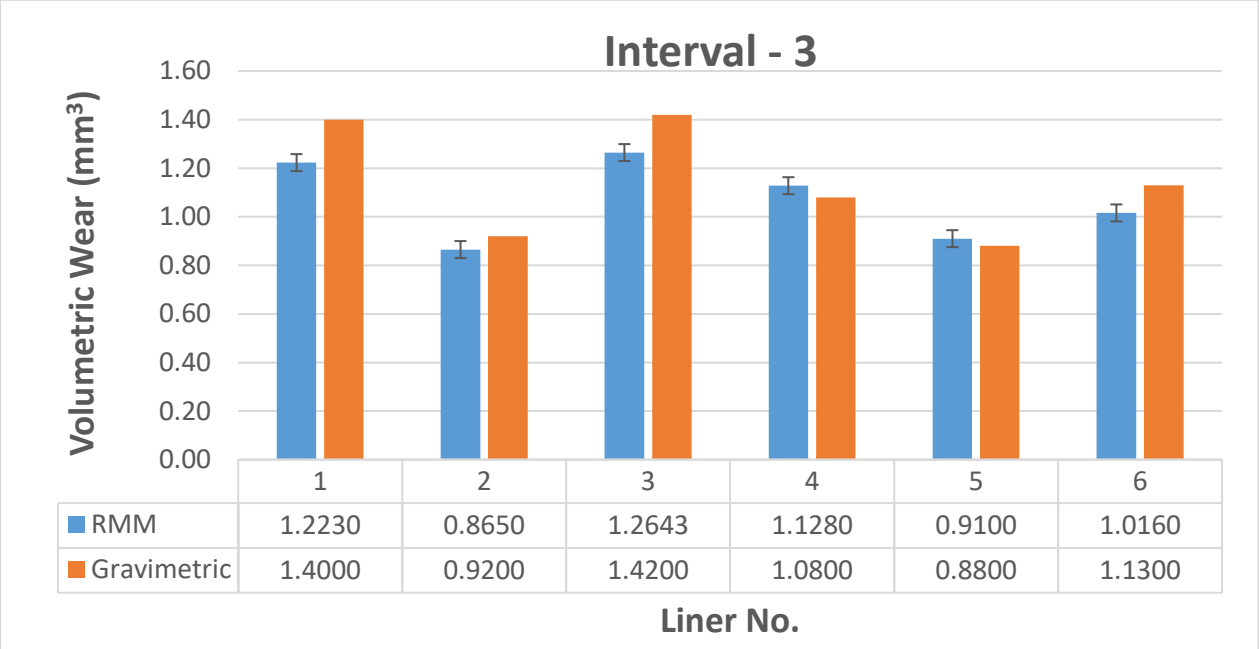

Figure 80: Bar graph displaying the maximum linear wear and volumetric wear of liners from cohort-C at interval-3.

Interval - 3						
Liner No.	**1**	**2**	**3**	**4**	**5**	**6**
RMM (mm3)	1.2230	0.8650	1.2643	1.1280	0.9100	1.0160
Gravimetric	1.4000	0.9200	1.4200	1.0800	0.8800	1.1300
Difference	0.1770	0.0550	0.1558	0.0480	0.0300	0.1140

Table 28: A table displaying the variations in the results obtained from the RMM method and the gravimetric method for liners of cohort C at interval 3.

The above bar graph displayed in figure 80, exhibits the volumetric wear results for interval 3 obtained through the RMM method and the gravimetric

method along with the linear wear penetration determined by the 3D surface obtained through the RMM method. However, a high variation in the quantified wear volumes can be speculated for liner 1 and liner 6. The above Table 28 shows the variation between the results obtained through the RMM method and the gravimetric method at third interval for all the six liners. By studying the tabulated variations results in Table 28 it can be noted that the variation in liner 1 and liner 6 are as high as 0.177 mm^3 and 0.114 mm^3 respectively. It was observed during the wear analysis process that wear distribution of liner 1, liner 3 and liner 6 was higher than the measuring height permitted by the gauge employed by the RMM. This means some part of the wear was left unassessed due to the gauge travel length limitation. The variation between results obtained by the RMM method and the gravimetric method ranged from as low as 0.030 mm^3 to 0.177 mm^3 for third interval. It was observed that the variation for the third interval had increased sign significantly compared to that of interval 1 and interval 2. The reason for this significant increment is that the RMM method is measuring considerably high wear volumes and more complex wear distribution compared to interval 1 and interval 2. However in terms of percentage variation, the variation percentage had decreased to the range of 3.41% to 12.64%.

5.4.1 RMM Repeatability

As the analysis process of the RMM method includes to the manual wear segmentation process, it was suspected that larger wear extent and wear volume can increase the repeatability error. In order to explore this, a repeatability test was performed on the measurement of third interval of liner C-6 as it had endured highest amount of volumetric wear. For repeatability test, the measurement was analysed ten times by a single operator. The operator followed the analysis process specifications outlined in section 4.2, this included form removal process as well as the required wear segmentation in order to estimate the volumetric wear.

	Result (mm^3)
Mean	1.143
Median	1.132
Range	1.093 – 1.206
Std. Deviation	0.034

Table 29: Results of the repeatability study conducted on the measurement of the third interval on liner C-6. This table displays the mean, median, range and std. deviation of the obtained results.

In the above Table 29, mean is the average of the ten measured values of Liner C-6, and range defines the lowest and the highest value obtained from those ten measurements. It can be observed that the analysis process displays high repeatability with the standard deviation found to be as low as 0.034 mm^3. However, the obtained standard deviation is higher compared to the results of the repeatability test conducted on liner A-6 in section 4.4. This is discrepancy is obtained due to the analysis of increased wear volume. As this is the highest standard deviation obtained among both the repeatability test, this value is used for the RMM error bars in all the displayed bar graphs.

Chapter 6: Discussion

In this chapter, the necessity of the volumetric wear assessment and the importance for method development is discussed. Along with that, the results obtained from the developed RMM and the CMM methods are compared against the results obtained through the gold standard gravimetric method. Both, the CMM method and the RMM method is compared with each other and their advantages and limitations are discussed. The results obtained through all the three methods, CMM, RMM and Gravimetric, are compared to test the performance of the CMM and the RMM method against the gold standard gravimetric method.

The fourth generation of Ceramic-on-Ceramic arthroplasty devices are well-recognised for their longevity through in-vitro studies and are encouraged to be implanted in younger and more active patient due to their excellent abrasive wear resistant properties and the inertness of ceramic materials. Despite the fact that ceramic materials are considered to be biologically inert when compared to other materials employed for the bearing surfaces of hip arthroplasty devices such as metal and polyethylene, bio-inertness of ceramic has been questioned by some studies. When ceramic debris are released in large amounts in the body they do trigger cellular response with similar intensity to that of metallic and polymeric debris [308]. A study by Yoon *et al.* concluded that ceramic wear particles could stimulate a foreign body response, leading to peri-prosthetic osteolysis [309]. An *in vivo* characterisation study performed by Lerouge et al. demonstrated that Zirconia and Alumina particles can induce foreign body reaction and are the major particles responsible of aseptic loosening associated with CoC bearings [310].

After studying the effects of wear debris on the performance of the CoC hip arthroplasty device, edge wear, which is the major source of wear generation in CoC bearings, is discussed. The edge wear occurs when the loading vector of contact of the femoral head articulates against the hard edge of the acetabular cup liner. The form of the bearing surface and uncontrolled

geometry of the as-manufactured edge of the unworn cohort B was examined. Through examination of cohort B, a tilt of two degree in coverage angle was observed in two liners from a set of six. This is a matter of concern as such high frequency of uneven coverage angle can induce or further encourage edge loading and causes higher edge wear even for a well-positioned acetabular liner. Controlling such uneven edge geometry through better manufacturing techniques can be advantageous as it can reduce the chances of edge loading in well-positioned acetabular liners. Edge wear being a well-recognised source of wear debris generation in CoC bearings makes the measurement of the volume of material loss through edge wear is of essential.

The wear debris from edge wear enters the bearing surface and contributes to wear in bearing surface by smearing onto the bearing surface. For metal-on-metal studies, all the existing geometric wear measurement methods employed to measure volumetric wear of a liner only accounted for the wear in bearing surface [17, 41-43, 289, 292, 306, 307, 311]. The existing wear measurement methods fit a basic geometric sphere in the bearing surface as a reference geometry of the unworn surface to determine volumetric wear. The edge and the bearing surface proximal to the edge is discounted from the measurement. Hence the quantified edge wear by the use of the existing methods in the previous studies accounted only for the wear in the bearing surface rather than the full extent of edge wear distribution and disregarded the major volume loss at the actual edge. Existing studies have reported edge wear [312, 313], however they did not measure wear beyond the edge. This explains the reason for the studies that reported metal ions released were more compared to that of the measured bearing wear [314]. Measurement of such essential material loss was previously not taken into account due to lack of a method that could reconstruct the unworn over-edge geometry of the acetabular liner.

For ceramic acetabular liners, reconstruction of the unworn surface was challenging because of the complex form obtained due to their manufacturing process. Ceramic liners had an uncontrolled elliptical edge geometry with an

occasional coverage tilt and a free form surface above the edge that did not allow for the reconstruction of the unworn geometry by the use of a revolving a planar curve. Such form of ceramic liners made it challenging to reconstruct a geometry that can imitate the unworn as manufactured surface.

The developed CMM method utilised the unworn surface of the acetabular liner to reconstruct the as manufactured surface geometry by the use of the vertical and horizontal planar sections. The deviation analysis performed between the reconstructed unworn surface geometry and the measured surface characterised the wear distribution and quantified of the depth of linear wear penetration over the surface geometry by the use of the given colour map. It must be noted that, unlike the existing methods, the CMM method developed in this study accounts for the wear not only in the bearing surface but also the full over-edge geometry. In terms of volumetric wear, the CMM method is capable of determining volumetric wear to a sub 0.1 mm^3 level.

The developed RMM method utilise the roundness traces measured on Talyrond 365 to determine volumetric wear. These roundness traces are stitched to form a 3D surface that provides a form removed 3-dimensional representation of the measured surface. This surface allows the user to visualise the extent and geometry of the edge wear area and depth of linear wear penetration over a freeform geometry by the use of a coloured height map. The RMM method has been proven to have the ability to determine volumetric wear to a sub 0.1mm^3 level through the developed analysis procedure. The RMM method, like the CMM method, can characterise and quantify edge wear beyond the bearing surface.

6.1 CMM Results from Method Development

To test the developed CMM method, a cohort of six simulated ceramic acetabular liners were assessed by the CMM method. The obtained test results provide confidence in the CMM measurement method and the novel volumetric

analysis process that is used to characterise and quantify wear volumes of the liners. Through examining the form of given liners, it was observed that each liner had unique ellipsoidal bearing surface and an uncontrolled edge geometry. The coverage angle for all the six liners ranged from 153.07° to 154.40°, however, a significant variation in the coverage angle from the centre axis of the bearing sphere was discovered in three out of the given six liners. Such significant variation resulted in a tilt as high as 2° in the coverage angle of the liners. This introduces a disparity of 4° in quartiles which considerably increases the possibility disrupting the coverage angle geometry and induces edge loading even for a well-positioned acetabular liner by positioning the edge into the articulation area of the loading axis. This possibility can lead to significant edge wear.

Deviation analysis of the CMM method allowed to characterise wear and found that each liner of Cohort-A had a singular area of localised wear and could quantify the maximum linear wear penetration ranging as low as 8.9μm to 29.1μm. Deviation analysis was also able to highlight that the edge wear distribution was spread out above the edge and into the bearing surface for all the six liners. Hence, an advantage of this method over the existing metrological methods is that it allows the user to measure the full extent of the edge wear as the existing metrological methods are limited to the bearing surface. The wear volumes determined by the CMM method ranged from 0.081 mm^3 to 0.311 mm^3. By comparing the volumetric wear results obtained by the CMM method to the volumetric wear results obtained through the gravimetric method, it is evident that there is a strong correlation between them. The Pearson's correlation coefficient was calculated to be 0.969 at a significance value of 0.001 also signified a strong correlation between the CMM and the gravimetric method. Hence it can be said that the developed CMM method is capable of measuring wear volumes as low as 0.1 mm^3 and it has a strong correlation with the gold standard gravimetric method.

A study was conducted to test the repeatability and the inter-operator variability of the CMM method. The results of this repeatability study as

displayed in Table 13 of section 3.10 exhibits a high repeatability of the analysis process with the standard deviation of 0.002 mm for the maximum linear wear penetration and 0.046 mm^3 for the volumetric wear. The results of the inter-operator variability as displayed in Table 14 of section 3.10 exhibits low variability with a standard deviation of 0.051 mm^3 with the variation range of 0.007 mm^3 to 0.178 mm^3. Hence it is evident that the analysis process of the CMM method has a high repeatability and good reproducibility between two operators. A Bland-Altman plot is displayed in Figure 55 of section 3.10 displays a good agreement between the results obtained by two operators and displays a non-proportional bias of the measurement. It was observed that the major factor contributing variations in the wear computation process was the manual selection of the vertical planar sections in order to reconstruct unworn surface geometry. The accuracy of the unworn surface geometry depends on the distance of the selected planar sections from the wear scar. The closer planar section is to the wear scar provides better accuracy of the unworn surface geometry.

6.2 RMM Results from Method Development

The same cohort of six ceramic liners was measured with the RMM method, and was successful at characterising and quantifying edge wear in the ceramic liners. Hence, there can be confidence in the RMM measurement method and its novel volumetric analysis process to characterise wear and quantify wear volumes. The 3-dimensional surface generated from the roundness traces efficiently characterise the edge wear distribution for all six liners. The surface map highlighted the phenomenon of wear smearing from the edge onto the bearing surface. An example of such smearing effect can be seen below in Figure 81. The Figure 81 displays the extent of the smear effect of acetabular liner-1 from cohort-A by filtering the higher peaks from the analysis in order to highlight smaller value of wear through smear effect. A singular area of localised wear was again observed on all the six liners from the generated 3D surfaces. The maximum linear wear penetration for all six

liners determined from the 3D surface ranged from 10.59μm to 29.48μm. The edge wear distribution was again observed to be spread out beyond the edge and into the bearing surface for all six liners. Hence it can be said that the RMM method is also capable to measure wear beyond the bearing surface which is an advantage over existing metrological methods to assess wear volumes in aceabular liners. The wear volumes deteremined by the RMM method ranged between 0.061 mm^3 to 0.362 mm^3. Further through comparison between the volumetric wear results obtained by the RMM method and the volumetric wear results obtained through the gravimetric method, it was evident that there exist a strong correlation between them. The Pearson's correlation coefficient was calculated to be 0.985 at a significance value of 0.001 also signified a strong correlation. Hence, just like the CMM method, the RMM method is also capable to measure wear as low as 0.1 mm^3 and can displays a strong correlation with the gold standard gravimetric method.

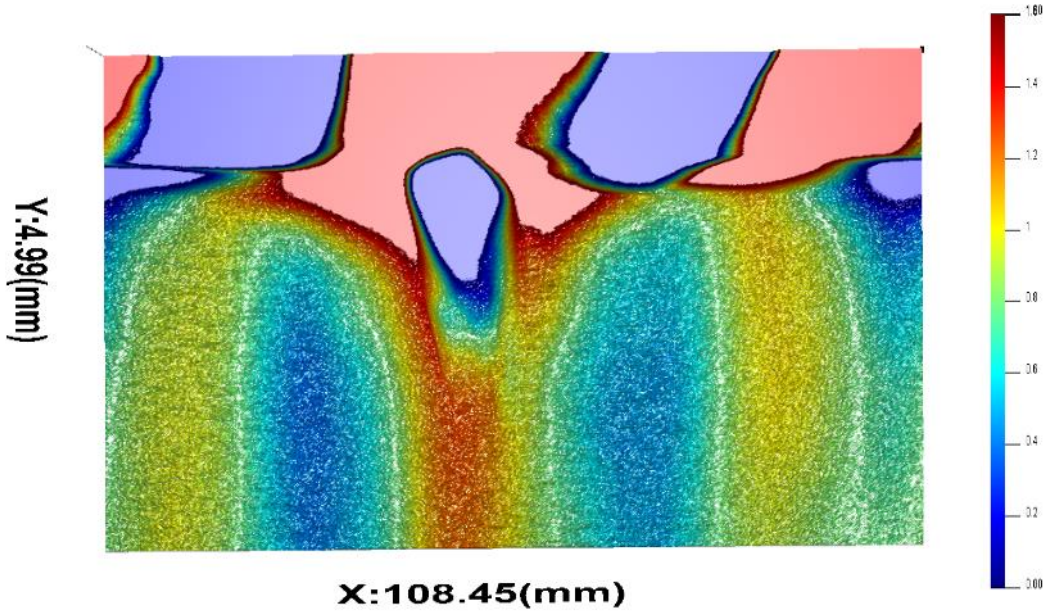

Figure 81: Image displaying the extent of smear effect highlighted after thresholding process [315].

An inter-operator variability study was conducted to test repeatability and inter-operator variability of the RMM method. The results of this study as displayed in Table 17 of section 4.4 exhibits a good agreement between the two users. The standard deviation of both measurement and analysis process

was determined to be 0.009 mm^3 and 0.003 mm^3 for first and second operators respectively. Hence it is evident that the method has a high repeatability for measurement and analysis process and good reproducibility between two operators. The results also displayed a good agreement between the users with the overall standard deviation of inter-operator variability of 0.004 mm^3. A Bland-Altman plot is displayed in Figure 68 of chapter 4.4 to graphically examine the agreement and non-proportional bias of the measurement. It was observed that the major factor affecting the wear computation is the manual wear boundary selection process and it affects the repeatability and reproducibility of the analysis process. The centring and levelling process of the employed RMM centres the components to the eccentricity of 1 µm and levels the component up till 89.995° which allows for minor measurement errors.

6.3 CMM Results from Interval study

Through the interval case study, it was observed that the CMM method was capable of measuring the increased wear distribution at each measurement interval and was able to assess volumetric wear for each interval. The deviation analysis successfully evaluated the linear wear penetration in all the six liners of cohort C at each interval. As observed previously, again the liners had a singular area of localised wear at all three intervals for all six liners. The linear wear penetration of all six liners of cohort C as measured by the CMM method for interval 1, interval 2 and interval 3 ranged from 0.0259mm to 0.0405mm, 0.0318mm to 0.044mm and 0.0323mm to 0.0551mm respectively. Again, for all six liners, the wear was distributed above the edge and into the bearing surface. The CMM method was able to reconstruct the as manufactured surface and determine the volumetric wear of all six liners of cohort-C at each interval. The results obtained by the CMM method were compared to the results obtained by the gravimetric method to test the variations and the range of variation was

observed to be 0.071mm^3 to 0.139mm^3 for the first interval, 0.009mm^3 to 0.101mm^3 for the second interval and 0.033mm^3 to 0.0434mm^3 for the third interval. The second interval had comparatively less variation which can be attributable to the planar selection process of the CMM analysis procedure. It was noted for some liners that the variation was higher than expected and the factors affecting such high variations when compared to the gravimetric method are discussed in subsequent section 6.6.

6.4 RMM results from Interval study

At each interval, subsequent to assessing volumetric wear through the CMM method, the liners of cohort C were assessed through the RMM method. Upon assessing the cohort C it was observed that the RMM method characterised the expanding wear distribution and was able to assess volumetric wear for each interval. The 3D surface displayed the wear distribution and determined the linear wear penetration in all the six liners of cohort C at each interval. Similar to the observation made by the CMM method, the liners had a singular area of localised wear and the wear was distributed above the edge and into the bearing surface. The linear wear penetration of all six liners of cohort C as measured by the RMM method for interval 1, interval 2 and interval 3 ranged from 0.026mm to 0.042mm, 0.032mm to 0.043mm and 0.032mm to 0.053mm respectively. Subsequent to assessing the linear wear penetration, the RMM method successfully determined volumetric wear of all six liners at each interval and the results are displayed in Table 25**Error! Reference source not found.** of section 5.3. The volumetric wear results obtained by the RMM method were compared to the results obtained by the gravimetric method to test the variations and the range of variation was observed to be 0.072mm^3 to 0.233mm^3 for the first interval, 0.030mm^3 to 0.0965mm^3 for the second interval and 0.030mm^3 to 0.177mm^3 for the third interval. Similar to the CMM method, it was noted for some liners that the variation was higher than expected and the factors

affecting such high variations when compared to the gravimetric method are discussed in detail in sections 6.6.

6.5 CMM vs RMM Advantages and Limitations

The results obtained from both the developed methods were studied to recognise the advantages and limitations of both the methods and to examine the suitability of methods in measuring edge wear. On comparing both the methods it was observed that the CMM method allows for the measurement of the acetabular liner from the pole to the rim, whereas the RMM method allows only for a limited area of 5.5mm height surrounding the edge wear. This limitation of RMM is due to the 2mm permissible gauge travel length of the employed RMM. From the interval study, it was speculated that in some liners that the RMM was not successful at measuring the complete wear distribution and minute smeared wear in the bearing surface was left unmeasured. However, this limitation can be overcome by employing a commercially available gauge with the travel length of 4mm which can allow for the measurement of a greater height around the edge wear distribution. The RMM measurement and analysis process both consumes considerably less time compared to the CMM measurement and analysis process. Due to the limitation of gauge travel length of the RMM method, it is more suitable when the wear distribution is exclusively at the edge of the liner. However, it is advantageous to use the CMM method for assessing the acetabular liners that have larger wear distribution in terms of height. Considering the precision of measurement, the CMM has a micro-meter precision with stated MPE and MPE/THP of 1.99µm+L/300 and 1µm@30sec, whereas the employed RMM possess a stated gauge resolution of 30nm with a spindle run-out value of 20nm. The CMM measurement employs Ø2mm ruby stylus that induces mechanical filtering errors, whereas RMM employs a diamond tip pointed stylus of 5µm that eliminates the mechanical filtering error. Hence when comparing the measurement of CMM and RMM, RMM measurements provide higher precision with extremely low mechanical filtering errors in measurement to that of CMM measurements. Also, the measurement cycle

time of the CMM per measurement is between 3-4 hours, whereas for the RMM the measurement cycle time is between 45-60 minutes. From the perspective of cost-efficiency, the CMMs are significantly more expensive compared to the RMMs. Hence it is quicker and cost effective to measure the acetabular liners on the RMM when compared to the CMM.

By comparing the analysis process of the CMM method and the RMM method, it is observed that the RMM method is more precise at characterising the wear distribution to that of the CMM method due to the nanometer precision of the RMM. The exported measurement data from the RMM provides for better resolution of wear distribution and the unwrapped 3D surface provided by RMM gives more precise visualisation of wear form as dispayed in Figure 82. However, unike the RMM method, the deviation analysis of the CMM method characterise the wear distribution on the true surface as displayed in Figure 83. This allows the user for better understanding of the location and the extent of wear distribution on the liner surface.

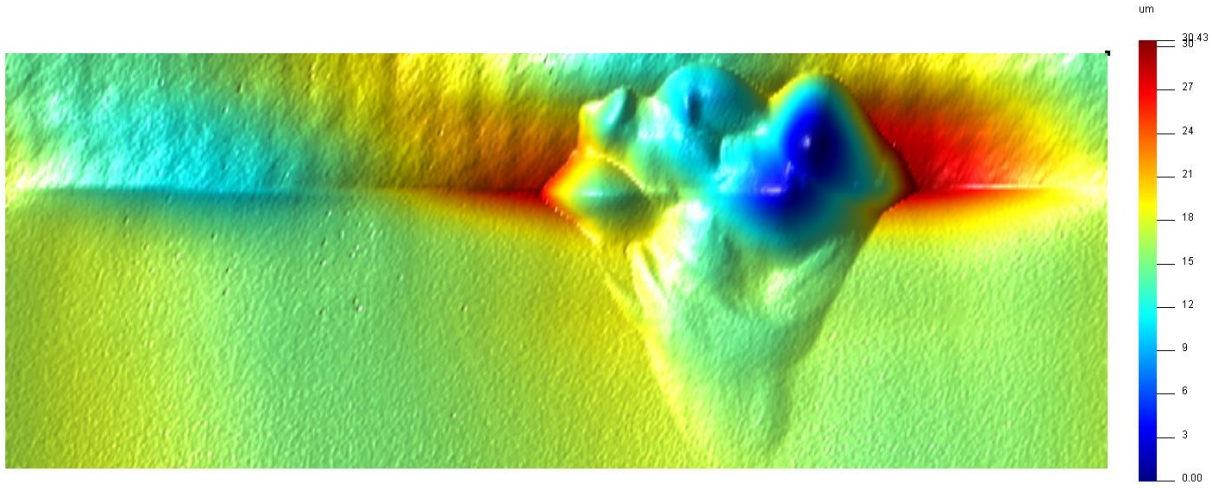

Figure 82: Image displays 3D surface of liner 5 from Cohort C at third interval.

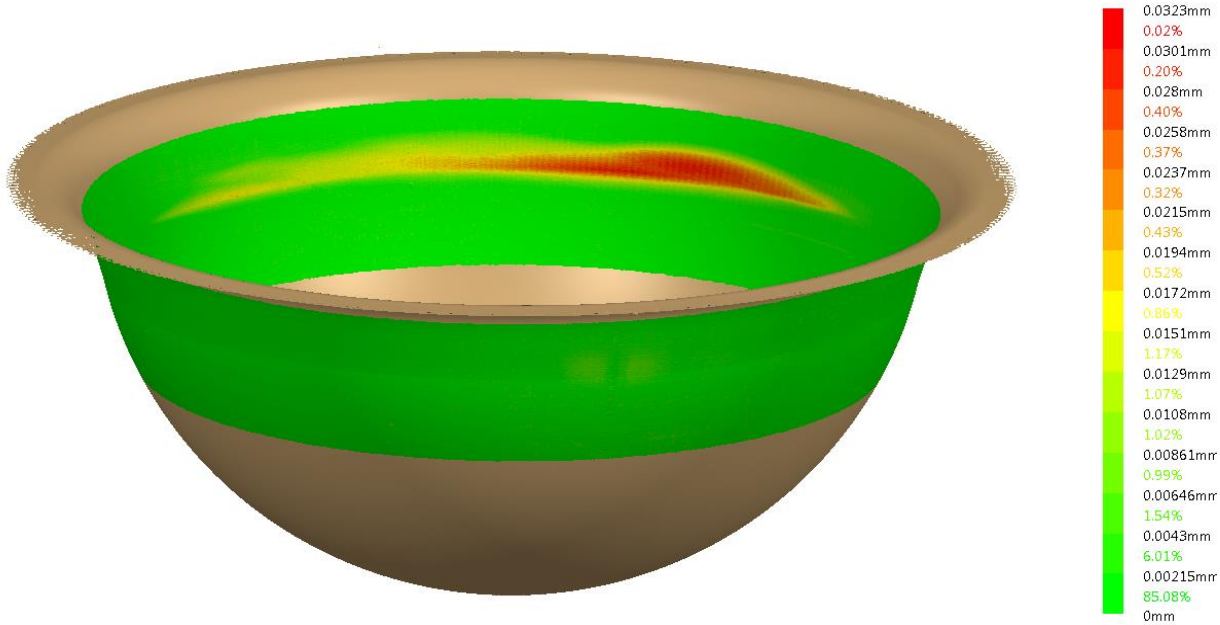

Figure 83: Deviation analysis of liner 5 of cohort C at third interval.

The volumetric wear assessments of the acetabular liner by the RMM method includes manual segmentation of wear scar from the measured data by the use of CloudCompare. This manual process makes the RMM method dependent on the wear identification skill of the operator. However the RMM method has displayed an inter-operator variability as low as 0.004 mm^3. Similarly, the as-manufactured geometry reconstruction process of the CMM method is also user dependent as it requires the operator to identify the wear scar on the mesh prior to deviation analysis in order select the required planar sections. The CMM method also displayed a low inter-operator variability of 0.051 mm^3. The volumetric wear assessment results of the interval study are displayed in bar graphs below for each interval in order to evaluate the variation in wear assessment by both methods.

Liner No.	Interval 1		Interval 2		Interval 3	
	CMM	RMM	CMM	RMM	CMM	RMM
1	0.6980	0.5152	0.9530	0.7861	1.3380	1.2230
2	0.4260	0.4140	0.6800	0.6590	0.7290	0.8650
3	0.5060	0.5370	0.9660	1.1180	1.2430	1.1670
4	0.4010	0.4290	0.7310	0.7002	0.8620	1.1280
5	0.3890	0.3871	0.6090	0.6645	0.9130	0.9100
6	0.4680	0.4732	0.8030	0.7825	0.6960	1.0160

Table 30: Volumetric wear results of cohort C obtained by the CMM and the RMM method at each interval.

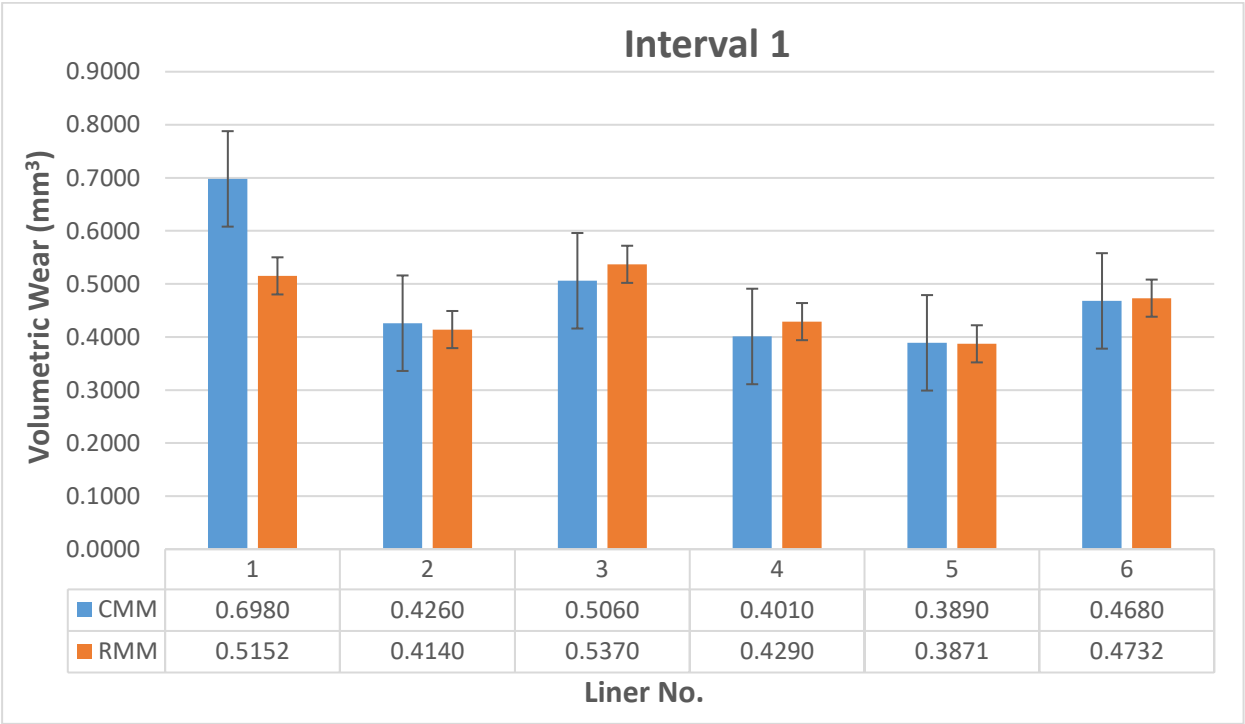

Figure 84: Image displays a bar graph that compares volumetric wear results of cohort C obtained by the CMM and the RMM method at interval 1.

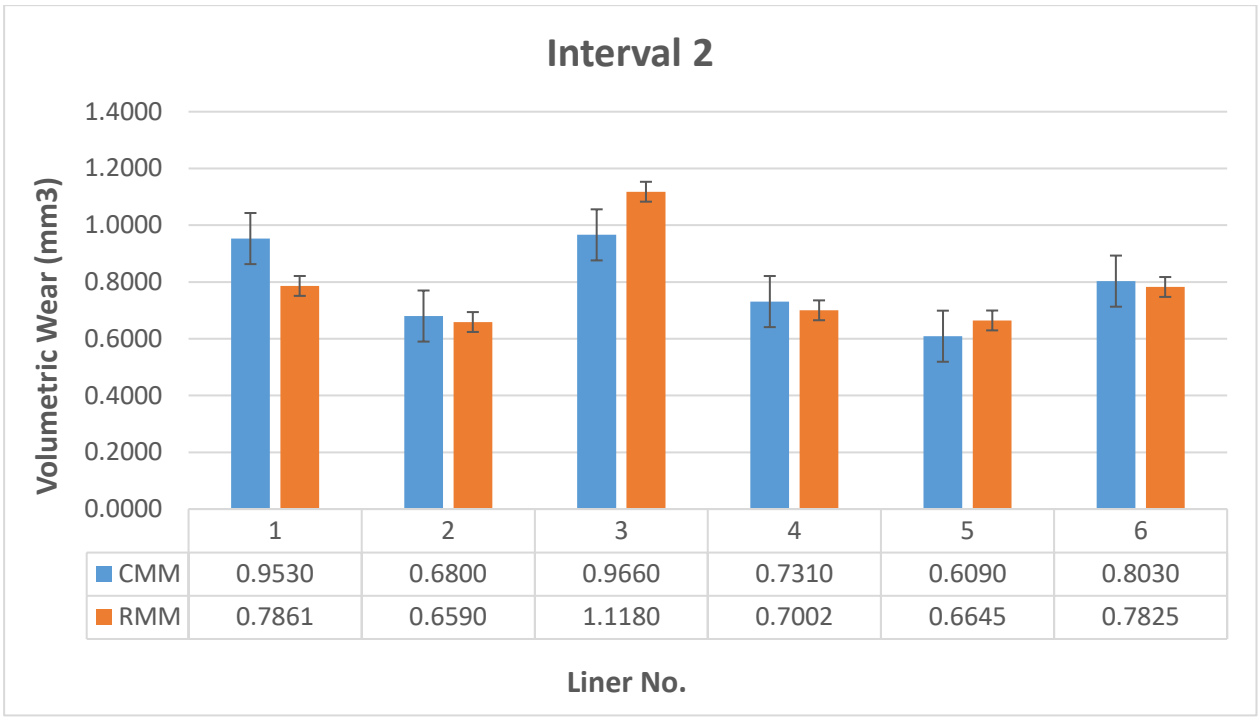

Figure 85: Image displays a bar graph that compares volumetric wear results of cohort C obtained by the CMM and the RMM method at interval 2.

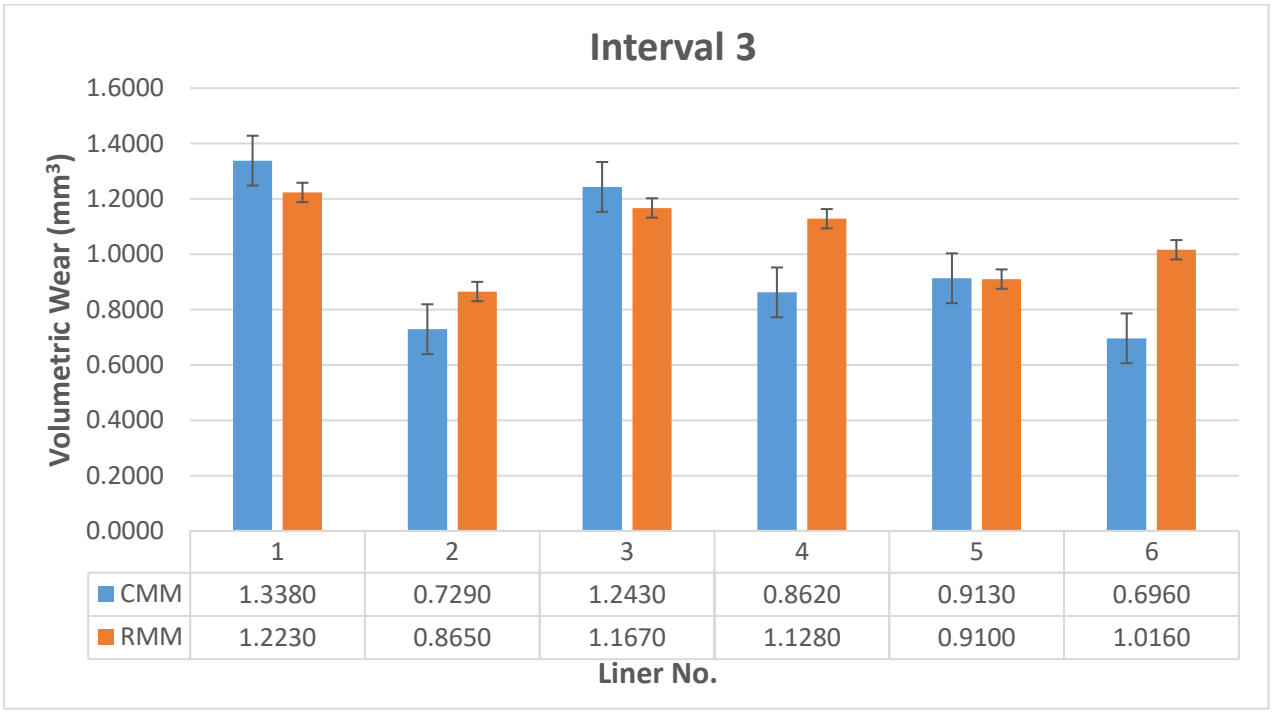

Figure 86: Image displays a bar graph that compares volumetric wear results of cohort C obtained by the CMM and the RMM method at interval 3.

From the above given graphs (Figure 84, Figure 85 and Figure 86) it can be noted that there are variations between the volumetric wear results determined by each method. For liner 1 at first interval and liner 6 at third interval the variations observed are significant. For both the measurement, liner 1 at first interval and liner 6 at third interval, the CMM measurements are treated as outliers. There are three major factors that cause the variation in wear assessment, i.e. the user dependent vertical planar section selection process for the reconstruction of the unworn surface for the CMM method, limited surface height measurement of the RMM method due to the limited gauge travel length and user dependent nature of the segmentation process of the RMM method.

6.6 Comparison of CMM, RMM and Gravimetric

After studying the volumetric wear results obtained from the CMM method and the RMM method and comparing them individually against results obtained by the gravimetric method, the volumetric wear results obtained through all the methods were compared. The obtained volumetric wear results of cohort A was tabulated against each other in Table 31: below and a bar graph is presented in Figure 87 for comparing the results obtained by the CMM method, the RMM method and the gravimetric method.

Total Volumetric Wear (mm^3)			
Liner	**CMM**	**RMM**	**Gravimetric**
1	0.0810	0.0610	0.1120
2	0.2500	0.2850	0.4140
3	0.0840	0.1090	0.1790
4	0.3110	0.3620	0.4320
5	0.1050	0.1140	0.1640
6	0.1290	0.1770	0.2470

Table 31: The given table compares the volumetric wear results of cohort-A as measured by the CMM, the RMM and the Gravimetric methods.

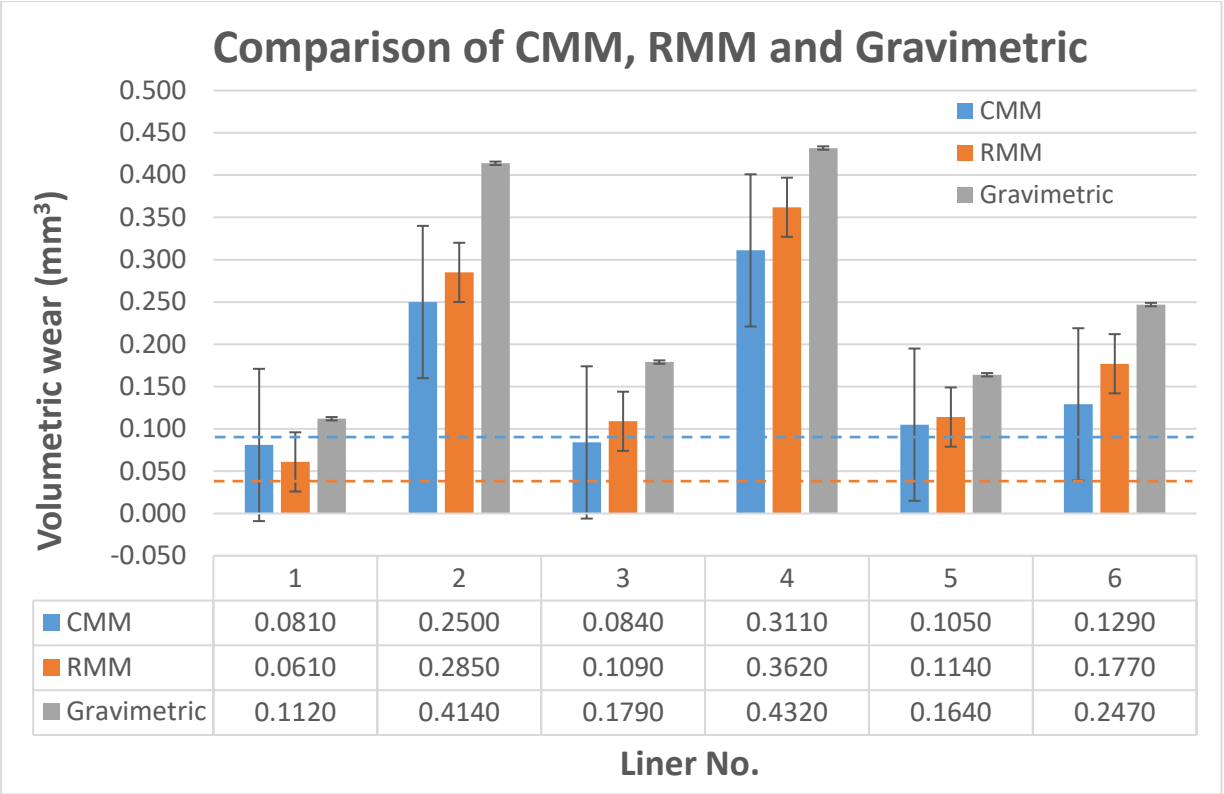

	1	2	3	4	5	6
CMM	0.0810	0.2500	0.0840	0.3110	0.1050	0.1290
RMM	0.0610	0.2850	0.1090	0.3620	0.1140	0.1770
Gravimetric	0.1120	0.4140	0.1790	0.4320	0.1640	0.2470

Figure 87: A bar graph displaying the volumetric wear results of cohort-A obtained from the CMM, the RMM and the gravimetric method. The dashed blue and orange line denotes the error range of the CMM and the RMM method respectively.

Upon comparing the obtained results of liners from cohort A, it can be noted that gravimetric method displays highest amount of wear consistently. This is because gravimetric method accounts for wear on the full liner including the wear from the clamping area of the liner, whereas the CMM method and the RMM method accounts for wear in only the measured area, i.e. the bearing surface and beyond. The results obtained by the CMM method and the RMM method display less variance however the RMM method results displays higher wear volumes than the CMM method except for liner 1. The suspected reason for this is the mechanical filtering error caused by the CMM measurements and nanometer precision of the employed RMM.

Further to comparing the volumetric wear results of cohort A, the interval volumetric results from cohort C were compared. For the comparison, individual graphs for each liner was created that displayed the volumetric wear of that liner at each interval measured by all three methods. This graph was

chosen to efficiently display the variation in all the three methods at each interval. Below given are the six graphs (Figure 88, Figure 89, Figure 90, Figure 91, Figure 92 and Figure 93) that display the volumetric wear results obtained at all three interval by all three methods for each liner.

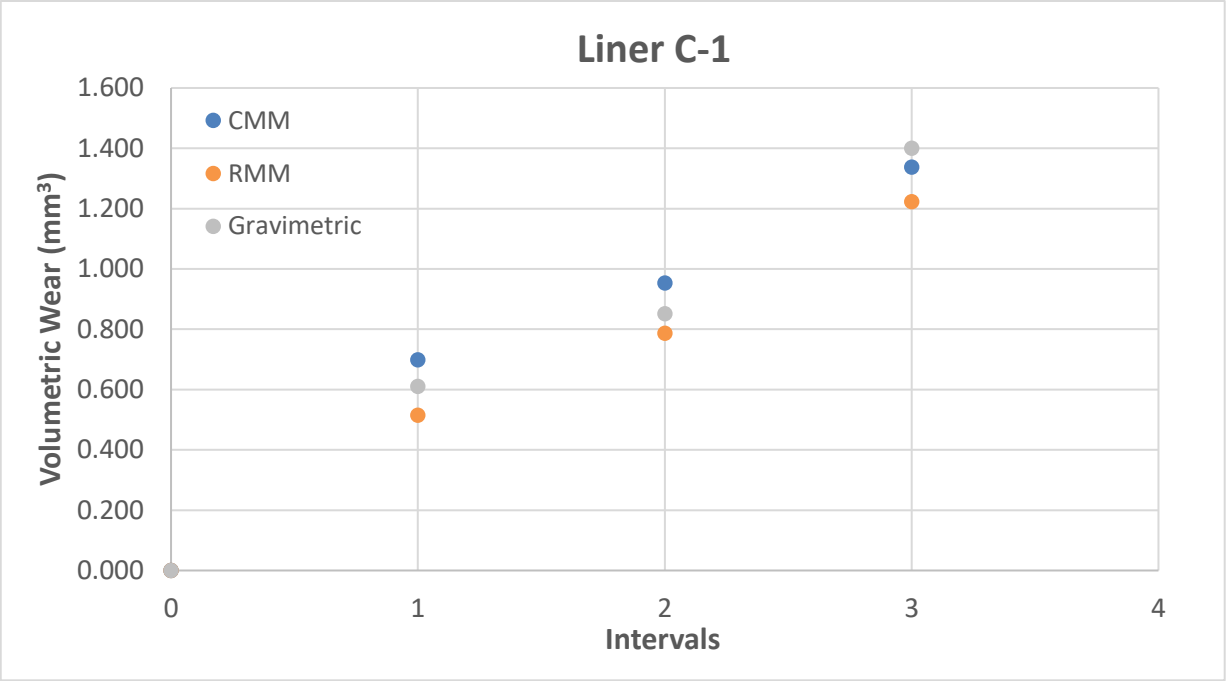

Figure 88: Graph displaying volumetric wear result obtained by CMM, RMM and Gravimetric at each interval for liner C-1.

The above graph (Figure 88) compares the volumetric wear results obtained through the CMM, the RMM and the Gravimetric method at each interval for liner C-1. It can be observed that the CMM method at interval 1 and interval 2 displays higher volumetric wear compared to gravimetric. Such higher volumetric wear reading is possibly attributable to the CMM method's analysis process of the planar section selection. Regardless, all three methods quantified volumetric wear within a variation as low as 0.2 mm^3 at each interval for liner C-1.

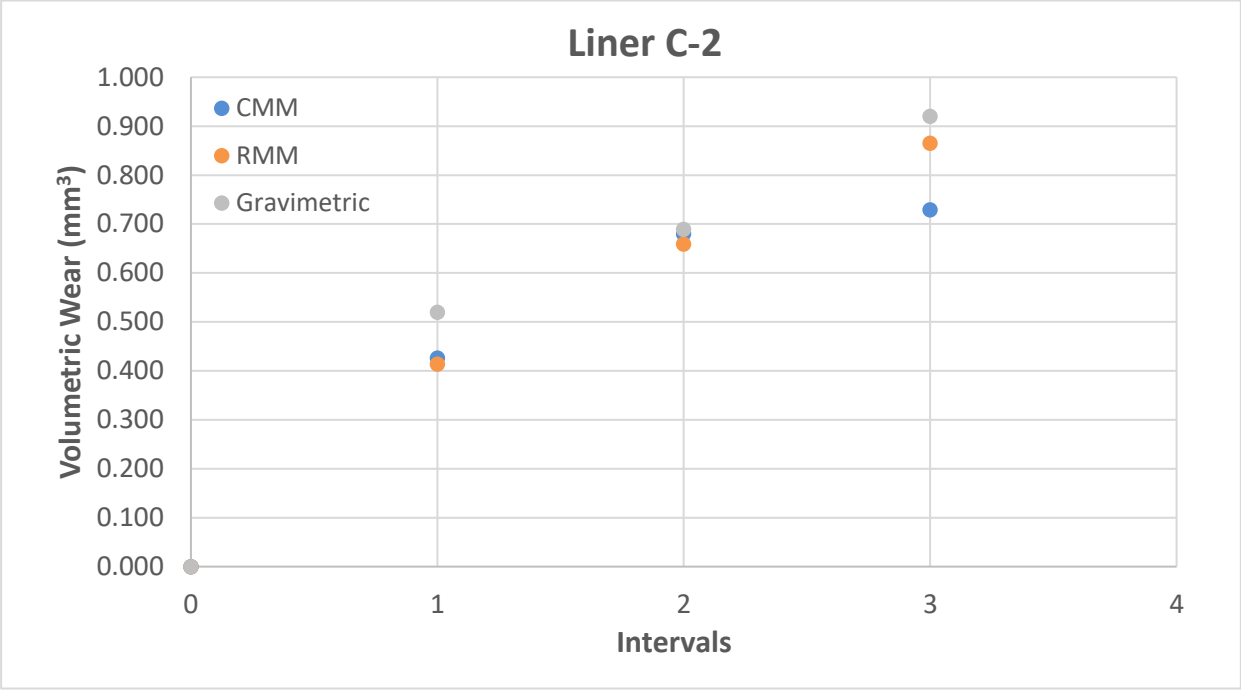

Figure 89: Graph displaying volumetric wear result obtained by CMM, RMM and Gravimetric at each interval for liner 2.

The above graph (Figure 89) compares the volumetric wear results obtained through the CMM, the RMM and the Gravimetric method at each interval for liner C-2. It can be observed that at interval 1, the CMM and the RMM method quantified equal amount of wear, but the gravimetric method displayed 0.1 mm^3 higher wear than that quantified by the CMM and the RMM method. Here, it is suspected that the wear has occured in area other than the edge and as the gravimetric method accounts for the overall wear of liner it displays higher wear than that the CMM and the RMM method. At interval 2 all the three methods quantified equal amount of volumetric wear with the variation of 0.03 mm^3. At interval 3, the RMM and the gravimetric method obtained wear volumes within 0.05 mm^3, however CMM quantified less volumetric wear compared to the RMM and the gravimetric methods. It must be noted that the result of liner C-2 as obtained by the CMM method is an outlier.

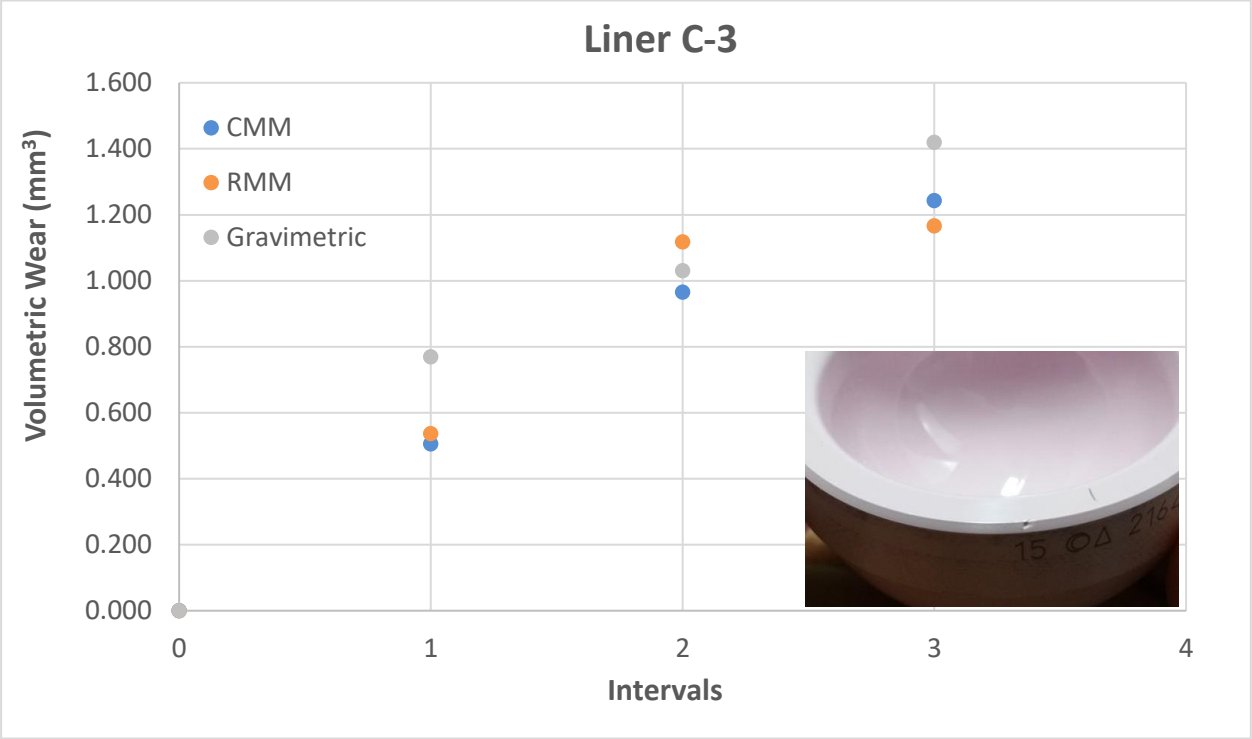

Figure 90: Graph displaying volumetric wear result obtained by CMM, RMM and Gravimetric at each interval for liner 3. The picture of the liner displays the chipped rim.

The above graph (Figure 90) compares the volumetric wear results obtained through the CMM, the RMM and the Gravimetric method at each interval for liner C-3. It can be observed that at interval 1, the CMM and the RMM method quantified equal amount of wear with a variation of 0.02 mm^3, but the gravimetric method displayed volumetric wear higher by 0.27 mm^3 than that quantified by the CMM and the RMM methods. Such high value of volumetric wear result as obtained by the gravimetric method was due to the chipping of the rim of liner C-3 which gravimetric cannot ignore. This is an indication that, even for simulation process, the wear can occur in other areas of the acetabular liner. At interval 2 all three methods quantified equal amount of volumetric wear with a variation of 0.15 mm^3. It should be noted that the from interval 2 the chipped part was compensated by the Leeds university group that assessed liners gravimetrically. As the study being blind, I had no influence on the compensation. At interval 3, the CMM and the RMM methods

displayed similar wear volumes with a variation of 0.07 mm^3, however, the gravimetric method quantified 0.2 mm^3 more volumetric wear compared to the CMM and the RMM methods.

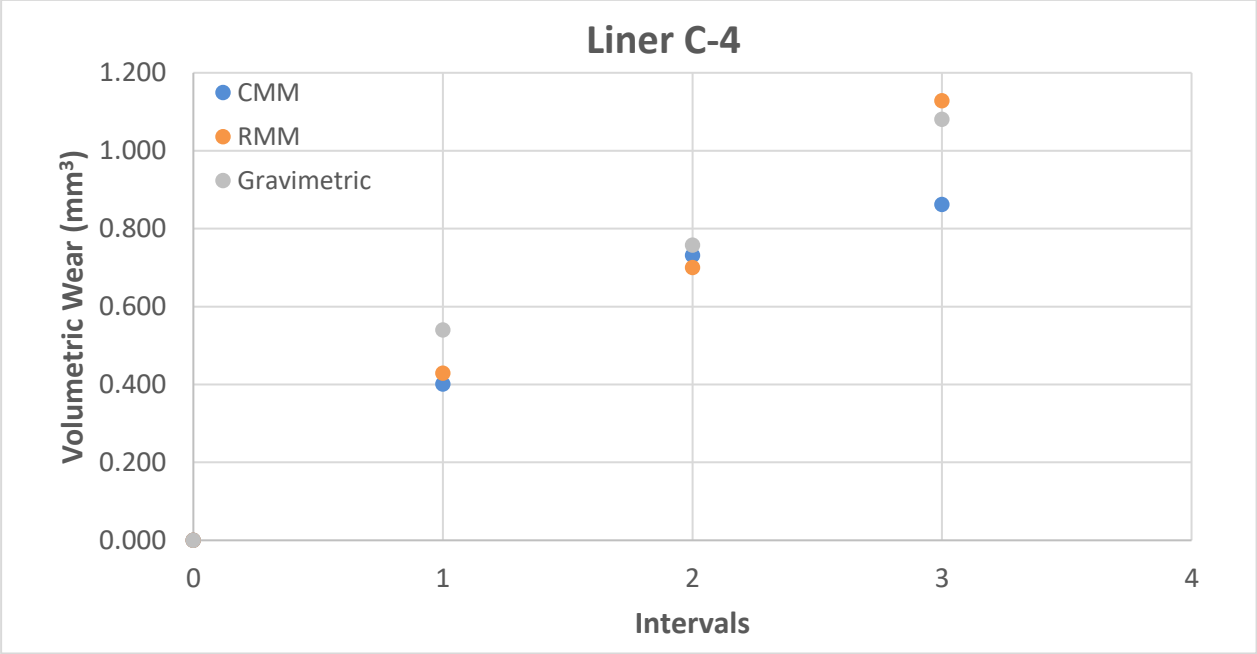

Figure 91: Graph displaying volumetric wear result obtained by the CMM, the RMM and the Gravimetric at each interval for liner 4.

The above graph (Figure 91) compares the volumetric wear results obtained through the CMM, the RMM and the Gravimetric method at each interval for liner C-4. It can be observed that at interval 1, CMM and RMM method quantified equal amount of wear with a variation of 0.028 mm^3, but the volumetric wear as obtained by the gravimetric method was 0.14 mm^3 higher than that quantified by the CMM and the RMM method. Here, it is suspected that the wear has occurred in area other than edge and as gravimetric method accounts for the overall wear of liner it displays higher wear than that CMM and RMM method. At interval 2 all three methods quantified equal amount of volumetric wear with variation of 0.05 mm^3. At interval 3, RMM and gravimetric methods displayed similar wear volumes with variation of 0.02 mm^3 however the CMM method quantified significantly low

(lower by 0.266 mm^3) volumetric wear compared to the RMM and the gravimetric method.

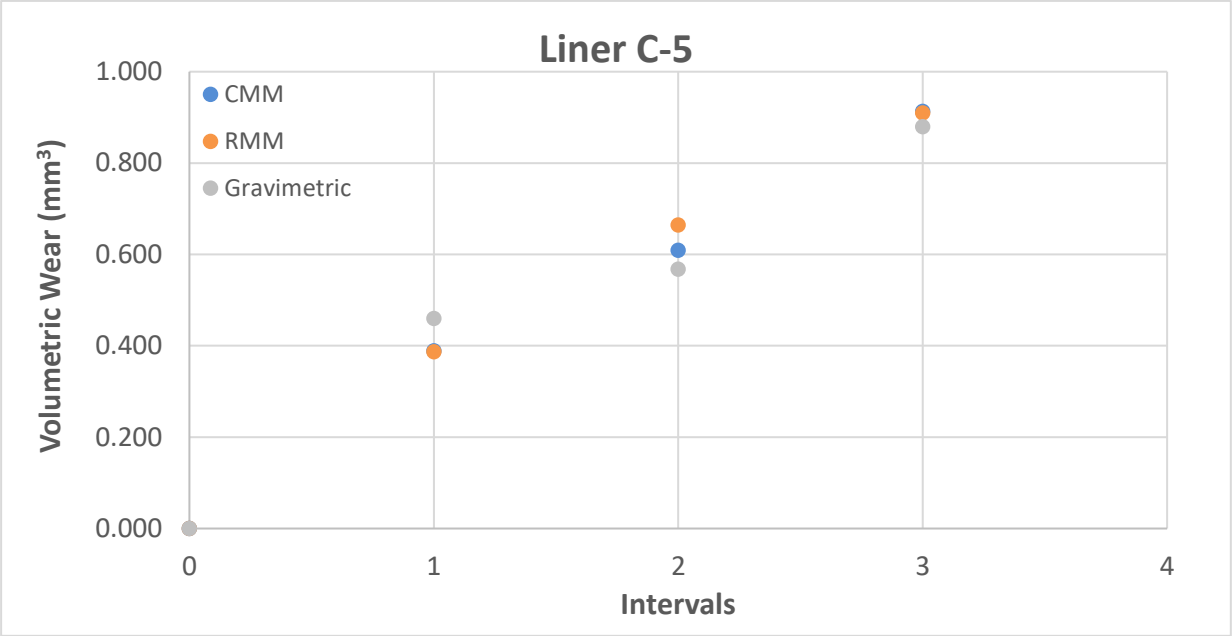

Figure 92: Graph displaying volumetric wear result obtained by the CMM, the RMM and the Gravimetric at each interval for liner 5.

The above graph (Figure 92) compares the volumetric wear results obtained through CMM, RMM and Gravimetric method at each interval for liner C-5. It can be observed that at interval 1, CMM and RMM method quantified exactly same amount of wear, but the volumetric wear obtained by the gravimetric method was 0.071 mm^3 higher than that quantified by the CMM and the RMM methods. At interval 2, CMM and RMM methods display higher value of quantified wear volumes to that of gravimetric method with a variation of 0.096 mm^3. At interval 3, again the CMM and the RMM method obtained exactly same amount of volumetric wear, however the volumetric wear measured by the gravimetric was lower by 0.033 mm^3 than that of the CMM and the RMM method. The measurements of liner C-5 serves as a good example for displaying good agreement between all the three methods.

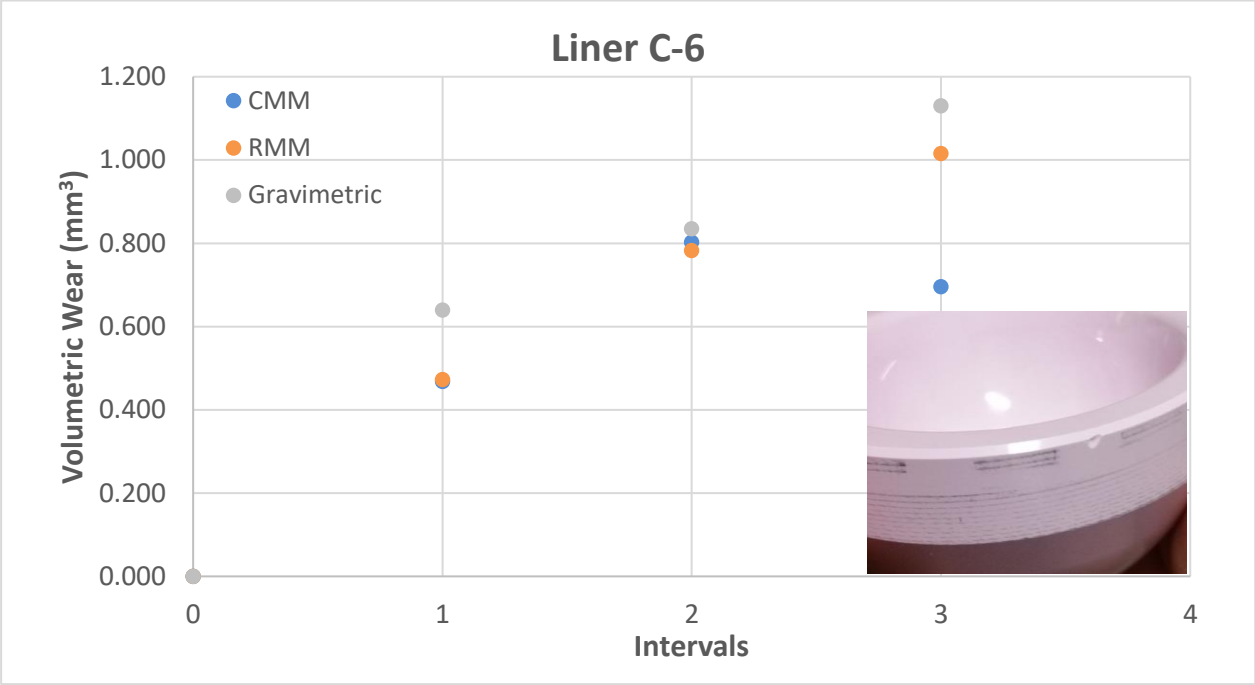

Figure 93: Graph displaying volumetric wear result obtained by the CMM, the RMM and the Gravimetric at each interval for liner 6. Picture of the liner displays the chipped rim.

The above graph (Figure 93) compares the volumetric wear results obtained through the CMM, the RMM and the Gravimetric method at each interval for liner C-6. It can be observed that at interval 1, the CMM and the RMM method quantified equal amount of wear, but the gravimetric method displayed higher wear than that quantified by the CMM and the RMM methods. The reason for higher value of volumetric wear as measured by gravimetric method was caused due to chipping of the rim of liner C-6 which gravimetric cannot ignore. At interval 2 all three methods quantified equal amount of volumetric wear. At interval 3, the gravimetric method displays highest volumetric wear, the RMM method measured similar amount of wear volumes as gravimetric, however, the results obtained from the CMM method displayed lower values of volumetric wear.

From the above discussion, it can be said that the CMM method and the RMM method, both can measure volumetric wear in ceramic acetabular liners. Both the methods are able to characterise edge wear distribution, determine

linear wear penetration and assess volumetric edge wear in simulated acetabular liners. Both, the CMM method and the RMM method, do not require any pre-wear data of the liner to characterise or quantify volumetric edge wear and hence are suitable for edge wear measurement of retrieved acetabular liners. The wear volumes observed in the ceramic liners are 10-folds lower than that observed in metal-on-metal components and hence this method can also be employed to measure the metal-on-metal acetabular components. Some retrieval studies stated that the measured volumetric wear and examined blood ions were not directly comparable [314]. This is due to the previously unmeasured edge wear beyond the bearing surface. However, the developed CMM and the RMM method allows for the volumetric wear measurement beyond the bearing surface and hence making it possible to directly compare the blood ions to the volumetric wear.

6.7 Novel Contribution

The novelties of this study are mentioned below:

- Unlike the existing CMM methods, the novel CMM method utilises planar section to reconstruct the unworn reference geometry allowing for the reconstruction of the complex freeform surfaces.
- The new unworn geometry reconstruction process of the CMM method allows for the reconstruction of beyond the bearing surface and hence allows for the characterisation and quantification of the complete edge wear.
- The developed CMM method allows for the volumetric wear measurement of sub 0.1 mm^3.
- The developed RMM method analyse the roundness traces by the use of developed programs in MATLAB to characterise and quantify volumetric wear.

- The 3D surface obtained from the RMM measurement displays unwrapped 3D surface of the measured data and allows the user to characterise edge wear distribution and measure linear wear penetration. Moreover, the 3D surface also allows for 2D assessment of the measurement.

Chapter 7: Conclusion

- Two methods, the CMM method and the RMM method, were successfully developed to characterise and quantify volumetric edge wear in ceramic acetabular liners. Both the methods are able to quantify volumetric wear as low as 0.1 and allow for the quantification of the volumetric wear above the edge geometry. This is essential to estimate a complete edge wear which was not possible prior to this study.
- The form of the unworn bearing surfaces of acetabular liners of cohort B has been investigated by measuring the roundness traces on the RMM and from this it was concluded that the bearing surfaces of the ceramic acetabular liners were ellipsoidal and had uncontrolled surface above the edge. This finding was important as this information was essential to develop a method for reconstruction of the unworn geometry of the measured surface.
- For the CMM method, the reference geometry of the unworn surface was successfully reconstructed in accordance with the studied uncontrolled ellipsoidal form of the bearing surface and the uncontrolled edge geometry of the ceramic acetabular liners.
- The surface reconstruction process was performed on acetabular liners of the unworn cohort B and the fitting of the reconstructed surface was tested through deviation analysis. The deviation analysis displayed that the surface reconstruction was successful with 98.7% of the reconstructed surface fitted under 2 microns. Such precise fit of the reconstructed reference geometry is essential to achieve the accuracy as required for the volumetric wear assessment of the ceramic liners.
- The investigation of cohort B gave an important insight regarding the coverage angle of the acetabular liners. The investigation led to the conclusion that two out of six acetabular liners had a tilt of more than 2° in the coverage angle. Hence this tilt causes a significant disparity of

4° in quartiles, which drastically increases the possibility of edge loading or edge wear even in a well-positioned acetabular liner.

- The novel unworn geometry reconstruction process of the CMM method encompass the complete edge wear, i.e. the wear in the bearing surface as well as in the surface above the edge. Hence, the deviation analysis of the CMM method is now able to characterise complete edge wear distribution and measure linear wear penetration of the complete edge wear.
- The 3D surface map generated from the RMM method displays an unwrapped and levelled form of the complete edge wear including the wear above the bearing surface. However, due to the limited gauge travel range of 2 mm of the given RMM, the measurement is limited to a well-defined area located on both the bearing surface and the edge surface of an acetabular liner. It should be noted that this limitation can be resolved by employing a commercially available gauge that has a travel length of 4 mm.
- The interval study concluded that the methods were able to characterise the progress and development of the wear scar at each interval along with providing information regarding the linear wear penetration and volumetric wear. The interval study displayed a good correlation between the volumetric wear results as obtained at each interval by all the three methods. This shows that the developed CMM method and the RMM method, both can quantify edge wear volumes as good as the gold standard gravimetric method.The range of the wear volumes measured by both, the CMM and the RMM method, was found to be 0.3871 mm^3 to 1.3380 mm^3. The interval study also points out two outliers in the CMM method at the third interval which requires further investigation.
- Both, the CMM and the RMM, method is effective at characterising the wear distribution and quantifying volumetric edge wear beyond the edge and the bearing surface. This breaks the limitation of edge-wear

measurement of ceramic acetabular liners which has yet been confined to the *in vitro* testing. This also allows for the measurement of volumetric wear in surface beyond the edge in metallic acetabular liners which has not yet been accounted for in the existing simulation or retrieval studies and hence left the wear volumes under-estimated

Chapter 8: Future Work

- Resolving the cause of errors induced through the planar section selection process of the CMM method that causes the outliers. The planar selection process is complex due to the free form edge and the freeform surface beyond the bearing area. It causes the planar sections require to be as close as possible to the wear area in order to reconstruct the unworn geometry more accurately. This can be done through increasing the number of vertical and horizontal planar sections and decreasing the distance between vertical planar section.

- Test both, the CMM and the RMM method, on a larger cohort and evaluate the uncertainties related to each method.

- Test the performance of both, the CMM and the RMM method, on various designs of ceramic-on-ceramic acetabular liners. Currently the methods are developed on a single design of ceramic-on-ceramic acetabular liner. However, there are various design of ceramic acetabular cups available on which the method requires to be tested in order to make it more robust with respect to other designs.

- Test both, the CMM and the RMM method, on retrieved ceramic-on-ceramic liners. Currently the methods have been developed on the acetabular liners that were simulated specifically for edge wear. However the scenario of retrieved liners can differ and hence the methods are required to be tested on retrieved components.

- Conduct the RMM measurement by employing an RMM that has gauge that permits higher travel range to encompass complete edge-wear. The employed RMM has a gauge travel range of 2 um which limited the RMM measurement to 5 mm height. However, there gauges with higher travel

range (4 um) are available on the market which can allow the user to measure more than 5 mm height of the acetabular liner and capture the wear scar thoroughly or even capture bigger wear areas.

- Test the performance of the CMM method on metal-on-metal acetabular components and compare it with the previous geometrical measurement methods. Previously, the metal-on-metal acetabular components were measured on using a different CMM method that limited the measurement to the bearing surface. Hence all the previously measured metal-on-metal acetabular components did not account for the wear beyond bearing surface. However the developed CMM method allows for the measurement beyond the bearing surface. Hence it provides an opportunity to compare the previous results with the results obtained by the developed CMM method.

References

1. *National Joint Registry - 14th Annual Report*. 2017.

2. Kurtz, S., et al., *Projections of primary and revision hip and knee arthroplasty in the United States from 2005 to 2030.* JBJS, 2007. **89**(4): p. 780-785.

3. Pabinger, C. and A. Geissler, *Utilization rates of hip arthroplasty in OECD countries.* Osteoarthritis and cartilage, 2014. **22**(6): p. 734-741.

4. Al-Hajjar, M., et al., *Wear of novel ceramic-on-ceramic bearings under adverse and clinically relevant hip simulator conditions.* Journal of Biomedical Materials Research Part B: Applied Biomaterials, 2013. **101**(8): p. 1456-1462.

5. Al-Hajjar, M., et al., *Wear of 36-mm BIOLOX® delta ceramic-on-ceramic bearing in total hip replacements under edge loading conditions.* Proceedings of the Institution of Mechanical Engineers, Part H: Journal of Engineering in Medicine, 2013. **227**(5): p. 535-542.

6. Vendittoli, P.-A., et al., *Metal ion release with large-diameter metal-on-metal hip arthroplasty.* The Journal of arthroplasty, 2011. **26**(2): p. 282-288.

7. Smeekes, C., et al., *Large fixed-size metal-on-metal total hip arthroplasty: higher serum metal ion levels in patients with pain.* International orthopaedics, 2015. **39**(4): p. 631-638.

8. Zijlstra, W.P., N. Bos, and J.J. van Raaij, *Large head metal-on-metal cementless total hip arthroplasty versus 28mm metal-on-polyethylene cementless total hip arthroplasty: design of a randomized controlled trial.* BMC musculoskeletal disorders, 2008. **9**(1): p. 136.

9. Lachiewicz, P.F., E.S. Soileau, and J.M. Martell, *Wear and osteolysis of highly crosslinked polyethylene at 10 to 14 years: the effect of femoral head size.* Clinical Orthopaedics and Related Research®, 2016. **474**(2): p. 365-371.

10. Stafford, G., S.U. Islam, and J. Witt, *Early to mid-term results of ceramic-on-ceramic total hip replacement: analysis of bearing-surface-related complications.* The Journal of bone and joint surgery. British volume, 2011. **93**(8): p. 1017-1020.

11. Jarrett, C.A., et al., *The squeaking hip: a phenomenon of ceramic-on-ceramic total hip arthroplasty.* JBJS, 2009. **91**(6): p. 1344-1349.

12. Keurentjes, J., et al., *High incidence of squeaking in THAs with alumina ceramic-on-ceramic bearings.* Clinical orthopaedics and related research, 2008. **466**(6): p. 1438-1443.

13. Sanders, A.P. and R.M. Brannon, *A simple surrogate test method to rank the wear performance of prospective ceramic materials under hip prosthesis edge-loading conditions.* Journal of Biomedical Materials Research Part B: Applied Biomaterials, 2014. **102**(2): p. 311-321.

14. Macdonald, N. and M. Bankes, *Ceramic on ceramic hip prostheses: a review of past and modern materials.* Archives of orthopaedic and trauma surgery, 2014. **134**(9): p. 1325-1333.

15. Walter, W.L., et al., *Edge loading in third generation alumina ceramic-on-ceramic bearings.* The Journal of Arthroplasty, 2004. **19**(4): p. 402-413.

16. Sagbas, B. and M. Numan Durakbasa, *Measurement of wear in orthopedic prosthesis.* Acta Physica Polonica-Series A General Physics, 2012. **121**(1): p. 131.

17. Bills, P.J., et al., *Volumetric wear assessment of retrieved metal-on-metal hip prostheses and the impact of measurement uncertainty.* Wear, 2012. **274**: p. 212-219.

18. Carmignato, S., et al., *Uncertainty evaluation of volumetric wear assessment from coordinate measurements of ceramic hip joint prostheses.* Wear, 2011. **270**(9-10): p. 584-590.

19. ISO, B., *14242-2: 2000: Implants for Surgery-Wear of Total Hip Joint Prostheses-Part 2: Methods of Measurement.* British Standards Institute, London, 2000.

20. Learmonth, I.D., C. Young, and C. Rorabeck, *The operation of the century: total hip replacement.* The Lancet, 2007. **370**(9597): p. 1508-1519.

21. Dudkiewicz, I., et al., *Total hip arthroplasty in patients younger than 30 years of age.* IMAJ-RAMAT GAN-, 2003. **5**(10): p. 709-712.

22. No-Author-Listed, *12th Annual Report - NJR.* National Joint Registry for England and Wales: 9th Annual report, 2012., 2015. **12**.

23. Rajpura, A., D. Kendoff, and T. Board, *The current state of bearing surfaces in total hip replacement.* Bone Joint J, 2014. **96**(2): p. 147-156.

24. Jameson, S.S., et al., *Lower rates of dislocation with increased femoral head size after primary total hip replacement: A five-year analysis of NHS patients in England.* Journal of Bone and Joint Surgery - Series B, 2011. **93**(7): p. 876-880.

25. Liu, F., et al., *Effect of head contact on the rim of the cup on the offset loading and torque in hip joint replacement.* Proceedings of the Institution of Mechanical Engineers, Part H: Journal of Engineering in Medicine, 2013. **227**(11): p. 1147-1154.

26. Neuerburg, C., et al., *Survivorship of second-generation metal-on-metal primary total hip replacement.* Archives of Orthopaedic and Trauma Surgery, 2012. **132**(4): p. 527-533.

27. Streicher, R.M., et al., *Metal-On-Metal Articulation for Artificial Hip Joints: Laboratory Study and Clinical Results.* Proceedings of the Institution of Mechanical Engineers, Part H: Journal of Engineering in Medicine, 1996. **210**(3): p. 223-232.

28. Ingham, E. and J. Fisher, *Biological reactions to wear debris in total joint replacement.* Proceedings of the Institution of Mechanical Engineers, Part H: Journal of Engineering in Medicine, 2000. **214**(1): p. 21-37.

29. Hu, D., et al., *Comparison of ceramic-on-ceramic to metal-on-polyethylene bearing surfaces in total hip arthroplasty: a meta-analysis of randomized controlled trials.* Journal of Orthopaedic Surgery and Research, 2015. **10**(1): p. 22.

30. D'Antonio, J.A., W.N. Capello, and M. Naughton, *Ceramic Bearings for Total Hip Arthroplasty Have High Survivorship at 10 Years.* Clinical Orthopaedics and Related Research®, 2012. **470**(2): p. 373-381.

31. Dumbleton, J.H., M.T. Manley, and A.A. Edidin, *A literature review of the association between wear rate and osteolysis in total hip arthroplasty.* The Journal of Arthroplasty, 2002. **17**(5): p. 649-661.

32. Kabo, J., et al., *In vivo wear of polyethylene acetabular components.* Bone & Joint Journal, 1993. **75**(2): p. 254-258.

33. Vendittoli, P.-A., et al., *Alumina on alumina versus metal on conventional polyethylene: a randomized clinical trial with 9 to 15 years follow-up.* Acta Orthop Belg, 2013. **79**(2): p. 181-190.

34. Capello, W.N., et al., *Ceramic-on-ceramic total hip arthroplasty: update.* The Journal of arthroplasty, 2008. **23**(7): p. 39-43.

35. Bascarevic, Z., et al., *Alumina-on-alumina ceramic versus metal-on-highly cross-linked polyethylene bearings in total hip arthroplasty: a comparative study.* International orthopaedics, 2010. **34**(8): p. 1129-1135.

36. Bierbaum, B.E., et al., *Ceramic/Ceramic Total Hip Replacement: The American Experience with Stryker Implants*, in *Bioceramics in Joint Arthroplasty: 9th BIOLOX® Symposium Paris, March 26–27, 2004 Proceedings*, J.-Y. Lazennec and M. Dietrich, Editors. 2004, Steinkopff: Heidelberg. p. 21-34.

37. Ikeda, T., et al., *Polyneuropathy caused by cobalt–chromium metallosis after total hip replacement.* Muscle & Nerve, 2010. **42**(1): p. 140-143.

38. Heffernan, E.J., et al., *The imaging appearances of metallosis.* Skeletal radiology, 2008. **37**(1): p. 59-62.

39. Lal, S., R.M. Hall, and J.L. Tipper, *A novel method for isolation and recovery of ceramic nanoparticles and metal wear debris from serum lubricants at ultra-low wear rates.* Acta Biomaterialia, 2016. **42**: p. 420-428.

40. Tipper, J.L., et al., *Characterisation of wear debris from UHMWPE on zirconia ceramic, metal-on-metal and alumina ceramic-on-ceramic hip prostheses generated in a physiological anatomical hip joint simulator.* Wear, 2001. **250**(1): p. 120-128.

41. Tuke, M., et al., *3D linear and volumetric wear measurement on artificial hip joints—Validation of a new methodology.* Precision Engineering, 2010. **34**(4): p. 777-783.

42. Lord, J., et al., *Volumetric wear assessment of failed metal-on-metal hip resurfacing prostheses.* Wear, 2011. **272**(1): p. 79-87.

43. Morlock, M., et al., *Biomechanical, morphological, and histological analysis of early failures in hip resurfacing arthroplasty.* Proceedings of the Institution of Mechanical Engineers, Part H: Journal of Engineering in Medicine, 2006. **220**(2): p. 333-344.

44. Philo, R., *Gray's Anatomy for Students, 2nd Ed. by Richard L. Drake, A. Wayne Vogl, and Adam W. M. Mitchell.* Clinical Anatomy, 2009. **22**(7): p. 846-847.

45. Ltd, T.S. *The Hip Joint*. 2017; Available from: http://teachmeanatomy.info/lower-limb/joints/hip-joint/.

46. Kung, M.S., et al., *The synovial lining and synovial fluid properties after joint arthroplasty.* Lubricants, 2015. **3**(2): p. 394-412.

47. Bronner, F. and M.C. Farach-Carson, *Bone and osteoarthritis*. Vol. 4. 2007: Springer Science & Business Media.

48. Pavlovich, R.I. and J. Lubowitz, *Current concepts in synovial tissue of the knee joint.* Orthopedics, 2008. **31**(2).

49. Brown, L., *The use of 3D surface analysis techniques to investigate the wear of matt surface finish femoral stems in total hip replacement*. 2006, University of Huddersfield.

50. Heuberger, M., et al., *Protein-mediated boundary lubrication in arthroplasty.* Biomaterials, 2005. **26**(10): p. 1165-1173.

51. Konttinen, Y.T., et al., *The microenvironment around total hip replacement prostheses.* Clinical orthopaedics and related research, 2005. **430**: p. 28-38.

52. Hills, B., *Boundary lubrication in vivo.* Proceedings of the Institution of Mechanical Engineers, Part H: Journal of Engineering in Medicine, 2000. **214**(1): p. 83-94.

53. Dowson, D., *New joints for the Millennium: wear control in total replacement hip joints.* Proceedings of the Institution of Mechanical Engineers, Part H: Journal of Engineering in Medicine, 2001. **215**(4): p. 335-358.

54. Unsworth, A., *Recent developments in the tribology of artificial joints.* Tribology International, 1995. **28**(7): p. 485-495.

55. Bills, P.J., *The development of a geometric methodology for the determination of volumetric wear in total joint replacements & development of a total knee replacement joint using new and novel measurement techniques*. 2007, University of Huddersfield.

56. Charlish, A., *The complete arthritis handbook: a self-help guide for people living with arthritis*. 1993.

57. Al-Hajjar, M., *Wear of hard-on-hard hip prostheses: influence of head size, surgical position, material and function*. 2012: University of Leeds.

58. Johnson, V.L. and D.J. Hunter, *The epidemiology of osteoarthritis.* Best practice & research Clinical rheumatology, 2014. **28**(1): p. 5-15.

59. Woolf, A.D. and B. Pfleger, *Burden of major musculoskeletal conditions.* Bulletin of the World Health Organization, 2003. **81**(9): p. 646-656.

60. Lawrence, R.C., et al., *Estimates of the prevalence of arthritis and other rheumatic conditions in the United States: Part II.* Arthritis & Rheumatology, 2008. **58**(1): p. 26-35.

61. Callaghan, J.J., A.G. Rosenberg, and H.E. Rubash, *The adult hip*. Vol. 1. 2007: Lippincott Williams & Wilkins.

62. Smolen, J.S., D. Aletaha, and I.B. McInnes, *Rheumatoid arthritis.* The Lancet, 2016. **388**(10055): p. 2023-2038.

63. Scott, D.L., F. Wolfe, and T.W.J. Huizinga, *Rheumatoid arthritis.* The Lancet, 2010. **376**(9746): p. 1094-1108.

64. Symmons, D., et al., *The prevalence of rheumatoid arthritis in the United Kingdom: new estimates for a new century.* Rheumatology, 2002. **41**(7): p. 793-800.

65. Costenbader, K.H., et al., *Geographic variation in rheumatoid arthritis incidence among women in the united states.* Archives of Internal Medicine, 2008. **168**(15): p. 1664-1670.

66. Kalla, A.A. and M. Tikly, *Rheumatoid arthritis in the developing world.* Best Practice & Research Clinical Rheumatology, 2003. **17**(5): p. 863-875.

67. Carlens, C., et al., *Smoking, use of moist snuff, and risk of chronic inflammatory diseases.* American journal of respiratory and critical care medicine, 2010. **181**(11): p. 1217-1222.

68. Hospitals, M. *HIGH PERFORMANCE TOTAL HIP REPLACEMENT SURGERY*. Available from: http://maxcurehospitals.com/blog/total-hip-replacement-surgery-in-india/.

69. Haboush, E., *A new operation for arthroplasty of the hip based on biomechanics, photoelasticity, fast-setting dental acrylic, and other considerations.* Bulletin of the Hospital for Joint Diseases, 1953. **14**(2): p. 242-277.

70. McKee, G. and J. Watson-Farrar, *Replacement of arthritic hips by the McKee-Farrar prosthesis.* Bone & Joint Journal, 1966. **48**(2): p. 245-259.

71. Ring, P., *Complete replacement arthroplasty of the hip by the Ring prosthesis.* Bone & Joint Journal, 1968. **50**(4): p. 720-731.

72. Müller, M.E., *The benefits of metal-on-metal total hip replacements.* Clinical orthopaedics and related research, 1995. **311**: p. 54-59.

73. Walker, P. and B. Gold, *The tribology (friction, lubrication and wear) of all-metal artificial hip joints.* Wear, 1971. **17**(4): p. 285-299.

74. Learmonth, I., S. Gheduzzi, and T. Vail, *Clinical experience with metal-on-metal total joint replacements: indications and results.* Proceedings of the Institution of Mechanical Engineers, Part H: Journal of Engineering in Medicine, 2006. **220**(2): p. 229-237.

75. Thompson, M.S. and A. MEng, *The design of a novel hip resurfacing prosthesis*. 2001, University of London.

76. Charnley, J. and Z. Cupic, *The nine and ten year results of the low-friction arthroplasty of the hip.* Clinical orthopaedics and related research, 1973. **95**: p. 9-25.

77. Charnley, J., *Total hip replacement.* Jama, 1974. **230**(7): p. 1025-1028.

78. Charnley, J., *Long-term results of low-friction arthroplasty.* The hip, 1981: p. 42-49.

79. Semlitsch, M., R. Streicher, and H. Weber, *The wear behavior of capsules and heads of CoCrMo casts in long-term implanted all-metal hip prostheses.* Der Orthopade, 1989. **18**(5): p. 377-381.

80. Schmidt, M., H. Weber, and R. Schön, *Cobalt chromium molybdenum metal combination for modular hip prostheses.* Clinical orthopaedics and related research, 1996. **329**: p. S35-S47.

81. McKellop, H., et al., *In Vivo Wear of 3 Types of Metal on Metal Hip Prostheses During 2 Decades of Use.* Clinical orthopaedics and related research, 1996. **329**: p. S128-S140.

82. Boutin, P., et al., *The use of dense alumina–alumina ceramic combination in total hip replacement.* Journal of Biomedical Materials Research Part A, 1988. **22**(12): p. 1203-1232.

83. Bizot, P., et al., *Ceramic/ceramic total hip arthroplasty.* Journal of orthopaedic science, 2000. **5**(6): p. 622-627.

84. Cales, B., *Zirconia as a sliding material: histologic, laboratory, and clinical data.* Clinical orthopaedics and related research, 2000. **379**: p. 94-112.

85. Streicher, R., et al., *Metal-on-metal articulation for artificial hip joints: laboratory study and clinical results.* Proceedings of the Institution of Mechanical Engineers, Part H: Journal of Engineering in Medicine, 1996. **210**(3): p. 223-232.

86. Willmann, G., *Ceramic femoral head retrieval data.* Clinical Orthopaedics and Related Research, 2000. **379**: p. 22-28.

87. Napier, R.J. and A.J. Shimmin. *Ceramic-on-ceramic bearings in total hip arthroplasty:"The future is now"*. in *Seminars in Arthroplasty*. 2016. Elsevier.

88. Firkins, P., et al., *A novel low wearing differential hardness, ceramic-on-metal hip joint prosthesis.* Journal of biomechanics, 2001. **34**(10): p. 1291-1298.

89. Kjærgaard, N., et al., *Thresholds for the Oxford Hip Score after total hip replacement surgery: a novel approach to postoperative evaluation.* Journal of Orthopaedics and Traumatology, 2017.

90. Spagnolo, A.M., et al., *Operating theatre quality and prevention of surgical site infections.* Journal of Preventive Medicine and Hygiene, 2013. **54**(3): p. 131-137.

91. Lidwell, O.M., et al., *Infection and sepsis after operations for total hip or knee-joint replacement: influence of ultraclean air, prophylactic antibiotics and other factors.* The Journal of Hygiene, 1984. **93**(3): p. 505-529.

92. Ghalme, S.G., A. Mankar, and Y. Bhalerao, *Biomaterials in hip joint replacement.* Int J Sci Eng, 2016. **4**(2): p. 113-125.

93. New, A.M.R., et al., *In vivo measurement of acetabular cement pressurization using a simple new design of cement pressurizer.* The Journal of Arthroplasty, 1999. **14**(7): p. 854-859.

94. Fisher, D., et al., *Cement-mantle thickness affects cement strains in total hip replacement.* Journal of biomechanics, 1997. **30**(11-12): p. 1173-1177.

95. eORTHOPOD. *ARTIFICIAL JOINT REPLACEMENT OF THE HIP*. Available from: http://www.houstonmethodist.org/orthopedics/where-does-it-hurt/hip/artificial-joint-replacement/.

96. Lai, K.-A., et al., *Failure of hydroxyapatite-coated acetabular cups Ten-year follow-up of 85 Landos Atoll arthroplasties.* Journal of Bone & Joint Surgery, British Volume, 2002. **84**(5): p. 641-646.

97. Cook, S.D., K.A. Walsh, and R.J. HADDAD Jr, *Interface mechanics and bone growth into porous Co-Cr-Mo alloy implants.* Clinical orthopaedics and related research, 1985. **193**: p. 271-280.

98. Pilliar, R., J. Lee, and C. Maniatopoulos, *Observations on the effect of movement on bone ingrowth into porous-surfaced implants.* Clinical orthopaedics and related research, 1986. **208**: p. 108-113.

99. Welsh, R.P., R.M. Pilliar, and I. Macnab, *Surgical Implants: THE ROLE OF SURFACE POROSITY IN FIXATION TO BONE AND ACRYLIC.* JBJS, 1971. **53**(5): p. 963-977.

100. Bobyn, J., et al., *The optimum pore size for the fixation of porous-surfaced metal implants by the ingrowth of bone.* Clinical orthopaedics and related research, 1980. **150**: p. 263-270.

101. Robertson, D.M., L. St Pierre, and R. Chahal, *Preliminary observations of bone ingrowth into porous materials.* Journal of Biomedical Materials Research Part A, 1976. **10**(3): p. 335-344.

102. Clemow, A., et al., *Interface mechanics of porous titanium implants.* Journal of Biomedical Materials Research Part A, 1981. **15**(1): p. 73-82.

103. Kienapfel, H., et al., *Implant fixation by bone ingrowth.* The Journal of arthroplasty, 1999. **14**(3): p. 355-368.

104. Steppacher, S.D., et al., *Managing length and stability: the role of the modular neck.* Orthopedics, 2008. **31**(9).

105. Skendzel, J.G., J.D. Blaha, and A.G. Urquhart, *Total hip arthroplasty modular neck failure.* The Journal of arthroplasty, 2011. **26**(2): p. 338. e1-338. e4.

106. Chmell, M.J., D. Rispler, and R. Poss, *The impact of modularity in total hip arthroplasty.* Clinical orthopaedics and related research, 1995. **319**: p. 77-84.

107. McCarthy, J.C., J.V. Bono, and P.J. O'donnell, *Custom and modular components in primary total hip replacement.* Clinical orthopaedics and related research, 1997. **344**: p. 162-171.

108. Barrack, R.L., *Modularity of prosthetic implants.* Journal of the American Academy of Orthopaedic Surgeons, 1994. **2**(1): p. 16-25.

109. Barrack, R., et al., *Complications related to modularity of total hip components.* Bone & Joint Journal, 1993. **75**(5): p. 688-692.

110. Bobyn, J.D., et al., *Concerns with modularity in total hip arthroplasty.* Clinical orthopaedics and related research, 1994. **298**: p. 27-36.

111. Collier, J.P., et al., *Mechanisms of failure of modular prostheses.* Clinical orthopaedics and related research, 1992. **285**: p. 129-139.

112. Collier, J.P., et al., *Corrosion between the components of modular femoral hip prostheses.* Bone & Joint Journal, 1992. **74**(4): p. 511-517.

113. Silverton, C.D., et al., *Midterm results of a femoral stem with a modular neck design: clinical outcomes and metal ion analysis.* The Journal of arthroplasty, 2014. **29**(9): p. 1768-1773.

114. Blakey, C., et al., *Mid-term results of the modular ANCA-Fit femoral component in total hip replacement.* Bone & Joint Journal, 2009. **91**(12): p. 1561-1565.

115. Pettersson, A., *High-performance base fluids for environmentally adapted lubricants.* Tribology international, 2007. **40**(4): p. 638-645.

116. Isaac, G., et al., *Metal-on-metal bearings surfaces: materials, manufacture, design, optimization, and alternatives.* Proceedings of the Institution of Mechanical Engineers, Part H: Journal of Engineering in Medicine, 2006. **220**(2): p. 119-133.

117. Fisher, J. and D. Dowson, *Tribology of total artificial joints.* Proceedings of the Institution of Mechanical Engineers, Part H: Journal of Engineering in Medicine, 1991. **205**(2): p. 73-79.

118. Taddei, P., et al., *May the surface roughness of the retrieved femoral head influence the wear behavior of the polyethylene liner?* Journal of Biomedical Materials Research Part B: Applied Biomaterials, 2016. **104**(7): p. 1374-1385.

119. Hall, R., et al., *The association between rates of wear in retrieved acetabular components and the radius of the femoral head.* Proceedings of the Institution of Mechanical Engineers, Part H: Journal of Engineering in Medicine, 1998. **212**(5): p. 321-326.

120. Liao, Y.-S., et al., *The effect of frictional heating and forced cooling on the serum lubricant and wear of UHMW polyethylene cups against cobalt–chromium and zirconia balls.* Biomaterials, 2003. **24**(18): p. 3047-3059.

121. Bergmann, G., et al., *Frictional heating of total hip implants, Part 1: measurements in patients.* Journal of Biomechanics, 2001. **34**(4): p. 421-428.

122. Bergmann, G., et al., *Frictional heating of total hip implants. Part 2: finite element study.* Journal of biomechanics, 2001. **34**(4): p. 429-435.

123. Smith, S.L., D. Dowson, and A.A.J. Goldsmith, *The lubrication of metal-on-metal total hip joints: A slide down the Stribeck curve.* Proceedings of the Institution of Mechanical Engineers, Part J: Journal of Engineering Tribology, 2001. **215**(5): p. 483-493.

124. Cubillos, P.O., et al., *Evaluation of Surface Finish and Dimensional Control of Tribological Metal-Ultra High Molecular Weight Polyethylene Pair of Commercially Available Hip Implants.* The Journal of Arthroplasty, 2018. **33**(3): p. 939-944.

125. Nyrén, O., et al., *Cancer risk after hip replacement with metal implants: a population-based cohort study in Sweden.* JNCI: Journal of the National Cancer Institute, 1995. **87**(1): p. 28-33.

126. Visuri, T., et al., *Cancer risk after metal on metal and polyethylene on metal total hip arthroplasty.* Clinical orthopaedics and related research, 1996. **329**: p. S280-S289.

127. Visuri, T.I., et al., *Cancer incidence and causes of death among total hip replacement patients: a review based on Nordic cohorts with a special emphasis on metal-on-metal bearings.* Proceedings of the Institution of Mechanical Engineers, Part H: Journal of Engineering in Medicine, 2006. **220**(2): p. 399-407.

128. Vendittoli, P.-A., et al., *Chromium and cobalt ion release following the Durom high carbon content, forged metal-on-metal surface replacement of the hip.* Bone & Joint Journal, 2007. **89**(4): p. 441-448.

129. *ASTM F138-13a*, in *Standard Specification for Wrought 18Chromium-14Nickel-2.5Molybdenum Stainless Steel Bar and Wire for Surgical Implants (UNS S31673)*. 2013, ASTM International: West Conshohocken, PA.

130. *ASTM F90-14*, in *Standard Specification for Wrought Cobalt-20Chromium-15Tungsten-10Nickel Alloy for Surgical Implant Applications (UNS R30605)*. 2014, ASTM International: West Conshohocken, PA, 2014.

131. *ASTM F75-12*, in *Standard Specification for Cobalt-28 Chromium-6 Molybdenum Alloy Castings and Casting Alloy for Surgical Implants (UNS R30075)*. 2012, ASTM International: West Conshohocken, PA.

132. *ASTM F562-13*, in *Standard Specification for Wrought 35Cobalt-35Nickel-20Chromium-10Molybdenum Alloy for Surgical Implant Applications (UNS R30035)*. 2013, ASTM International: West Conshohocken, PA.

133. Long, M. and H.J. Rack, *Titanium alloys in total joint replacement—a materials science perspective*. 1998, Elsevier Ltd: ENGLAND. p. 1621-1639.

134. Kawalec, J.S., et al., *Mixed-metal fretting corrosion of Ti6Al4V and wrought cobalt alloy.* Journal of Biomedical Materials Research Part A, 1995. **29**(7): p. 867-873.

135. *ASTM F136-13*, in *Standard Specification for Wrought Titanium-6Aluminum-4Vanadium ELI (Extra Low Interstitial) Alloy for Surgical Implant Applications (UNS R56401)*. 2013, ASTM International: West Conshohocken, PA.

136. Kurtz, S.M. and S.M. Kurtz, *UHMWPE Biomaterials Handbook: Ultra High Molecular Weight Polyethylene in Total Joint Replacement and Medical Devices*. 2nd;2; ed. 2009, US: Academic Press.

137. Charnley, J., *2 Total Hip Replacement by Low-Friction Arthroplasty.* Clinical orthopaedics and related research, 1970. **72**: p. 7-21.

138. Li, S. and A.H. Burstein, *Ultra-high molecular weight polyethylene. The material and its use in total joint implants.* JBJS, 1994. **76**(7): p. 1080-1090.

139. McKellop, H., et al., *Development of an extremely wear-resistant ultra high molecular weight polythylene for total hip replacements.* Journal of Orthopaedic Research, 1999. **17**(2): p. 157-167.

140. Wang, A., et al., *Effect of radiation dosage on the wear of stabilized UHMWPE evaluated by hip and knee joint simulators.* Trans Soc Biomater, 1997. **23**: p. 394.

141. Musib, M.K., *A review of the history and role of UHMWPE as a component in total joint replacements.* International Journal of Biological Engineering, 2011. **1**(1): p. 6-10.

142. Birman, M.V., et al., *Cracking and impingement in ultra–high-molecular-weight polyethylene acetabular liners.* The Journal of arthroplasty, 2005. **20**: p. 87-92.

143. Tower, S.S., et al., *Rim cracking of the cross-linked longevity polyethylene acetabular liner after total hip arthroplasty.* JBJS, 2007. **89**(10): p. 2212-2217.

144. Oral, E., et al., *Wear resistance and mechanical properties of highly cross-linked, ultrahigh–molecular weight polyethylene doped with vitamin E.* The Journal of arthroplasty, 2006. **21**(4): p. 580-591.

145. Chaudhry, S. and D. Dunlop, *Bone cement in arthroplasty.* Orthopaedics and Trauma, 2012. **26**(6): p. 391-396.

146. Vaishya, R., M. Chauhan, and A. Vaish, *Bone cement.* Journal of clinical orthopaedics and trauma, 2013. **4**(4): p. 157-163.

147. Breusch, S.J., *The Well-Cemented Total Hip Arthroplasty*. 2005: Springer. 125-140.

148. Webb, J. and R. Spencer, *The role of polymethylmethacrylate bone cement in modern orthopaedic surgery.* Bone & Joint Journal, 2007. **89**(7): p. 851-857.

149. Charnley, J., *Anchorage of the femoral head prosthesis to the shaft of the femur.* Bone & Joint Journal, 1960. **42**(1): p. 28-30.

150. Gillani, R., et al., *Nanofunctionalized zirconia and barium sulfate particles as bone cement additives.* International journal of nanomedicine, 2010. **5**: p. 1.

151. Cisneros-Pineda, O.G., et al., *Combined influence of barium sulfate content and co-monomer concentration on properties of PMMA bone cements for vertebroplasty.* Journal of Biomaterials Science, Polymer Edition, 2011. **22**(12): p. 1563-1580.

152. Sabokbar, A., et al., *Radio-opaque agents in bone cement increase bone resorption.* J Bone Joint Surg Br, 1997. **79**(1): p. 129-134.

153. Combs, S.P. and A.S. Greenwald, *The effects of barium sulfate on the polymerization temperature and shear strength of surgical simplex P.* Clinical orthopaedics and related research, 1979. **145**: p. 287-291.

154. *Instruction for use*. 2017, PALACOS R: Germany.

155. Hamadouche, M. and L. Sedel, *Ceramics in orthopaedics.* Bone & Joint Journal, 2000. **82**(8): p. 1095-1099.

156. Vallet-Regi, M., *Bioceramics with clinical applications*. 2014: Wiley-Blackwell.

157. Basu, B. and M. Kalin, *Tribology of ceramics and composites: a materials science perspective*. 2011: John Wiley & Sons.

158. Slonaker, M. and T. Goswami, *Review of wear mechanisms in hip implants: paper II–ceramics IG004712.* Materials & design, 2004. **25**(5): p. 395-405.

159. Clarke, I., et al., *Biomechanical stability and design Wear.* Annals of the New York Academy of Sciences, 1988. **523**(1): p. 292-296.

160. Nizard, R.S., et al., *Ten-year survivorship of cemented ceramic-ceramic total hip prosthesis.* Clinical orthopaedics and related research, 1992(282): p. 53-63.

161. Sedel, L., et al., *Alumina-on-alumina hip replacement. Results and survivorship in young patients.* Bone & Joint Journal, 1990. **72**(4): p. 658-663.

162. Sedel, L., et al., *Alumina-alumina hip replacement in patients younger than 50 years old.* Clinical orthopaedics and related research, 1994. **298**: p. 175-183.

163. De Aza, A., et al., *Crack growth resistance of alumina, zirconia and zirconia toughened alumina ceramics for joint prostheses.* Biomaterials, 2002. **23**(3): p. 937-945.

164. Cales, B., *Zirconia as a sliding material: histologic, laboratory, and clinical data.* Clinical Orthopaedics and Related Research (1976-2007), 2000. **379**: p. 94-112.

165. Kokubo, T., *Bioceramics and their clinical applications*. 2008: Elsevier.

166. Paton, R., *Basic Orthopaedic Sciences: The Stanmore Guide*. 2008, The Royal College of Surgeons of England.

167. Marlowe, D.E., J.E. Parr, and M.B. Mayor, *Modularity of orthopedic implants*. Vol. 1301. 1997: ASTM International.

168. Burger, W. and H. Richter. *High strength and toughness alumina matrix composites by transformation toughening and'in situ'platelet reinforcement (ZPTA)-The new generation of bioceramics*. in *Key Engineering Materials*. 2001. Trans Tech Publ.

169. Basu, B. and M. Kalin, *Tribology of ceramics and composites: materials science perspective*. 2011: John Wiley & Sons.

170. Lombardi, A.V., et al., *Delta Ceramic-on-Alumina Ceramic Articulation in Primary THA: Prospective, Randomized FDA-IDE Study and Retrieval Analysis.* Clinical Orthopaedics and Related Research®, 2010. **468**(2): p. 367-374.

171. Hamilton, W.G., et al., *THA With Delta Ceramic on Ceramic: Results of a Multicenter Investigational Device Exemption Trial.* Clinical Orthopaedics and Related Research®, 2010. **468**(2): p. 358-366.

172. Livermore, J., D. Ilstrup, and B. Morrey, *Effect of femoral head size on wear of the polyethylene acetabular component.* JBJS, 1990. **72**(4): p. 518-528.

173. Clarke, I., et al., *Charnley wear model for validation of hip simulators' ball diameter versus polytetrafluoroethylene and polyethylene wear.* Proceedings of the Institution of Mechanical Engineers, Part H: Journal of Engineering in Medicine, 1997. **211**(1): p. 25-36.

174. Derbyshire, B., et al., *Comparative study of the wear of UHMWPE with zirconia ceramic and stainless steel femoral heads in artificial hip joints.* Medical engineering & physics, 1994. **16**(3): p. 229-236.

175. Endo, M., et al., *Comparison of wear, wear debris and functional biological activity of moderately crosslinked and non-crosslinked polyethylenes in hip prostheses.* Proceedings of the Institution of Mechanical Engineers, Part H: Journal of Engineering in Medicine, 2002. **216**(2): p. 111-122.

176. Galvin, A., et al., *Wear of crosslinked polyethylene under different tribological conditions.* Journal of Materials Science: Materials in Medicine, 2006. **17**(3): p. 235-243.

177. Archard, J., *Contact and rubbing of flat surfaces.* Journal of applied physics, 1953. **24**(8): p. 981-988.

178. Geller, J.A., et al., *Large diameter femoral heads on highly cross-linked polyethylene: minimum 3-year results.* Clinical orthopaedics and related research, 2006. **447**: p. 53-59.

179. Bragdon, C.R., et al., *Radiostereometric analysis comparison of wear of highly cross-linked polyethylene against 36-vs 28-mm femoral heads.* The Journal of arthroplasty, 2007. **22**(6): p. 125-129.

180. Lachiewicz, P.F., et al., *Femoral head size and wear of highly cross-linked polyethylene at 5 to 8 years.* Clinical Orthopaedics and Related Research®, 2009. **467**(12): p. 3290.

181. Waewsawangwong, W. and S.B. Goodman, *Unexpected failure of highly cross-linked polyethylene acetabular liner.* The Journal of arthroplasty, 2012. **27**(2): p. 323. e1-323. e4.

182. Furmanski, J., et al., *Clinical fracture of cross-linked UHMWPE acetabular liners.* Biomaterials, 2009. **30**(29): p. 5572-5582.

183. Duffy, G.P., et al., *Fracture of a cross-linked polyethylene liner due to impingement.* The Journal of arthroplasty, 2009. **24**(1): p. 158. e15-158. e19.

184. Premnath, V., et al., *Gamma sterilization of UHMWPE articular implants: an analysis of the oxidation problem.* Biomaterials, 1996. **17**(18): p. 1741-1753.

185. Cole, J.C., J.E. Lemons, and A.W. Eberhardt, *Gamma irradiation alters fatigue-crack behavior and fracture toughness in 1900H and GUR 1050 UHMWPE.* Journal of Biomedical Materials Research Part A, 2002. **63**(5): p. 559-566.

186. Huot, J.C., et al., *The effect of radiation dose on the tensile and impact toughness of highly cross-linked and remelted ultrahigh-molecular weight polyethylenes.* Journal of Biomedical Materials Research Part B: Applied Biomaterials, 2011. **97**(2): p. 327-333.

187. Schroder, D.T., et al., *Retrieved highly crosslinked UHMWPE acetabular liners have similar wear damage as conventional UHMWPE.* Clinical Orthopaedics and Related Research®, 2011. **469**(2): p. 387-394.

188. Ingham, E. and J. Fisher, *The role of macrophages in osteolysis of total joint replacement.* Biomaterials, 2005. **26**(11): p. 1271-1286.

189. Kadoya, Y., et al., *Wear particulate species and bone loss in failed total joint arthroplasties.* Clinical orthopaedics and related research, 1997. **340**: p. 118-129.

190. Kobayashi, A., et al., *Number of polyethylene particles and osteolysis in total joint replacements.* J Bone Joint Surg Br, 1997. **79**(5): p. 844-848.

191. McGee, M.A., et al., *Implant retrieval studies of the wear and loosening of prosthetic joints: a review.* Wear, 2000. **241**(2): p. 158-165.

192. Maloney, W.J., et al., *Endosteal erosion in association with stable uncemented femoral components.* JBJS, 1990. **72**(7): p. 1025-1034.

193. Schmalzried, T., M. Jasty, and W.H. Harris, *Periprosthetic bone loss in total hip arthroplasty. Polyethylene wear debris and the concept of the effective joint space.* JBJS, 1992. **74**(6): p. 849-863.

194. Santavirta, S., et al., *Aggressive granulomatous lesions in cementless total hip arthroplasty.* Bone & Joint Journal, 1990. **72**(6): p. 980-984.

195. Savio, J., L. Overcamp, and J. Black, *Size and shape of biomaterial wear debris.* Clinical Materials, 1994. **15**(2): p. 101-147.

196. Bobyn, J., et al., *The susceptibility of smooth implant surfaces to periimplant fibrosis and migration of polyethylene wear debris.* Clinical orthopaedics and related research, 1995. **311**: p. 21-39.

197. Devane, P.A., et al., *Measurement of Polyethylene Wear in Metal-Backed Acetabular Cups: I. Three-Dimensional Technique.* Clinical orthopaedics and related research, 1995. **319**: p. 303-316.

198. Nashed, R.S., D.A. Becker, and R.B. Gustilo, *Are Cementless Acetabular Components the Cause of Excess Wear and Osteolysis in Total Hip Arthroplasty?* Clinical orthopaedics and related research, 1995. **317**: p. 19-28.

199. Bos, I., et al., *Comparative investigations of regional lymph nodes and pseudocapsules after implantation of joint endoprostheses.* Pathology-Research and Practice, 1990. **186**(6): p. 707-716.

200. Hicks, D.G., et al., *Granular histiocytosis of pelvic lymph nodes following total hip arthroplasty. The presence of wear debris, cytokine production, and immunologically activated macrophages.* JBJS, 1996. **78**(4): p. 482-96.

201. Shea, K.G., et al., *Analysis of lymph nodes for polyethylene particles in patients who have had a primary joint replacement.* JBJS, 1996. **78**(4): p. 497-504.

202. Sieber, H.-P., C. Rieker, and P. Köttig, *Analysis of 118 second-generation metal-on-metal retrieved hip implants.* J Bone Joint Surg Br, 1999. **81**(1): p. 46-50.

203. Weber, B., M. Semlitsch, and R. Streicher, *Total hip joint replacement using a CoCrMo metal-metal sliding pairing.* Nihon Seikeigeka Gakkai Zasshi, 1993. **67**(5): p. 391-398.

204. Willert, H.G. and M. Semlitsch, *Reactions of the articular capsule to wear products of artificial joint prostheses.* Journal of Biomedical Materials Research Part A, 1977. **11**(2): p. 157-164.

205. Medley, J.B., et al., *Comparison of alloys and designs in a hip simulator study of metal on metal implants.* Clinical orthopaedics and related research, 1996. **329**: p. S148-S159.

206. Semlitsch, M. and H.-G. Willert, *Implant materials for hip endoprostheses: old proofs and new trends.* Archives of orthopaedic and trauma surgery, 1995. **114**(2): p. 61-67.

207. Smith-Petersen, M.N., *Evolution of mould arthroplasty of the hip joint.* The Journal of bone and joint surgery. British volume, 1948. **30B**(1): p. 59-75.

208. Charnley, J., *Surgery of the hip-joint.* British medical journal, 1960. **1**(5176): p. 821.

209. Freeman, M., H. Cameron, and G. Brown, *Cemented double cup arthroplasty of the hip: a 5 year experience with the ICLH prosthesis.* Clinical orthopaedics and related research, 1978(134): p. 45-52.

210. Furuya, K., M. Tsuchiya, and S. Kawachi, *Socket-cup arthroplasty.* Clinical orthopaedics and related research, 1978(134): p. 41-44.

211. Tanaka, S., *Surface replacement of the hip joint.* Clinical orthopaedics and related research, 1978(134): p. 75-79.

212. Amstutz, H.C., et al., *Total hip articular replacement by internal eccentric shells: the "tharies" approach to total surface replacement arthroplasty.* Clinical Orthopaedics and Related Research®, 1977. **128**: p. 261-284.

213. Wagner, H., *Surface replacement arthroplasty of the hip.* Clinical orthopaedics and related research, 1978(134): p. 102-130.

214. McMinn, D. and J. Daniel, *History and modern concepts in surface replacement.* Proceedings of the Institution of Mechanical Engineers, Part H: Journal of Engineering in Medicine, 2006. **220**(2): p. 239-251.

215. Goldsmith, A., et al., *A comparative joint simulator study of the wear of metal-on-metal and alternative material combinations in hip replacements.* Proceedings of the Institution of Mechanical Engineers, Part H: Journal of Engineering in Medicine, 2000. **214**(1): p. 39-47.

216. Fisher, J., et al., *Wear of surface engineered metal-on-metal hip prostheses.* Journal of Materials Science: Materials in Medicine, 2004. **15**(3): p. 225-235.

217. Dowson, D., et al., *A hip joint simulator study of the performance of metal-on-metal joints: Part II: design.* The Journal of arthroplasty, 2004. **19**(8): p. 124-130.

218. Scholes, S., S. Green, and A. Unsworth, *The wear of metal-on-metal total hip prostheses measured in a hip simulator.* Proceedings of the Institution of Mechanical Engineers, Part H: Journal of Engineering in Medicine, 2001. **215**(6): p. 523-530.

219. Rieker, C.B., R. Schön, and P. Köttig, *Development and validation of a second-generation metal-on-metal bearing: laboratory studies and analysis of retrievals.* The Journal of arthroplasty, 2004. **19**(8): p. 5-11.

220. Chan, F.W., et al., *Wear and Lubrication of Metal-on-Metal Hip Implants.* Clinical orthopaedics and related research, 1999. **369**: p. 10-24.

221. Tipper, J., et al., *Quantitative analysis of the wear and wear debris from low and high carbon content cobalt chrome alloys used in metal on metal total hip replacements.* Journal of materials science: materials in medicine, 1999. **10**(6): p. 353-362.

222. Scholes, S. and A. Unsworth, *The tribology of metal-on-metal total hip replacements.* Proceedings of the Institution of Mechanical Engineers, Part H: Journal of Engineering in Medicine, 2006. **220**(2): p. 183-194.

223. Jacobs, M., et al., *Three-to six-year results with the Ultima metal-on-metal hip articulation for primary total hip arthroplasty.* The Journal of arthroplasty, 2004. **19**(7): p. 48-53.

224. Lombardi, A.V., et al., *Mid-term results of a polyethylene-free metal-on-metal articulation.* The Journal of arthroplasty, 2004. **19**(7): p. 42-47.

225. Blac, J., *Systemic effects of biomaterials.* Biomaterials, 1984. **5**(1): p. 11-18.

226. Black, J., et al., *Metallosis associated with a stable titanium-alloy femoral component in total hip replacement. A case report.* JBJS, 1990. **72**(1): p. 126-130.

227. Willert, H.-G., et al., *Metal-on-metal bearings and hypersensitivity in patients with artificial hip joints: a clinical and histomorphological study.* JBJS, 2005. **87**(1): p. 28-36.

228. J., L.D., et al., *The effect of component size and orientation on the concentrations of metal ions after resurfacing arthroplasty of the hip.* The Journal of Bone and Joint Surgery. British volume, 2008. **90-B**(9): p. 1143-1151.

229. R., D.H., et al., *Revision of metal-on-metal resurfacing arthroplasty of the hip.* The Journal of Bone and Joint Surgery. British volume, 2008. **90-B**(9): p. 1158-1163.

230. Hesketh, J., et al., *Biotribocorrosion of metal-on-metal hip replacements: How surface degradation can influence metal ion formation.* Tribology International, 2013. **65**: p. 128-137.

231. Miller, E.H., et al., *Self-bearing, uncemented, ceramic total hip replacement arthroplasty.* Instructional course lectures, 1986. **35**: p. 188-202.

232. Bierbaum, B.E., et al., *Ceramic-on-ceramic bearings in total hip arthroplasty.* Clinical Orthopaedics and Related Research®, 2002. **405**: p. 158-163.

233. Hannouche, D., et al., *Fractures of ceramic bearings: history and present status.* Clinical orthopaedics and related research, 2003. **417**: p. 19-26.

234. Boutin, P., *Total arthroplasty of the hip by fritted alumina prosthesis. Experimental study and 1st clinical applications.* Orthopaedics & Traumatology: Surgery & Research, 2014. **100**(1): p. 15-21.

235. Kim, Y.-H., J.-W. Park, and J.-S. Kim, *Alumina Delta-on-Alumina Delta Bearing in Cementless Total Hip Arthroplasty in Patients Aged <50 Years.* The Journal of Arthroplasty, 2016. **31**(10): p. 2209-2214.

236. Park, Y.S., S.J. Park, and S.J. Lim, *Ten-year results after cementless THA with a sandwich-type alumina ceramic bearing.* Orthopedics, 2010. **33**(11).

237. Murphy, S.B., T.M. Ecker, and M. Tannast, *Two-to 9-year clinical results of alumina ceramic-on-ceramic THA.* Clinical orthopaedics and related research, 2006. **453**: p. 97-102.

238. Kress, A.M., et al., *Excellent results with cementless total hip arthroplasty and alumina-on-alumina pairing: minimum ten-year follow-up.* International orthopaedics, 2011. **35**(2): p. 195-200.

239. Lee, Y.-K., et al., *Alumina-on-alumina total hip arthroplasty: a concise follow-up, at a minimum of ten years, of a previous report.* JBJS, 2010. **92**(8): p. 1715-1719.

240. Nevelos, J., et al., *Wear of HIPed and non-HIPed alumina–alumina hip joints under standard and severe simulator testing conditions.* Biomaterials, 2001. **22**(16): p. 2191-2197.

241. Nevelos, J., et al., *Microseparation of the centers of alumina-alumina artificial hip joints during simulator testing produces clinically relevant wear rates and patterns.* The Journal of arthroplasty, 2000. **15**(6): p. 793-795.

242. Fisher, J., et al., *PRESIDENTIAL GUEST LECTURE: Tribology of Alternative Bearings.* Clinical orthopaedics and related research, 2006. **453**: p. 25-34.

243. Higuchi, Y., et al., *Significantly Lower Wear of Ceramic-on-Ceramic Bearings Than Metal-on-Highly Cross-Linked Polyethylene Bearings: A 10- to 14-Year Follow-Up Study.* The Journal of Arthroplasty, 2016. **31**(6): p. 1246-1250.

244. Kaddick, C. and H. Pfaff, *1.3 Results of Hip Simulator Testing with Various Wear Couples.* Bioceramics in Joint Arthroplasty: Proceedings, 2002: p. 16.

245. Jeffers, J. and W. Walter, *Ceramic-on-ceramic bearings in hip arthroplasty.* J Bone Joint Surg Br, 2012. **94**(6): p. 735-745.

246. Nevelos, J., et al., *Comparative analysis of two different types of alumina-alumina hip prosthesis retrieved for aseptic loosening.* Bone & Joint Journal, 2001. **83**(4): p. 598-603.

247. Lombardi, A.V., et al., *An in vivo determination of total hip arthroplasty pistoning during activity.* The Journal of Arthroplasty, 2000. **15**(6): p. 702-709.

248. Sadoghi, P., et al., *The incidence of implant fractures after total hip arthroplasty.* International orthopaedics, 2014. **38**(1): p. 39-46.

249. Walter, W.L., et al., *Squeaking in ceramic-on-ceramic hips: the importance of acetabular component orientation.* The Journal of arthroplasty, 2007. **22**(4): p. 496-503.

250. Migaud, H., et al., *Do the Reasons for Ceramic-on-ceramic Revisions Differ From Other Bearings in Total Hip Arthroplasty?* Clinical Orthopaedics and Related Research®, 2016. **474**(10): p. 2190-2199.

251. Charnley, J., *Low friction arthroplasty of the hip: theory and practice*. 2012: Springer Science & Business Media.

252. Back, D., et al., *Early results of primary Birmingham hip resurfacings.* Bone & Joint Journal, 2005. **87**(3): p. 324-329.

253. Walter, W., et al., *Retrieval analysis of squeaking alumina ceramic-on-ceramic bearings.* J Bone Joint Surg Br, 2011. **93**(12): p. 1597-1601.

254. Walter, W.L., et al., *Squeaking hips.* The Journal of Bone and Joint Surgery. American volume., 2008. **90**(Suppl 4): p. 102.

255. Levine, D., J. Richards, and M. Whittle, *Whittle's Gait analysis*. 5th ed. 2012, Edinburgh: Churchill Livingstone Elsevier.

256. Bergmann, G., et al., *Standardized Loads Acting in Hip Implants.* PLOS ONE, 2016. **11**(5): p. e0155612.

257. Whittle, M.W., *Gait analysis: an introduction*. 2014: Butterworth-Heinemann.

258. Foucher, K.C., D.E. Hurwitz, and M.A. Wimmer, *Relative importance of gait vs. joint positioning on hip contact forces after total hip replacement.* Journal of Orthopaedic Research, 2009. **27**(12): p. 1576-1582.

259. Paul, J., *Quantification of Disability: Techniques of Gait Analysis*. 1974, SAGE Publications.

260. Bergmann, G., et al., *Hip contact forces and gait patterns from routine activities.* Journal of Biomechanics, 2001. **34**(7): p. 859-871.

261. Donath, L., et al., *Effects of stair-climbing on balance, gait, strength, resting heart rate, and submaximal endurance in healthy seniors.* Scandinavian Journal of Medicine & Science in Sports, 2014. **24**(2): p. e93-e101.

262. Paul, J.P., *Paper 8: Forces Transmitted by Joints in the Human Body.* Proceedings of the Institution of Mechanical Engineers, Conference Proceedings, 1966. **181**(10): p. 8-15.

263. Colgan, G., et al., *Gait analysis and hip extensor function early post total hip replacement.* Journal of Orthopaedics, 2016. **13**(3): p. 171-176.

264. Bergmann, G., F. Graichen, and A. Rohlmann, *Hip joint loading during walking and running, measured in two patients.* Journal of biomechanics, 1993. **26**(8): p. 969-990.

265. Brand, R.A., et al., *Comparison of hip force calculations and measurements in the same patient.* The Journal of Arthroplasty, 1994. **9**(1): p. 45-51.

266. Hodge, W., et al., *Contact pressures from an instrumented hip endoprosthesis.* JBJS, 1989. **71**(9): p. 1378-1386.

267. Rydell, N.W., *Forces acting on the femoral head-prosthesis: a study on strain gauge supplied prostheses in living persons.* Acta Orthopaedica Scandinavica, 1966. **37**(sup88): p. 1-132.

268. Ke, Z., et al., *A SoC for pressure balance measurement application in total knee arthroplasty.* AASRI Procedia, 2012. **1**: p. 267-275.

269. Morais, R., et al., *Double permanent magnet vibration power generator for smart hip prosthesis.* Sensors and Actuators A: Physical, 2011. **172**(1): p. 259-268.

270. Silva, N.M., et al., *Power management architecture for smart hip prostheses comprising multiple energy harvesting systems.* Sensors and Actuators A: Physical, 2013. **202**: p. 183-192.

271. Takeda, R., et al., *Gait posture estimation using wearable acceleration and gyro sensors.* Journal of Biomechanics, 2009. **42**(15): p. 2486-2494.

272. Mayagoitia, R.E., A.V. Nene, and P.H. Veltink, *Accelerometer and rate gyroscope measurement of kinematics: an inexpensive alternative to optical motion analysis systems.* Journal of Biomechanics, 2002. **35**(4): p. 537-542.

273. Rueterbories, J., et al., *Methods for gait event detection and analysis in ambulatory systems.* Medical Engineering & Physics, 2010. **32**(6): p. 545-552.

274. Pappas, I.P., et al., *A reliable gait phase detection system.* IEEE Transactions on neural systems and rehabilitation engineering, 2001. **9**(2): p. 113-125.

275. Bergmann, G., F. Graichen, and A.a. Rohlmann, *Is staircase walking a risk for the fixation of hip implants?* Journal of biomechanics, 1995. **28**(5): p. 535-553.

276. Hashimoto, N., et al., *Dynamic Analysis of the Resultant Force Acting on the Hip Joint During Level Walking.* Artificial Organs, 2005. **29**(5): p. 387-392.

277. Rydell, N., *Intravital measurements of forces acting on the hip joint.* Studies on the anatomy and function of bone and joints. Springer, Berlin Heidelberg New York, 1966: p. 52-68.

278. Davy, D., et al., *Telemetric force measurements across the hip after total arthroplasty.* JBJS, 1988. **70**(1): p. 45-50.

279. Pedotti, A., *Simple equipment used in clinical practice for evaluation of locomotion.* IEEE Transactions on Biomedical Engineering, 1977(5): p. 456-461.

280. Scholes, S. and A. Unsworth, *The effects of proteins on the friction and lubrication of artificial joints.* Proceedings of the Institution of Mechanical Engineers, Part H: Journal of Engineering in Medicine, 2006. **220**(6): p. 687-693.

281. Liu, D., et al., *A measuring model study of a new coordinate-measuring machine based on the parallel kinematic mechanism.* Measurement Science and Technology, 1999. **10**(11): p. 1020.

282. Hocken, R.J. and P.H. Pereira, *Coordinate Measuring Machines and Systems, Second Edition*. 2011, Baton Rouge, UNITED STATES: CRC Press.

283. Fan, K.-C. and M.C. Leu, *Intelligent planning of CAD-directed inspection for coordinate measuring machines.* Computer Integrated Manufacturing Systems, 1998. **11**(1): p. 43-51.

284. Zahwi, S. and A.M. Mekawi, *Some effects of stylus force on scratching surfaces.* International Journal of Machine Tools and Manufacture, 2001. **41**(13): p. 2011-2015.

285. Blunt, L., et al., *The role of tribology and metrology in the latest development of bio-materials.* Wear, 2009. **266**(3-4): p. 424-431.

286. Bills, P., et al. *A metrology solution for the orthopaedic industry*. in *Journal of Physics: Conference Series*. 2005. IOP Publishing.

287. Raimondi, M.T., R. Sassi, and R. Pietrabissa, *A method for the evaluation of the change in volume of retrieved acetabular cups.* Proceedings of the Institution of Mechanical Engineers, Part H: Journal of Engineering in Medicine, 2000. **214**(6): p. 577-587.

288. Becker, A., et al., *Metal-on-metal bearings I: The influence of 3D measurement accuracy on the calculated wear of a ball head using a new mathematical approach.* micron, 2006. **1**(5): p. 10.

289. Bills, P., L. Blunt, and X. Jiang, *Development of a technique for accurately determining clinical wear in explanted total hip replacements.* Wear, 2007. **263**(7-12): p. 1133-1137.

290. Spinelli, M., et al., *Integrated friction measurements in hip wear simulations: short-term results.* Proceedings of the Institution of Mechanical Engineers, Part H: Journal of Engineering in Medicine, 2010. **224**(7): p. 865-876.

291. Affatato, S., et al., *Ceramic-On-Metal for Total Hip Replacement: Mixing and Matching Can Lead to High Wear.* Artificial organs, 2010. **34**(4): p. 319-323.

292. Anissian, H.L., et al., *The wear pattern in metal-on-metal hip prostheses.* Journal of Biomedical Materials Research: An Official Journal of The Society for Biomaterials, The Japanese Society for Biomaterials, and The Australian Society for Biomaterials and the Korean Society for Biomaterials, 2001. **58**(6): p. 673-678.

293. Morlock, M.M., et al., *Modes of implant failure after hip resurfacing: morphological and wear analysis of 267 retrieval specimens.* JBJS, 2008. **90**: p. 89-95.

294. Estok, D.M., et al., *The measurement of creep in ultrahigh molecular weight polyethylene: a comparison of conventional versus highly cross-linked polyethylene.* The Journal of arthroplasty, 2005. **20**(2): p. 239-243.

295. Muratoglu, O.K., et al., *Knee-simulator testing of conventional and cross-linked polyethylene tibial inserts.* The Journal of arthroplasty, 2004. **19**(7): p. 887-897.

296. Spinelli, M., et al., *CMM–based procedure for polyethylene non-congruous unicompartmental knee prosthesis wear assessment.* Wear, 2009. **267**(5-8): p. 753-756.

297. Mizoue, T., et al., *Validation of acetabular cup wear volume based on direct and two-dimensional measurements: hip simulator analysis.* Journal of orthopaedic science, 2003. **8**(4): p. 491-499.

298. Bowden, A., S. Kurtz, and A. Edidin, *Validation of a micro-CT technique for measuring volumetric wear in retrieved acetabular liners.* Journal of Biomedical Materials Research Part B: Applied Biomaterials, 2005. **75**(1): p. 205-209.

299. Al-Hajjar, M., et al. *Severe edge loading and increased wear in ceramic-on-ceramic THRs due to rotational and translational surgical mal-positioning*. in *Orthopaedic Proceedings*. 2016. The British Editorial Society of Bone & Joint Surgery.

300. Nevelos, J., et al., *Analysis of retrieved alumina ceramic components from Mittelmeier total hip prostheses.* Biomaterials, 1999. **20**(19): p. 1833-1840.

301. Hatton, A., et al., *Alumina–alumina artificial hip joints. Part I: a histological analysis and characterisation of wear debris by laser capture microdissection of tissues retrieved at revision.* Biomaterials, 2002. **23**(16): p. 3429-3440.

302. Tipper, J.L., et al., *Alumina–alumina artificial hip joints. Part II: Characterisation of the wear debris from in vitro hip joint simulations.* Biomaterials, 2002. **23**(16): p. 3441-3448.

303. 14, A.F.-. *Standard Guide for Characterization of Wear from the Articulating Surfaces in Retrieved Metal-on-Metal and other Hard-on-Hard Hip Prostheses*. 2014: West Conshohocken.

304. Scheerlinck, T., *Cup positioning in total hip arthroplasty.* Acta Orthop Belg, 2014. **80**(03): p. 336-347.

305. Hart, A., et al., *Cup inclination angle of greater than 50 degrees increases whole blood concentrations of cobalt and chromium ions after metal-on-metal hip resurfacing.* Hip International, 2008. **18**(3): p. 212-219.

306. Witzleb, W.-C., et al., *In vivo wear rate of the Birmingham hip resurfacing arthroplasty: a review of 10 retrieved components.* The Journal of arthroplasty, 2009. **24**(6): p. 951-956.

307. Carmignato, S. and E. Savio, *Traceable volume measurements using coordinate measuring systems.* CIRP Annals-Manufacturing Technology, 2011. **60**(1): p. 519-522.

308. Bitar, D. and J. Parvizi, *Biological response to prosthetic debris.* World journal of orthopedics, 2015. **6**(2): p. 172.

309. Yoon, T.R., et al., *Osteolysis in association with a total hip arthroplasty with ceramic bearing surfaces.* JBJS, 1998. **80**(10): p. 1459-67.

310. Lerouge, S., et al., *Characterization of in vivo wear debris from ceramic—ceramic total hip arthroplasties.* Journal of Biomedical Materials Research Part A, 1996. **32**(4): p. 627-633.

311. Uddin, M., C. Mak, and S. Callary, *Evaluating hip implant wear measurements by CMM technique.* Wear, 2016. **364**: p. 193-200.

312. Underwood, R.J., et al., *Edge loading in metal-on-metal hips: low clearance is a new risk factor.* Proceedings of the Institution of Mechanical Engineers, Part H: Journal of Engineering in Medicine, 2012. **226**(3): p. 217-226.

313. Al-Hajjar, M., et al., *Effect of femoral head size on the wear of metal on metal bearings in total hip replacements under adverse edge-loading conditions.* Journal of Biomedical Materials Research Part B: Applied Biomaterials, 2013. **101B**(2): p. 213-222.

314. De Haan, R., et al., *Correlation between inclination of the acetabular component and metal ion levels in metal-on-metal hip resurfacing replacement.* The Journal of bone and joint surgery. British volume, 2008. **90**(10): p. 1291-1297.

315. Kapadia, D., et al., *Method for volumetric assessment of edge-wear in ceramic-on-ceramic acetabular liners.* Wear, 2017. **376**: p. 236-242.